

1311.05  
August 1988

Final Report - Phase II

PROVIDING STRUCTURAL MODULES WITH  
SELF-INTEGRITY MONITORING

Prepared for

NASA  
JET PROPULSION LABORATORY  
Pasadena, California  
(NASA SBIR Phase II Contract NAS7-961)

(NASA-CR-190887) PROVIDING  
STRUCTURAL MODULES WITH  
SELF-INTEGRITY MONITORING Final  
Report (Anco Engineers) 353 p

N93-18374

Unclass

G3/39 0121293

## PROJECT SUMMARY

An important aspect of ensuring the safety of individuals who will work in the U.S. space station, as well as the continual functioning of it is the ability to detect any structural damage that might result from 1) shuttle docking problems 2) direct impact from objects, such as a space vehicle, and 3) hostile action. The focus of this damage detection research is on the use of modules (substructures). This was done to maximize the possibility of detecting damage in large complex structures.

Several methods of detecting module damage, some of which were independent from the others, were developed; they are 1) damage indicator--it is used to detect slight changes in the MIMO Module transfer function matrix (MTFM, a method for calculating it had to be developed); 2) modal strain energy distribution method--it is used to locate damage that has been detected by the damage indicator method; the modes which have not been affected by the damage are found and used by the method; 3) time domain module identification--this is a nonlinear time domain parameter estimation approach applied to a module that remains attached to the global system; and 4) general system identification methods--these are nonlinear parameter estimation schemes. Also, a preliminary semi-detailed design of a module damage detection hardware system was made.

The research resulted in 1) determining a non-robust method for determining a MTFM--it can be determined but must be done using force appropriation, 2) determining that the damage indicators can be used to easily establish the occurrence of damage, 3) establishing that the strain energy method works well for nonsymmetric modules, and works for symmetric modules but indicates that there is damage at certain "symmetrical" structural locations, 4) established that the time domain module identification method works well only for global modes whose motion is mostly local to the module, and 5) identifying some refinements for some general system identification methods for module identification.

**ANCO**

## Final Report

**PROVIDING STRUCTURAL MODULES WITH  
SELF-INTEGRITY MONITORING**

Prepared for

**NASA**  
**JET PROPULSION LABORATORY**  
 Pasadena, California  
 (NASA SBIR Phase II Contract NAS7-961)

## Approval Signatures

W. Walton 8/1/88 D. Hiney 8/4/88  
 Project Mgr./Date Cog. Prin./Date

[Signature] 8/4/88 Perel. Kays 8/4/88  
 Technical QA/Date Editorial QA/Date

[Signature] 8/4/88  
 Chief Engineer/Date

Prepared by

The Technical Staff  
**ANCO ENGINEERS, INC.**  
 9937 Jefferson Boulevard  
 Culver City, California 90232-3591  
 (213) 204-5050

August 1988

## ACKNOWLEDGMENT

This report was prepared for the National Aeronautics and Space Administration (NASA) through NASA Small Business Innovation and Research (SBIR) Contract NAS7-961. The opportunity to perform the structural damage detection research is gratefully acknowledged.

The Principal Investigators for this project were Mr. W.B. Walton and Dr. P. Ibanez of ANCO Engineers, Inc. Mr. Walton also served as the Project Manager. Mr. G. Yessaie, of ANCO, also contributed considerably to the project. Other ANCO Technical Staff involved in the work were Mr. B. Johnson and Dr. C. Aboim.

In addition to the ANCO staff, Dr. J.L. Beck of the California Institute of Technology served as a general consultant for the entire project and performed specific research in the area of time domain system identification for damage detection.

Dr. J-C Chen of the Jet Propulsion Laboratory, Pasadena, California, is gratefully acknowledged for his general guidance.

# TABLE OF CONTENTS

	<u>Page</u>
1.0 SUMMARY.....	1-1
2.0 INTRODUCTION.....	2-1
2.1 References.....	2-3
3.0 MODULE TRANSFER FUNCTION MATRIX.....	3-1
3.1 Theoretical Discussion.....	3-1
3.2 Examples of Module Transfer Function.....	3-12
3.3 References.....	3-67
4.0 OBSERVING CHANGES IN THE MODULE TRANSFER FUNCTION.....	4-1
4.1 Damage Indicator.....	4-1
4.2 Example Problems.....	4-2
5.0 TIME DOMAIN MODULE MODAL IDENTIFICATION.....	5-1
5.1 Space Truss Example Problem.....	5-1
5.2 References.....	5-14
6.0 MODAL STRAIN ENERGY DISTRIBUTION METHOD.....	6-1
6.1 Theoretical Discussion.....	6-2
6.2 Case Study.....	6-7
6.3 References.....	6-12
7.0 SYSTEM IDENTIFICATION AS A METHOD OF LOCATING DAMAGE.....	7-1
7.1 A Few Recommendations for Performing System Identification to Detect Damage.....	7-4
7.2 References.....	7-6
8.0 SELF-INTEGRITY MONITORING HARDWARE SYSTEM.....	8-1
8.1 Functional Requirements.....	8-1
8.2 DAPS Architecture.....	8-3
8.3 Temperature Stabilization.....	8-15
8.4 Calibration and Compensation.....	8-17
8.5 System Power.....	8-18
8.6 System Installation and Integration.....	8-20
8.7 Reliability.....	8-21
8.8 Maintenance.....	8-23
9.0 CONCLUSIONS AND COMMENTS.....	9-1
9.1 Module Transfer Function Matrix.....	9-1
9.2 Damage Indicators.....	9-2
9.3 Time Domain Module Identification.....	9-2
9.4 Modal Strain Energy Distribution Method.....	9-2

# TABLE OF CONTENTS (concluded)

	<u>Page</u>
9.5 System Identification.....	9-3
9.6 Module Damage Detection Hardware System.....	9-3
APPENDIX A: MOUDLE TRANSFER FUNCTION MATRIX--DERIVATION DETAILS.....	A-1
APPENDIX B: THEORETICAL BASIS OF MAC/RAN IV AND MULTI-INPUT SINGLE-OUTPUT TRANSFER FUNCTION COMPUTATIONS.....	B-1
APPENDIX C: EXAMPLES OF MULTI-INPUT MULTI-OUTPUT MODULE TRANSFER FUNCTION MATRIX FOR NUMERICAL TWO BOUNDARY POINT PROBLEM.....	C-1
APPENDIX D: NONUNIFORM ENFORCED MOTION USING LARGE MASS METHOD.....	D-1
APPENDIX E: DERIVATION DETAILS FOR A DAMAGE INDICATOR.....	E-1
APPENDIX F: CASE STUDY USING TIME DOMAIN SYSTEM IDENTIFICATION.....	F-1
APPENDIX G: MODAL STRAIN ENERGY DISTRIBUTION METHOD SOFTWARE.....	G-1
APPENDIX H: MODAL STRAIN ENERGY DISTRIBUTION PLOTS FOR SIMPLY SUPPORTED BEAM.....	H-1

## 1.0 SUMMARY

An important aspect of ensuring the safety of individuals who will work in the U.S. space station, as well as the continual functioning of it is the ability to detect any structural damage that might result from 1) shuttle docking problems 2) direct impact from objects, such as a space vehicle, and 3) hostile action. The focus of this damage detection research is on the use of modules (substructures). This was done to maximize the possibility of detecting damage in large complex structures.

Several methods of detecting module damage, some of which were independent from the others, were developed; they are 1) damage indicator--it is used to detect slight changes in the MIMO Module transfer function matrix (MTFM, a method for calculating it had to be developed); 2) modal strain energy distribution method--it is used to locate damage that has been detected by the damage indicator method; the modes which have not been affected by the damage are found and used by the method; 3) time domain module identification--this is a nonlinear time domain parameter estimation approach applied to a module that remains attached to the global system; and 4) general system identification methods--these are nonlinear parameter estimation schemes. Also, a preliminary semi-detailed design of a module damage detection hardware system was made.

The research resulted in 1) determining a non-robust method for determining a MTFM--it can be determined but must be done using force appropriation, 2) determining that the damage indicators can be used to easily establish the occurrence of damage, 3) establishing that the strain energy method works well for nonsymmetric modules, and works for symmetric modules but indicates that there is damage at certain "symmetrical" structural locations, 4) established that the time domain module identification method works well only for global modes whose motion is mostly local to the module, and 5) identifying some refinements for some general system identification methods for module identification.

## 2.0 INTRODUCTION

With the advent of complex space structures (i.e., U.S. Space Station), the need for methods for remotely detecting structural damage will become greater. Some of these structures will have hundreds of individual structural elements (i.e., strut members). Should some of them become damaged, it could be virtually impossible to detect it using visual or similar inspection techniques. The damage of only a few individual members may or may not be a serious problem. However, should a significant number of the members be damaged, a significant problem could be created. The implementation of an appropriate remote damage detection scheme would greatly reduce the likelihood of a serious problem related to structural damage ever occurring. This report presents the results of the research conducted on remote structural damage detection approaches and the related mathematical algorithms. The research was conducted for the Small Business Innovation and Research (SBIR) Phase II National Aeronautics and Space Administration (NASA) Contract NAS7-961.

The Phase II research conducted was an extension of that done for the corresponding Phase I contract (NASA Contract NAS7-937) [1]. The Phase I work involved the following items:

- literature survey of structural damage detection methods;
- study (analytical and experimental of one simple system) to determine those quantities (structural variables) which are most sensitive to damage;
- defined substructure (module) transfer function matrix and investigated how it changed with damage level for the simple system tested;
- defined a damage indicator which is a function of the substructure (module) transfer function matrix and studied the influence of damage on it for the system tested;
- studied possibility of using modal strain energy distribution of the structural modes in locating damage of the system tested;
- investigated two parameter estimation approaches to locating damage; and
- sketched out with some detail some of the possible microcomputer requirements and a possible conceptual computer design for use in implementing the damage detection schemes which was felt would be the most successful.



Overall, the Phase I research yielded some approaches to the remote damage detection problem which it was felt could be developed into useful detection schemes for complex structures. The detection schemes which appeared to have the most promise for successful implementation in a practical detection hardware/software system were: 1) damage indicator approach including the concept of the substructure transfer function, and 2) modal strain energy distribution method for locating damage.

Upon the award of the NASA Phase II contract to extend the Phase I research results, work was performed in the following areas:

- established the validity of defining a substructure (module) transfer function matrix; this was done rigorously for the general case and demonstrated using several numerical examples (i.e., finite element model with random/transient excitation and obtain a transfer function using a time series analysis computer code);
- development and implementation of a number of independent damage indicators (they are functions of the substructure transfer function matrix) which were used primarily in the detection of the occurrence of damage; the work involved the calibration of the indicator output with the level of structural damage, studying the effect of different levels of damage on the shape of the indicator plots, determining which indicators are most sensitive to damage, and determining which indicators can be best used with the modal strain energy distribution method;
- study and implement the modal strain energy distribution method for locating damage; the work involved assessing the number of modes and the value of certain parameters needed for the accurate location of damage, the value of the approach for use with symmetric structures, and the determination of the levels of damage for which the method works well;
- use the concept of the substructure transfer function and the damage indicator method to locate damage by using various substructures within a substructure (module);
- study briefly the parameter estimation methods used to assess the damage state; and
- develop a more detailed microcomputer system design for exciting the modules and collecting the transducer signal data and calculation quantities which give an indication of the level of structural damage.

The sections of this report which follow document in detail the NASA Phase II research which was performed and the results of the research.

## 2.1 References

1. "Providing Structural Modules With Self-Integrity Monitoring," ANCO Final Report 1311.05, May 1985, for the National Aeronautics and Space Administration.

### 3.0 MODULE TRANSFER FUNCTION MATRIX

The structural damage detection schemes that have been developed and are discussed in Sections 4.0 and 6.0 can be used for detecting damage in a structural system taken as a whole with no substructuring done. However, the intent of the research was to develop damage detection schemes which could be used for substructures as well as the global structure. This was done for the NASA SBIR Phase I and II research. A theoretical discussion and some examples of the substructure transfer function follow.

#### 3.1 Theoretical Discussion

All but one of the structural damage detection methods developed use the concept of the multi-input multi-output transfer function--a matrix function, e.g.,

$$X(\omega) = H(\omega) L(\omega) \quad (3-1)$$

Where  $X(\omega)$  = system response vector\* (nx1)  
 $H(\omega)$  = system transfer function matrix (nx1)  
 $L(\omega)$  = system input "load" vector (lx1)  
 $\omega$  = the transform frequency

\* A vector is a column matrix.

The "load" vector can consist of forces, accelerations or other input quantities. For a substructure the responses are the responses of the substructure at its interior points--does not include the boundary points. The input "loads" are the forces or motions (i.e., displacements) at the boundary of the substructure and any forces applied to the interior of the substructure.

As a part of the use of the above definition of the substructure transfer function matrix to help in the detection of structural damage, its existence was demonstrated analytically. Two types of substructure response were looked at; they are 1) absolute response and 2) relative response. Also, two types of boundary inputs were looked at; they are 1) motions and 2) forces. The results of these investigations are presented below.

### 3.1.1 Consideration of Substructure Absolute Responses and Boundary Motions

As will be shown, it is possible to define a substructure transfer function using either absolute or relative substructure responses. The reasons for looking at the two types of responses is discussed later. The substructure input "loads" at its boundary are motions and not forces.

The matrix equation for the dynamic response of an entire structural system was Fourier transformed and partitioned.

$$M\ddot{x}(t) + C\dot{x}(t) + Kx(t) = f(t) \quad (3-2)$$

where  $M$ ,  $C$ , and  $K$  are the mass, damping and stiffness matrices, respectively, and  $x(t)$  and  $f(t)$  are the displacement and applied load vectors, respectively. The dot, " $\cdot$ ", represents the first derivative with respect to time,  $t$ . Taking the Fourier transform of Equation 3-2 yields the following matrix equation:

$$(-\omega^2 M + i\omega C + K)X(\omega) = F(\omega) \quad (3-3)$$

or

$$\tilde{K}(\omega)X(\omega) = F(\omega)$$

where  $\omega$  = the transform frequency

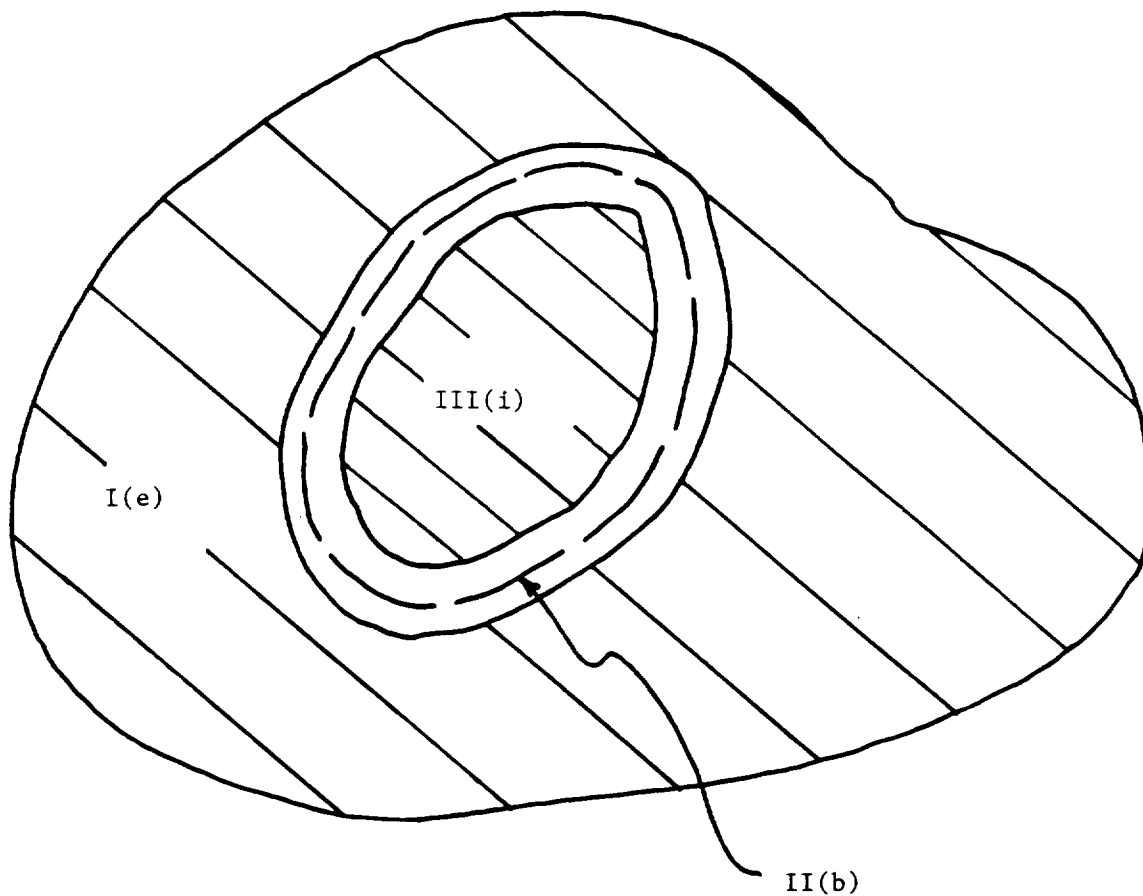
$$i = \sqrt{-1}$$

$X(\omega)$  = system response vector, Fourier transform of

$F(\omega)$  = system input load vector, Fourier transform of

$\tilde{K}(\omega)$  = system "dynamic stiffness" matrix

Equation 3-3 was then partitioned using three zones (domains) of the entire system (see Figure 3.1)--actually two substructures. One substructure was the one for which damage was being detected--the module, and the other substructure consisted of the other substructures for which damage was not being detected at the present time--damage is detected one substructure at a time.



<u>Zone</u>	<u>Description</u>
I	Total structure less the module--structure <u>external</u> to the Module (e).
II	Module <u>boundary</u> (b).
III	Module <u>interior</u> --part of system for which damage is being detected (i).

Figure 3.1: Partitioning Structure Into Three Zones

$$\begin{bmatrix} \tilde{K}_{ee} & \tilde{K}_{eb} & \tilde{K}_{ei} \\ \tilde{K}_{be} & \tilde{K}_{bb} & \tilde{K}_{bi} \\ \tilde{K}_{ie} & \tilde{K}_{ib} & \tilde{K}_{ii} \end{bmatrix} \begin{Bmatrix} X_e(\omega) \\ X_b(\omega) \\ X_i(\omega) \end{Bmatrix} = \begin{Bmatrix} F_e(\omega) \\ F_b(\omega) \\ F_i(\omega) \end{Bmatrix} \quad (3-4)$$

where  $X_e, X_b, X_i$  = absolute displacement vectors corresponding to motions in Zones I, II, and III, respectively, Fourier transform of; and

$F_e, F_b, F_i$  = applied force vectors for Zones I, II, and III, respectively, Fourier transform of.

The elements of the matrix and vectors are themselves matrices and vectors, respectively.

Equation 3-4 can be expanded to yield three matrix equations.

$$\tilde{K}_{ee}X_e + \tilde{K}_{eb}X_b + \tilde{K}_{ei}X_i = F_e \quad (3-5a)$$

$$\tilde{K}_{be}X_e + \tilde{K}_{bb}X_b + \tilde{K}_{bi}X_i = F_b \quad (3-5b)$$

$$\tilde{K}_{ie}X_e + \tilde{K}_{ib}X_b + \tilde{K}_{ii}X_i = F_i \quad (3-5c)$$

It can be shown from the concept of the static and dynamic influence coefficient that  $\tilde{K}_{ie} = 0$  (see Appendix A). Thus, it is possible to solve for  $X_e$  as a function of  $X_b$  and  $F_e$ , and  $X_i$  as a function of  $X_b$  and  $F_i$ . These relationships can be used in Equation 3-5b to solve for  $X_b$ . The motions within the two substructures can then be determined. Of course, the purpose of this effort is not to solve the substructure problem. It is to develop an expression for the module transfer function matrix.

Equation 3-5c can be used to solve for  $X_i$  as a function of  $X_b$  (see Appendix A).

$$\begin{aligned}
X_i &= \tilde{K}_{ii}^{-1} F_i - \tilde{K}_{ii}^{-1} \tilde{K}_{ib} X_b \\
&= \tilde{K}_{ii}^{-1} [I \mid - \tilde{K}_{ib}] \begin{Bmatrix} F_i \\ X_b \end{Bmatrix}
\end{aligned} \tag{3-6}$$

The transfer function matrix for the module is

$$\tilde{K}_{ii}^{-1} [I \mid - \tilde{K}_{ib}]$$

for both externally applied forces  $F_i$  and boundary displacements  $X_b$ . For the case of either no boundary motions or no applied forces within the module, the transfer function matrix can be found from Equation 3-6.

In calculating the transfer function matrix (see Equation 3-1) from the system inputs and outputs, it is necessary to use all the nonzero system inputs to be able to determine any elements of it. If all the inputs and one output is known, it is possible to determine the single row of the transfer function matrix corresponding to the given output. The more outputs that are known, the more rows of the transfer function matrix can be determined. The transfer function matrices that can be identified using Equation 3-6 correspond to knowing all outputs. Furthermore, they correspond to the inclusion of all components of the input vector, i.e., possible applied forcing at all degrees-of-freedom. Of course, there is nothing wrong with using the entire transfer function matrix when only some of the possible inputs are nonzero and only some of the outputs are of interest. It is just necessary to keep track of which rows and columns of the matrix must be retained.

The matrices in Equation 3-6 can be partitioned by identifying the nonzero and zero boundary displacements and module internal forces, and the module internal displacements which are to be used and not used. When this is done and the resulting equation expanded, the following matrix equation is found:

$$X_i^u = T_{ii}^{u u_f} F_i^u - \left( T_{ii}^{u f} \tilde{K}_{ib}^{u f u_b} + T_{ii}^{u n_f} \tilde{K}_{ib}^{n_f u_b} \right) X_b^u \tag{3-7}$$

where the superscripts u and n refer to the variables being used and not used, respectively. For the boundary displacements and forces applied to

the module interior, the variables which are used and not used are those which are not zero and are zero, respectively. Thus,

$$X_b = \begin{Bmatrix} u_b \\ X_b \\ n_b \\ X_b \end{Bmatrix} = \begin{Bmatrix} u_b \\ X_b \\ 0 \end{Bmatrix}$$

$$F_i = \begin{Bmatrix} u_f \\ F_i \\ n_f \\ F_i \end{Bmatrix} = \begin{Bmatrix} u_f \\ F_i \\ 0 \end{Bmatrix}$$

where the terms within the brackets are block vectors. For the displacements within the module, the variables which are used and not used are those which are and are not selected for investigation, respectively. Thus,

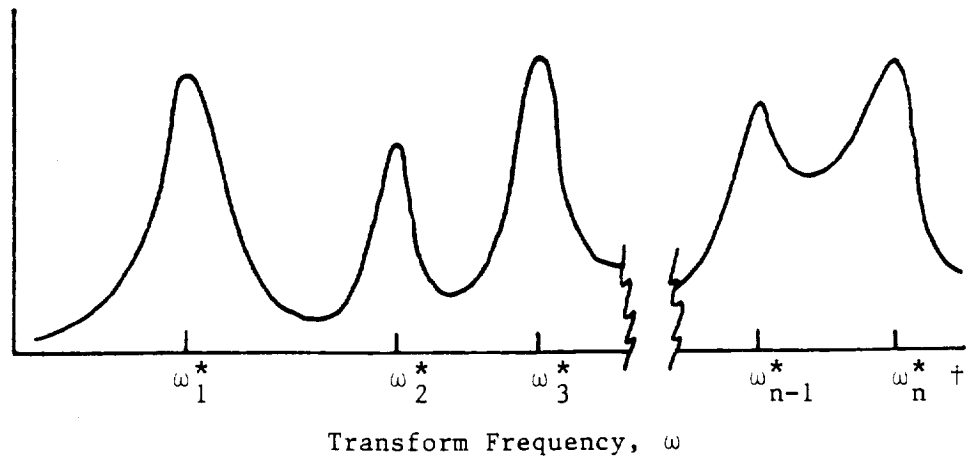
$$X_i = \begin{Bmatrix} u_i \\ X_i \\ n_i \\ X_i \end{Bmatrix}$$

Also, the matrices  $\tilde{K}_{ii}^{-1}$  and  $\tilde{K}_{ib}$  are partitioned appropriately and  $T_{ii} = \tilde{K}_{ii}^{-1}$ .

The transfer function for the case of some of the module responses used and some of the possible substructure inputs being zero, can be found from Equation 3-7. It is similar to that found from Equation 3-6.

There can be a difference between the set of all poles of the transfer functions obtained from Equations 3-6 and 3-7. The difference would not be in the value of the poles but in the number of unique poles for the two functions. This is represented by Figure 3.2. In this figure, the natural frequencies for the module are indicated as corresponding to the "pole frequencies". These natural frequencies correspond to the boundary of the module being completely constrained. This can be understood by comparing the method for determining the transfer function poles with that of determining the clamped boundary module eigenvalues. For the case of all possible applied module internal forces being nonzero and using all internal responses, the poles of the module transfer function matrix are found from

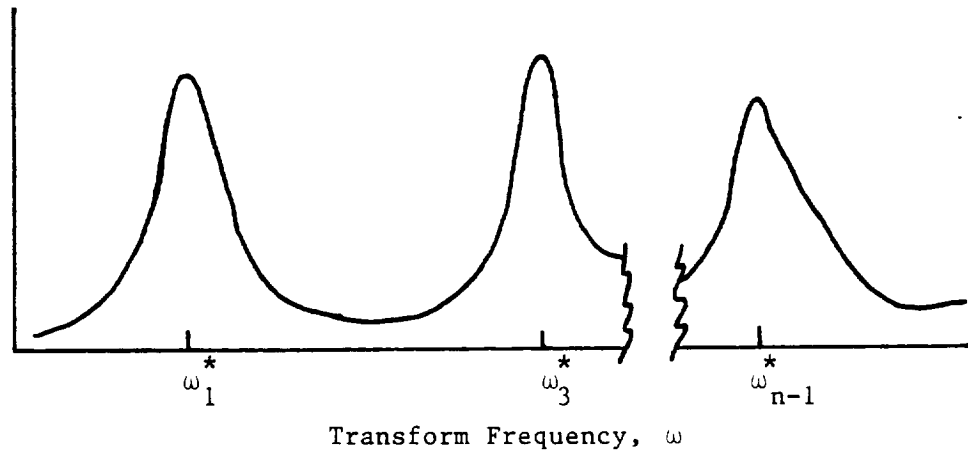




a) "Transfer function" for all possible inputs and outputs.

---

† A natural frequency of the substructure is represented by  $\omega_k^*$ .



b) "Transfer function" for only some inputs nonzero and only some output used.

Figure 3.2: Conceptual Representation of Transfer Function Matrix for Different Input and Output Conditions

$$\text{Det}[\tilde{K}_{ii}(\omega_k^p)] = \begin{cases} 0, & \text{no damping} \\ \text{minima,} & \text{damping present} \end{cases} \quad (3-8)$$

where  $\text{Det}[\ ] =$  determinant of a matrix.

$$\tilde{K}_{ii}(\omega_k^p) = -(\omega_k^p)^2 M_{ii} + i(\omega_k^p) C_{ii} + K_{ii}$$

$\omega_k^p =$  the kth pole of the module transfer function matrix.

The clamped boundary module eigenvalue problem is solved in part by solving Equation 3-8--the eigenvalues are found by doing this. Thus, the poles of the transfer function are the same as the natural frequencies found from the fixed boundary module problem.

### 3.1.2 Consideration of Substructure Relative Responses and Boundary Motions

The previous discussion on the module transfer function matrix was for absolute module responses. During the research effort it was decided that module relative responses should be looked at also. The absolute response of a substructure has large parts of it which are due to the global system response. There are smaller parts of it which are due to the excitation of the substructure fixed boundary modes. It is desired to focus in this subsection on the latter described parts of the absolute response--the relative response.

The starting point for this development is with Equation 3-5c.

$$\tilde{K}_{ib} X_b + \tilde{K}_{ii} X_i = F_i \quad (3-9)$$

The approach used to obtain the relative responses is the so-called "pseudo-static method" for non-uniform base enforced motion [1,2]. The absolute substructure response,  $X_i$ , can be expressed as follows:

$$X_i(\omega) = S_i(\omega) + R_i(\omega) \quad (3-10)$$

where  $S_i =$  vector of Fourier transform of the "pseudo-static components" of the structural response (which represents the "static" effects of the multiple support movements on the response of the structure); and

$R_i$  = vector of Fourier transform of components of the fixed boundary dynamic response of the substructure interior; these are relative responses.

The vector  $S_i$  is given by the following:

$$S_i = PX_b$$

where  $P = -K_{ii}^{-1}K_{ib}$

From these equations, the following is found:

$$\tilde{K}_{ii}R_i = F_i - \omega^2 M_{ii}K_{ii}^{-1}K_{ib}X_b \quad (3-11)$$

This equation can be used to obtain the transfer function matrix equation for relative responses of the module.

$$R_i(\omega) = \tilde{K}_{ii}^{-1}[I - \omega^2 M_{ii}K_{ii}^{-1}K_{ib}] \begin{Bmatrix} F_i(\omega) \\ X_b(\omega) \end{Bmatrix} \quad (3-12)$$

It is seen that Equations 3-6 and 3-12 are very similar.

Equation 3-11 can be inverse transformed to yield the following:

$$M_{ii}\ddot{r}_i(t) + C_{ii}\dot{r}_i(t) + K_{ii}r_i(t) = f_i(t) + M_{ii}K_{ii}^{-1}K_{ib}\ddot{x}_b(t) \quad (3-13)$$

This equation has the same form as the standard dynamic equation for the relative response of a structure undergoing nonuniform base motion. The only difference is that the applied force term is not usually included in the standard equation for base motion. The details of the development presented in this subsection are given in Appendix A.

### 3.1.3 Two Possible Definitions of the Module Input Vector

In the preceding two subsections (Sections 3.1.1 and 3.1.2), the module input vector was taken to be

$$\begin{Bmatrix} F_i \\ \vdots \\ X_b \end{Bmatrix}$$

For this case, a transfer function matrix was

$$T_{ii}[I \mid -\tilde{K}_{ib}]$$

It is possible to define the input vector differently. This can be done by grouping two matrices together as follows:

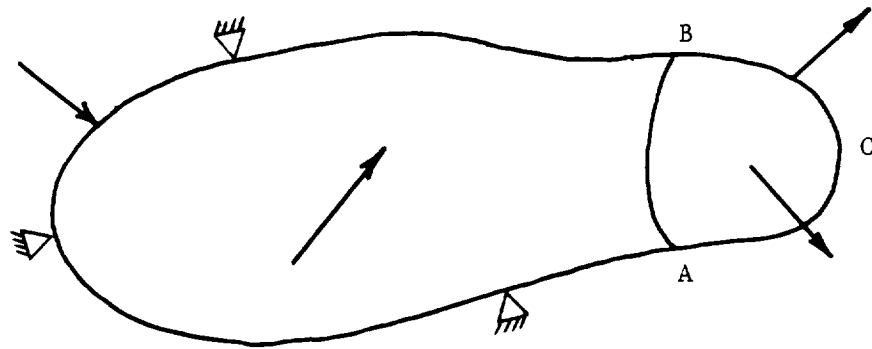
$$\begin{aligned} X_i &= \tilde{K}_{ii}^{-1}(F_i - \tilde{K}_{ib}X_b) \\ &= \tilde{K}_{ii}^{-1}[I \mid I] \begin{Bmatrix} F_i \\ \vdots \\ X'_b \end{Bmatrix} \end{aligned}$$

where  $X'_b = -\tilde{K}_{ib}X_b$

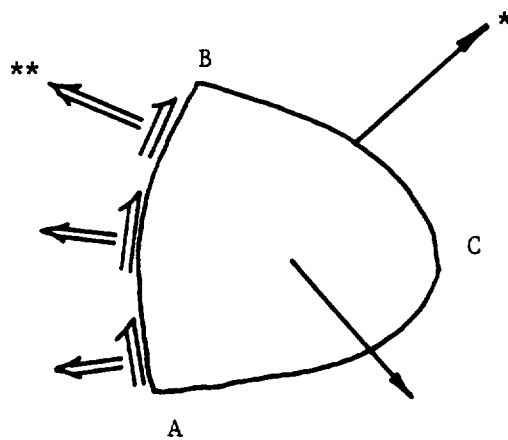
Either input can be used; however, there are advantages and disadvantages to each. If  $X_b$  is taken as an input it will not be necessary to determine  $\tilde{K}_{ib}$  explicitly; however, the transfer function obtained will involve  $\tilde{K}_{ib}$ . When  $\tilde{K}_{ib}X_b$  is taken as an input, it will be necessary to determine  $\tilde{K}_{ib}$  before determining the transfer function; however, the transfer function will basically be  $\tilde{K}_{ii}^{-1}$ . The work performed for this project involved the use of the boundary motion,  $X_b$ , as an input. (Appendix A contains some notes on this.)

#### 3.1.4 Consideration of Substructure Absolute Responses and Boundary Forces

This final analytically oriented discussion on the module transfer function deals with the use of boundary forces instead of boundary motions. Boundary forces are introduced into the substructure problem by simply free-bodying the module from the remainder of the total structure--create a free-body. Of course, it is necessary to include the structural system internal forces/stresses at the module boundary in the free-body. The module response is then characterized using the structural dynamic equations for it together with the interface forces and any other externally applied forces. An example of this is shown in Figure 3.3.



a) Global structural system.



b) Free-body with internal interface and external loads.

- 
- \* External load.
  - \*\* Internal load.

Figure 3.3: Free-body of Part of a Structural System

The matrix equation for a free-body can be written as follows:

$$M_f \ddot{q}_f + C_f \dot{q}_f + K_f q_f = f_f(t) \quad (3-14)$$

where  $M_f$ ,  $C_f$  and  $K_f$  are the mass, damping and stiffness matrices for the free-body, respectively, and  $q_f(t)$  and  $f_f(t)$  are the displacement and applied load vectors for the free-body, respectively. The free-body is a free-free structure--no displacements or rotations are prescribed on the interface surfaces of the free-body, i.e., on Surface A-B in Figure 3.3. The applied force  $f_f$  term includes all forces applied to the free-body, including the interface forces.

Given a free-body together with all applied loads, the solution to Equation 3-14 will be the same as the part of the solution of the global problem corresponding to the domain of the free-body.

The module (in this case, a free-body) transfer function matrix is determined by Fourier transforming Equation 3-14. The following is found:

$$(-\omega^2 M_f + i\omega C_f + K_f) Q_f(\omega) = F_f(\omega)$$

or

(3-15)

$$\tilde{K}_f Q_f(\omega) = F_f(\omega)$$

Thus,

$$Q_f(\omega) = \tilde{K}_f^{-1} F_f(\omega) \quad (3-16)$$

and the transfer function matrix is seen to be  $\tilde{K}_f^{-1}$ . The poles of the function occur when

$$\text{Det}(\tilde{K}_f) = 0$$

which also corresponds to the eigenvalues of the free-free module.

### 3.2 Examples of the Module Transfer Function

Three examples of the module transfer function are presented. The examples are simple (a few degree-of-freedom), but clearly illustrative of the concept.

### 3.2.1 Module With One Boundary Point - Analytical Study

The module and global system studied is pictured in Figure 3.4. The system is excited by a harmonic force at Node 1. The module transfer function modulus for this case is

$$|\tilde{K}_{ii}^{-1}| = |X_2/X_1|$$

where  $X_1$  and  $X_2$  are the global structure responses--modulus of the steady-state response. A plot of the function is given in Figure 3.5. There is one pole  $(\omega^p)^2 = 2\omega_1^2 = 2 K/M$ . The one natural frequency of the module with the boundary fixed is seen to be equal to  $\omega^p$ .

### 3.2.2 Substructure With One Boundary Point - Numerical Study

This numerical study involved a single substructure boundary point--a single input to the substructure (there were no forces applied to the substructure interior). For this study, several different locations for the boundary were chosen (see Figure 3.6). For a given substructure, a transfer function was calculated by dividing the Fourier transform of an output by the Fourier transform of the boundary motion\*. The response of the global system was determined using the static and dynamic structural digital computer code COSMOS/M.\*\*

A single approach was used to excite the global system--it was base (at Node 1) motion. Figures 3.7 and 3.8 show a sample of the type of input used and a sample of the outputs obtained, respectively. The first transfer function obtained was for the global structure (see Figure 3.9). This was done to verify that the correct method and parameters were being used to obtain the transfer functions. Because of the nature of the excitation, not all the modes were excited. A comparison was made between the poles of the

\* This was done using the digital computer code MAC/RAN IV [3]. This is a proprietary code developed and marketed by University Software Systems, El Segundo, California.

\*\* A finite element code developed and marketed by Structural Research and Analysis Corporation, Inc., Santa Monica, California.

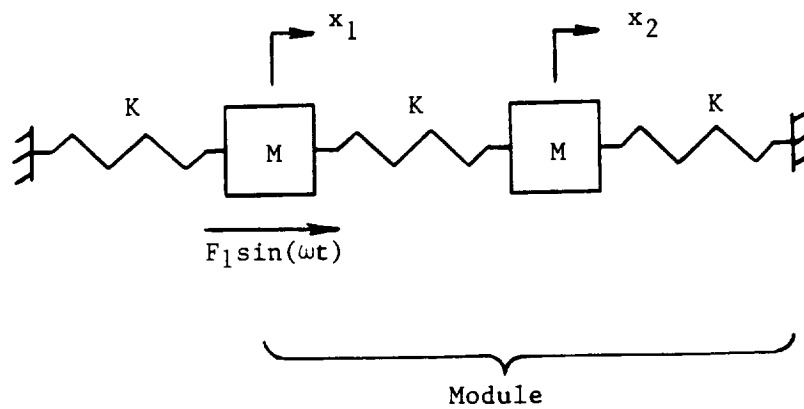
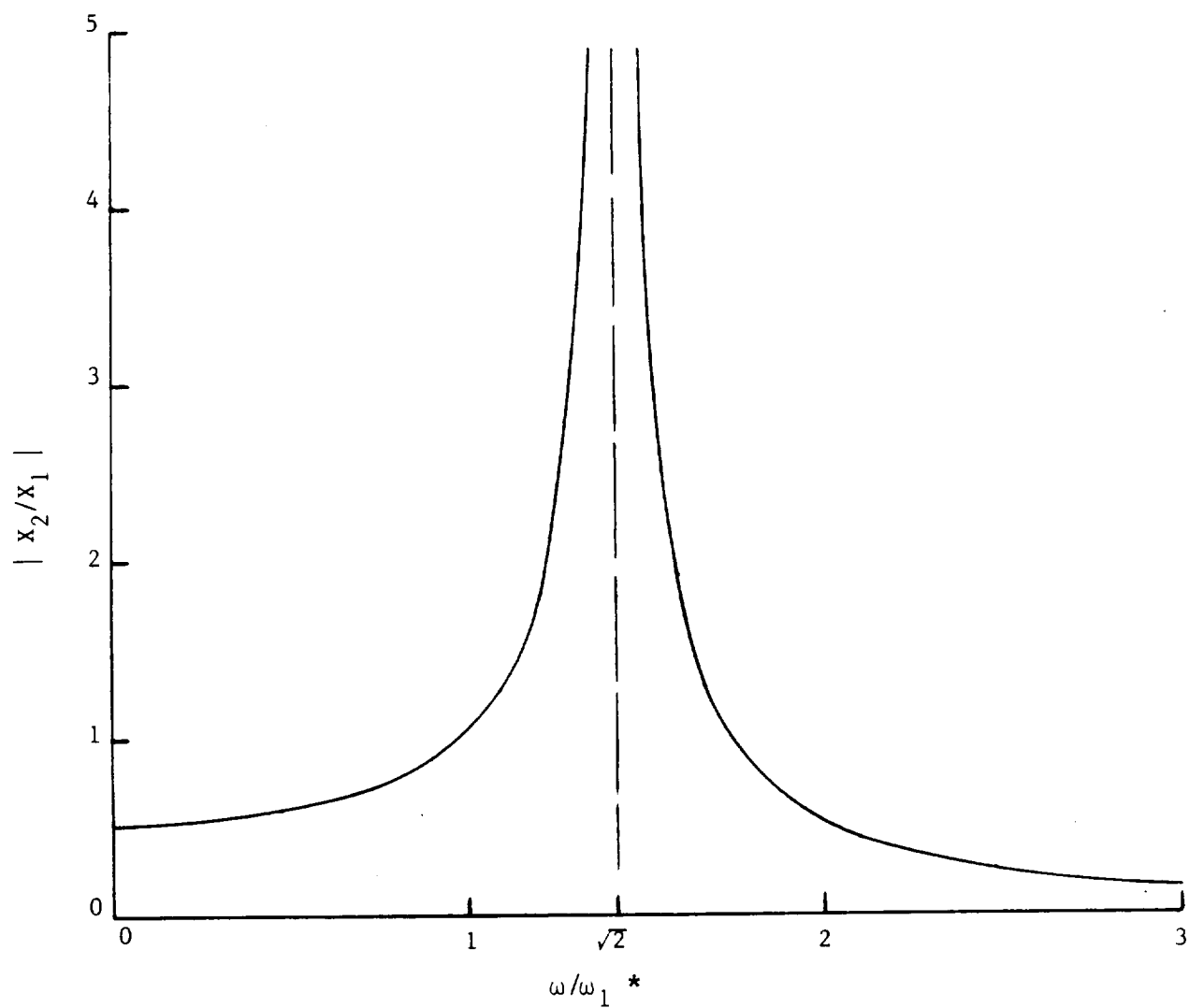


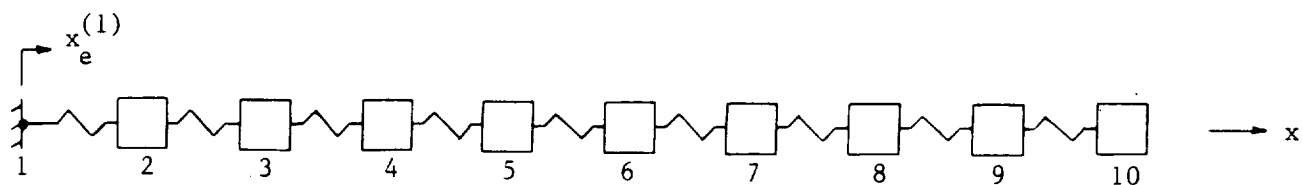
Figure 3.4: Two Degree-of-Freedom Lumped Spring and Mass System--Module With One Boundary Point





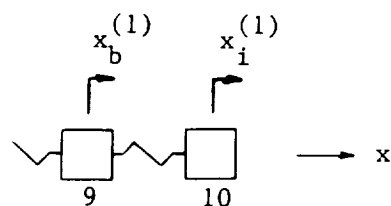
\*  $\omega_1$  is the first natural frequency of the global system. Its square is equal to  $K/M$ .

Figure 3.5: Modulus of Module Transfer Function--One Boundary Analytical Problem

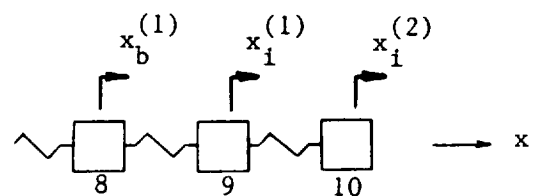


a) Global Structural System\*

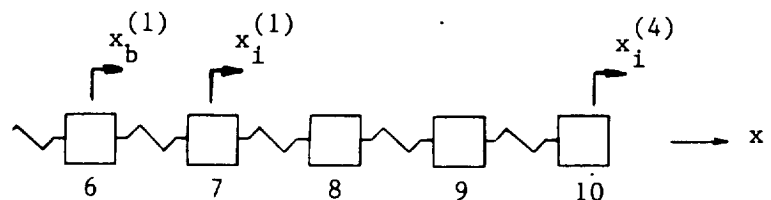
b) Module 1--Boundary at Node 9



c) Module 2--Boundary at Node 8



d) Module 3--Boundary at Node 6



\* The masses move in only the x-Direction.

Figure 3.6: Nine Degree-of-Freedom Lumped Spring and Mass System--Various Modules With Single Boundary Point

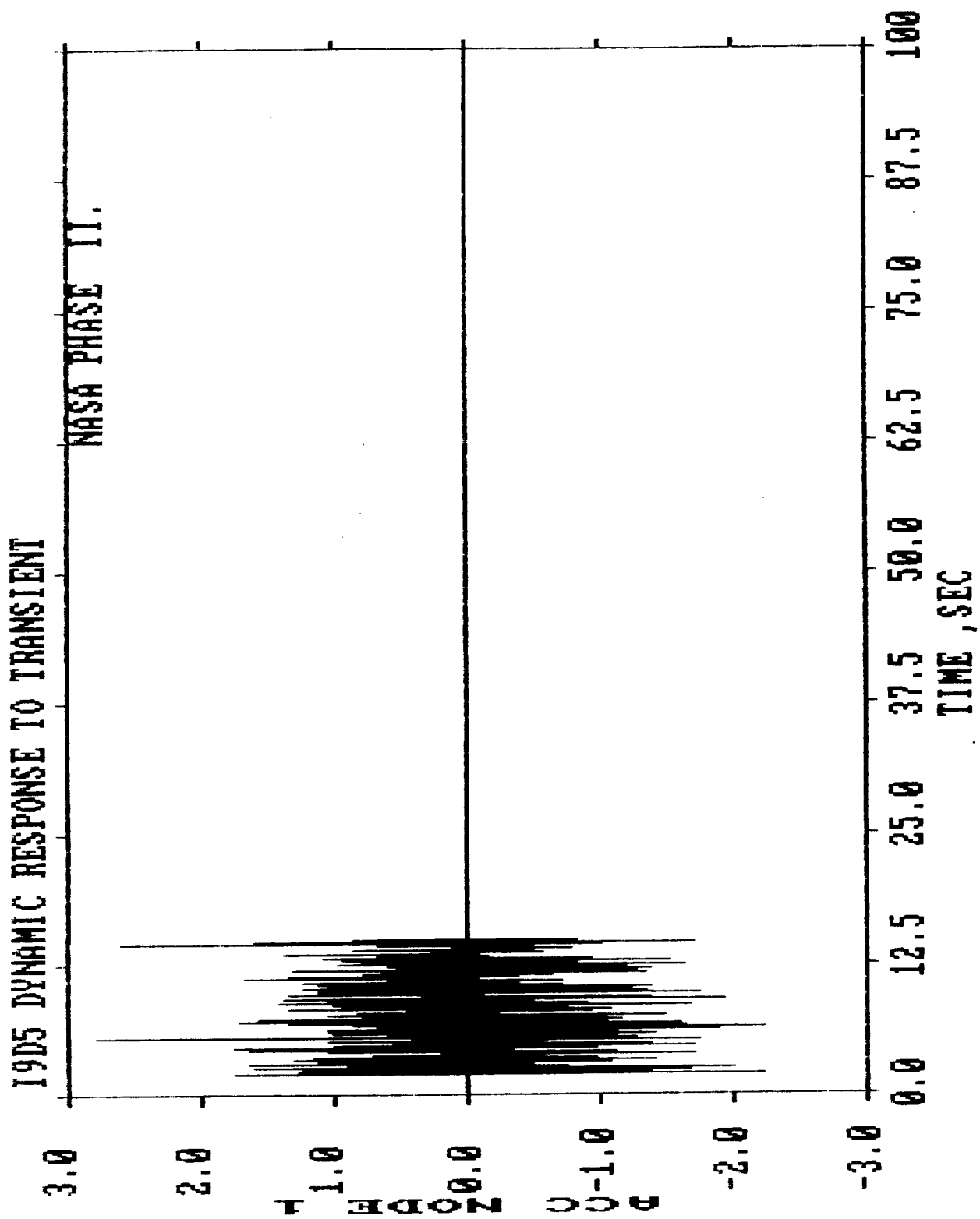
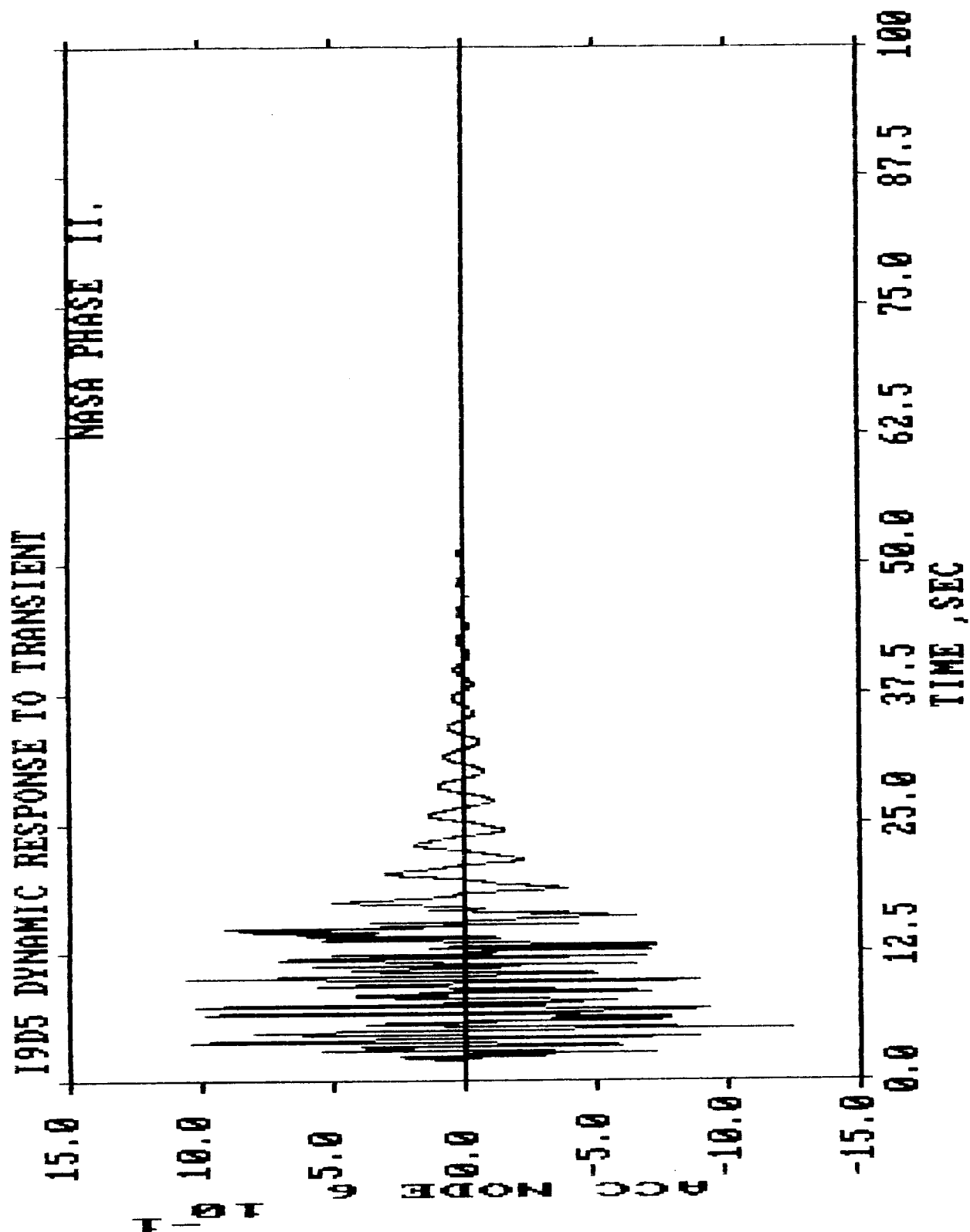
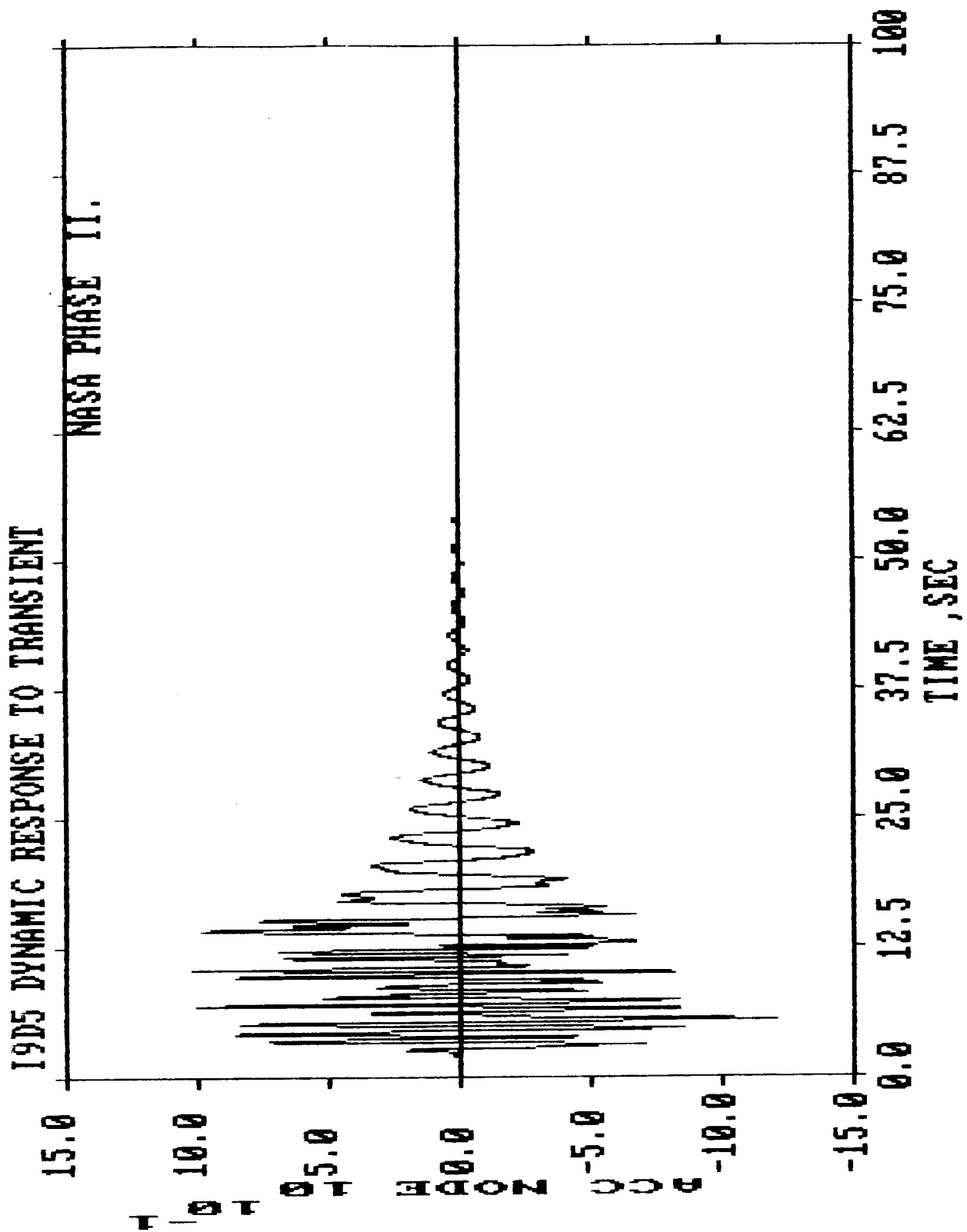


Figure 3.7: Base Motion at Node 1--Zero Motion, Then Random and Finally Long Duration Zero Motion



a) Acceleration of Node 6

Figure 3.8: Sample of Outputs Obtained From Transient Solution of Base Motion Problem



b) Acceleration of Node 10

Figure 3.8 (concluded)

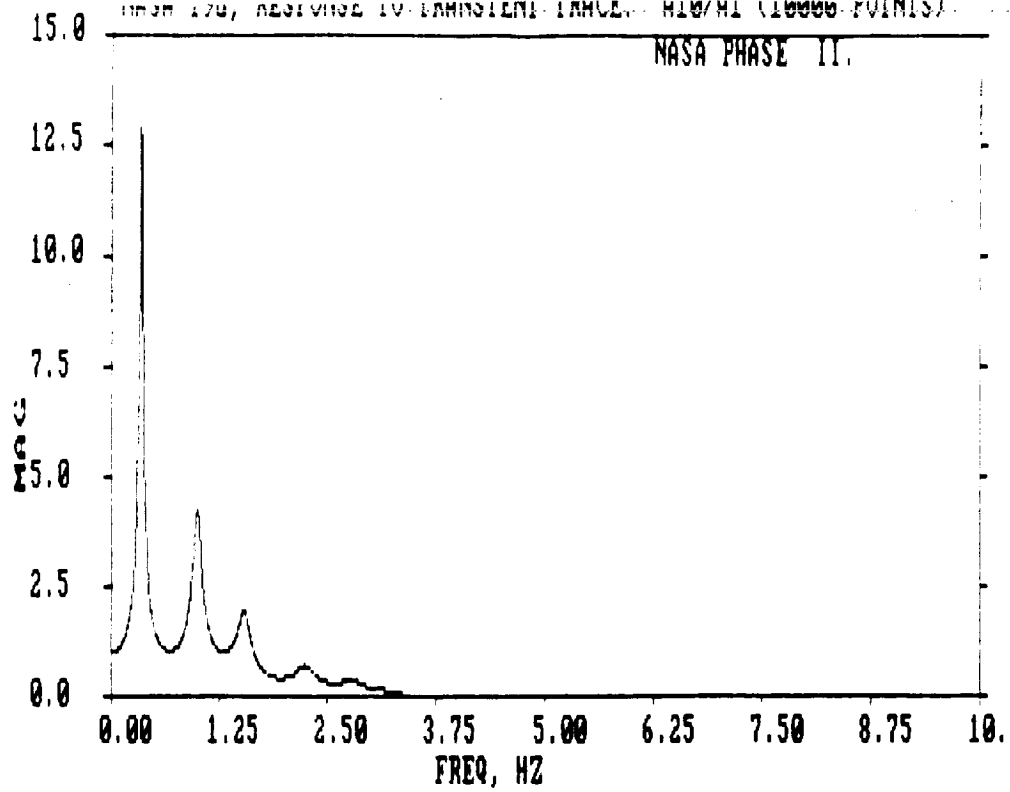
global transfer function and the natural frequencies obtained from an eigenvalue extraction--there was excellent agreement between them. Also, the damping obtained from the global transfer function was compared to that used in the simulation--the comparison was excellent.

Transfer functions were then obtained for the modules defined in Figure 3.6. They are shown in Figures 3.10 through 3.12. The results are completely consistent with the theoretical results discussed in Section 3.1. Table 3.1 is a comparison between the poles of the selected transfer function for the module and the real natural frequencies obtained from the fixed boundary module eigenvalue problem. It should be noted that the module poles are different from the global system natural frequencies (see Figure 3.13).

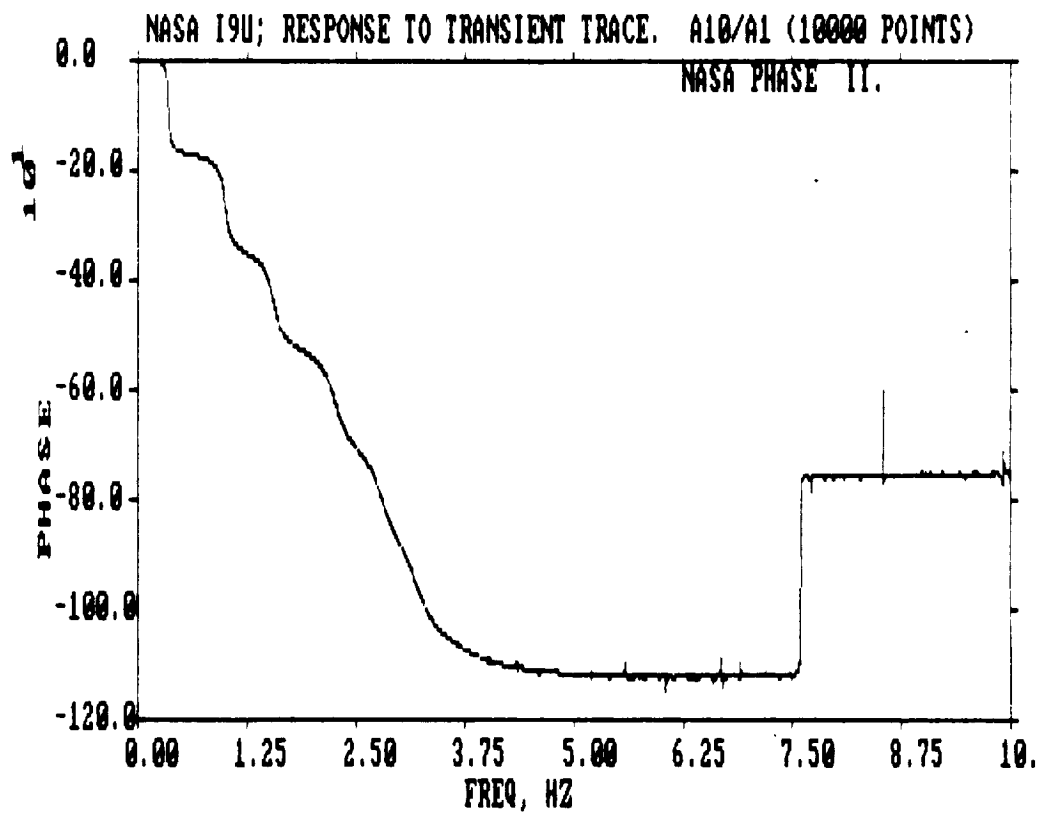
The last thing to be discussed for the one boundary point module problem with base excitation is the effect of changes in the structural system external to and at the boundary of the module on the module transfer function. Theoretically the module transfer function should not be changed by changes external to it and at the module boundary. It was decided to look at this for the numerical example being studied. This was done by reducing the mass at Nodes 2 through 6 and obtaining a transfer function for Module 3. This was done for two levels of mass reduction--25% and 50% reduction\*. The results are shown in Figure 3.14. The transfer function (e.g.,  $A_{10}/A_6$ ) remained virtually unchanged. The largest changes in the modulus (magnitude) occurred at the first resonant peak (at 0.69 Hz). The "peak frequency" remained unchanged, however, the amplitude at the peak changed slightly. This is probably due to the fact that the module transfer function peaks occur at frequencies which are between the global structure frequencies; hence, the module transfer function peaks occurred at frequencies where the input was quite small. Thus, numerical problems may have caused the slight variation in the peak height of the first resonant peak. The phase remained virtually unchanged for the three resonant peaks.

---

\* These reductions in mass, 25% and 50%, represented a 13.8% and 27.5% reduction in the total mass of the global system.

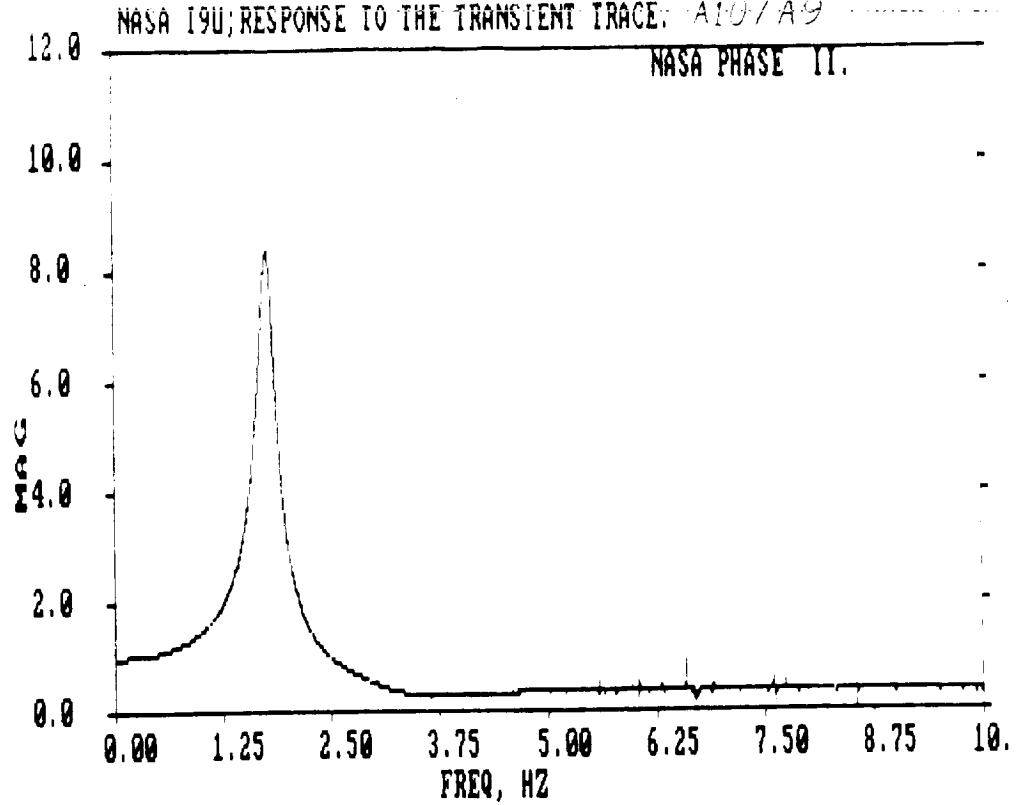


a) Modulus--Input is A1 and Output is A10

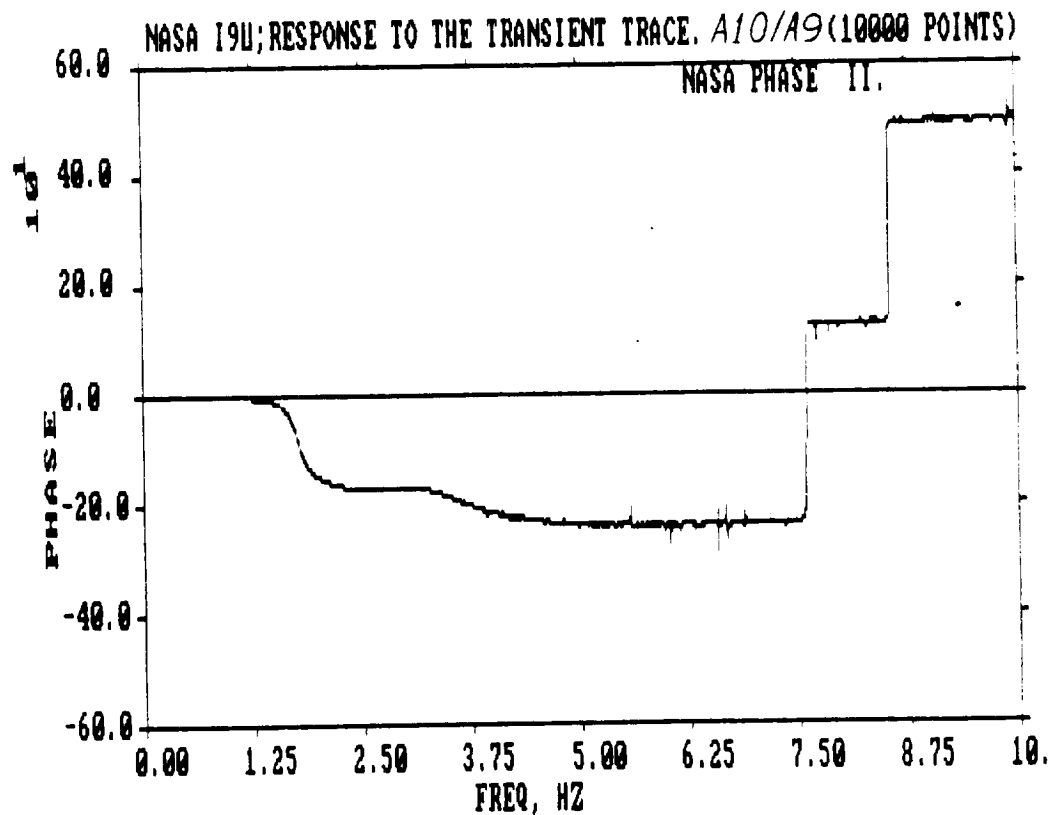


b) Phase

Figure 3.9: Global Transfer Function--Node 1 is the Base and Nodes 2 Through 10 are Other Structure Points



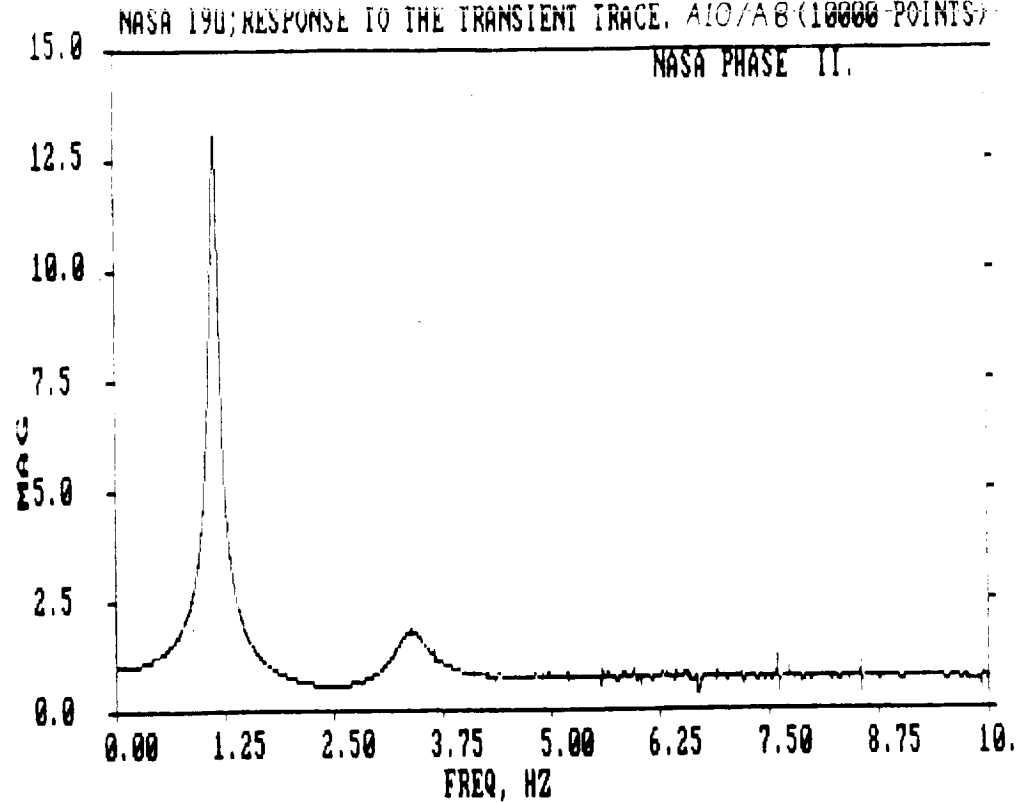
a) Modulus--Input is A9 and Output is A10.



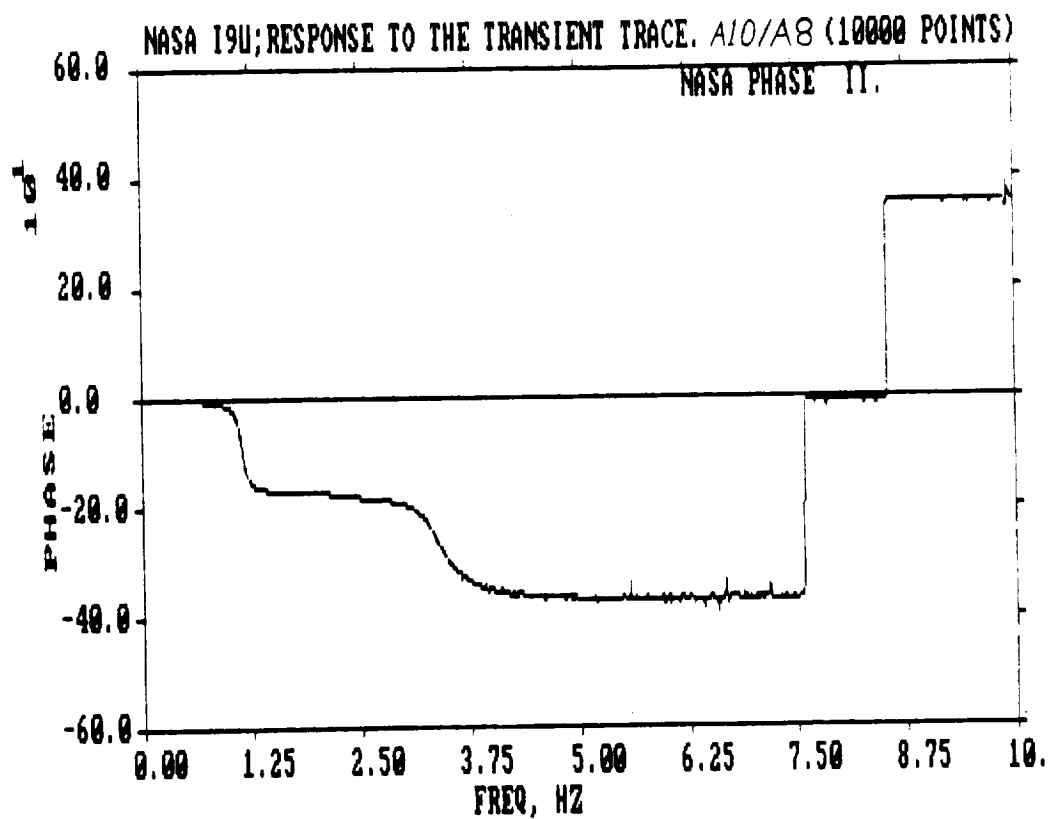
b) Phase

Figure 3.10: Module Transfer Function--Node 9 is the Boundary and Node 10 is the Interior Point



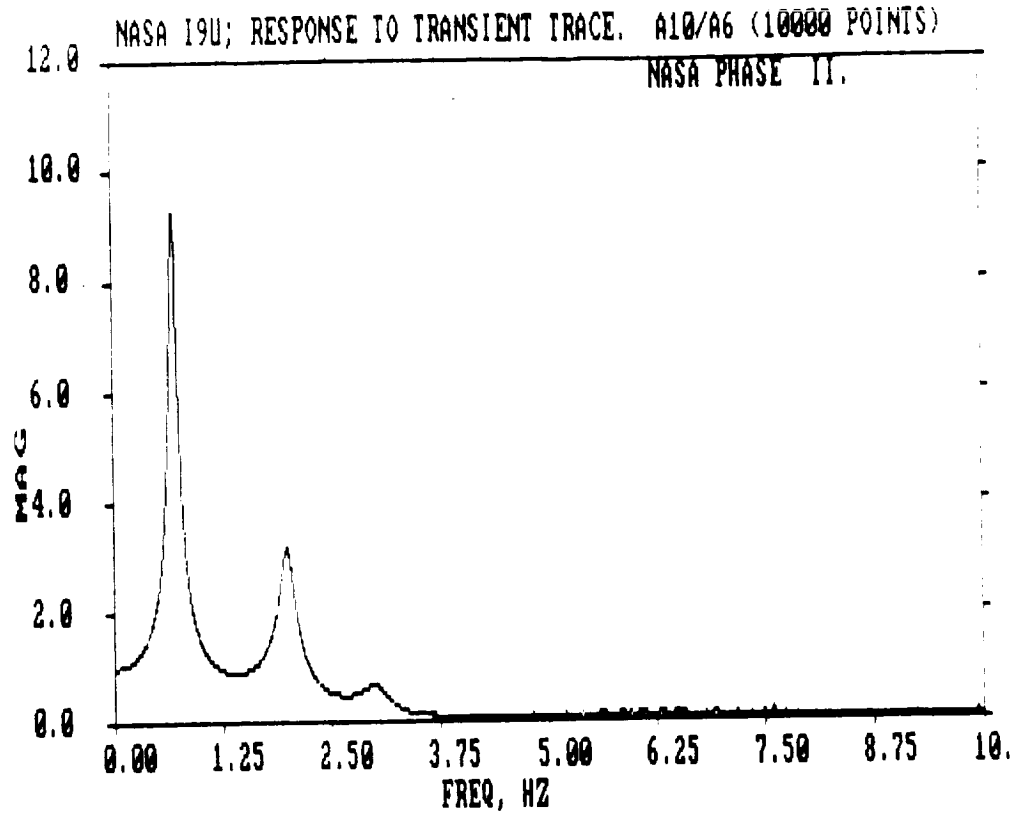


a) Modulus--Input is A8 and Output is A10

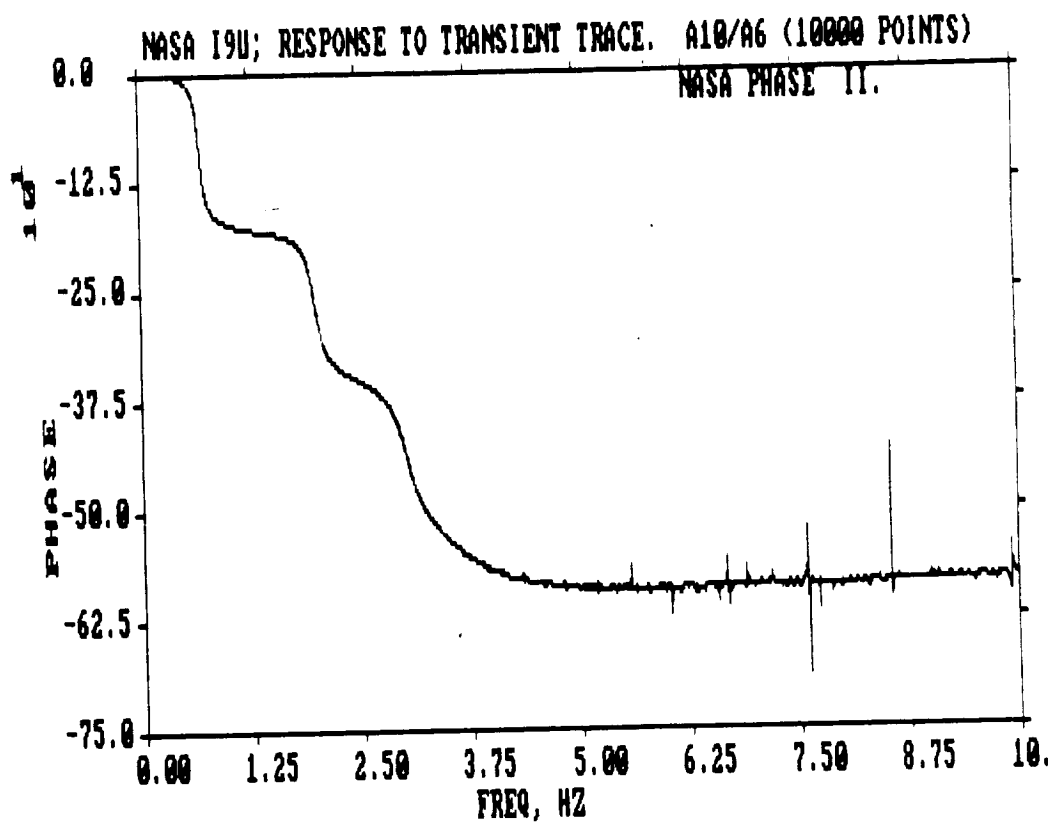


b) Phase

Figure 3.11: Module Transfer Function--Node 8 is the Boundary and Nodes 9 and 10 are Interior Points



a) Modulus--Input is A6 and Output is A10



b) Phase

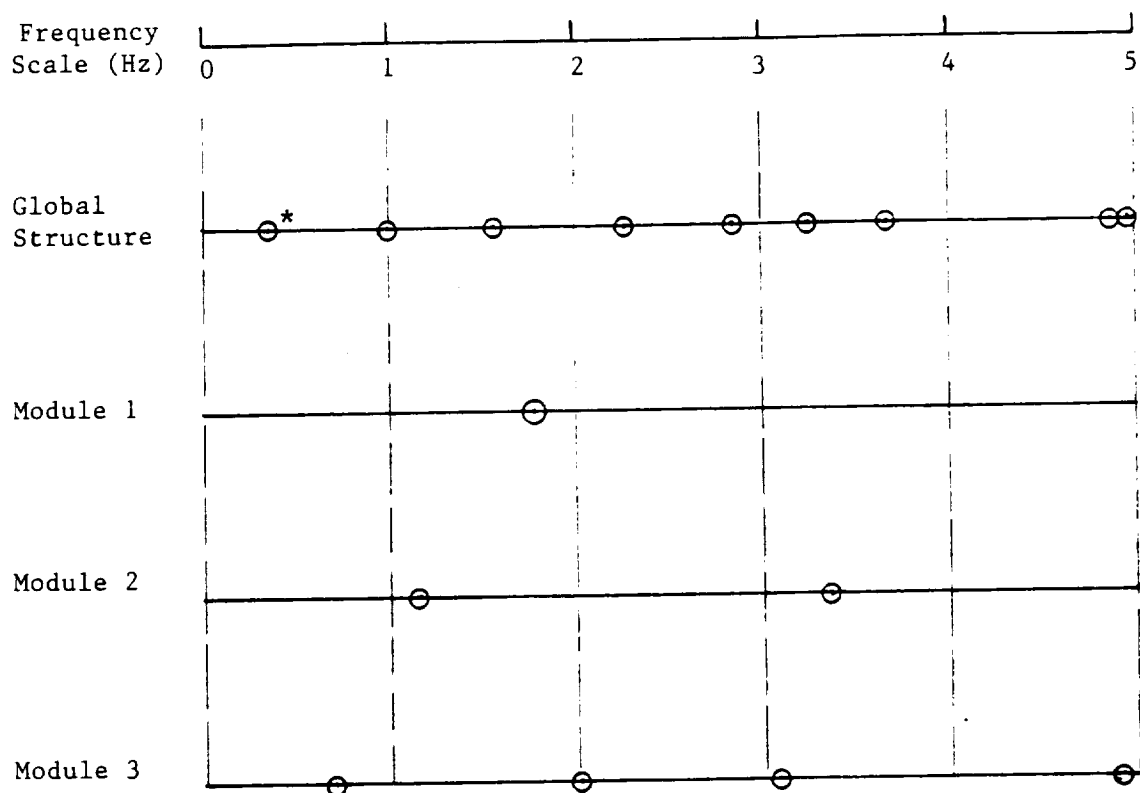
Figure 3.12: Module Transfer Function--Node 6 is the Boundary and Nodes 7 Through 10 are Interior Points

TABLE 3.1: COMPARISON OF MODULE TRANSFER FUNCTION POLES  
AND MODEL NATURAL FREQUENCIES

Module	Observed Pole (Hz)*	Natural Frequency (Hz)**
1	1.78	1.78
2	1.13	1.15
	3.40	3.38
3	0.69	0.70
	1.99	2.01
	2.99	3.09
	-	4.91

\* The frequencies were obtained from the transfer function plots; thus, there will be a small amount of error in the reported results. The fourth frequency for Module 3 was not detected probably because of the nature of the global system excitation.

\*\* The natural frequencies were obtained from the fixed boundary module eigenvalue problem.



\* The location of the circles represent the natural frequencies.

Figure 3.13: Comparison of Fixed Boundary Module Natural Frequencies With Global Natural Frequencies

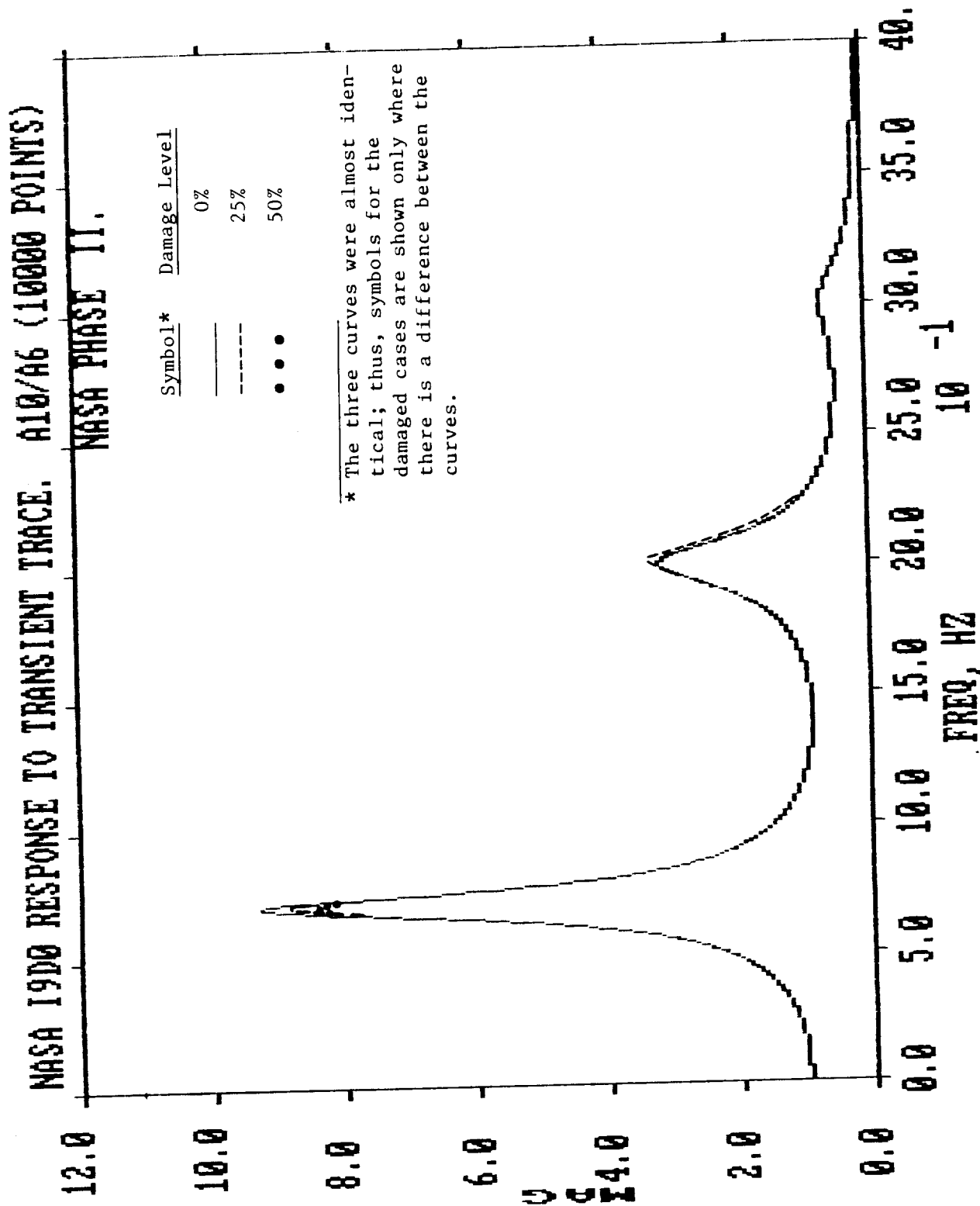


Figure 3.14: Module Transfer Function A10/A6--Different Levels of Damage External to and at the Boundary of the Module

# NASA 19D0 RESPONSE TO TRANSIENT TRACE. A10/A6 (10000 POINTS)

NASA PHASE II.

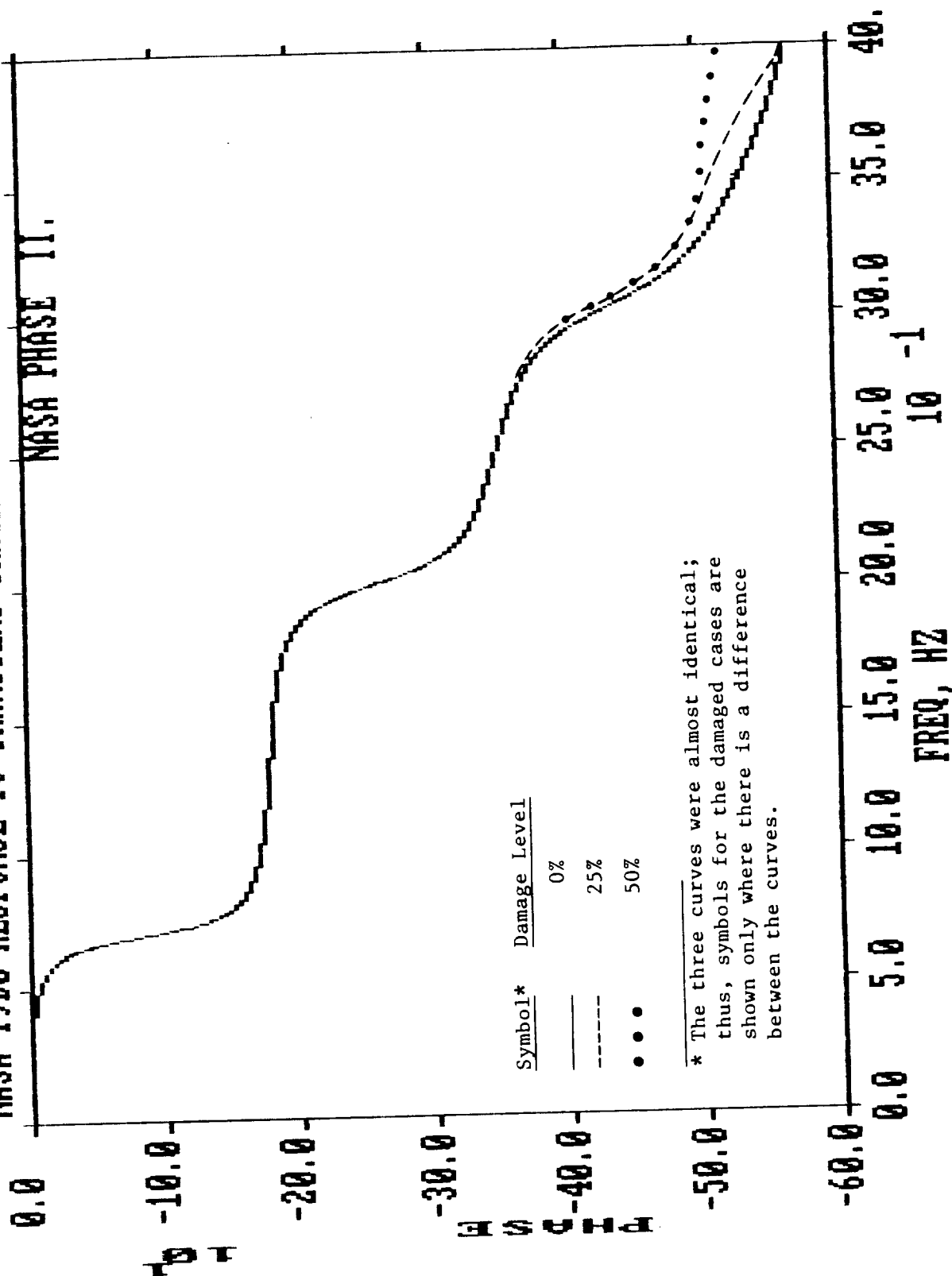


Figure 3.14 (concluded)

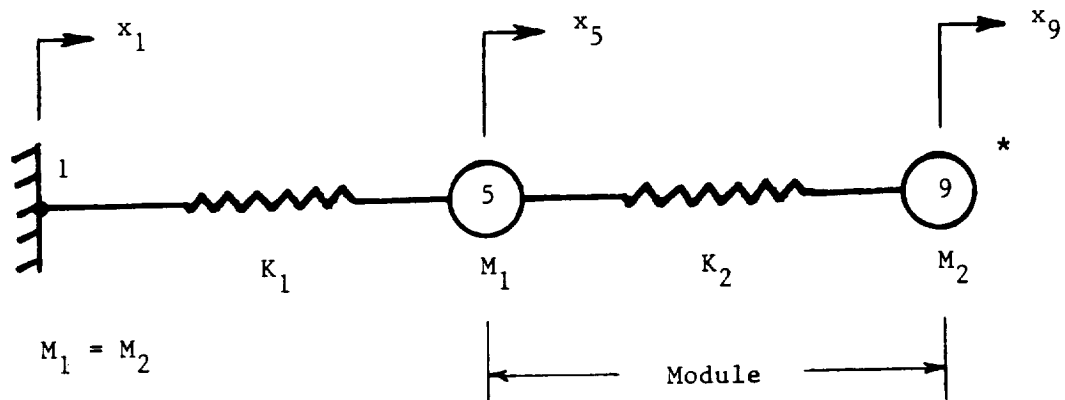
### 3.2.3 Module With One Boundary Point - Two-Degree-of-Freedom System With A Local Mode

In the previous subsection (3.2.2), the module had a single boundary point (one degree-of-freedom at the boundary). There was a slight error in the module transfer function modulus for the 25% and 50% damage outside of the module (reference Figure 3.14). It was decided to investigate this problem further using a simpler lumped mass and spring system (see Figure 3.15). Further, the system was tuned so there were cases with only global modes or a local mode whose motion was largely restricted to the physical domain of the module.

The first case looked at is somewhat similar to the previous one - the modes are global (see Figure 3.16) and there is a slight change in the amplitude of the module transfer function modulus near its resonant peak for damage outside the module (see Figure 3.17). For a 50% increase in stiffness outside of the module (resulting in a 15% increase in the global fundamental frequency), the indicated resonant peak for the module increased in height by 7.5%. This result is not new.

The next case consisted of tuning the model so one of the global system modes has its motion local to the module only--a local mode was generated (see Figure 3.16). The structure was damaged outside of the module in the same way as for the global case (50% increase in stiffness). However, because the first mode's motion was local to the module, the fundamental global frequency essentially did not change--0.4615 Hz and 0.4698 Hz undamaged and damaged, respectively (a 1.8% change). There was virtually no change in the module transfer function modulus near its resonant frequency (see Figure 3.18).

When a global mode's motion is "local to a given module", any excitation external to the substructure will be transmitted to its boundary fairly well unmodified within a narrow frequency band containing the modes natural frequency. (It is assumed that the adjacent modes are not too close in frequency.) This can be seen by looking at the local mode shape for this example and the corresponding Fourier transform of the base excitation and system response at Node 5 (see Figure 3.19). If the base excitation is broad band white noise, the substructure boundary motion will be essentially the same. Thus, it will be possible to determine the module transfer

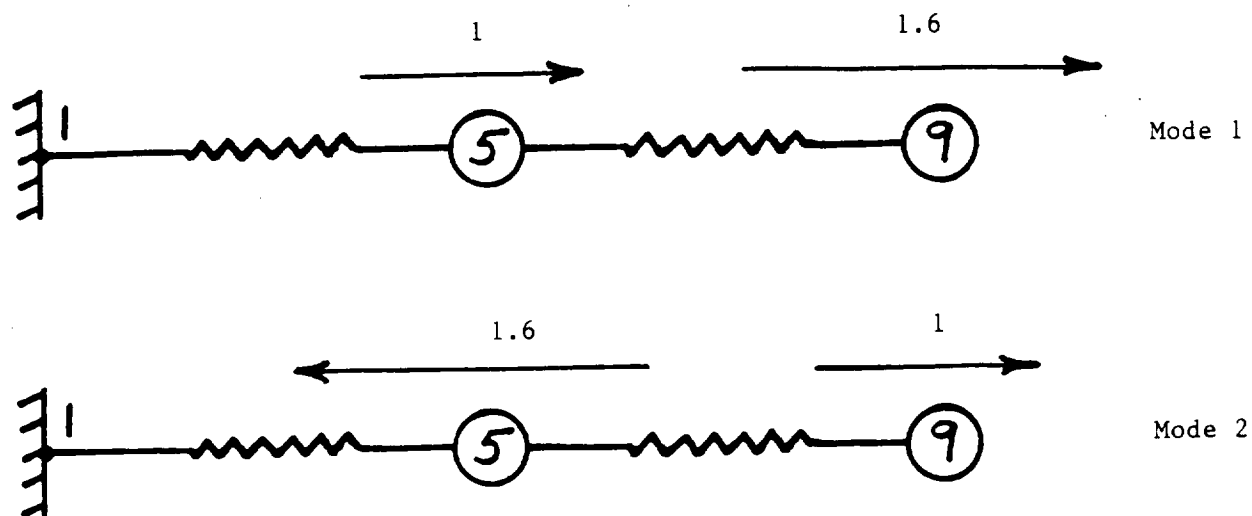


Case	System Modes	Undamaged Stiffness
		Ratio, $K_2/K_1$
1	Global	1
2	Local/Global	1/10

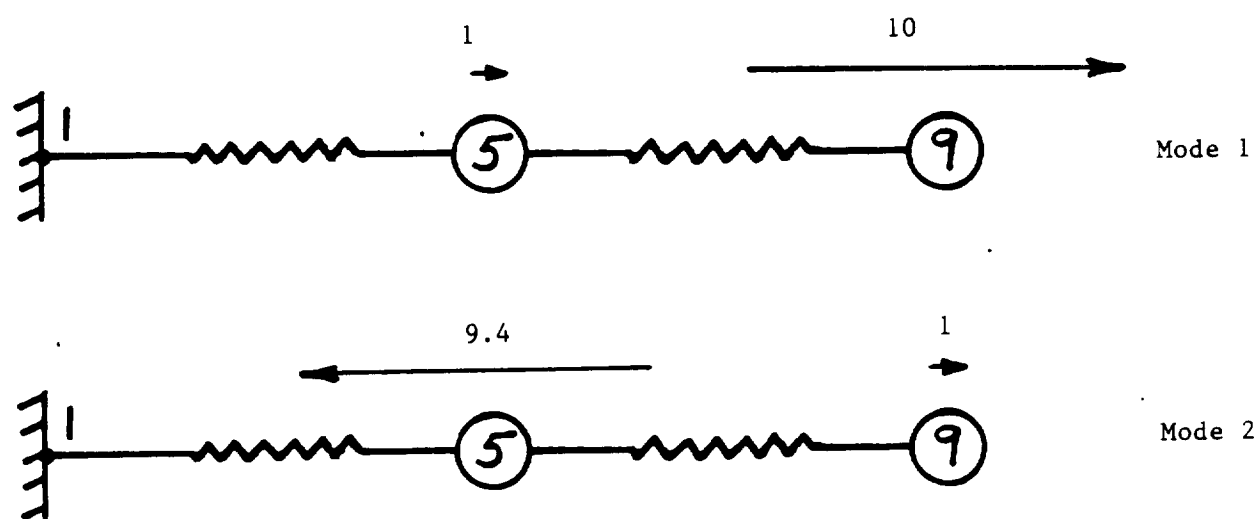
\* There were nodes which were intermediate to the nodes shown. They have not been shown here because the mass associated with them was much less than  $M_1$  or  $M_2$ .

Figure 3.15: Two Degree-of-Freedom System With and Without a Local Mode





a) Case 1 - Global Modes



b) Case 2 - Local/Global Modes

Figure 3.16: Mode Shapes for Two Degree-of-Freedom Undamaged System

# NASA W2D0G RESPONSE TO TRANSIENT TRACE. A9/A5 (10,000 PNTS)

COSMOS/M NASA 1311.0

Symbol*	Damage Level
—	0%
••••	50%

\* These two curves were almost identical; thus, symbols for the damaged case are shown only where there is a difference between the curves.

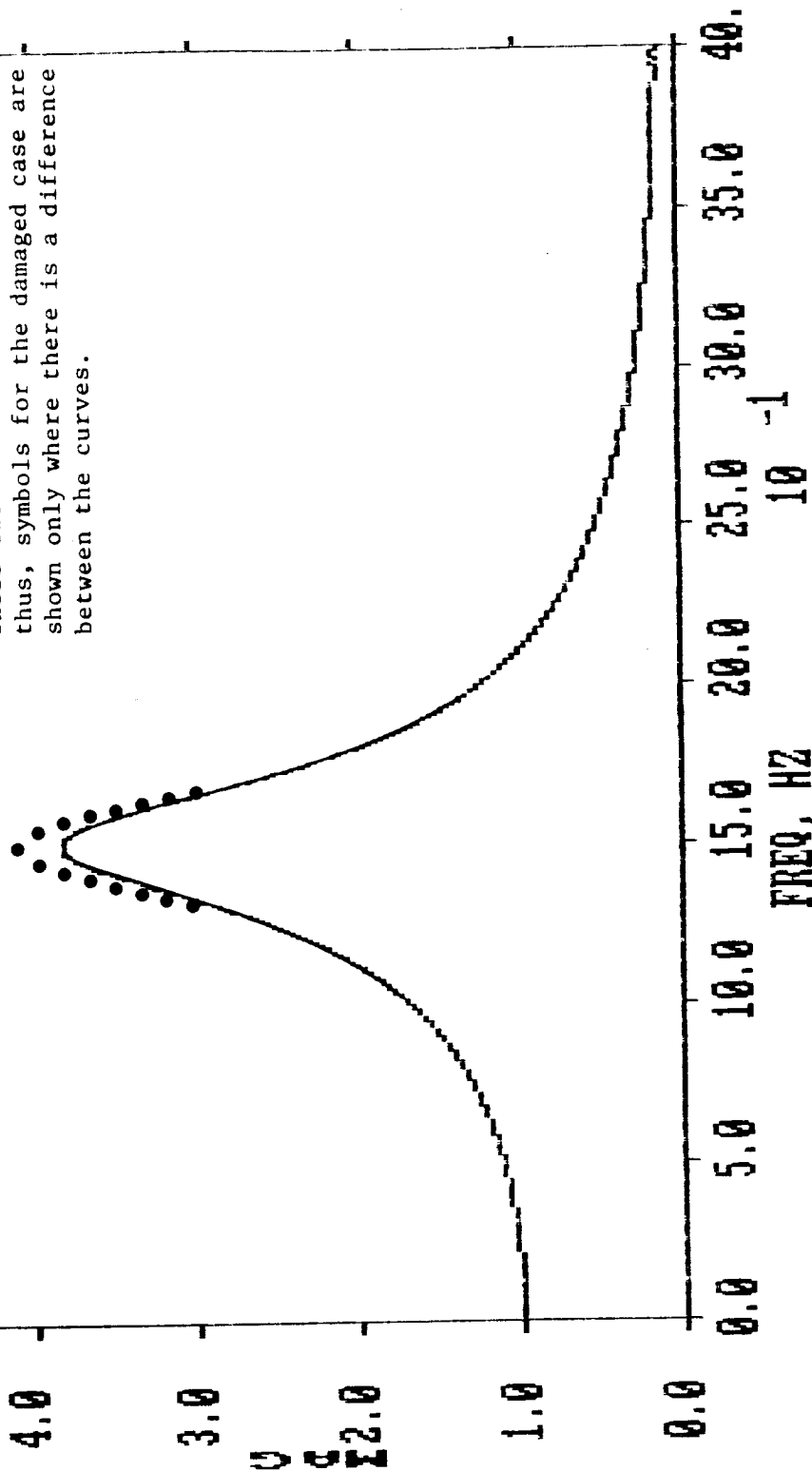
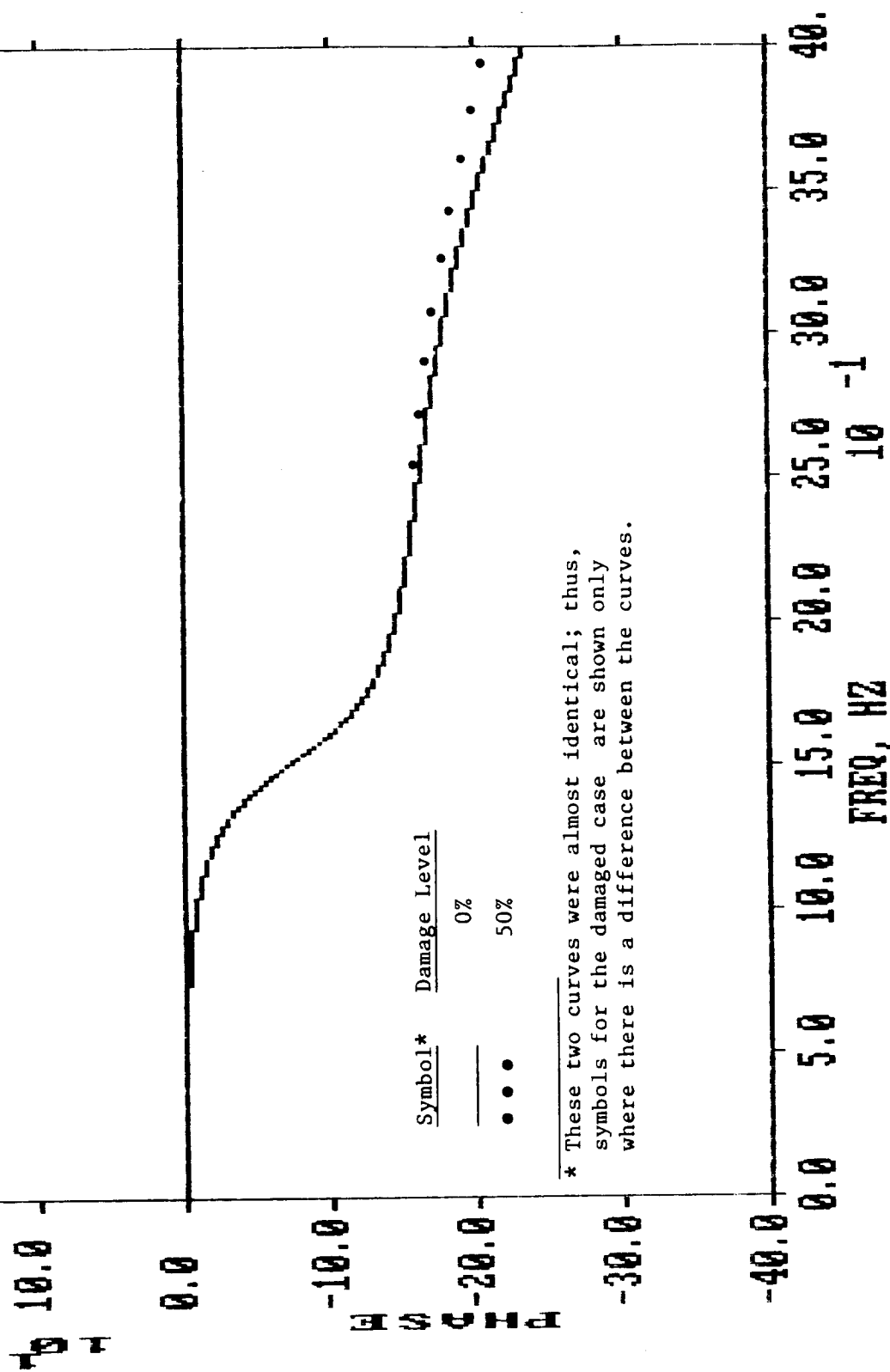


Figure 3.17: Change in Module Transfer Function (A9/A5) Due to Change in Stiffness Outside of Module--Global Mode Case

# NASA W2D0G RESPONSE TO TRANSIENT TRACE. A9/A5 (10,000 PNTS)

COSMOS/M NASA 1311.0



\* These two curves were almost identical; thus, symbols for the damaged case are shown only where there is a difference between the curves.

Figure 3.17 (concluded)

# NASA W2U RESPONSE TO TRANSIENT TRACE. A9/A5 (10,000 PNTS)

COSMOS/M NASA 1311.0

Symbol*	Damage Level
—	0%
...	50%

\* These two curves were virtually identical; the only difference was in the amplitude very close to the peak at about 0.5 Hz.

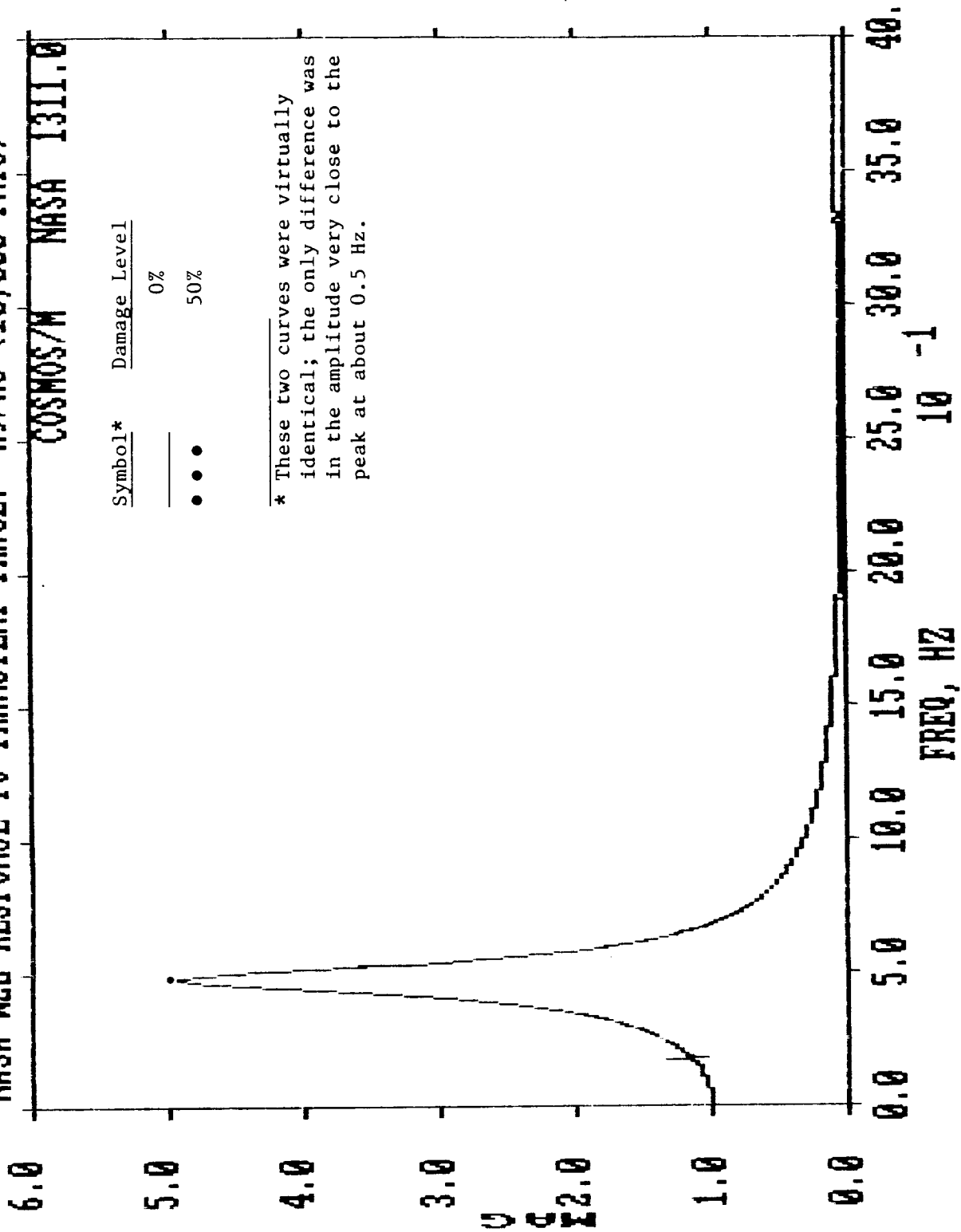


Figure 3.18: Change in Module Transfer Function (A9/A5) Due to Change in Stiffness Outside of Module--Local/Global Mode Case

# NASA W2U RESPONSE TO TRANSIENT TRACE. A9/A5 (10,000 PNTS)

COSMOS/M NASA 1311.0

Symbol*	Damage Level
—	0%
•••	50%

\* These two curves were almost identical; thus, symbols for the damaged case are shown only where there is a difference between the curves.

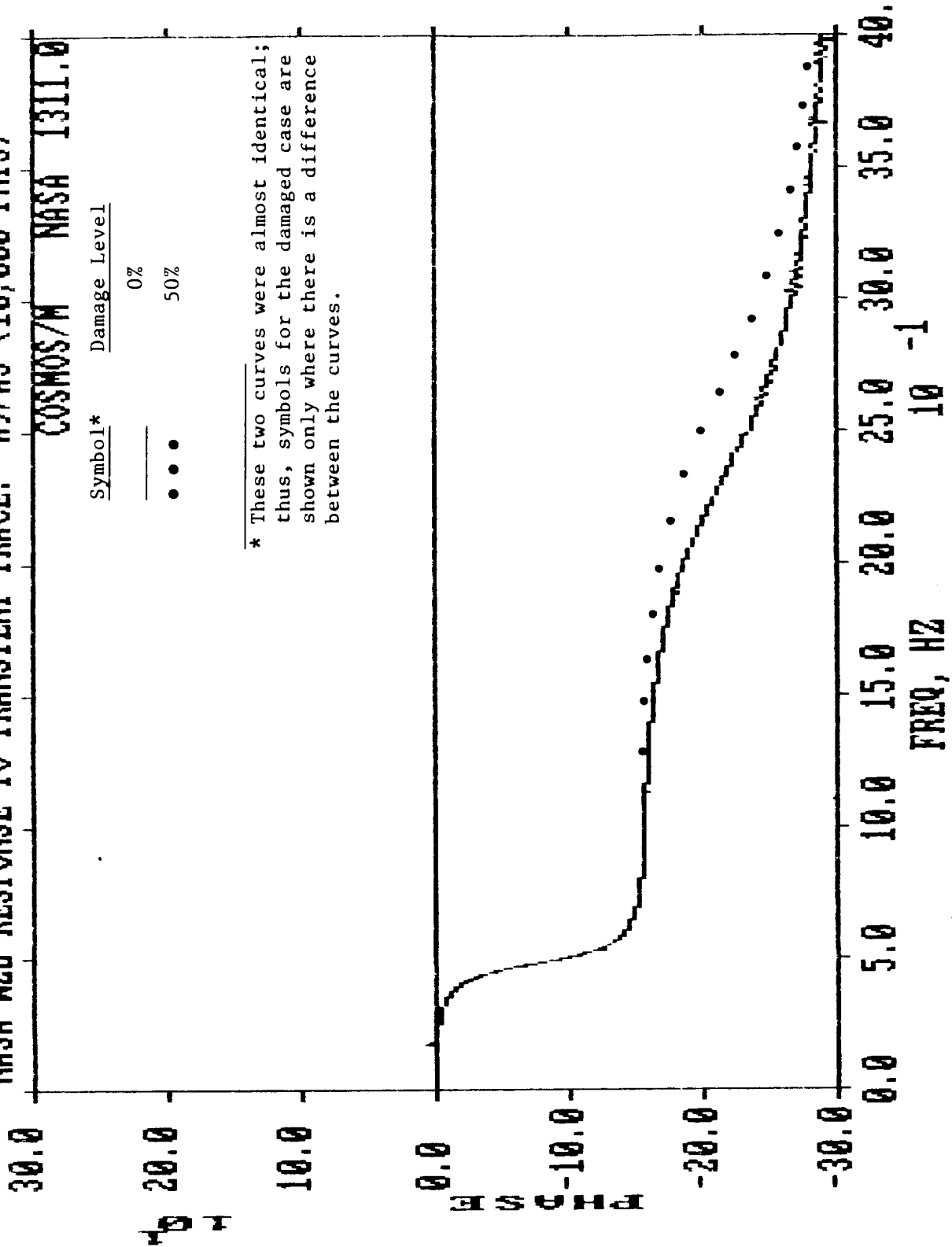


Figure 3.18 (concluded)

# NASA W2U RESPONSE TO TRANSIENT TRACE. A5/A1 (10,000 PNTS)

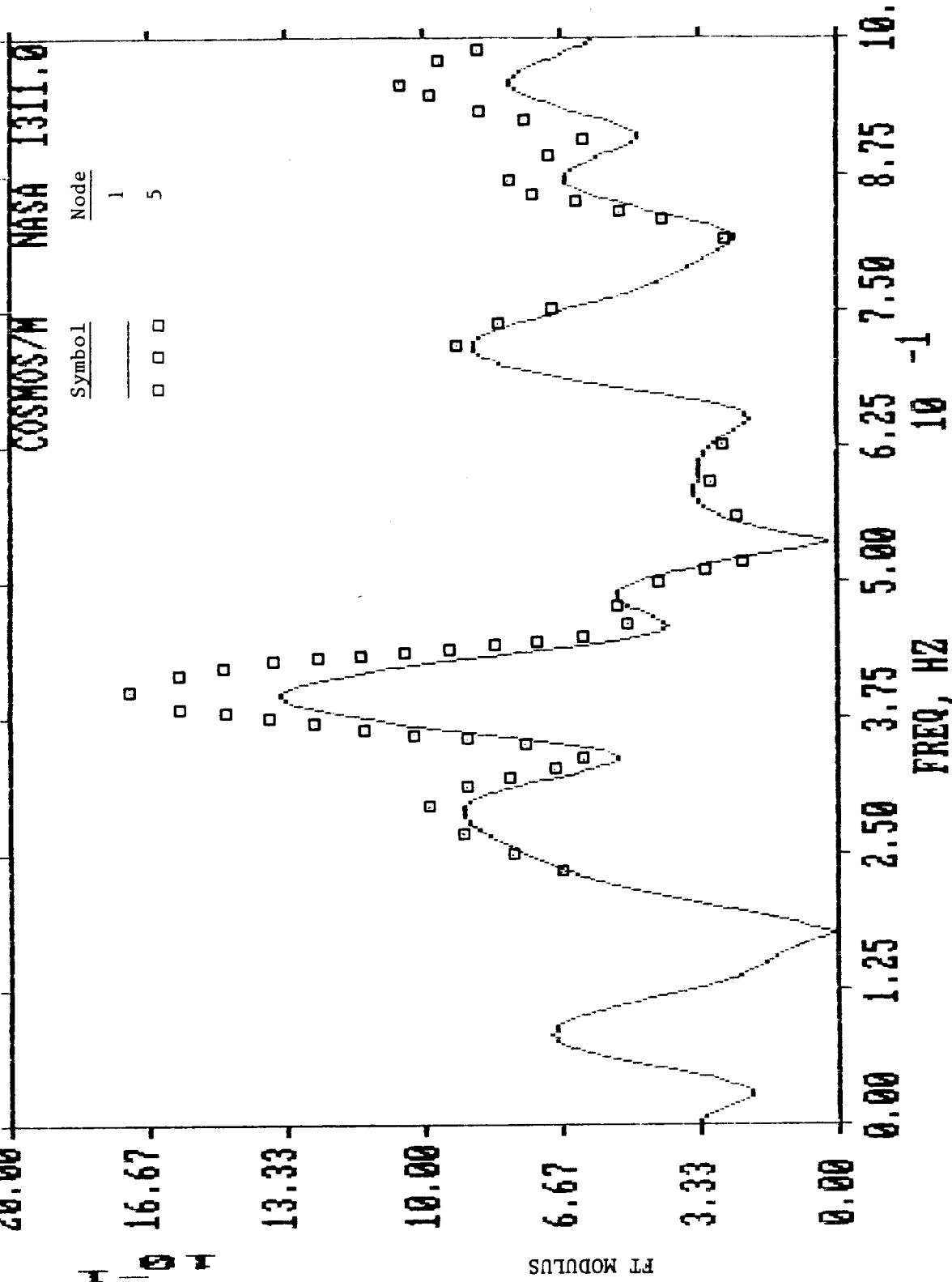


Figure 3.19: Comparison of Fourier Transform of Motion at Base (Node 1) and Response Point at Node 5 Around Fundamental Frequency--- Local/Global Mode Case

function within the frequency band with a good degree of accuracy. This would be true for sine dwell excitation if the narrow frequency band was "swept".

There appears to be somewhat of a problem in obtaining the module transfer function when the structure outside of it modifies the excitation. If the excitation to the global system is broad-band white noise the structure changes it so the substructure boundary motion is not white noise within frequency domains containing global modes. Thus, the corresponding module transfer functions cannot be determined using external excitation. Excitation from within a substructure will be investigated later in this section.

### 3.2.4 Module With Two Boundary Points

The module to be discussed is pictured in Figure 3.20. There are three springs (each with spring constant  $K$ ) and two masses (each with mass  $M$ ) within. The structure outside the substructure is not defined yet. The various matrices needed to determine  $\tilde{K}_{ii}$  are given as follows:

$$K_{ii} = \begin{bmatrix} 2K & -K \\ -K & 2K \end{bmatrix}, \quad M_{ii} = \begin{bmatrix} M & 0 \\ 0 & M \end{bmatrix}$$

For this example, take  $E_1 = 0$ ; thus, a "complete" module transfer function matrix is

$$-\tilde{K}_{ii}^{-1} \tilde{K}_{ib}$$

The matrix  $K_{ib}$  is

$$K_{ib} = \begin{bmatrix} -K & 0 \\ 0 & -K \end{bmatrix}$$

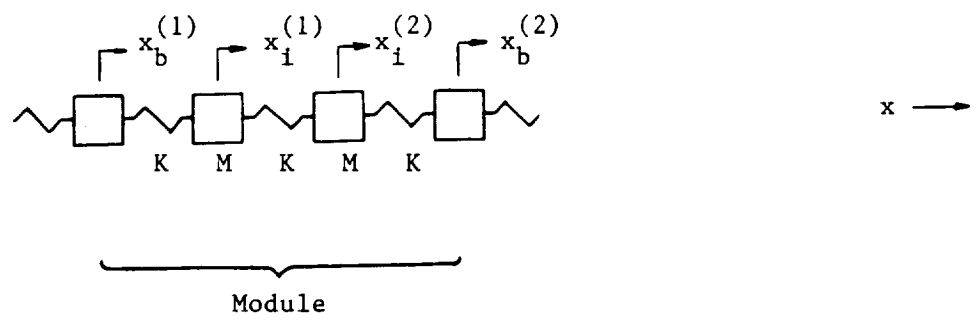


Figure 3.20: Module With Two Boundary Points



Because the global mass matrix is diagonal  $\tilde{K}_{ib} = K_{ib}$ . Thus.

$$-\tilde{K}_{ii}^{-1}\tilde{K}_{ib} = \frac{1}{\text{Det}(\tilde{K}_{ii})} \begin{bmatrix} K(2K - \omega^2 M) & K^2 \\ K^2 & K(2K - \omega^2 M) \end{bmatrix}$$

where  $\text{Det}(\tilde{K}_{ii}) = (K - \omega^2 M)(3K - \omega^2 M)$

The 1,1 element of the transfer function matrix is represented by the plot in Figure 3.21. The square of the transfer function poles are given by  $K/M$  and  $3K/M$ , which are equal to the fixed boundary module eigenvalues.

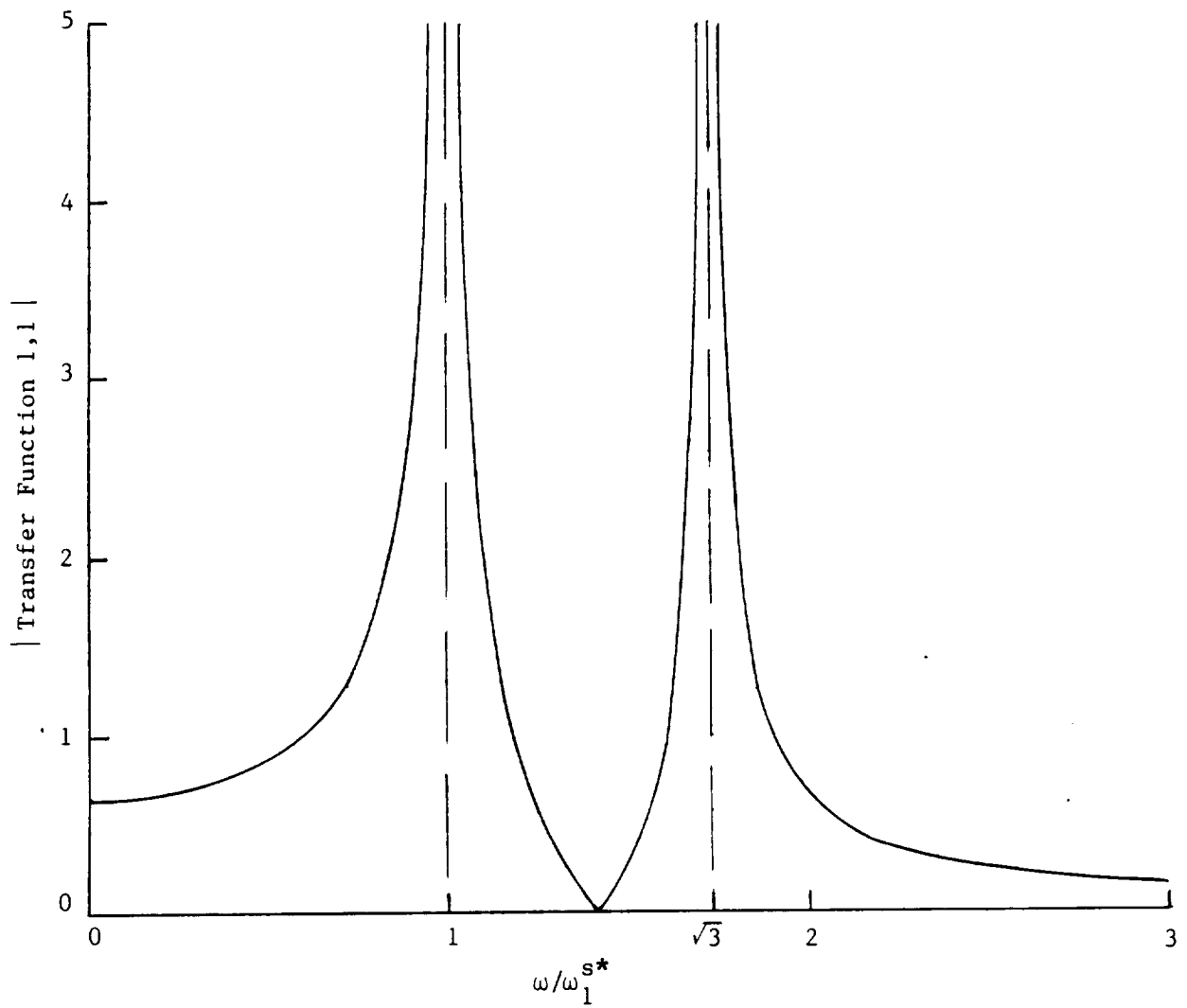
#### 3.2.4.1 Numerical Example of Two Boundary Point Problem

The previously defined module with two boundary points was incorporated into a system, with the total system containing nine lumped spring and eight lumped masses (see Figure 3.22). The global system was initially excited using base motion at Nodes 1 and 10--the motion was random, equal for the two bases and in only the x-Direction. The transient problem was solved using modal superposition. The global system responses for Nodes 4 through 7 were saved and used for the module problem. The global responses at Nodes 4 and 7 were taken as the inputs to the substructure--the boundary motions. The substructure responses were taken as the motion at Nodes 5 and 6. Table 3.2 is a listing of the undamaged global system and fixed-boundary module natural frequencies.

The transfer function matrix (a 2 x 2 matrix) corresponding to this module was obtained using ANCO's macro MIMO; the macro solves the multi-input multi-output transfer function problem\*. Figures 3.23 and 3.24 are plots of the modulus for two of the elements of the transfer function matrix (Appendix C contains all the plots corresponding to this matrix). The plots correspond to a system state defined as undamaged and two damaged states.

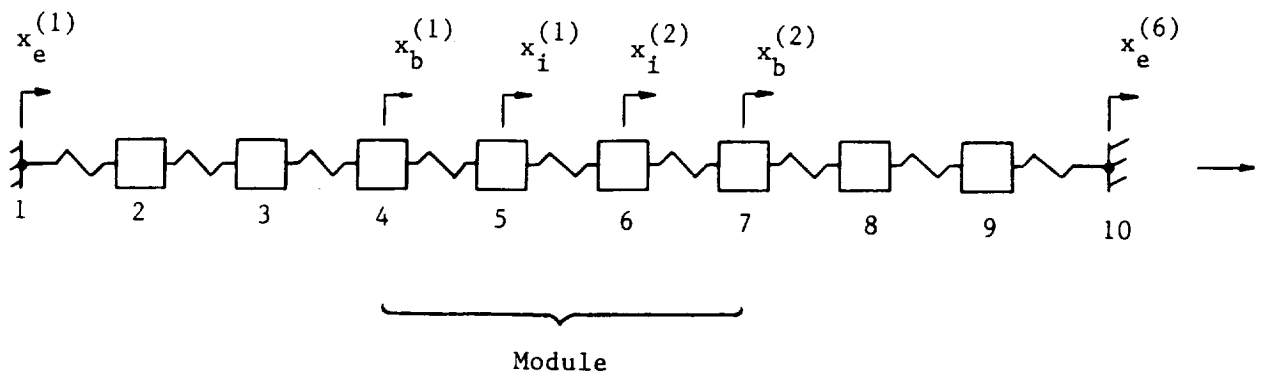
---

\* The macro MIMO uses the computer code MAC/RAN IV to solve the multi-input single output transfer function problem for a linear system. Appendix B briefly discusses the theoretical bases used for these computations in MAC/RAN IV.



\*  $\omega_1^s$  is the first natural frequency of the substructure with fixed boundary.

Figure 3.21: Modulus of Module Transfer Function Matrix (Two Boundary Point Structure)--Element 1,1



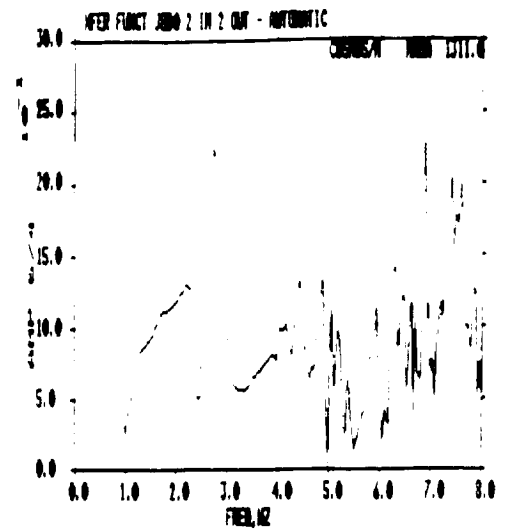
Note: The masses move in only the x-Direction.

Figure 3.22: System With Lumped Springs and Masses--Module With Two Boundary Points

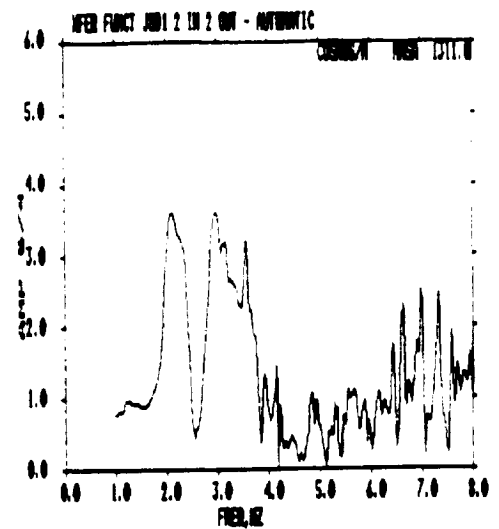
TABLE 3.2: UNDAMAGED GLOBAL SYSTEM AND MODULE (FIXED-BOUNDARY)  
NATURAL FREQUENCIES

Mode	Natural Frequency (Hz)	
	Global System	Module
1	0.746	2.460
2	1.407	4.753
3	2.226	
4	2.594	
5	3.159	
6	3.675	
7	4.865	
8	4.956	

a) Undamaged System (Initial Configuration)



b) System Damaged Outside of Module--  
Fundamental Global Natural Frequency  
Changed By -23.5%



c) System Damaged Outside of Module--  
Fundamental Global Natural Frequency  
Changed By 23.3%

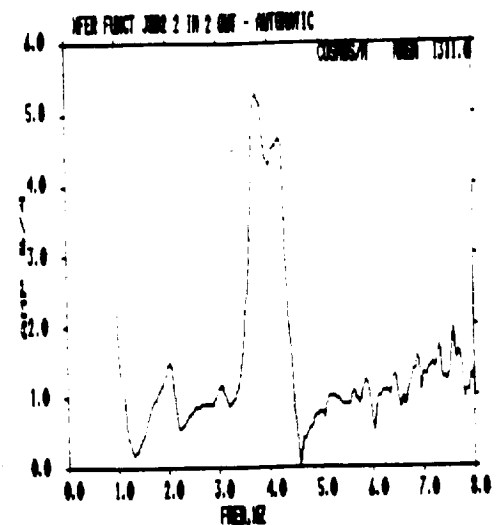
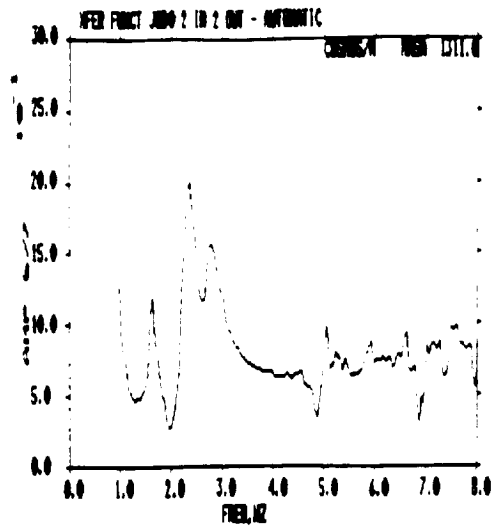
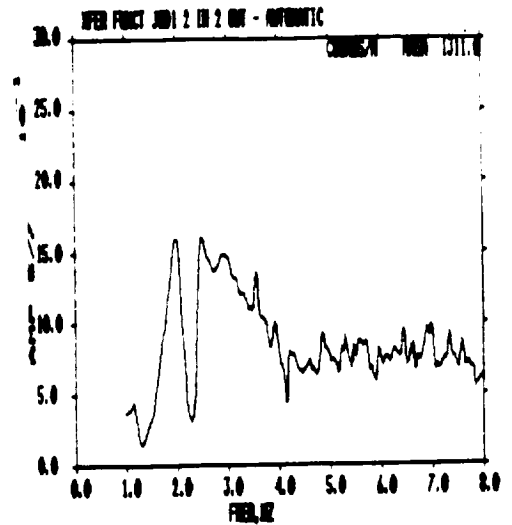


Figure 3.23: Comparison of MIMO Transfer Function Moduli for J8 Model; Element Output 5, Input 4

a) Undamaged System (Initial Configuration)



b) System Damaged Outside of Module--  
Fundamental Global Natural Frequency  
Changed By -23.5%



c) System Damaged Outside of Module--  
Fundamental Global Natural Frequency  
Changed By 23.3%

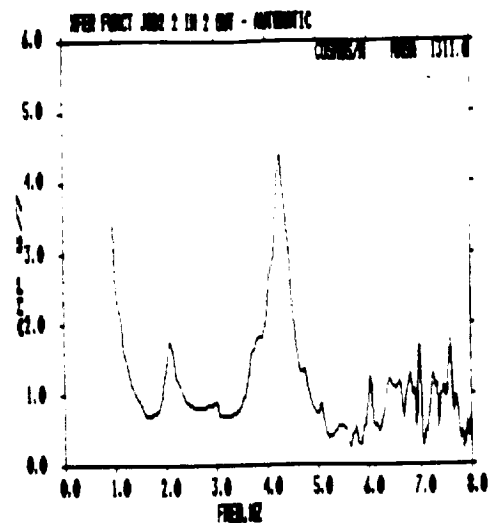


Figure 3.24: Comparison of MIMO Transfer Function Moduli for J8 Model;  
Element Output 5, Input 7

The damage corresponds to changes being made to the global structure outside of the module. Thus, no changes were made to the module transfer function. However, the module transfer functions computed for different damage levels clearly were different. The "transfer functions" computed are not the desired functions--these are not transfer functions, they are merely functions of frequency which are dependent on the global structure properties.

Why was this result obtained? The procedure used to obtain the module transfer function is based on the current technology used to solve the multi-input multi-output transfer function problem. One major assumption used in developing this theory is that all the inputs to the linear system are independent of each other. This is certainly not the case for this or related problems--the inputs (boundary motions) to the module are dependent on each other because they are responses of the global system. Because of this and what is to be presented, it will be shown that determining the module transfer function matrix is very difficult and probably not possible for a completely general case.

The transfer function computations described above used absolute module responses. It was decided to perform the same computations except using relative module responses. Instead of computing the relative responses by the pseudostatic method described earlier, they were obtained by defining a separate free-free structure and including only those mass degrees-of-freedom which corresponded to the global system module (see Figure 3.25). Large masses were assigned to those degrees-of-freedom corresponding to the module boundary points. Then, forces equal the large masses times the corresponding module boundary accelerations were applied to the large masses. The resulting absolute motions of the free-free system matched well with those of the corresponding global degrees-of-freedom. This approach to the enforced motion problem is discussed in Appendix D. The relative response of the module was then obtained by using only the third and fourth modes of the free-free system in obtaining the solution to the transient response problem\*.

---

\* The first two modes were rigid body and near rigid body (very low frequency) modes, whereas the third and fourth modes were essentially fixed base modes--Nodes 4 and 7 were virtually fixed.

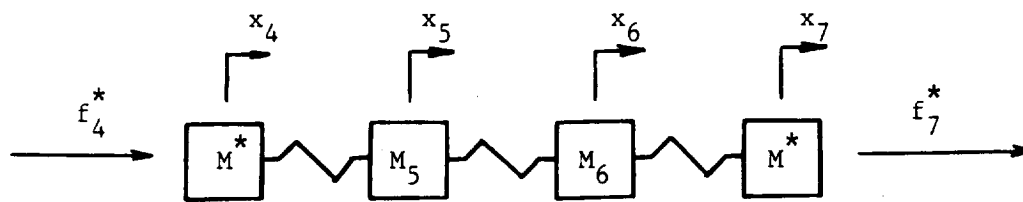


Figure 3.25: Free-Free System, J4, Used to Determine Relative Response of J8 System



The 2 x 2 module transfer function matrix for relative module responses was then calculated (see Figures 3.26 and 3.27 and Appendix C). Problems similar to those for the absolute module responses are evident here also--the transfer function changed with damage outside of the module. The transfer function poles corresponded to global, as well as module, natural frequencies. No additional insight was gained by looking at the single-input single-output (SISO) relative transfer functions (see Figures 3.28 and 3.29). The global resonances were clearly evident. The only thing that was an improvement was that there was no evidence of the fundamental global natural frequency--using relative responses eliminated the peak corresponding to the fundamental global frequency.

It was tentatively concluded that the module transfer function matrix for the case of multiple boundary points and excitation outside of the module could not be calculated by the approach used and described herein. This is true for absolute or relative module responses. It was decided to see if exciting the global system by applying a force(s) within the module would help in the determination of the module transfer function. The general idea is that if the forcing within the module can be chosen such that the response of the module is due largely to it and only slightly to the boundary motion, possibly the problem may be reduced largely to a SISO transfer function calculation. This can be seen by looking at Equation 3-11. If

$$F_i \gg \omega^2 M_{ii} K_{ii}^{-1} K_{ib} X_b$$

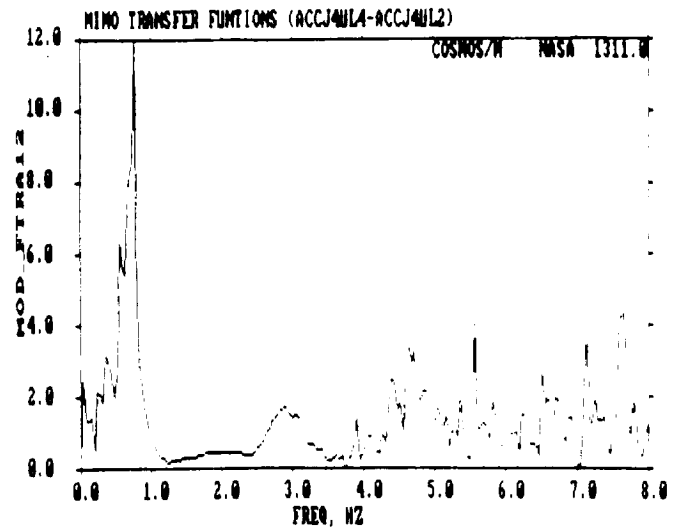
within a given frequency domain, then within this domain

$$\tilde{K}_{ii} R_i \approx F_i$$

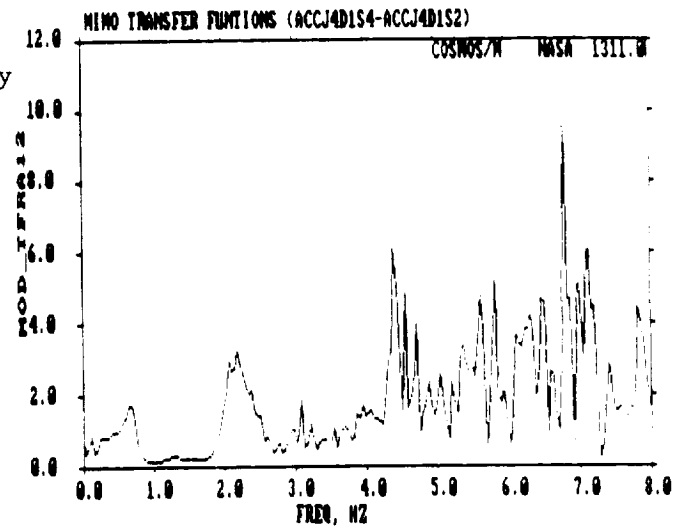
and the module transfer function matrix can be easily calculated using the MIMO procedure described herein.

This was done for the subject numerical example using relative module responses. A force,  $f_5(t)$ , was applied to Node 5 of the global system. The previously described procedure for determining module relative responses was followed--for the J4 model (see Figure 3.25) the masses at Nodes 4 and 7 were driven to obtain motions equal to the corresponding ones of the global system and the force  $f_5$  was applied to Node 5. As before, this produced

- a) Undamaged System (Initial Configuration)



- b) System Damaged Outside of Module--  
Fundamental Global Natural Frequency  
Changed By -23.5%



- c) System Damaged Outside of Module--  
Fundamental Global Natural Frequency  
Changed By 23.3%

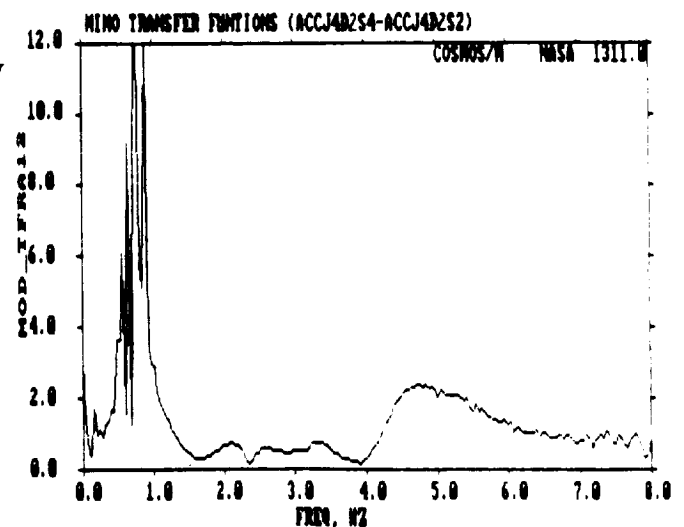
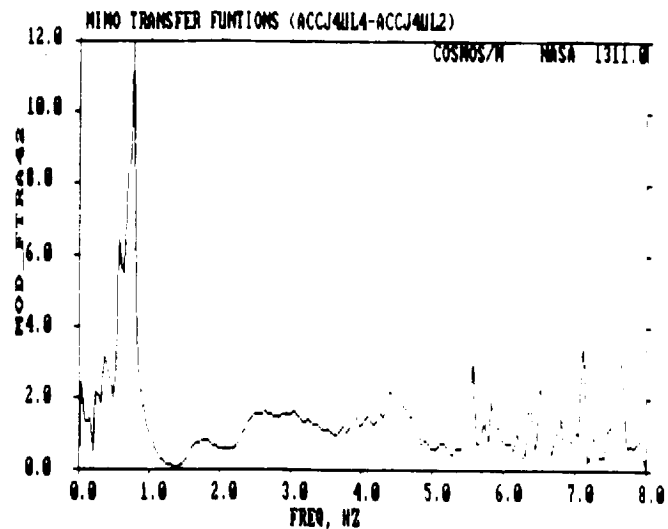
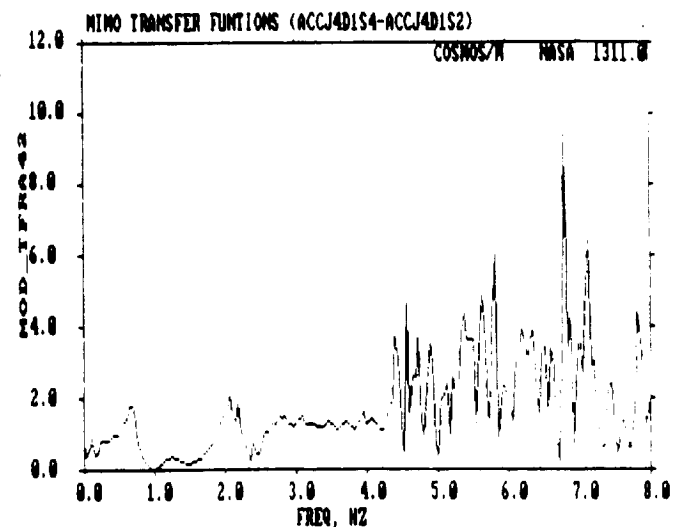


Figure 3.26: Comparison of MIMO Transfer Function Moduli for Relative Response of J4 Model; Element Output 5, Input 4

- a) Undamaged System (Initial Configuration)



- b) System Damaged Outside of Module--  
Fundamental Global Natural Frequency  
Changed By -23.5%



- c) System Damaged Outside of Module--  
Fundamental Global Natural Frequency  
Changed By 23.3%

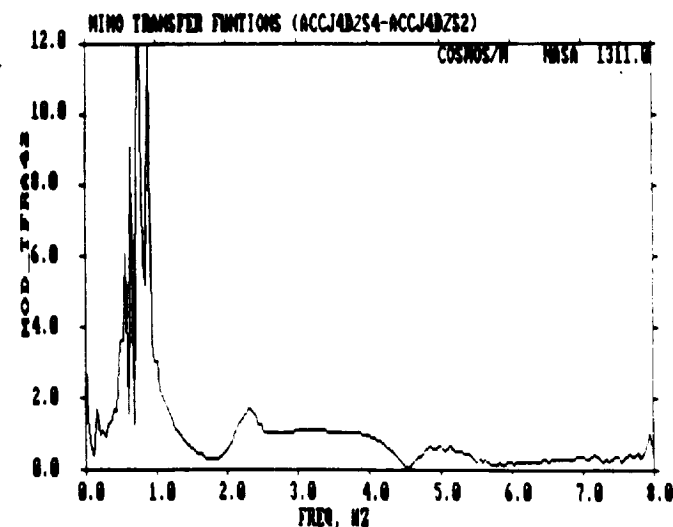
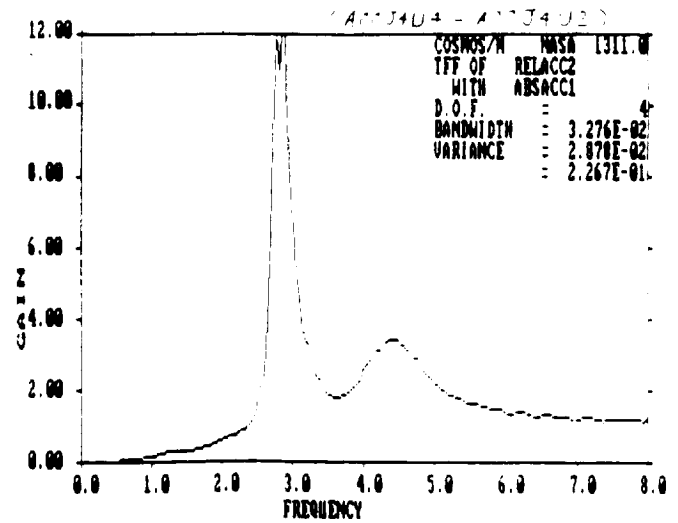
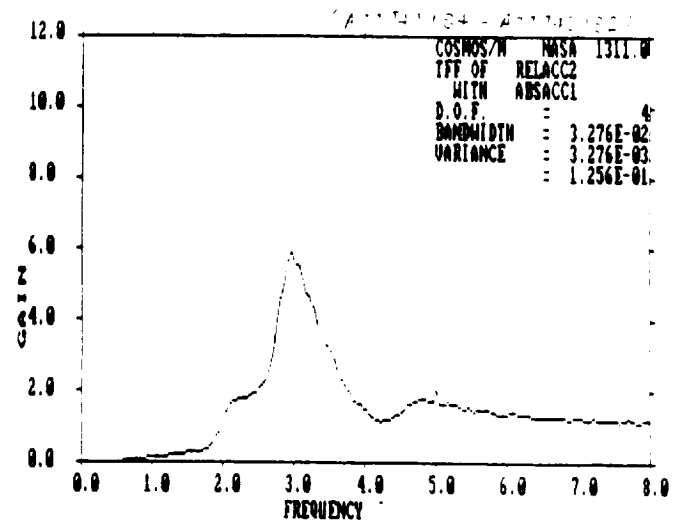


Figure 3.27: Comparison of MIMO Transfer Function Moduli for Relative Response of J4 Model; Element Output 5, Input 7

- a) Undamaged System (Initial Configuration)



- b) System Damaged Outside of Module--  
Fundamental Global Natural Frequency  
Damaged By -23.5%



- c) System Damaged Outside of Module--  
Fundamental Global Natural Frequency  
Changed By 23.3%

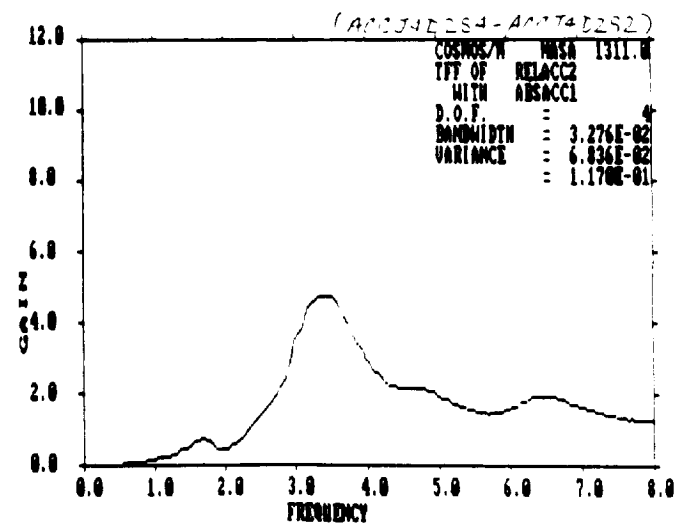
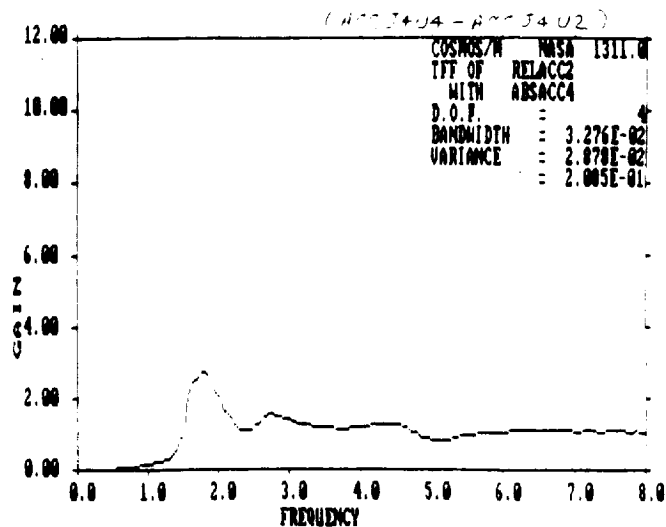
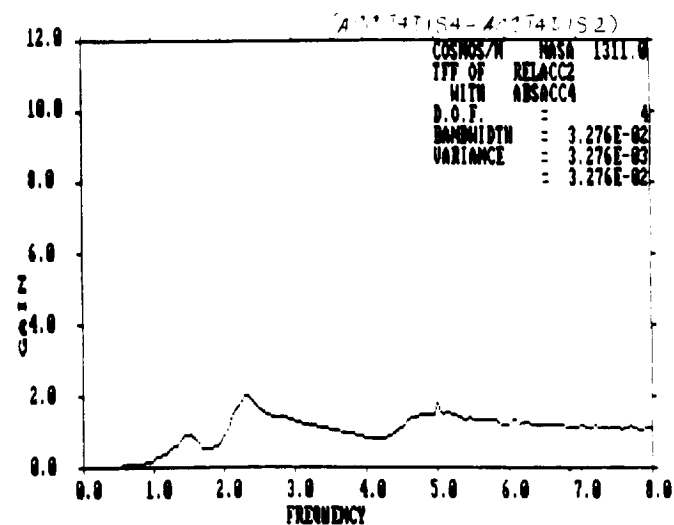


Figure 3.28: Comparison of SISO Transfer Function Moduli for Relative Response of J4 Model; Element Output 5, Input 4

a) Undamaged System (Initial Configuration)



b) System Damaged Outside of Module--  
Fundamental Global Natural Frequency  
Damaged By -23.5%



c) System Damaged Outside of Module--  
Fundamental Global Natural Frequency  
Changed By 23.3%

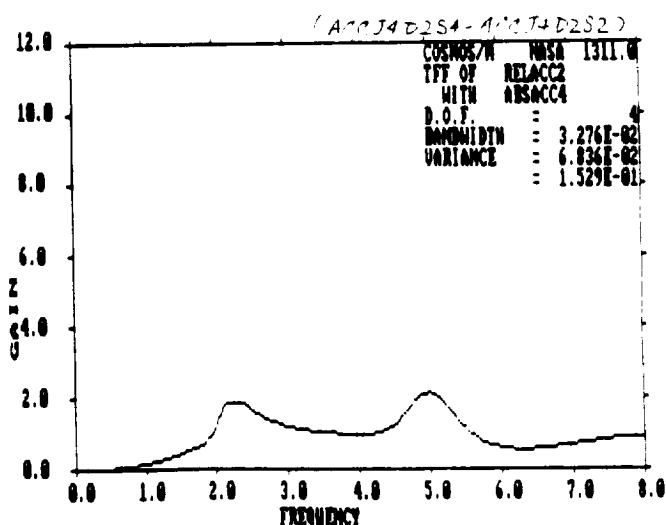


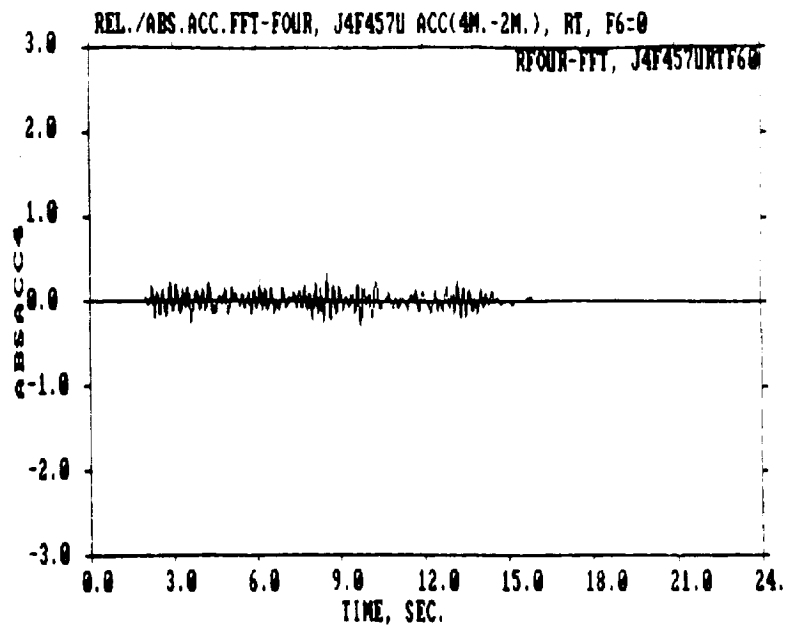
Figure 3.29: Comparison of SISO Transfer Function Moduli for Relative Response of J4 Model; Element Output 5, Input 7

motions which matched well those of the global J8 system. Modes three and four were used to obtain the relative responses. Figures 3.30 (time histories) and 3.31 (Fourier transforms) present the absolute boundary motions and relative responses of the module. It is seen that the relative response of Node 5 is considerably greater than the absolute motion of Nodes 4 and 7 (boundary points) in the frequency domain 4 Hz to 5 Hz. If the motions of the boundary points within this domain was somewhat lower, the problem would almost be a fixed-boundary problem with a single input (the force at Node 5). This would indeed be a simple problem within this frequency domain.

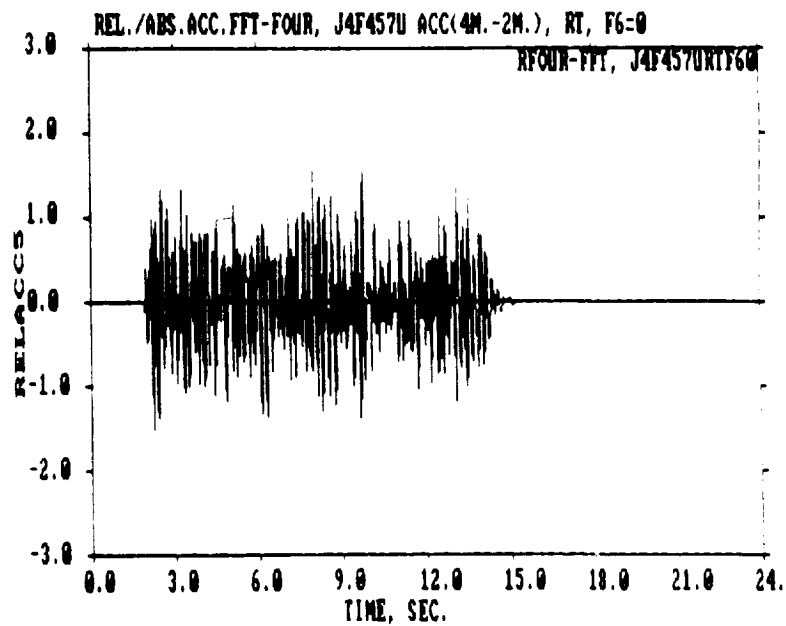
At this point it is worth looking at the difference between the absolute and relative (as calculated) module responses for this problem (see Figures 3.32 and 3.33). The major difference is that the relative responses do not have a peak corresponding to the fundamental global natural frequency, whereas the absolute responses do. There are other differences, but they appear to be minor.

The 2 x 3 relative module transfer function matrix was then calculated (see Figure 3.34 and Appendix C). There is evidence of global motion effecting the calculated module transfer function matrix. The results are poor; it was hoped that they would be better because of the excitation being a force at Node Point 5. Some basic work/research needs to be done dealing with this kind of MIMO problem--the problem with dependent inputs.

One last thing will be discussed concerning this problem. For the global excitation consisting of a single force applied to Node 5, it is useful to determine how much of the module relative response is due to the force at Node 5 and how much is due to the boundary motion. Figure 3.35 shows plots of the Fourier transform of the relative response of Node 5 for various applied loading conditions. Because the problem is linear the net response (response due to the boundary motions and applied force at Node 5 acting simultaneously) is equal to the sum of the response due to the boundary motions and applied load acting separately. It is seen that the majority of the response within the frequency domain 4 Hz to 5 Hz is due to the force on Node 5. This is good because when the J4 system (see Figure 3.25) is excited only by force  $f_5$ , the masses at Node Points 4 and 7,  $M^*$ , do

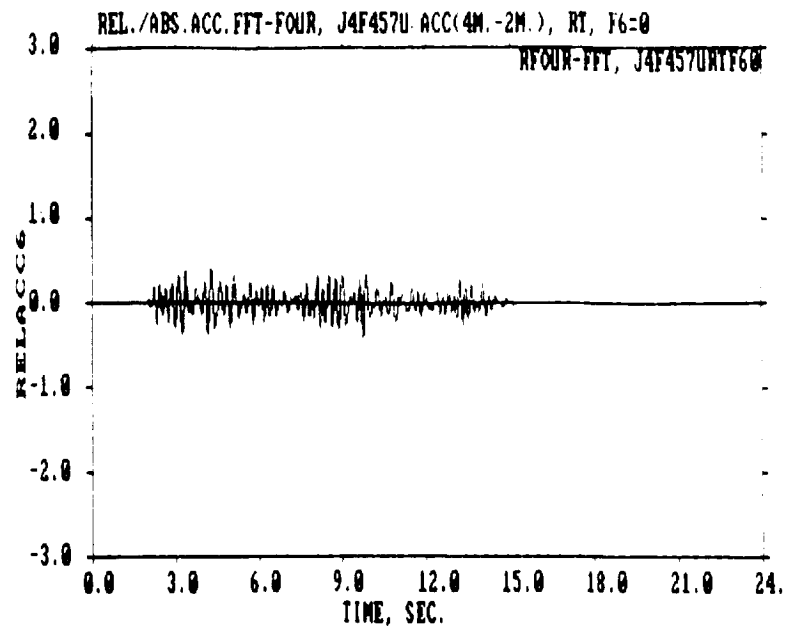


a) Absolute acceleration of module boundary point at Node 4.

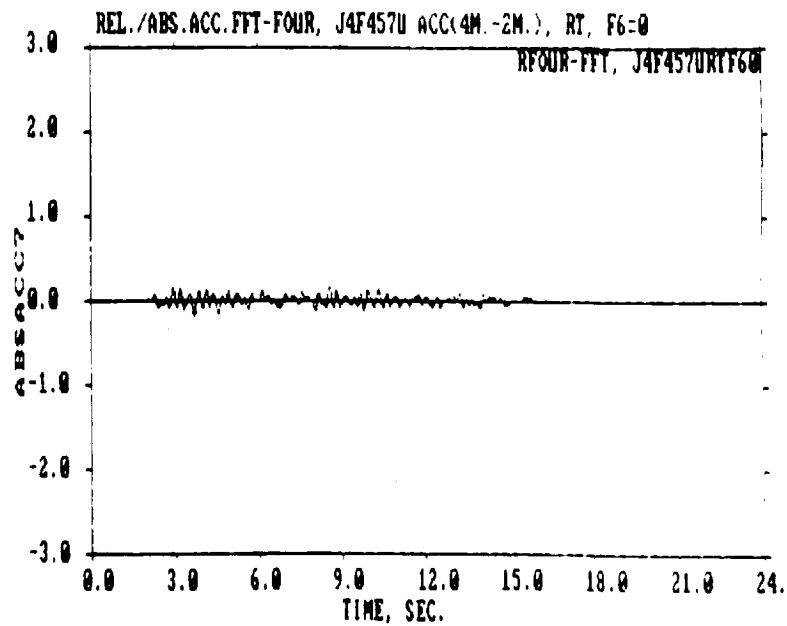


b) Relative acceleration of module internal point at Node 5.

Figure 3.30: Time History Motion of Module With Force Applied to Node 5



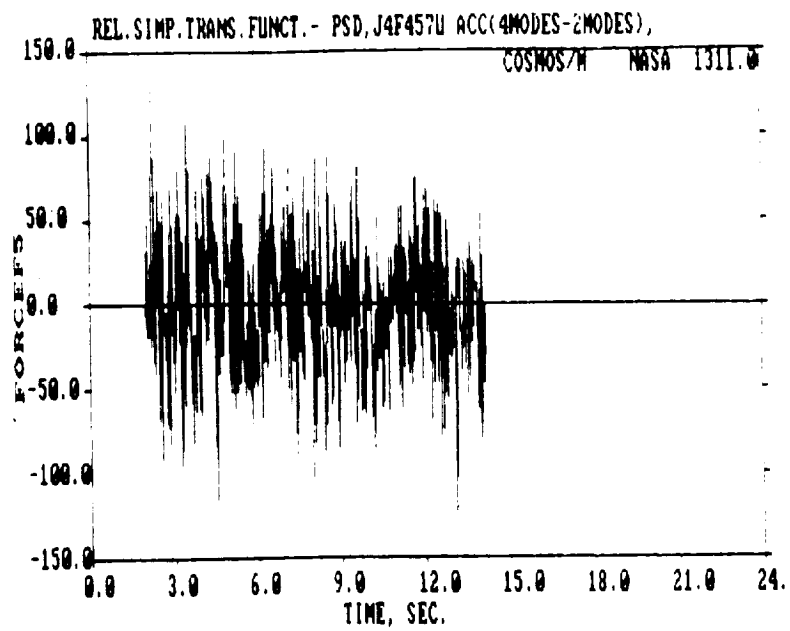
c) Relative acceleration of module internal point at Node 6.



d) Absolute acceleration of module boundary point at Node 7.

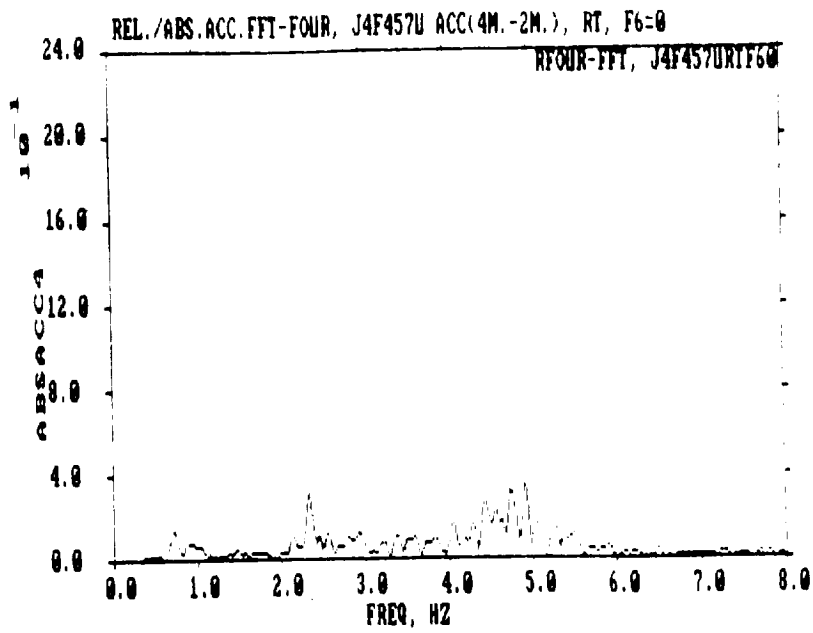
Figure 3.30 (continued)



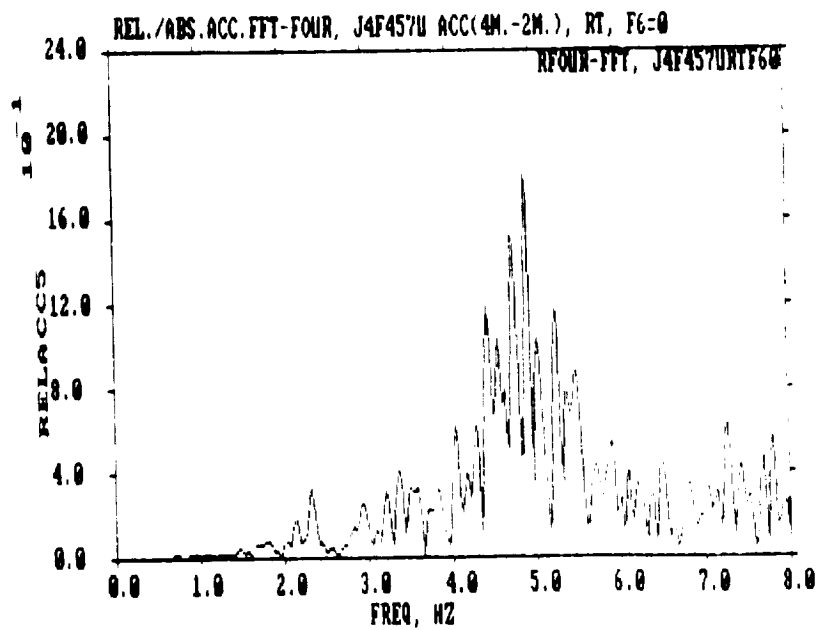


e) Force applied at Node 5.

Figure 3.30 (concluded)

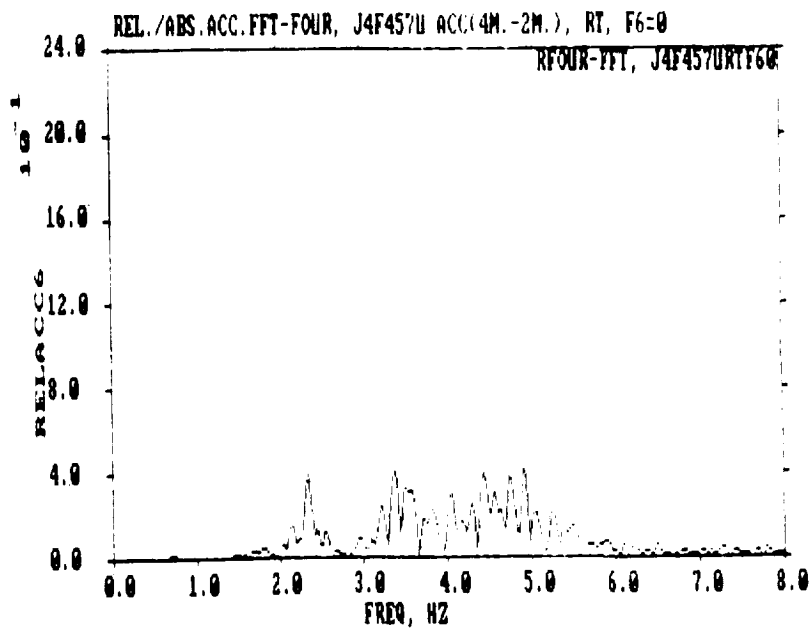


a) Absolute acceleration of module boundary point at Node 4.

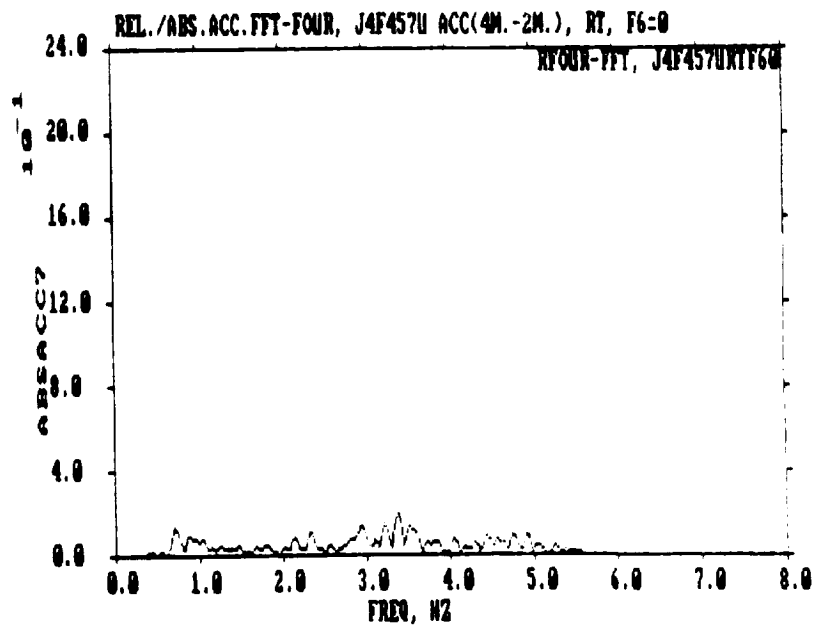


b) Relative acceleration of module internal point at Node 5.

Figure 3.31: Fourier Transform Moduli of Module Motion With Force Applied at Node 5

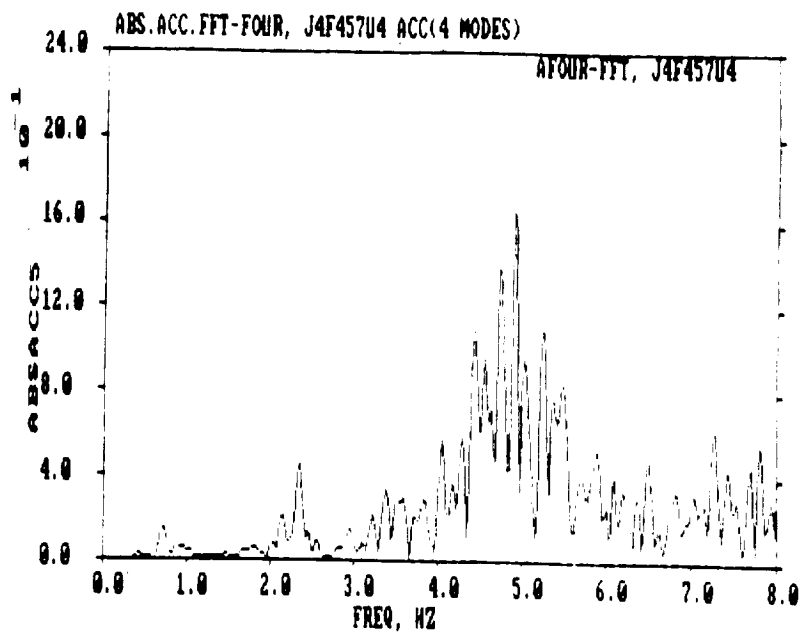


c) Relative acceleration of module internal point at Node 6.

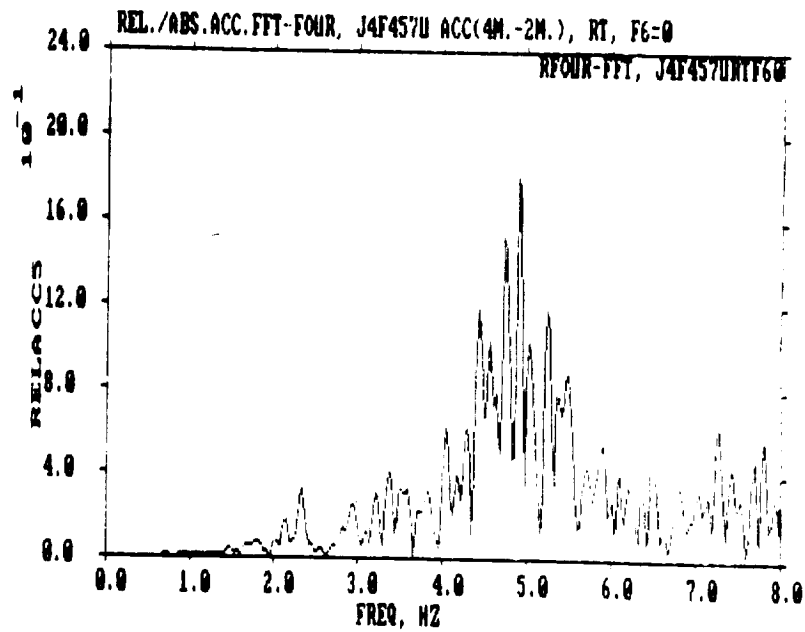


d) Absolute acceleration of module boundary point at Node 7.

Figure 3.31 (concluded)

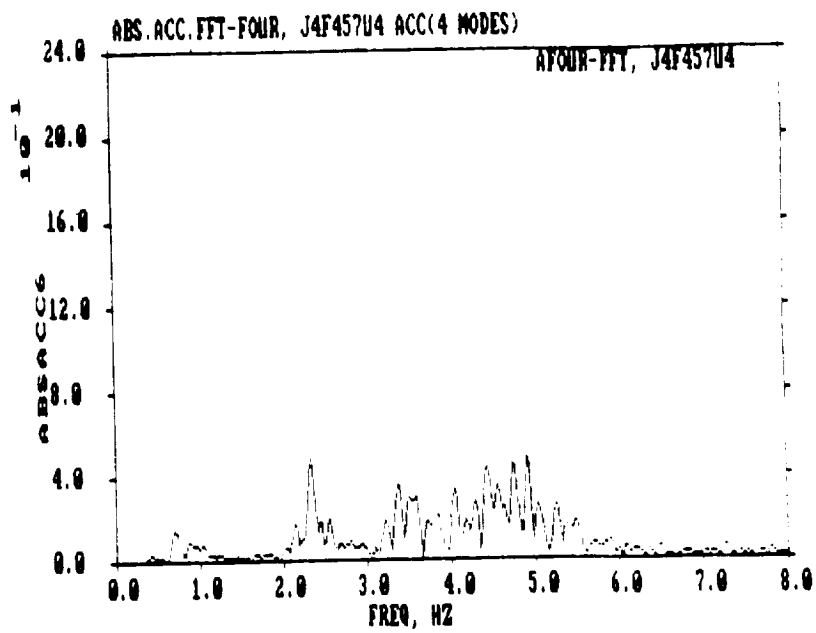


a) Absolute acceleration of Node 5.

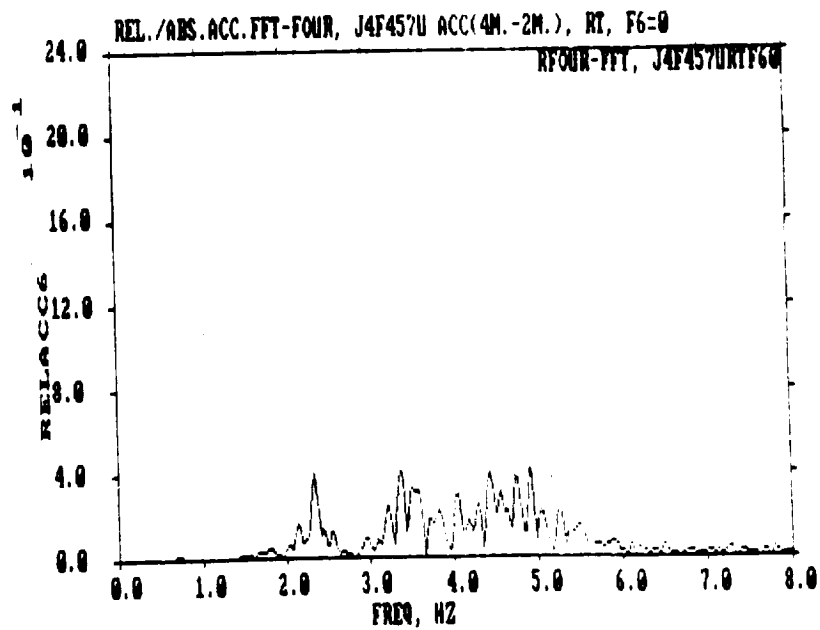


b) Relative acceleration of Node 5.

Figure 3.32: Difference Between Absolute and Relative Module Response--Fourier Transform

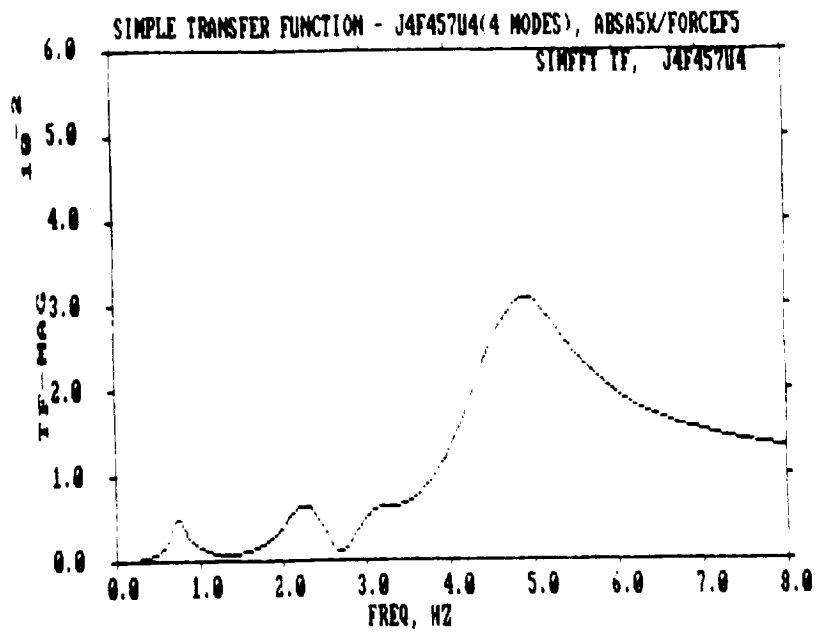


c) Absolute acceleration of Node 6.

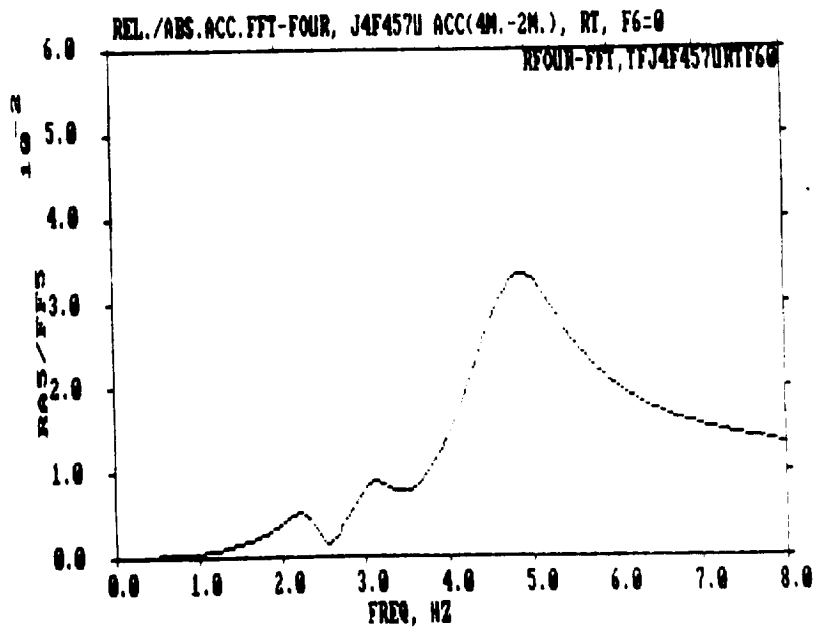


d) Relative acceleration of Node 6.

Figure 3.32 (concluded)

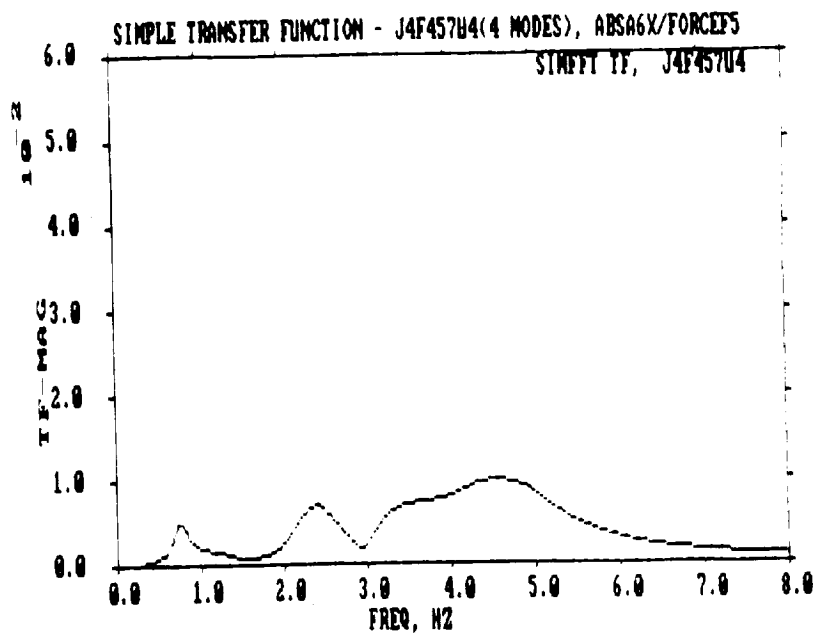


a) Absolute acceleration of Node 5.

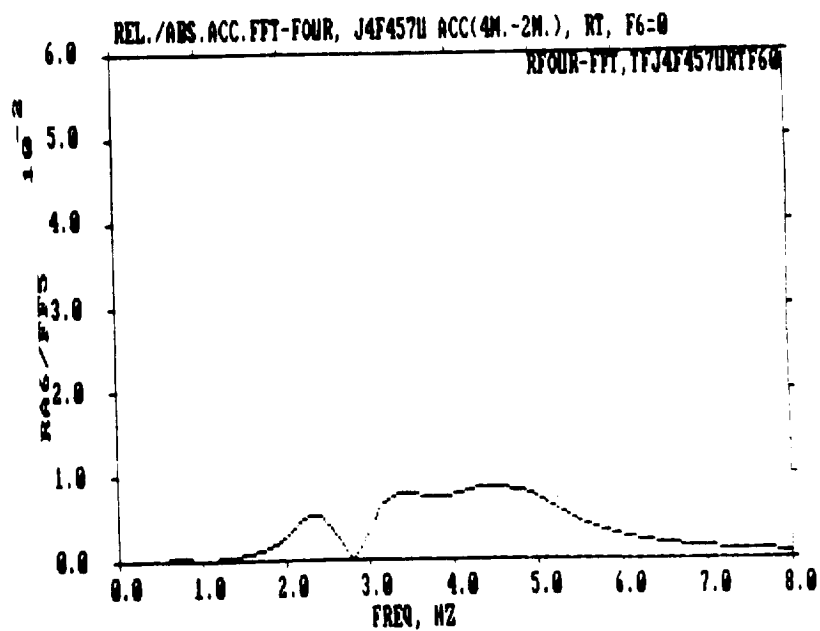


b) Relative acceleration of Node 5

Figure 3.33: Difference Between Absolute and Relative Module Response--SISO Transfer Function

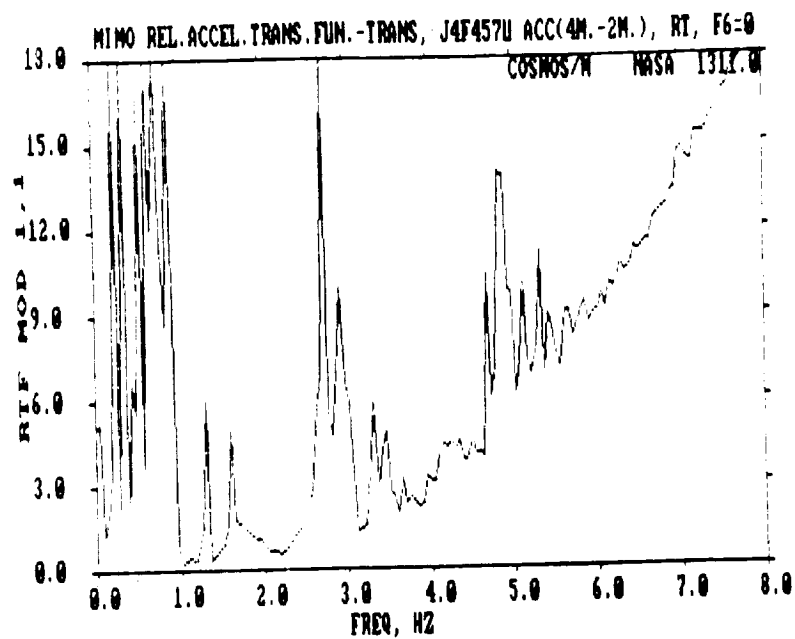


c) Absolute acceleration of Node 6.

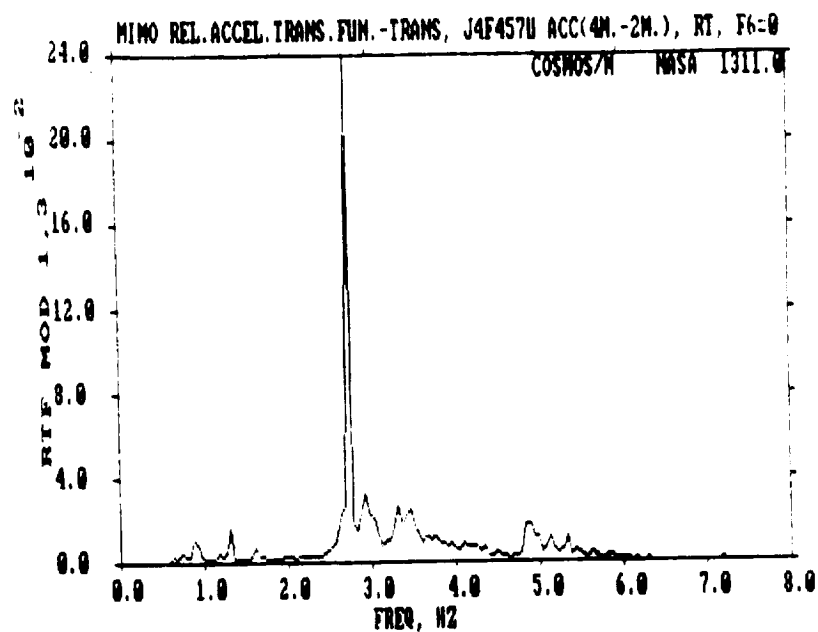


d) Relative acceleration of Node 6.

Figure 3.33 (concluded)



a) Element corresponding to output at Node 5,  
input from Node 4.

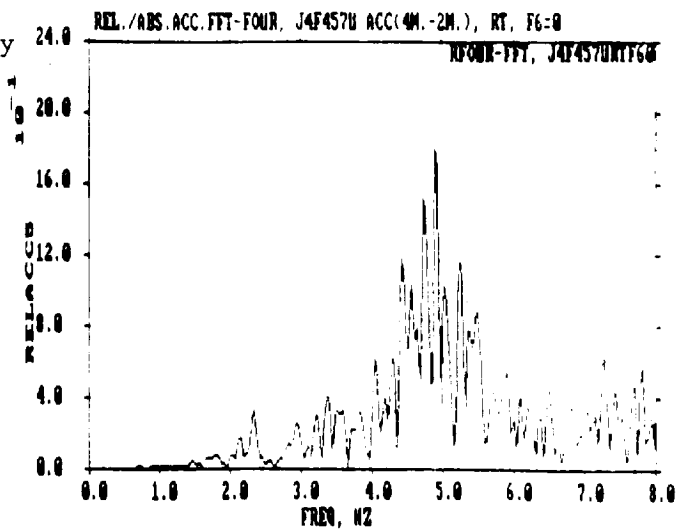


b) Element corresponding to output at Node 5,  
input from Force at Node 5.

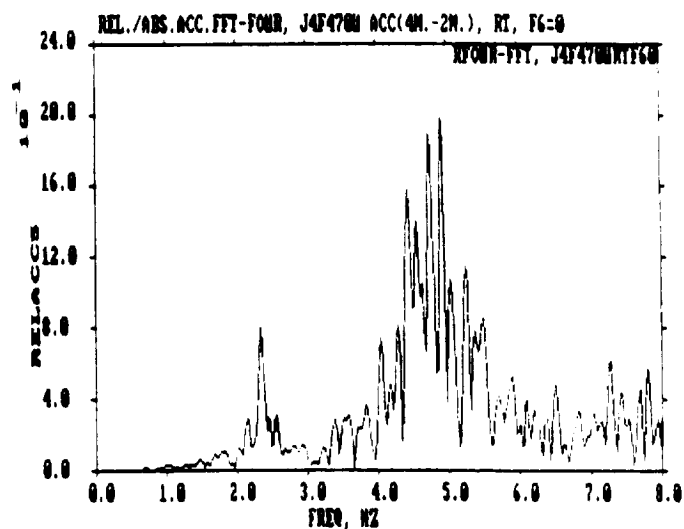
Figure 3.34: MIMO Relative Module Transfer Function Moduli



- a) All "Loading" Acting Simultaneously  
Enforced Boundary Motion and  
Applied Force at Node 5



- b) Only Force at Node 5 Acting



- c) Only Enforced Motions at Boundary  
Acting

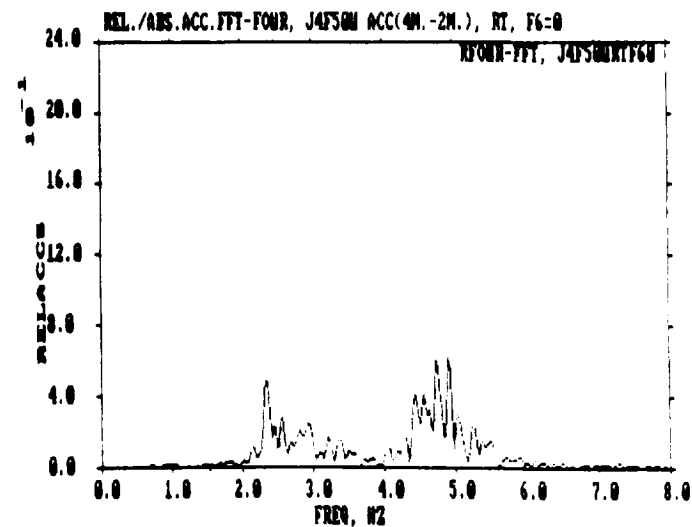
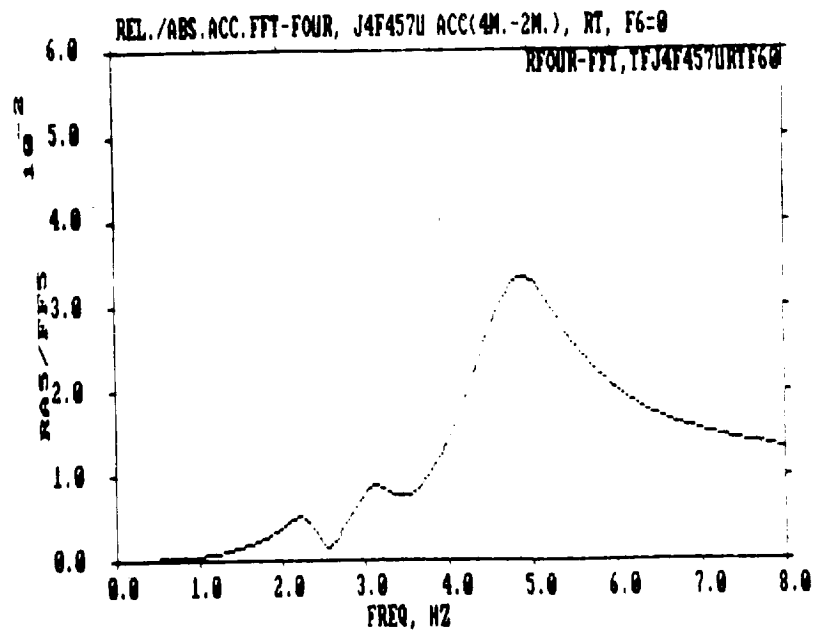


Figure 3.35: Contribution of Applied "Loading" to Net Relative Response of Module

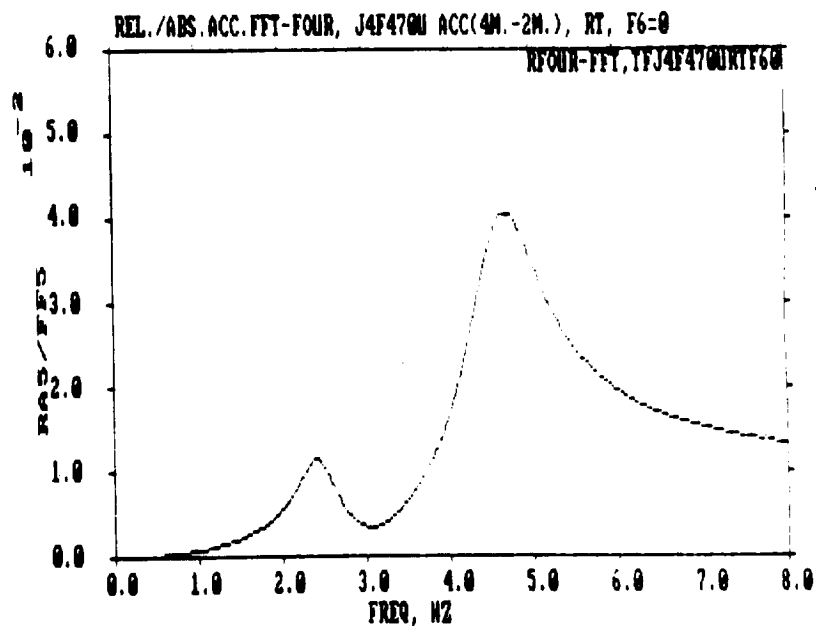
not move and the solution to the problem corresponds to a fixed-base problem with random excitation--the true module transfer function can be obtained from this SISO data. A SISO relative module transfer function using the force  $f_5$  as input was obtained for the case of all inputs to the module acting simultaneously and only force  $f_5$  acting (see Figure 3.36). It is seen that around 5 Hz they are similar and above 5 Hz they are almost identical. This is an expected result. However, the SISO module transfer function corresponding to all inputs is in error around 5 Hz and cannot be used to represent the modules true transfer function.

What is suggested by the above is a non-robust method for obtaining a module transfer function. It deals with the selection of applied force locations/directions (force appropriation). The approach is to apply a set of forces to the global system, with at least one force being applied within the module. They are applied in such a way that the module boundary motion is zero within a frequency domain of interest. Then, within this domain the module transfer function problem becomes a fixed boundary problem and the transfer function can be determined easily. As the global system is damaged (anywhere within the structure) the force locations/directions must be preserved within the module, but may have to be changed outside of the module so as to have no boundary motion within the frequency domain of interest. This is not a very practical method of determining a module transfer function, it is still best to try to develop a method of solving the MIMO transfer function problem with some dependent inputs.

Another but very limiting approach to solving the module transfer function problem is to focus only on those frequency domains where the corresponding modal motion is due to only global modes whose motion is local to the module in question. Of course, for this case the problem again becomes a fixed-boundary problem within the specified frequency domains. There are some good and bad points to this approach. The good points are obvious. The bad points include: 1) there may not be the kind of frequency domain described above--the global and global/local modes may be well mixed together and closely spaced, and 2) there is a considerable amount of effort involved in determining if the motion within a frequency domain is due to only a global/local mode.

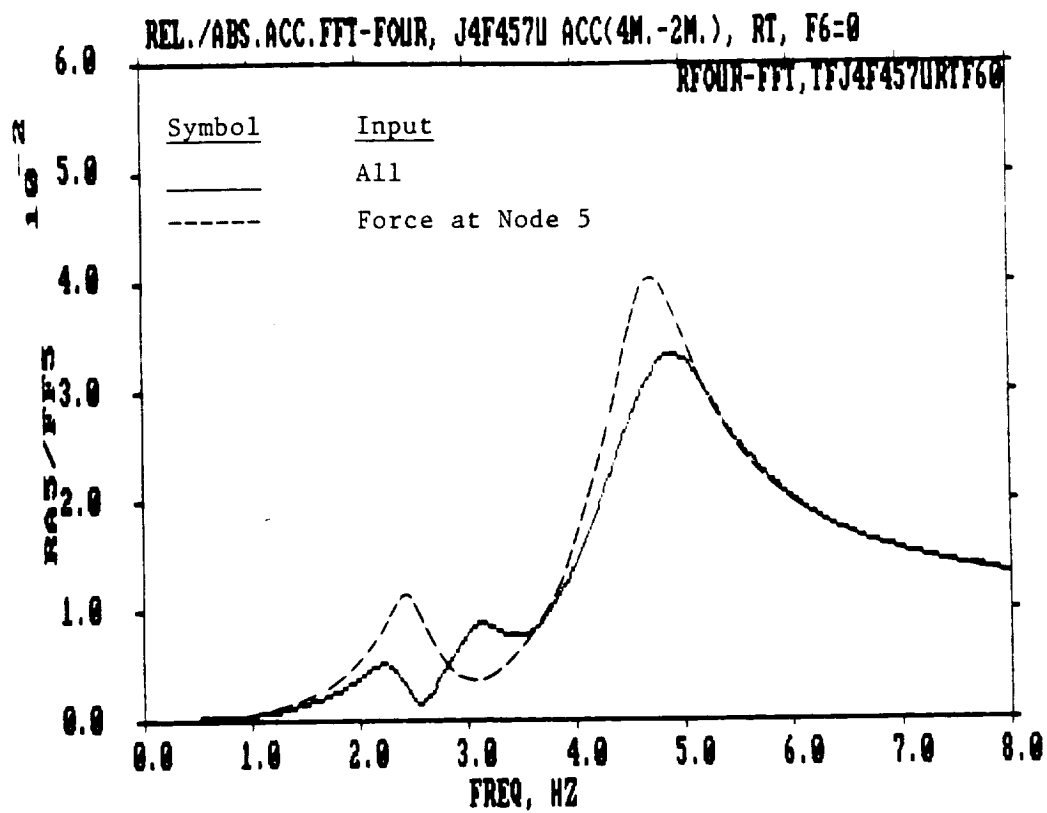


a) All inputs acting simultaneously--enforced boundary motion and applied force at Node 5.



b) Only force at Node 5 acting.

Figure 3.36: Comparison of SISO Relative Module Transfer Function for Different Inputs Acting



c) Overlay of subfigures a) and b).

Figure 3.36 (concluded)

#### 3.2.4.2 Module Transfer Function Via Time Domain System Identification

Another approach to determining the module transfer function matrix is by determining the module modal properties by using time or frequency domain system identification techniques. Once the modal properties have been determined the module transfer function can be determined. A basic approach to this problem is to use the matrix equation of motion for a module for absolute or relative module response, i.e., Equation 3-13 for relative response in the time domain. Use the corresponding linear transformation between the physical and modal domain to transform the equation of motion into the modal domain. Define an objective function which expresses the difference between the model and experimental response. Then determine those module modal parameter values which correspond to a best match between the model and experiment. Then, determine the module transfer function.

There is an approach that can be used to deal with the details of this problem--it was developed by Beck [2] and described in Section 5.0. The approach was used to obtain the module modal properties for a truss system for different levels of damage.

#### 3.3 References

1. R.W. Clough and J. Penzien, "Dynamic of Structures," McGraw-Hill, Inc., 1975.
2. S.D. Werner, J.L. Beck and M.B. Levine, "Seismic Response Evaluation of Meloland Road Overpass Using 1979 Imperial Valley Earthquake Records," Earthquake Engineering and Structural Dynamics, Vol. 15, 249-274, John Wiley & Sons, Ltd., 1987.
3. MAC/RAN IV, Time Series Data Analysis System, University Software Systems, El Segundo, California 90245, 1973.

#### 4.0 OBSERVING CHANGES IN THE MODULE TRANSFER FUNCTION

In the last section the module transfer function matrix was discussed. Given that the transfer function matrix for a given module is determined for various levels of damage including the case of no damage, for a structural system, it is necessary to be able to automatically (numerically) determine changes in it. This is so a hardware/software system can be used to determine if a structural module has incurred any damage. There are an unlimited number of ways to detect changes in a module transfer function matrix. This section discusses a few approaches to doing this. Also, two examples, for which this was done, are presented.

##### 4.1 Damage Indicator

It is possible to "look at" individual elements of a module transfer function matrix to detect if changes in it have occurred. This might be the most effective method of doing this if a maximum amount of information on the damage state is desired. Another way of looking at any changes in the matrix is to define various scalar functions of the matrix. The advantage of doing this is that fewer pieces of information have to be looked at and more effort can be spent on analyzing the data; also, the approach would possibly be simpler and be faster.

The approach used herein is to use various scalar functions to look at changes in the module transfer function matrix. A basic scalar function used is given as follows (see Appendix E for the derivation):

$$D = 1 - \frac{Q^T H^0 L}{Q^T X}$$

where  $D$  = damage indicator; it is a function of the transform variable,  $\omega$ ;

$X$  = system response vector, Fourier transform of;

$L$  = system input "load" vector, Fourier transform of;

$H^0$  = system transfer function matrix at state "0"; and

$Q$  = arbitrary vector; various variables can be chosen to produce different damage indicators.

One damage indicator was for  $Q = X$ ,  $D(1)$ ,

$$D(1) = 1 - \frac{X^T H^0 L}{X^T X}$$

Another damage indicator arrived at is

$$D = 1 - \frac{\sum_{\beta,j} (a H_{\beta j}^0 H_{\beta j}^0 + b H_{\beta j}^0 H_{\beta j}^0 + c X_{\beta j}^0 L_j)}{\sum_{\alpha,i} (a H_{\alpha i}^0 H_{\alpha i}^0 + b H_{\alpha i}^0 H_{\alpha i}^0 + c X_{\alpha i}^0 L_i)}$$

where  $\beta, j, \alpha, i$  = indices

$a, b, c$  = scalar multipliers

The previously described indicator,  $D(1)$ , is a special case of this indicator ( $a = b = 0$ ). Several other indicators were calculated using the latter expression. A second indicator,  $D(2)$ , is

$$D(2) = 1 - \frac{\sum_{\beta,j} H_{\beta j}^0 H_{\beta j}^0}{\sum_{\alpha,i} H_{\alpha i}^0 H_{\alpha i}^0}$$

Only results for these two indicators are provided herein. This is because the other indicators did not provide any other useful results.

It is probably best to use only that damage indicator data which is near the module natural frequencies. Away from these frequencies the indicator data may be confusing and erroneous. Further, the weighting function  $Q$  should be selected such that the sensitivity of the damage indicator,  $D$ , is maximized. An example of this is that if  $Q$  is chosen such that it eliminates the more unimportant responses from the calculation of  $D$ , it will be less subject to noise related problems.

#### 4.2 Example Problems

Two numerical problems are discussed in connection with the damage indicator. The first one is for a lumped spring and mass system with eight mass degrees-of-freedom. The other is for a truss structure. The major

function of them is to provide some insight as to how a damage indicator might be used.

#### 4.2.1 Lumped Parameter System--Global System Approach

The system analyzed is shown schematically in Figure 4.1. It has eight mass degrees-of-freedom. The two end point input motions used were independent of each other (see Figure 4.2). Some corresponding system responses are given in Figure 4.3. The problem was dealt with as a global system problem--no modules were used. The transfer function computation was a multi-input (two inputs) multi-output (MIMO) problem. Various damage levels were looked at. Figure 4.4 is a sample of the transfer function data obtained. A comparison of the resonant peaks with calculated system fixed-base natural frequencies was made (see Table 4.1). Also, half-power damping calculations were performed (values ranging from 10.1% to 10.4% were obtained for the first three modes) and a comparison made with the value used in the numerical simulation (10% for all modes). It is believed that the MIMO transfer function calculations performed yielded good results.

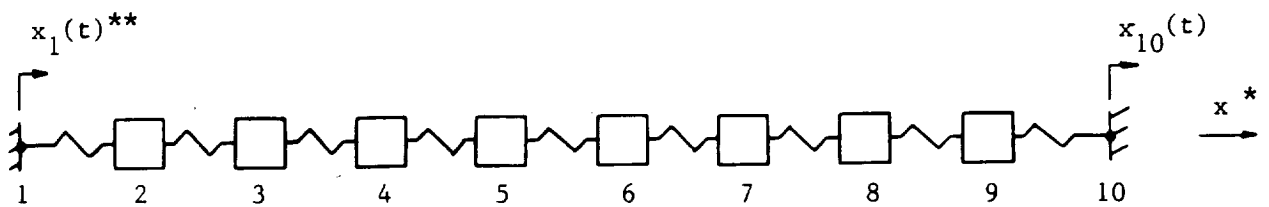
Next, damage indicator calculations were performed. Two sets of calculations were made; they are for 1) no structural damage but two different sets of base motion inputs and 2) structural damage. The case of no structural damage was looked at to obtain an approximate damage indicator level, for which if damage indicator values were at or below it, it could be assumed that no damage had occurred. Figure 4.5 is plots of the two damage indicators as a function of frequency. It is seen that even though there was no damage, the plots were not "flat".

Also, Figure 4.5 is plots of the two indicators for a uniform damage to the structure--each mass was reduced by 25 percent. In comparing the a) and b) type plots in the figure it is seen that the damage indicators are fairly sensitive to damage. The uniform decrease in mass would increase the fundamental frequency by about 15 percent. However, the increase in the

---

\* In computing the values of the damage indicators, the final computed value was one (1) minus the damage indicator discussed above. This means that for no damage and the same inputs, the modulus and phase are unity and zero, respectively.

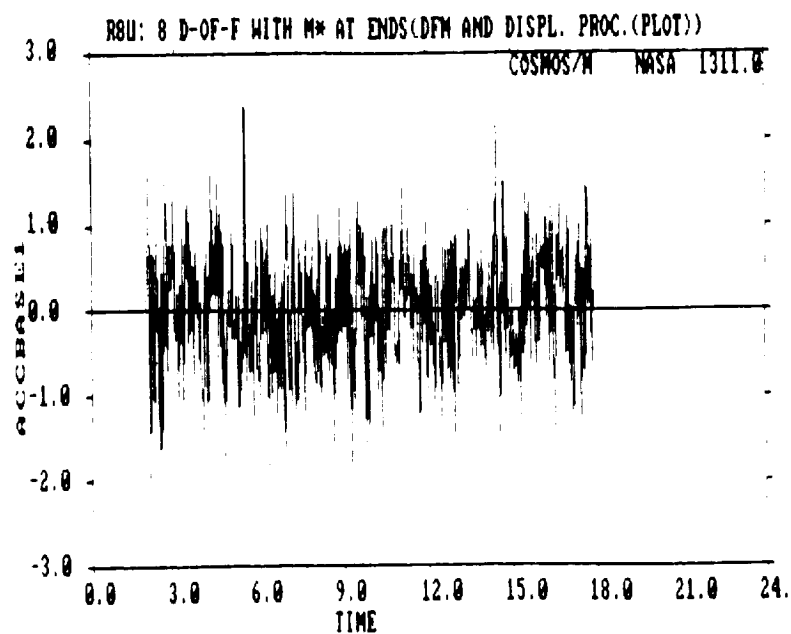




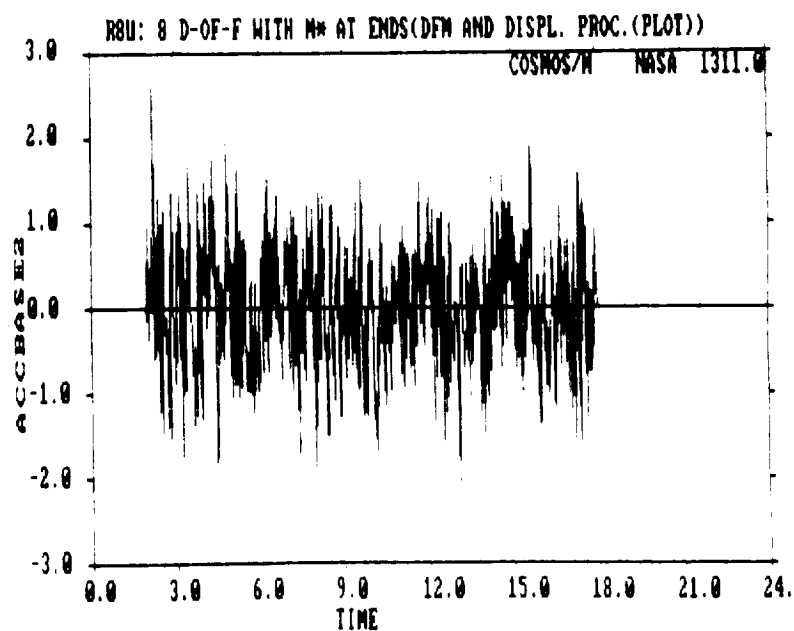
\* The masses moved in only the x-Direction.

\*\* The enforced motions  $x_1$  and  $x_{10}$  were different from each other--they were independent.

Figure 4.1: Lumped Parameter System With Different Enforced Motions at Ends

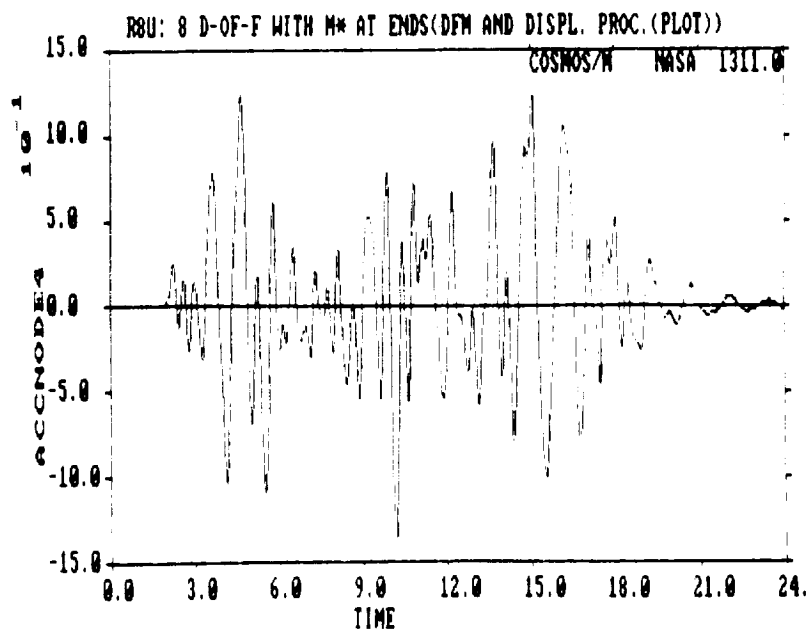


a) Base motion at Node Point 1.

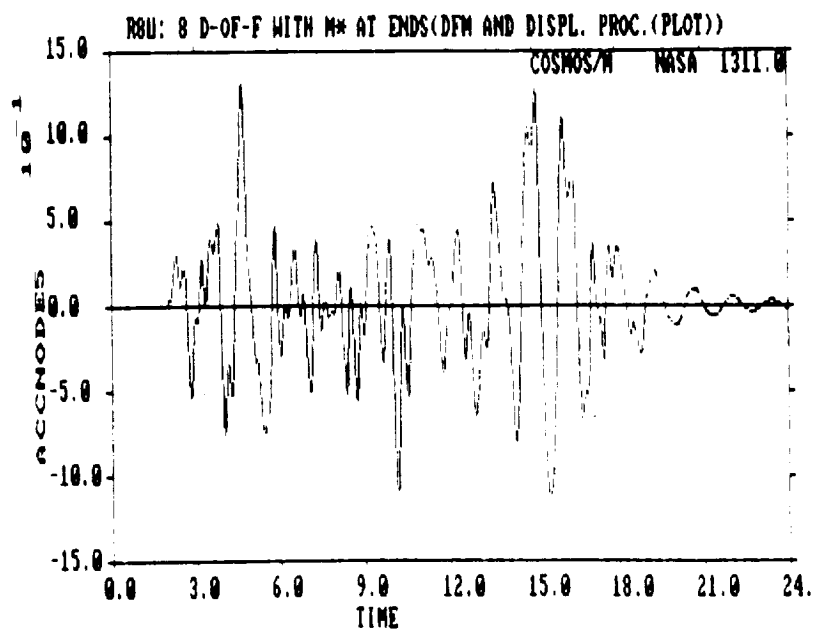


b) Base motion at Node Point 10

Figure 4.2: Independent Enforced Base Motions

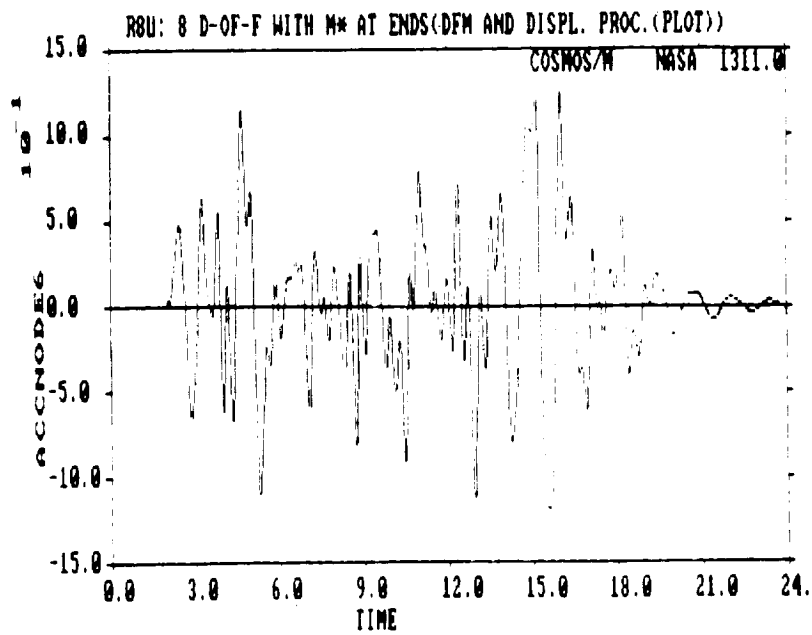


a) Absolute acceleration for Node 4.

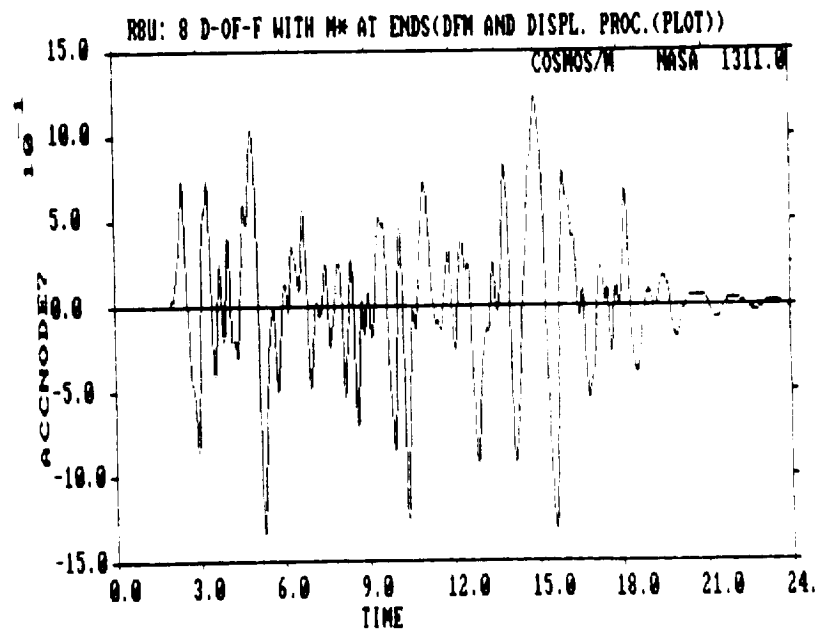


b) Absolute acceleration for Node 5.

Figure 4.3: Representative System Responses for Independent Base Motions

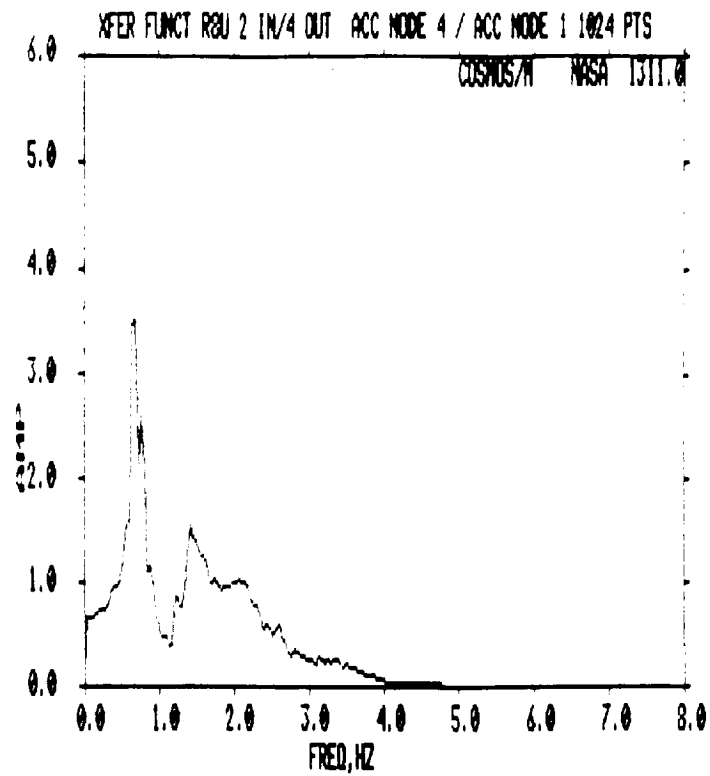


c) Absolute acceleration for Node 6.

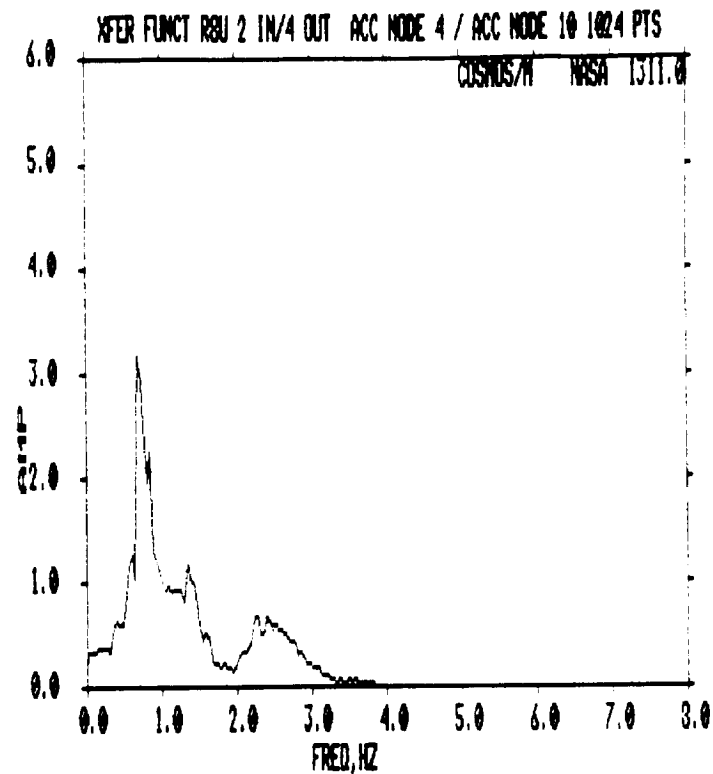


d) Absolute acceleration for Node 7.

Figure 4.3 (concluded)

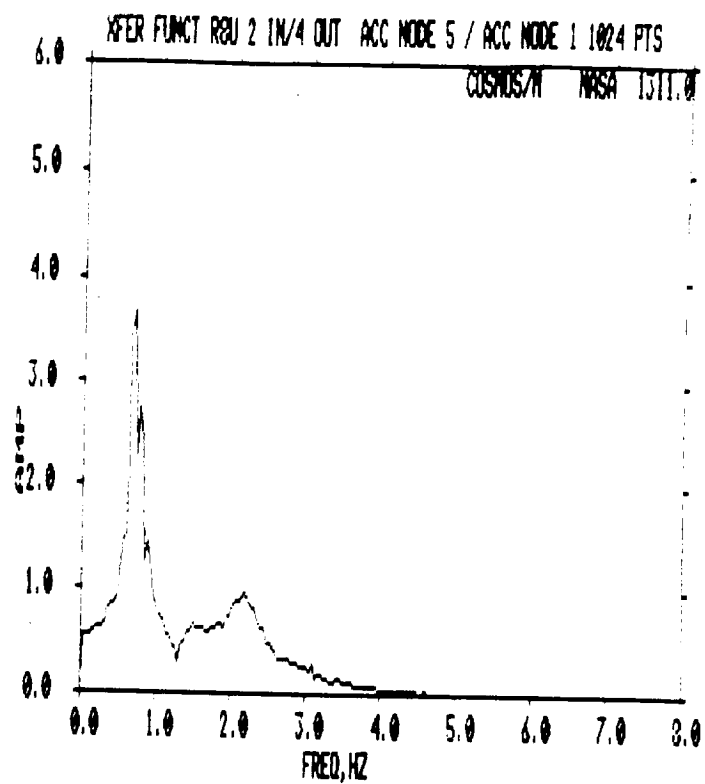


a) Element 1,1--Modulus

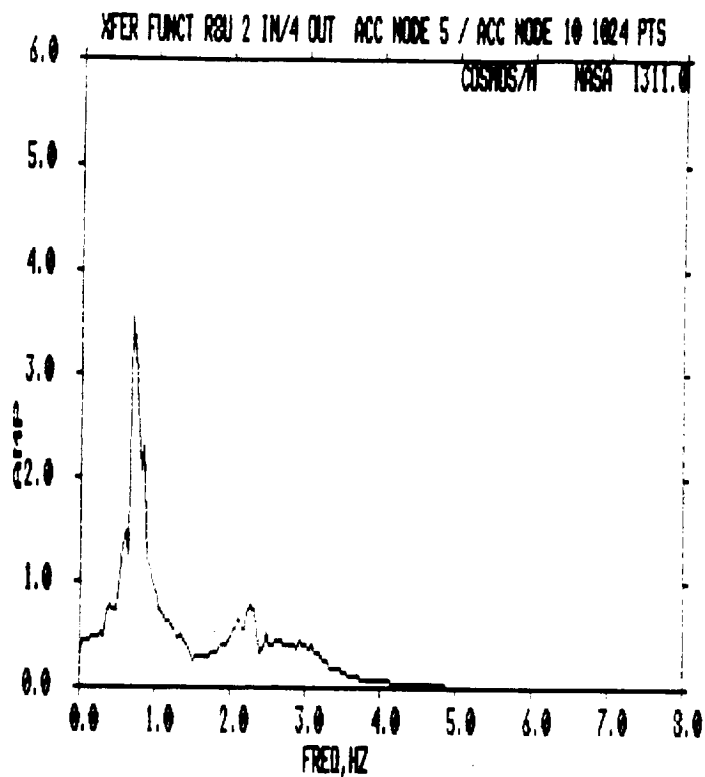


b) Element 1,2--Modulus

Figure 4.4: MIMO Absolute Global Transfer Function Matrix for Independent Base Inputs



c) Element 2,1--Modulus



d) Element 2,2--Modulus

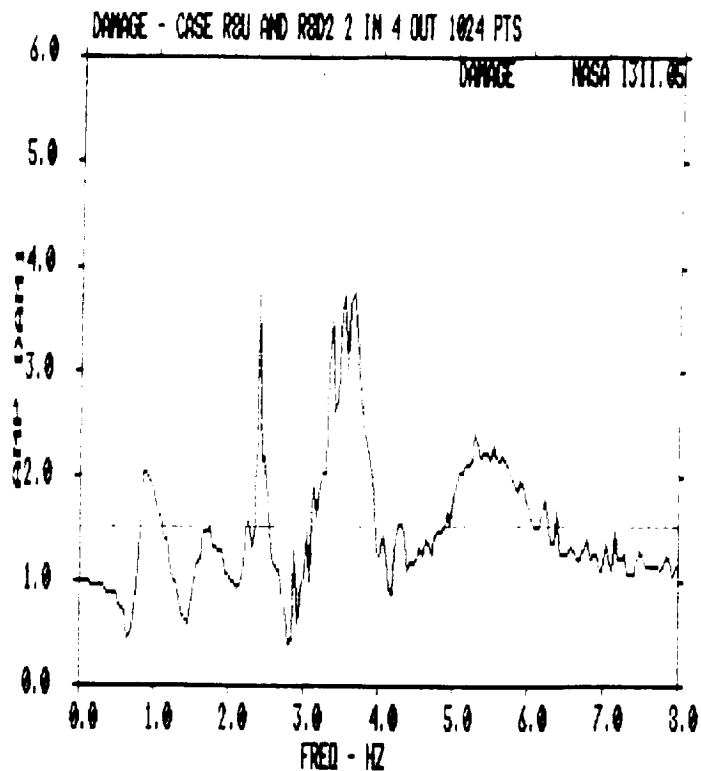
Figure 4.4 (concluded)

TABLE 4.1: COMPARISON OF RESONANT PEAK FREQUENCIES  
WITH CALCULATED NATURAL FREQUENCIES

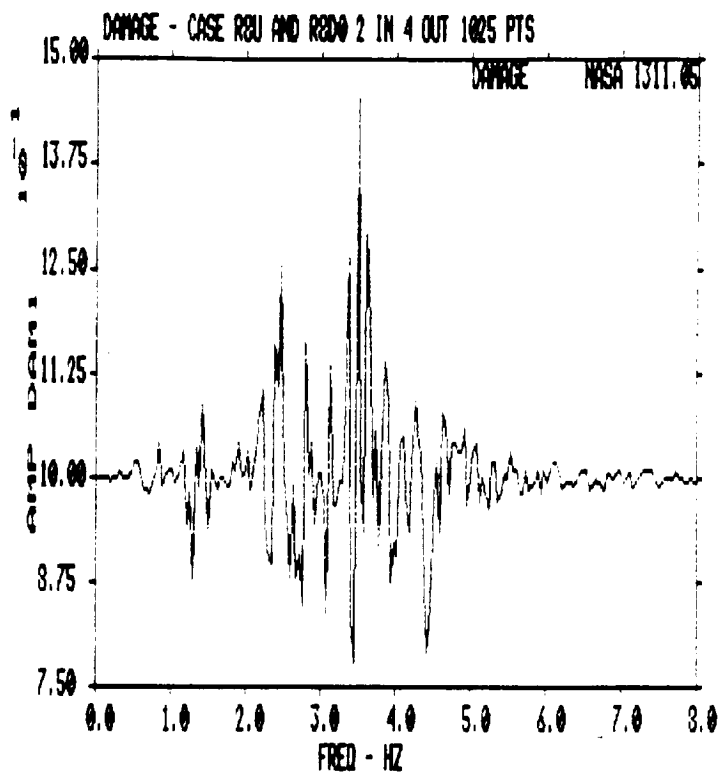
Mode	Resonant Peak Frequency (Hz)*	Calculated Natural Frequency (Hz)**	Percent Difference (%)
1	0.71	0.746	5.0
2	1.41	1.407	0.2
3	2.17	2.226	2.5

\* These were obtained from the transfer function plots.

\*\* These were obtained from an eigenvalue extraction.



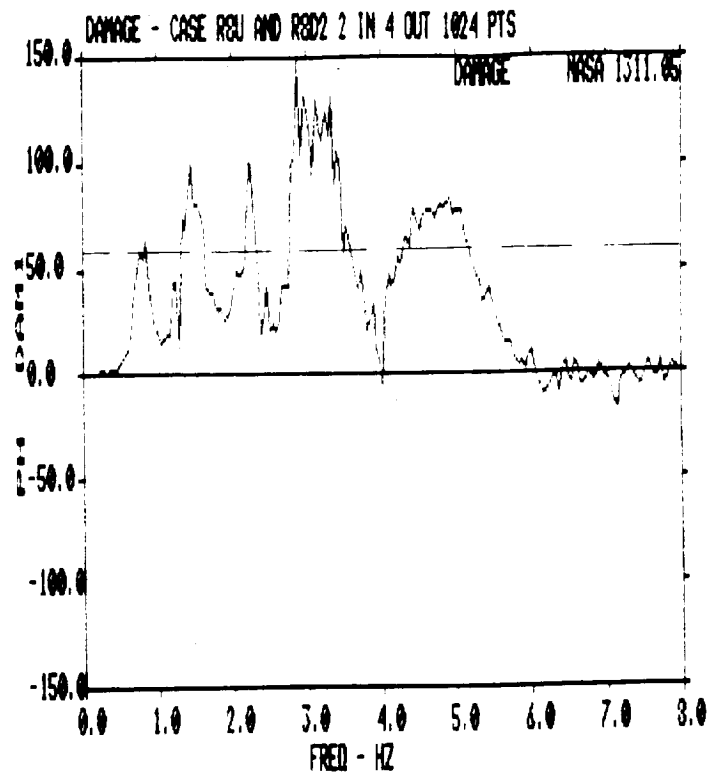
a) Damage Indicator One Modulus--Damaged Case



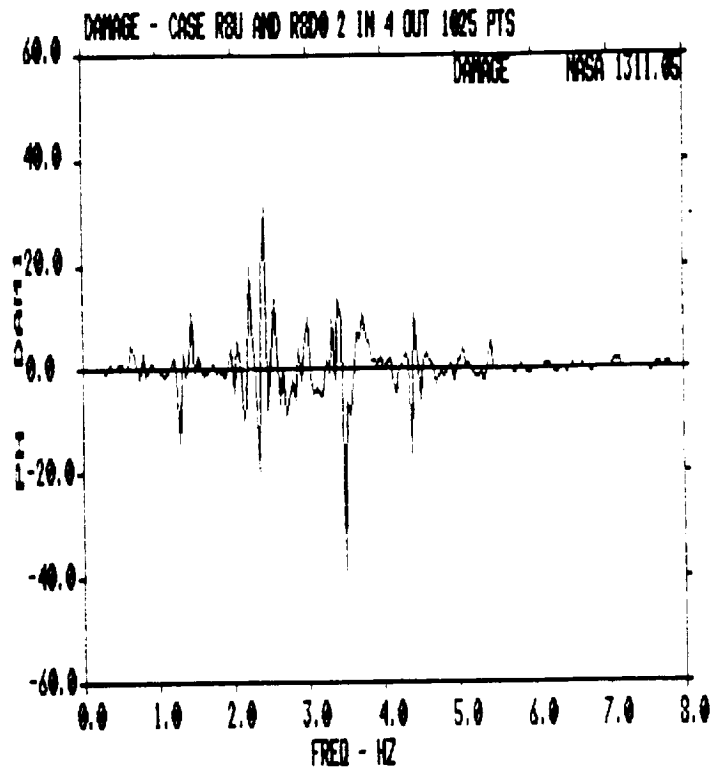
b) Damage Indicator One Modulus--Undamaged Case

Figure 4.5: Comparison of Damage Indicators for Uniform Global Damage and No Damage for Independent Base Motions



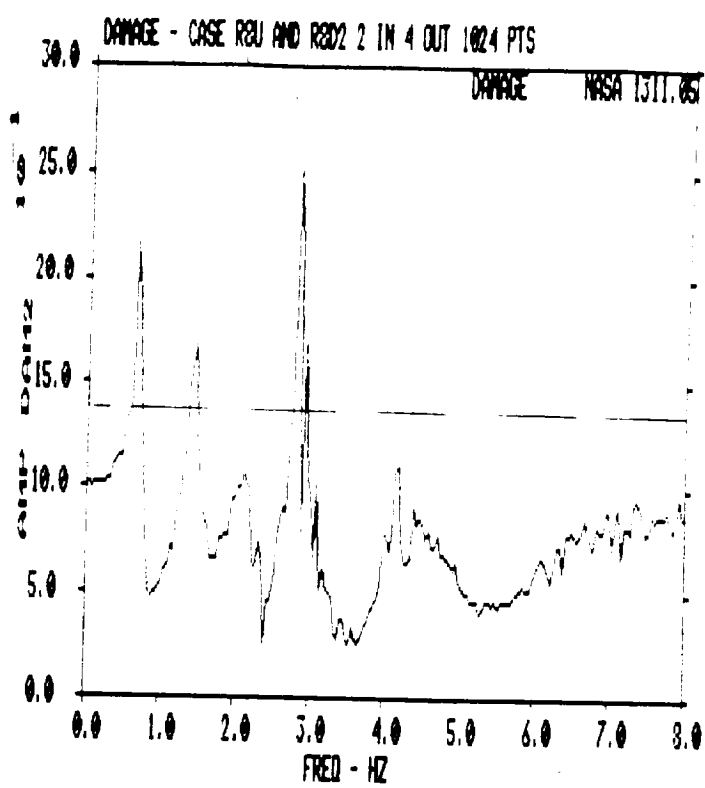


a2) Damage Indicator One Phase--Damaged Case

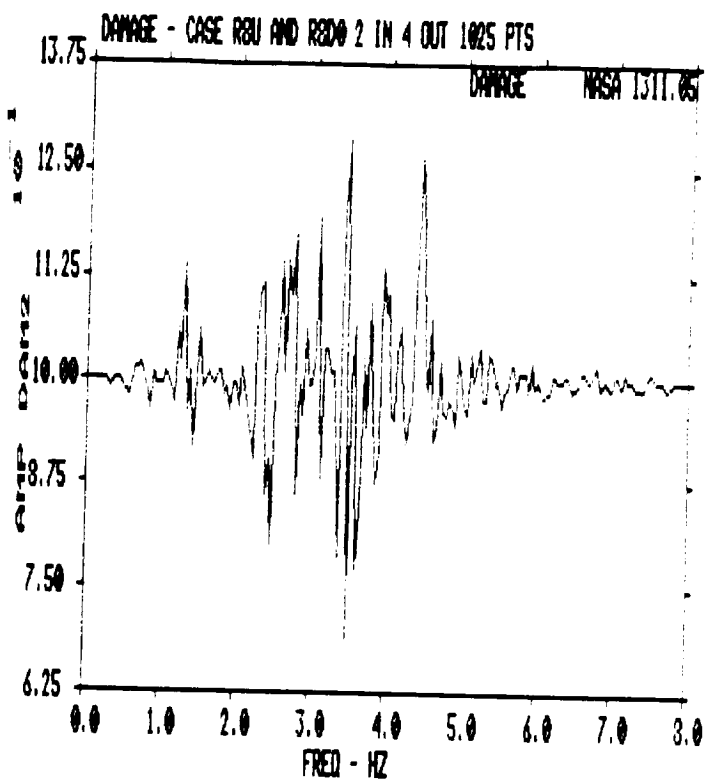


b2) Damage Indicator One Phase--Undamaged Case

Figure 4.5 (continued)

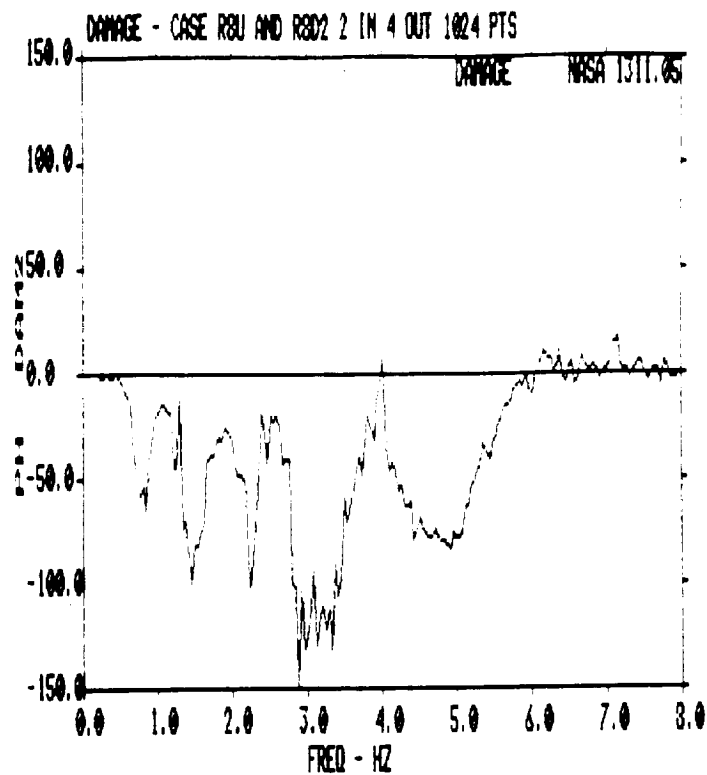


a3) Damage Indicator Two Modulus--Damaged Case

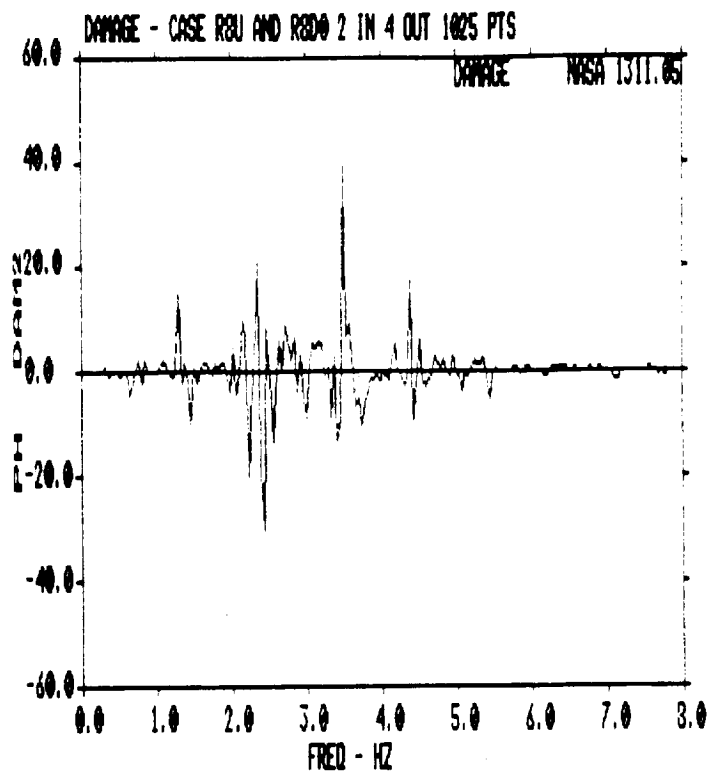


b3) Damage Indicator Two Modulus--Undamaged Case

Figure 4.5 (continued)



a4) Damage Indicator Two Phase--Damaged Case



b4) Damage Indicator Two Phase--Undamaged Case

Figure 4.5 (concluded)

peak values of the amplitudes for the two damage indicators was from about 10% to 115%, with most being above 50%.

In looking at the plots of the damage indicators it is seen that the amplitude (modulus) peaks greater than one correspond to "undamaged" and "damaged" natural frequencies for damage indicators  $D(2)$  and  $D(1)$ , respectively. The peaks for the phase plots occur between the "undamaged" and "damaged" natural frequencies. This will be discussed further in Section 6.0 (the modal strain energy distribution method of locating damage).

The damage indicators can be used to some degree to quantify the level of damage in a structural module. For uniform damage, it is possible to determine the change of a damage indicator peak for a given "undamaged" natural frequency with a change in the level of damage. Because the level of uniform damage can be represented by a scalar variable,  $\lambda$ , it is possible to plot a damage indicator level as a function of this variable, i.e., Plot  $D^{(2)}(f_1^u)$  as a function of  $\lambda$ , where  $f_1^u$  is the fundamental "undamaged" natural frequency. This was done and is shown by Figure 4.6. Given the damage indicator level the uniform damage level can be found.

For an actual physical system it would probably be necessary to use a numerical model of it to obtain an estimate of the functional relationship between an indicator, at a resonant frequency, and the uniform damage level variable,  $\lambda$ . In determining this relationship any possible error inherent in the model would need to be taken into account--an upper and lower bound functional relationship would have to be found.

It would be considerably more difficult to determine a functional relationship between the damage indicator and fraction of local damage than for uniform damage. This is solely due to the fact that there are an unlimited number of possible different local damage locations or combinations of locations. Even if essentially all local damage indicator relationships were known, it would be necessary to know where the local damage was in order to be able to select the proper relationship. It might be helpful to divide the module into a few regions and look at the damage as being uniform within a given region and zero within the others for the case of a single local damage.

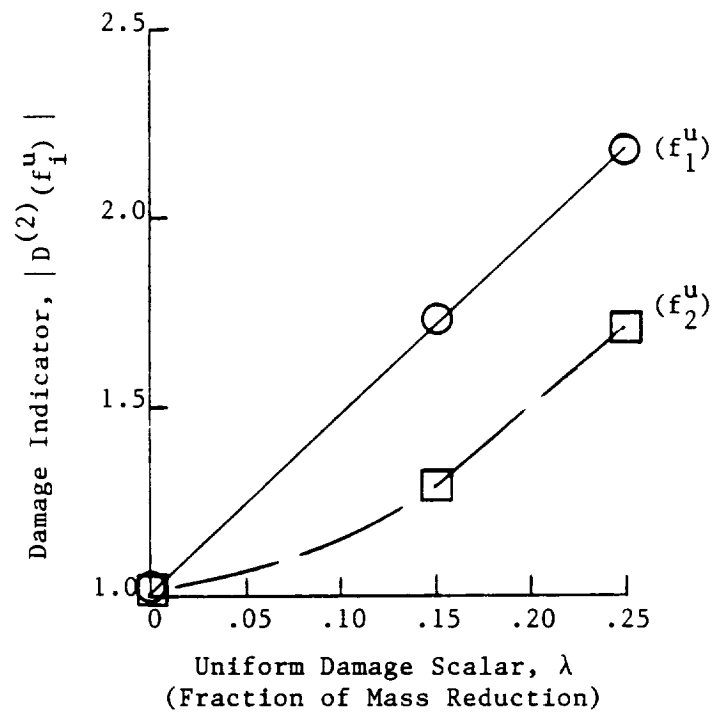


Figure 4.6: Damage Indicator Level as a Function of the Uniform Damage Scalar

#### 4.2.2 Truss Structure--Module Approach Using Local Modes

The structure used for this numerical example is shown in Figure 4.7. It is a 54 degree-of-freedom 2-dimensional system (motion is in the x-y plane). The excitation is uniform enforced base motion at Nodes 1 and 15 (at left end of structure). The module used starts at Nodes 6 and 20 and goes to the right to Nodes 14, 10, 24 and 28.

The model structure was designed so there would be global modes whose elastic motion would be only within the selected module--local modes were created. Figure 4.8 contains plots of some global and local modes. Table 4.2 is a list of the system's natural frequencies and uniform base motion participation factors. It can be seen that by using x-direction base motion the third mode (a local mode) can be excited very well, while Modes 1, 2, 4, 5 and 6 are essentially not excited. Also, by low-pass filtering the base excitation at 10 Hz (as was done) it is possible to minimize the excitation of any modes above 10 Hz. This makes possible the selective excitation of a local mode, and hence, a single-input single-output (SISO) module transfer function can be calculated easily (see Figure 4.9).\*

Using the SISO transfer function within input and output being at Nodes 6 and 9, respectively, the two damage indicators were calculated for a damage case (see Figures 4.10 and 4.11). The comments made concerning the damage indicators for the previous numerical case hold for this case. Because of the excitation of only a single mode the shape of the curves for the damage indicators is quite simple as opposed to those for the prior case. Basically, the concept of a damage indicator is fairly simple. The difficult thing to do is to correlate the maxima of peaks related to resonances with the level of module damage.

---

\* What was done for this frame structure can be generalized for some other structures. However, this approach is not useful for a general structure because 1) there may not be any local modes with motion in the desired areas, 2) of possible high modal density of global modes around the local modes, and 3) for additional reasons, of the inability to excite only local modes.

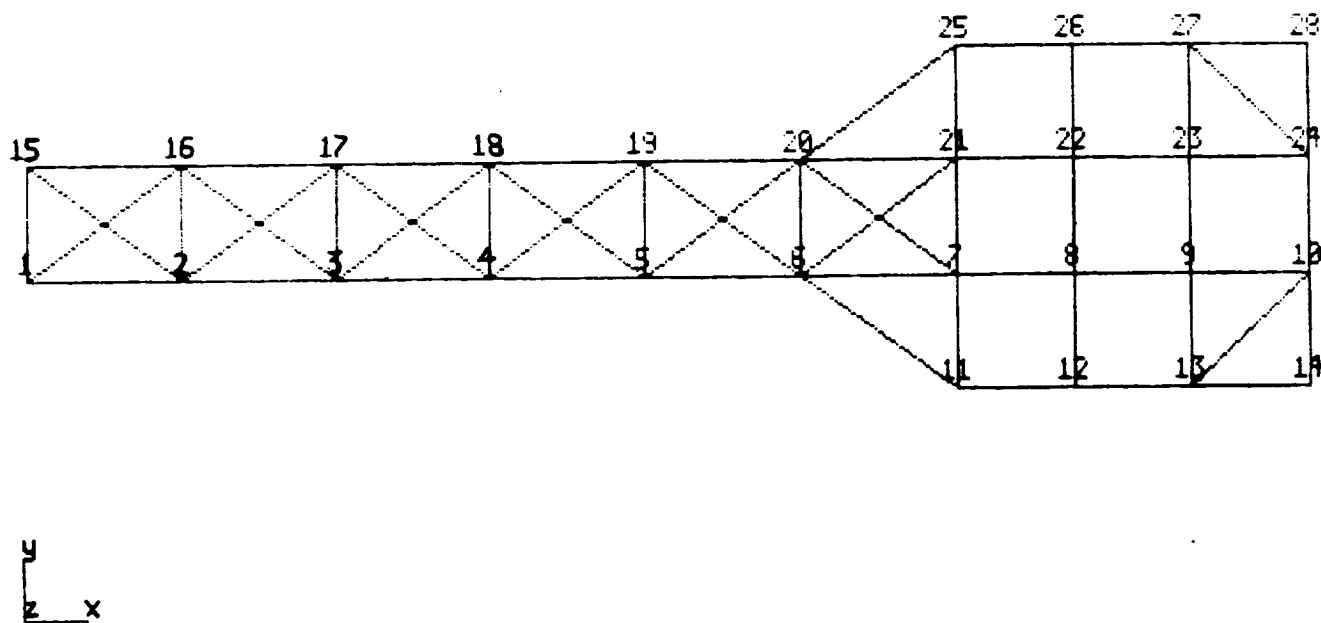


Figure 4.7: Numerical Model of a Truss Structure

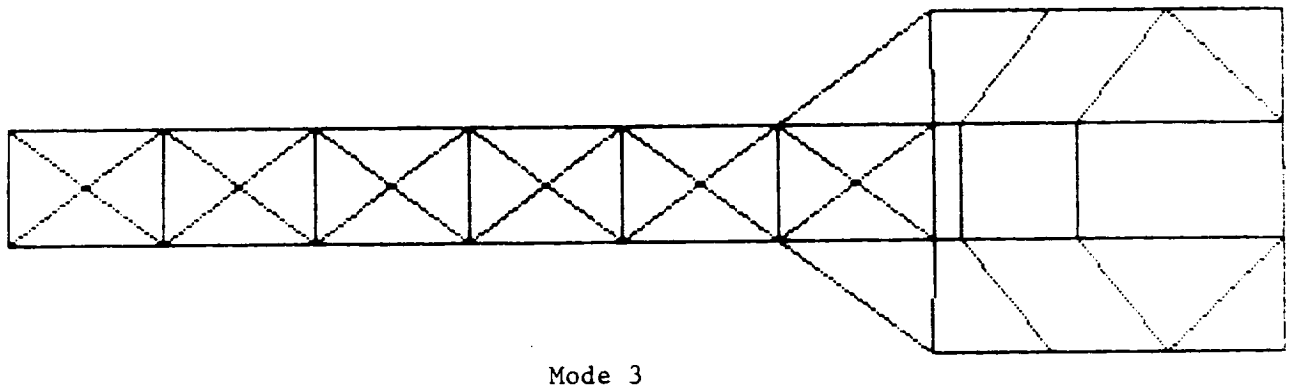
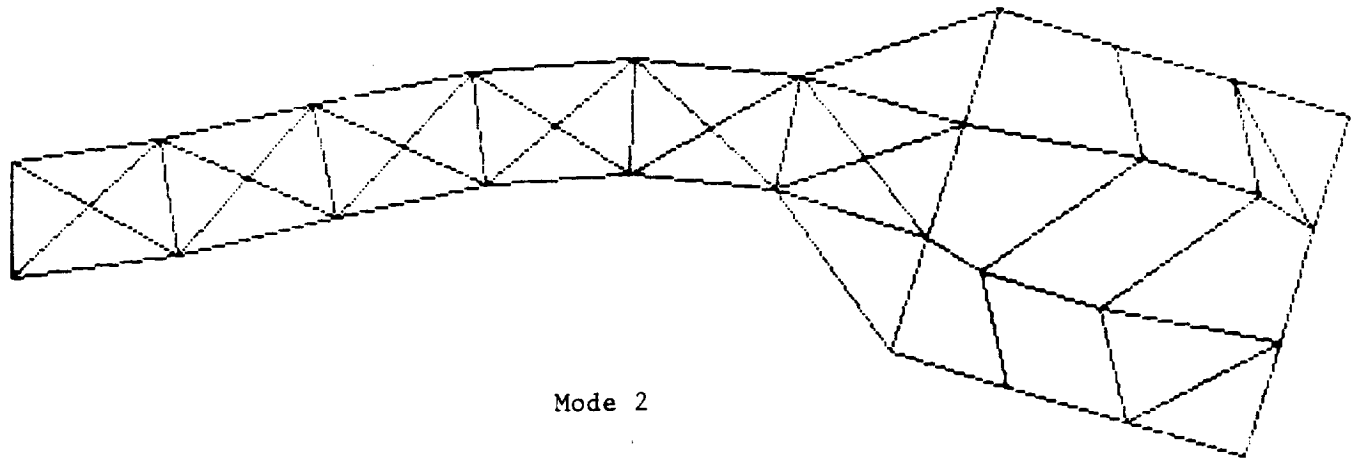
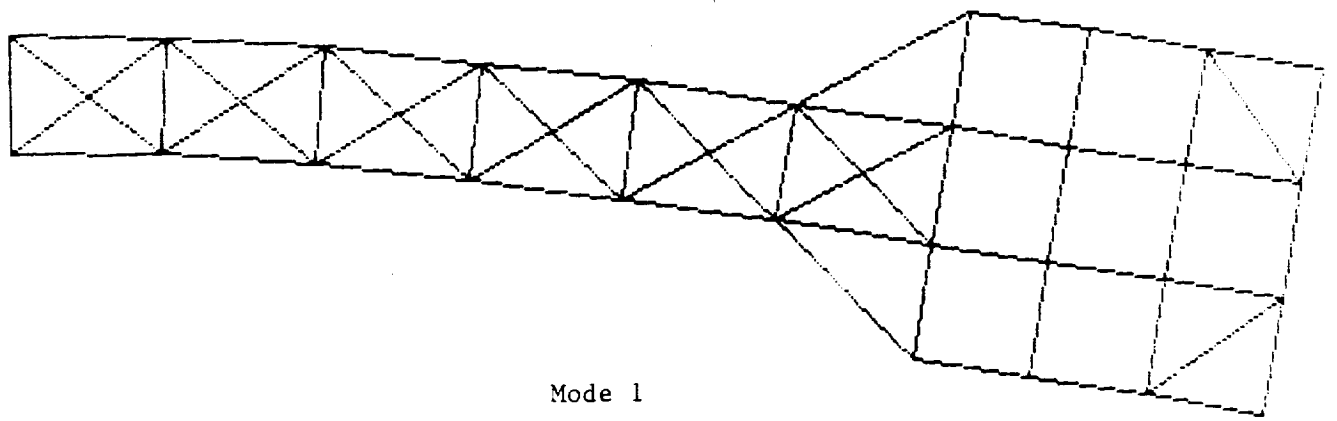
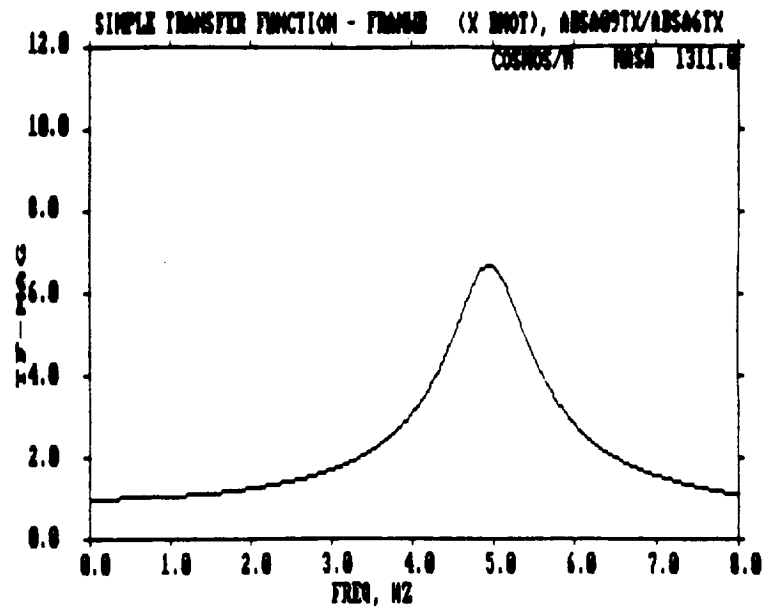


Figure 4.8: Truss Structure--Mode Shapes

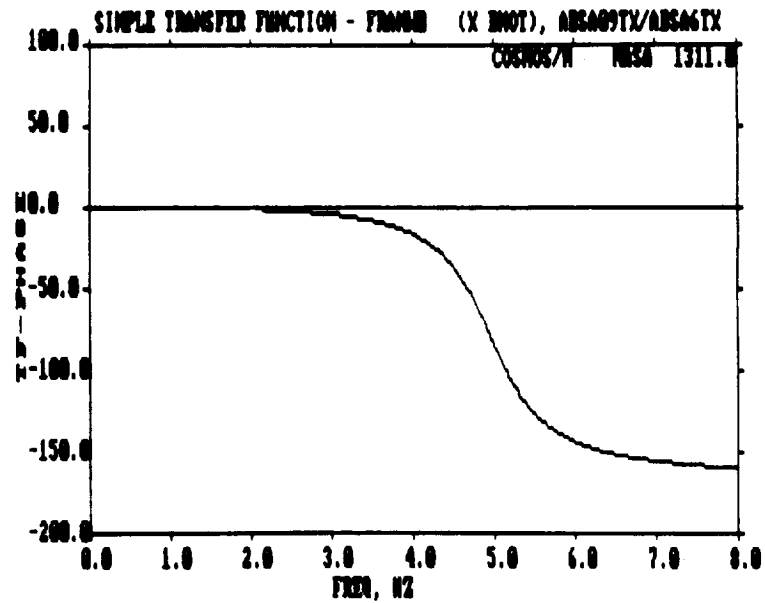


TABLE 4.2: TRUSS STRUCTURE GLOBAL NATURAL FREQUENCIES  
AND PARTICIPATION FACTORS (UNDAMAGED SYSTEM)

Mode	Natural Frequency (Hz)*	Participation Factor	
		x-Direction	y-Direction
1	0.703	$-0.475 \times 10^{-6}$	$0.189 \times 10^2$
2	4.519	$0.705 \times 10^{-5}$	$-0.968 \times 10^1$
3	4.932	$0.106 \times 10^2$	$0.662 \times 10^{-6}$
4	5.219	$-0.965 \times 10^{-5}$	$-0.323 \times 10^1$
5	8.842	$-0.729 \times 10^{-1}$	$-0.968 \times 10^{-6}$
6	8.855	$-0.893 \times 10^{-5}$	$-0.161 \times 10^{-2}$
7	10.316	$0.187 \times 10^2$	$0.112 \times 10^{-5}$
8	13.495	$-0.191 \times 10^{-5}$	$0.587 \times 10^1$



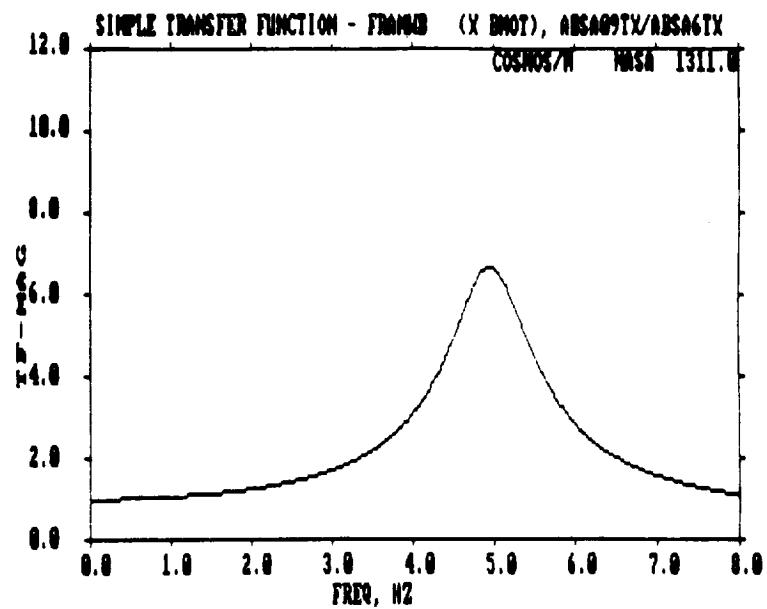
a) Modulus



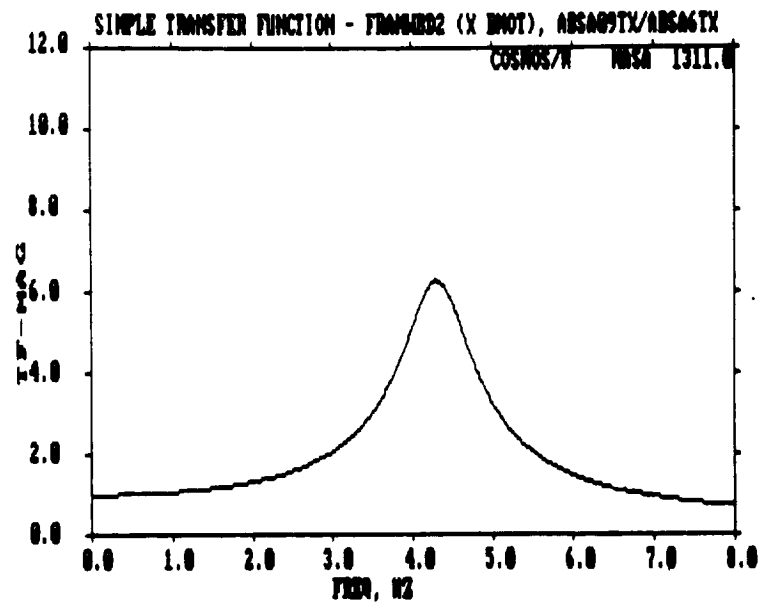
b) Phase

Figure 4.9: SISO Module Transfer Function (A9/A6)  
for Truss Structure

ORIGINAL SOURCE  
OF POOR QUALITY



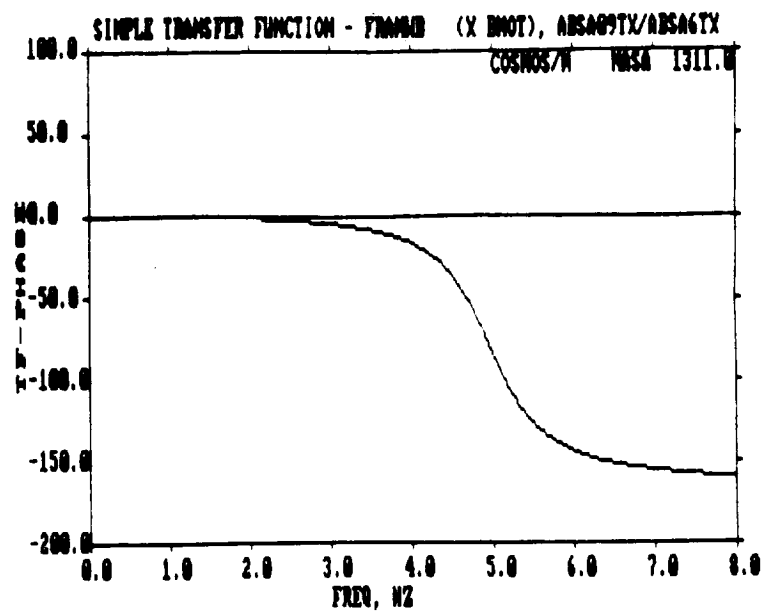
a) Undamaged Global System--Modulus



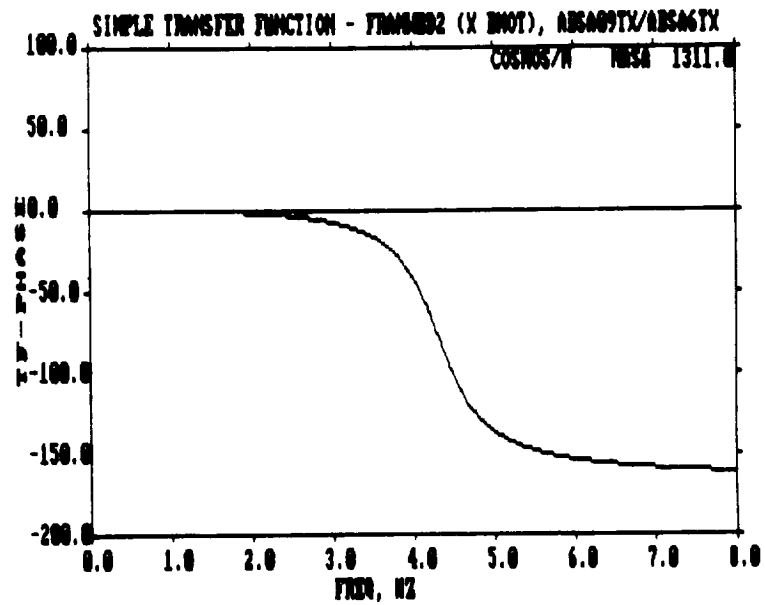
b) Damaged Module--Modulus

Figure 4.10: SISO Module Transfer Function for Two Damage Levels

GRAPHICAL FORM  
OF DATA

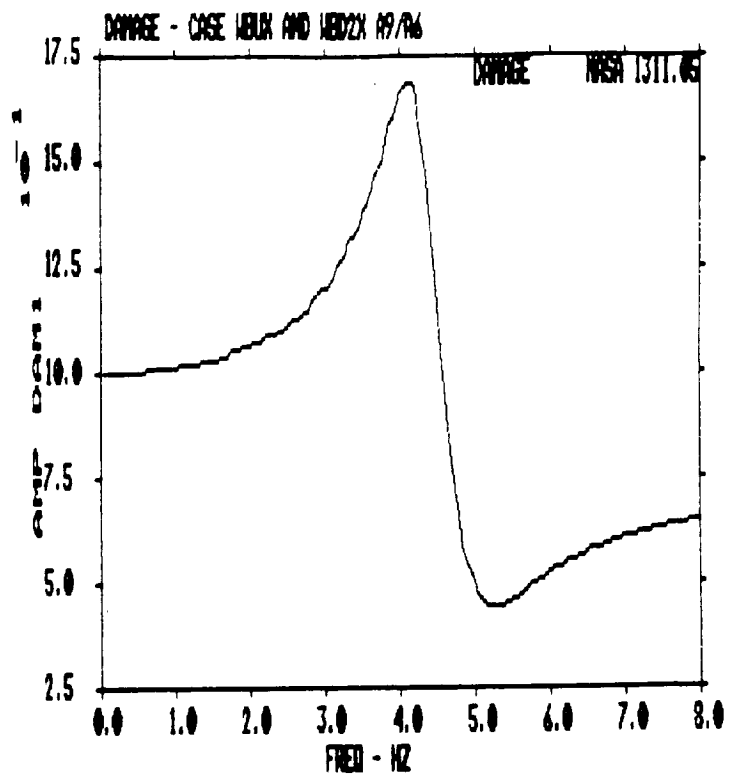


c) Undamaged Global System--Phase

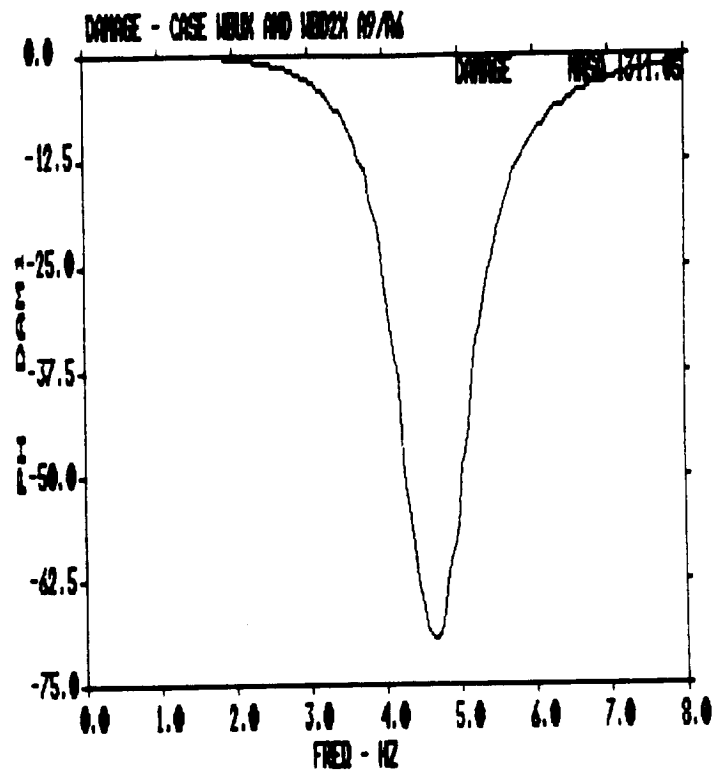


d) Damaged Module--Phase

Figure 4.10 (concluded)

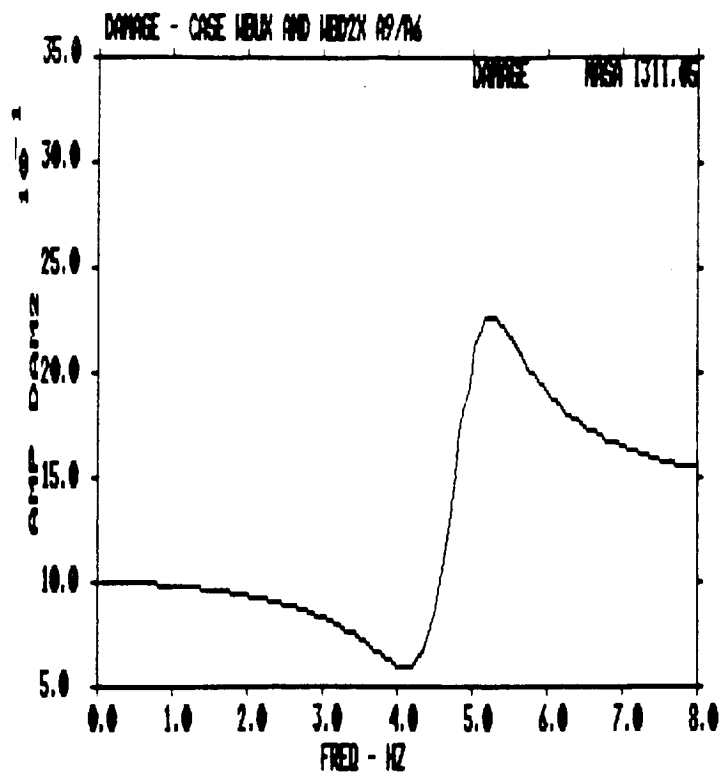


a) First Indicator--Modulus

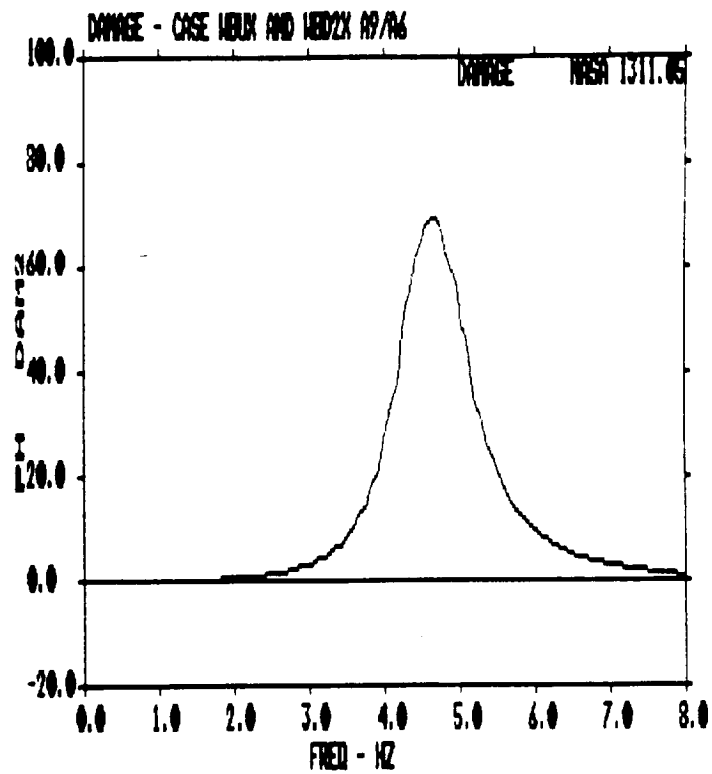


b) First Indicator--Phase

Figure 4.11: Damage Indicators for Module - Damage



c) Second Indicator--Modulus



d) Second Indicator--Phase

Figure 4.11 (concluded)

A module transfer function was not calculated using global and local modes for this problem because of the inability to determine it using a robust approach. It would have been possible to follow the non-robust approach described at the end of Section 3.0--using forces inside and outside of a module and appropriating them, ensuring that the module boundary does not move for a desired frequency domain.

## 5.0 TIME DOMAIN MODULE MODAL IDENTIFICATION

As mentioned previously in this report (Section 3.0), an approach that can be used to obtain module modal properties is system identification using the equations of motion for a module (Equation 3-6 or 3-12). There are different ways that this problem can be approached. The method used herein is that developed by Beck [1,2]. Conceptually, it involves determining the module modal properties (fixed-boundary) that result in a best fit (match) between the prediction given by Equation 3-13 and the experimental data (module responses).

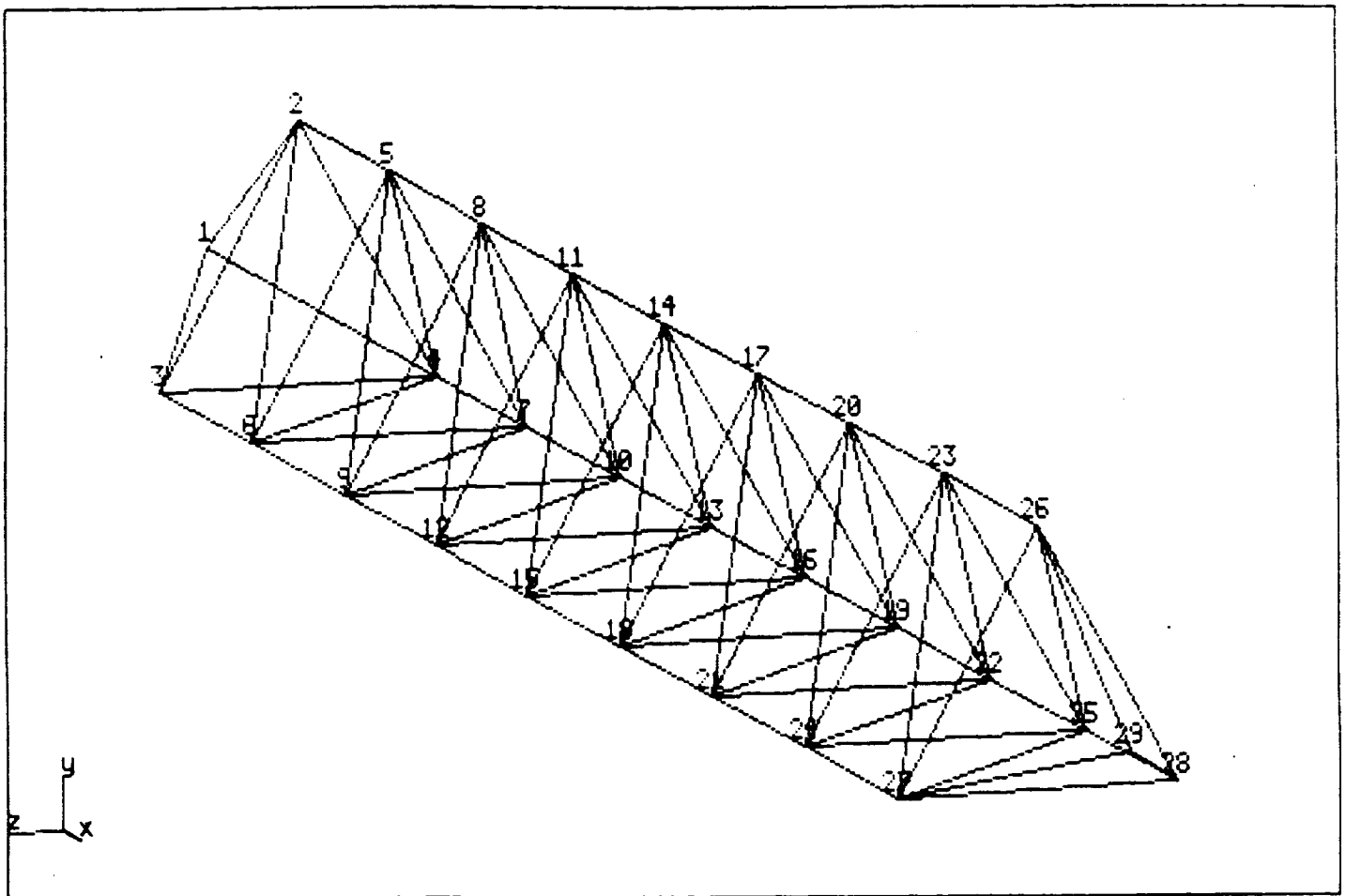
His approach was developed for use with civil structures undergoing seismic (earthquake) excitation--nonuniform enforced base motion. Hence, it did not include the  $f_i(t)$  term on the right-hand side of Equation 3-13. However, it is possible to cast the right-hand side of the equation into a form that looks like the corresponding term in the Beck equation. Thus, conceptually the forces can be treated as though they are a "type" of boundary motion. Thus, with Beck's approach implemented in his computer code MODE-ID, it was straight forward to apply it to the type of problem addressed in this report. (An example of the prior use of his method/code in successfully solving a problem is presented in Appendix F.) In the following part of this section, results are presented from the use of the MODE-ID computer code.

### 5.1 Space Truss Example Problem

The model structure used for determining if the Beck approach could be used for a general type of structure/module that might be used in space is pictured in Figure 5.1. Its first two global mode shapes are given in Figure 5.2. The module selected for use in the investigation was defined using Node Points 8 through 22 (see Figure 5.3). The boundary points are Node Points 8, 9, 10 and 20, 21, 22. The structure was excited by applying forces at Node Points 11 and 14 and in the y-direction. They were independent of each other and random/transient traces.

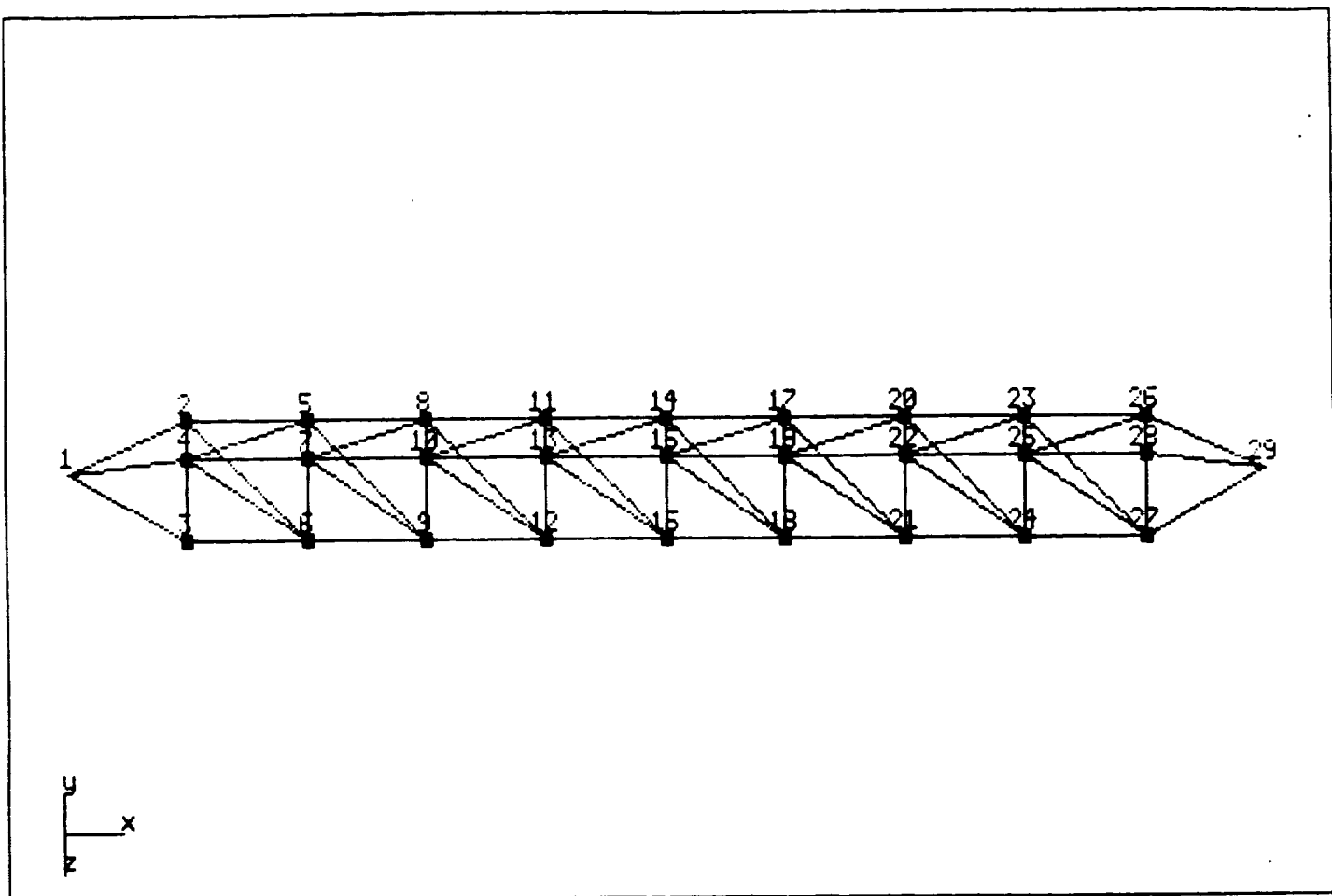
The first identification performed was that of the global system. For this there were no boundary motions--Node Points 1 and 29 were fixed (constrained from movement) for the entire study. It was possible to use MODE-ID to correctly identify the lower global modes. This effort was





a) View 1

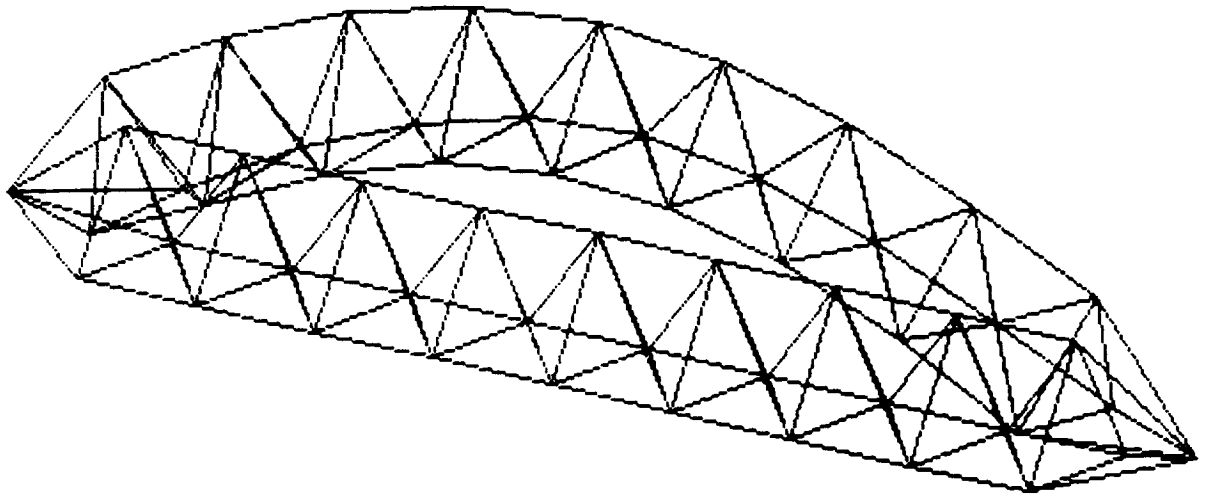
Figure 5.1: Model Structure--COFSMAST



b) View 2

Figure 5.1 (concluded)

MODE:1

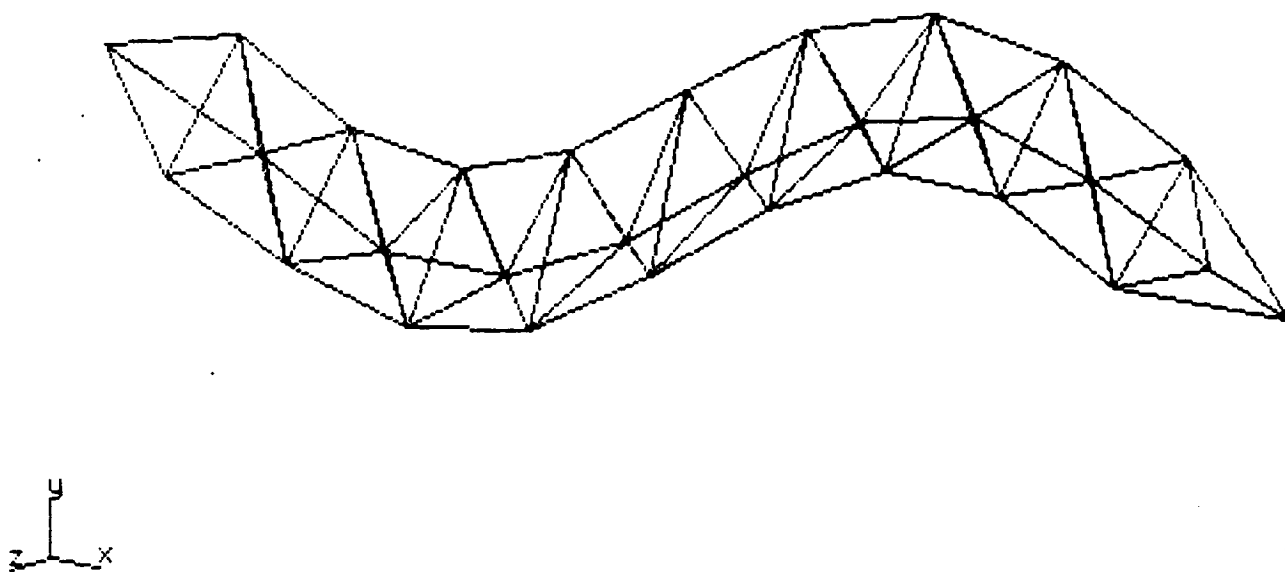


a) First Mode

Figure 5.2: COFSMAST Global Mode Shapes

MODE:2

1



b) Second Mode

Figure 5.2 (concluded)

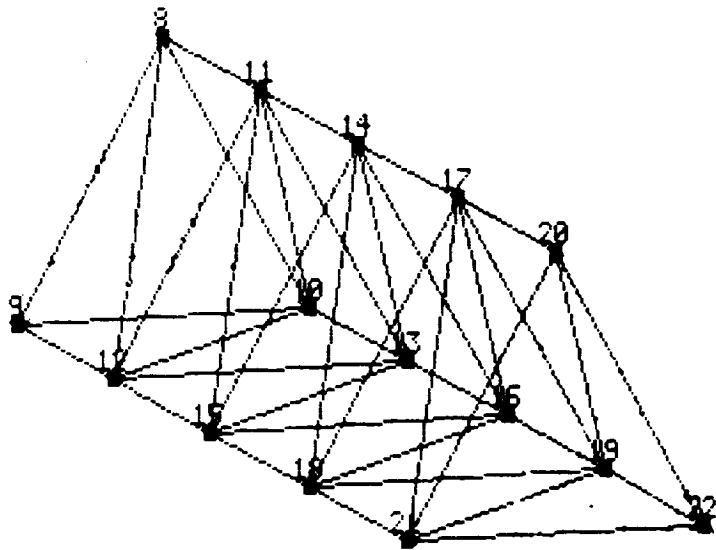


Figure 5.3: COFSMAST Module Studied

performed just to verify that MODE-ID could correctly handle forces applied to the module interior.

The next effort was to determine the fixed boundary undamaged module modal properties using MODE-ID. The problem inputs were the twelve boundary motions and two applied forces. The problem outputs were chosen to be the motions at Node Points 11, 14, 16 and 17 in the y-direction. Simplistically, the program estimates the pseudostatic influence matrix,

$$P = -K_{ii}^{-1}K_{ib} \quad (5-1)$$

which relates the pseudostatic part of the module response to the boundary motions by

$$s_i = Px_b \quad (5-2)$$

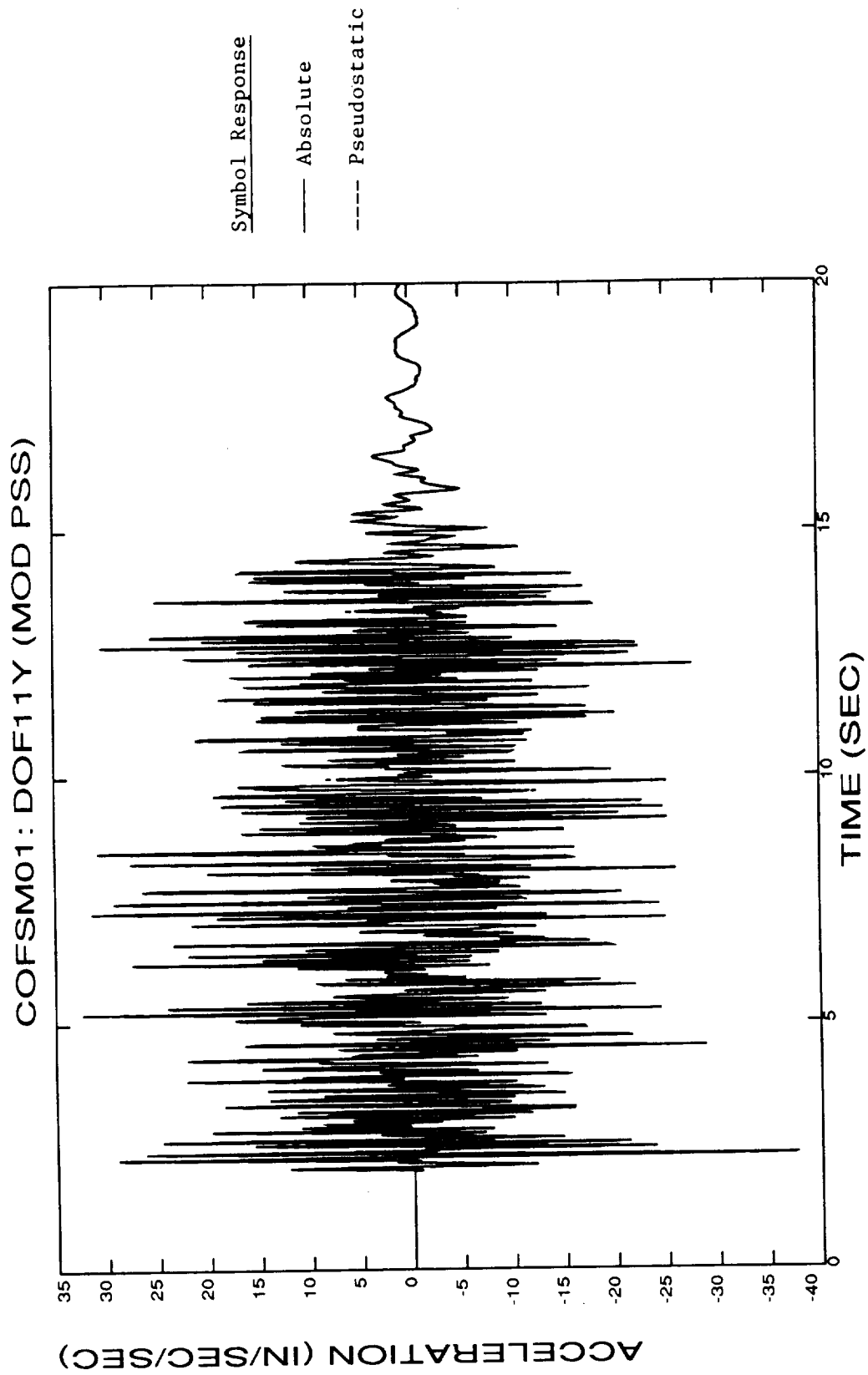
Once this is done the "dynamic" response (relative response) of the module is found from

$$r_i = x_i - s_i \quad (5-3)$$

With this information, the fixed boundary module modal properties are determined. Actually, this is an iterative parameter estimation process which alternates between updating the pseudostatic matrix estimates and the modal parameter estimates.

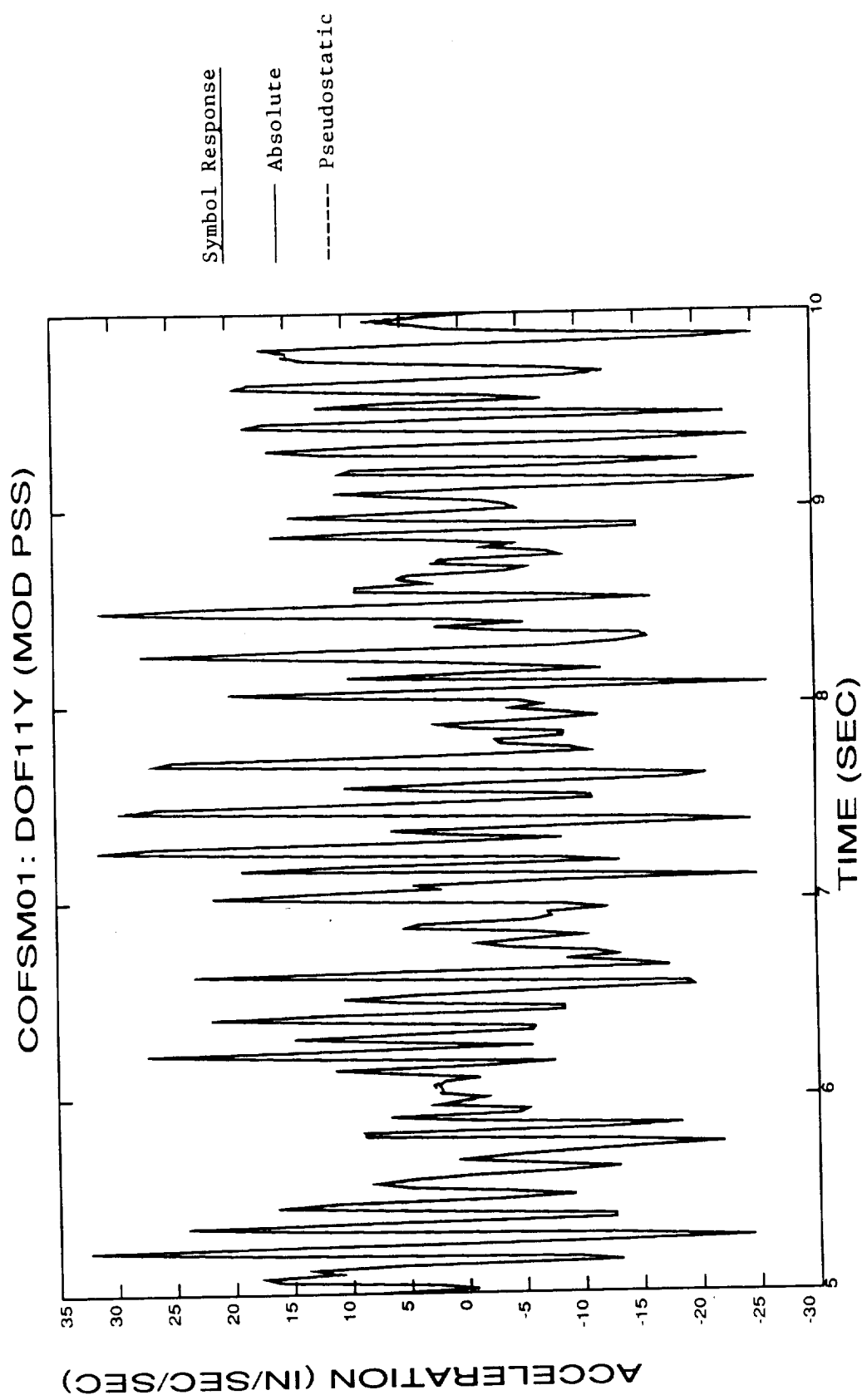
During the first MODE-ID iteration, the pseudostatic influence matrix determination resulted in almost a perfect match between the pseudostatic part of the response of the module and the absolute module response (see Figure 5.4). Thus, the relative response determined was essentially zero. This mode is impossible to determine the fixed-boundary module modal properties. It was found that the identified pseudostatic influence matrix was very different from that determined from the numerical model--the identified influence matrix did not just represent the static properties of the structure. This came about because of the large number of boundary motions being related to each other through the dynamics of the global system.

To show how different the two pseudostatic influence matrices were, the corresponding pseudostatic module responses were plotted in Figure 5.5. As



a) Node 11, y-direction, 0 to 20 seconds.

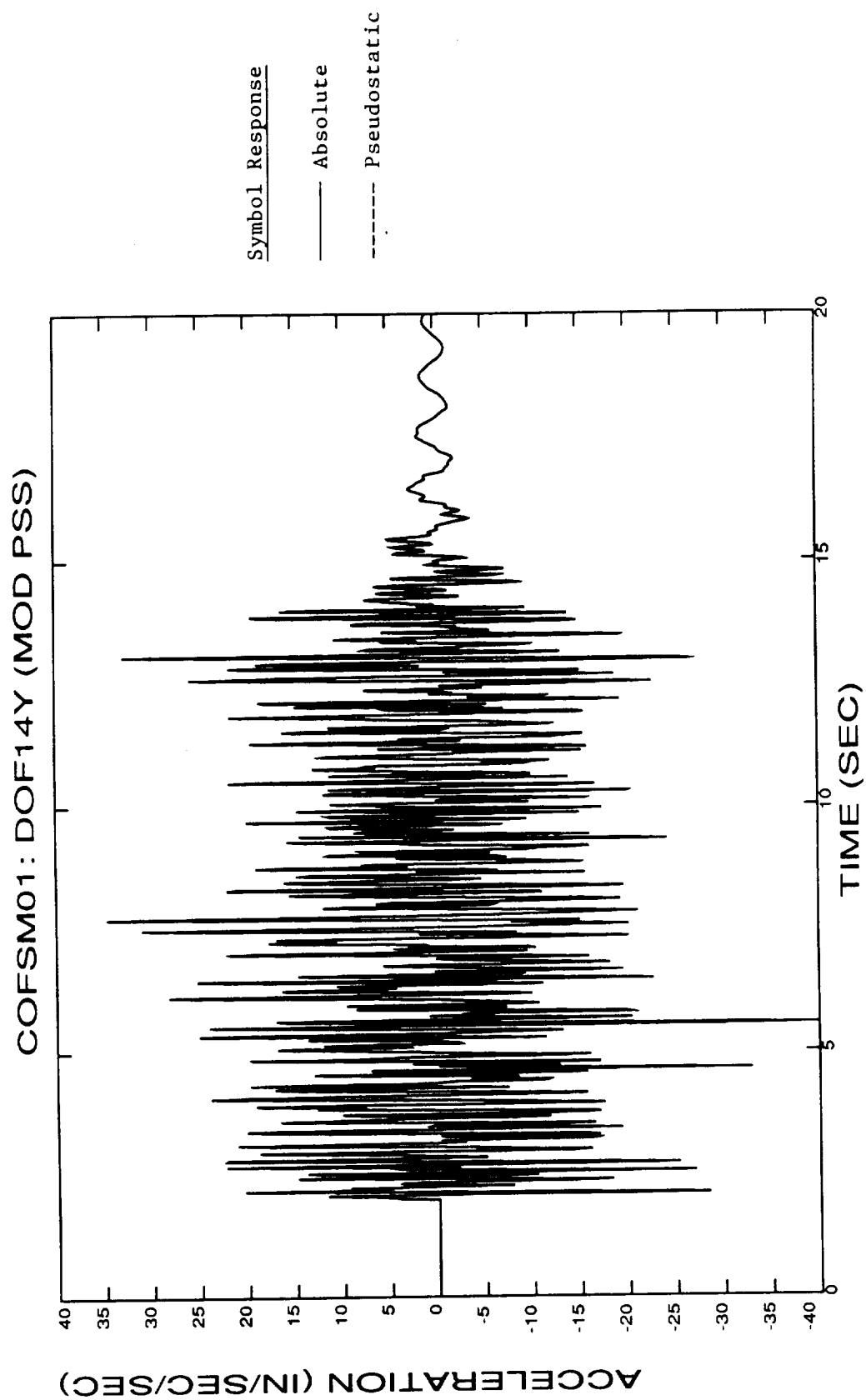
Figure 5.4: Comparison Between Absolute and Identified Pseudostatic Module Responses



b) Node 11, y-direction, 5 to 10 seconds.

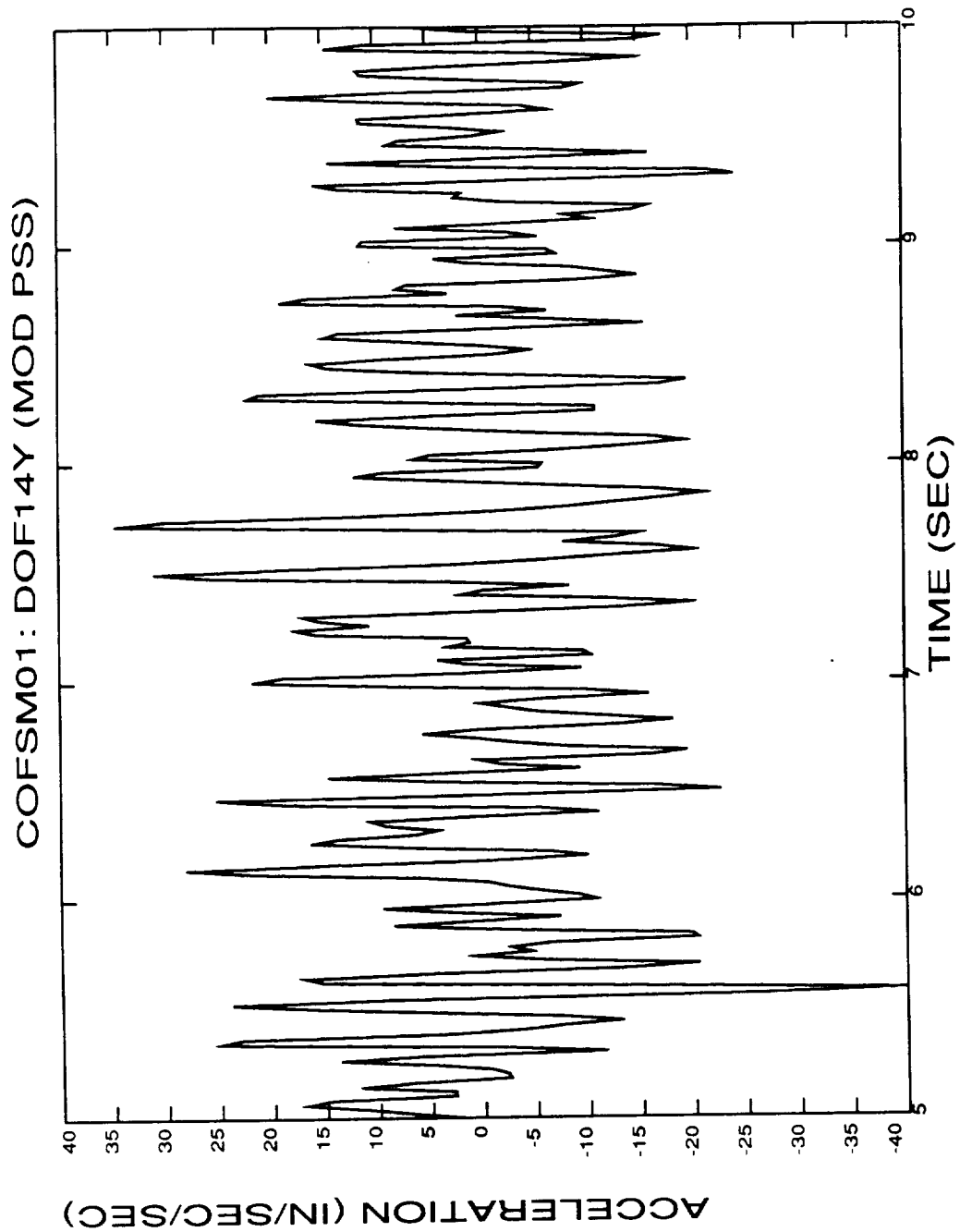
Figure 5.4 (continued)





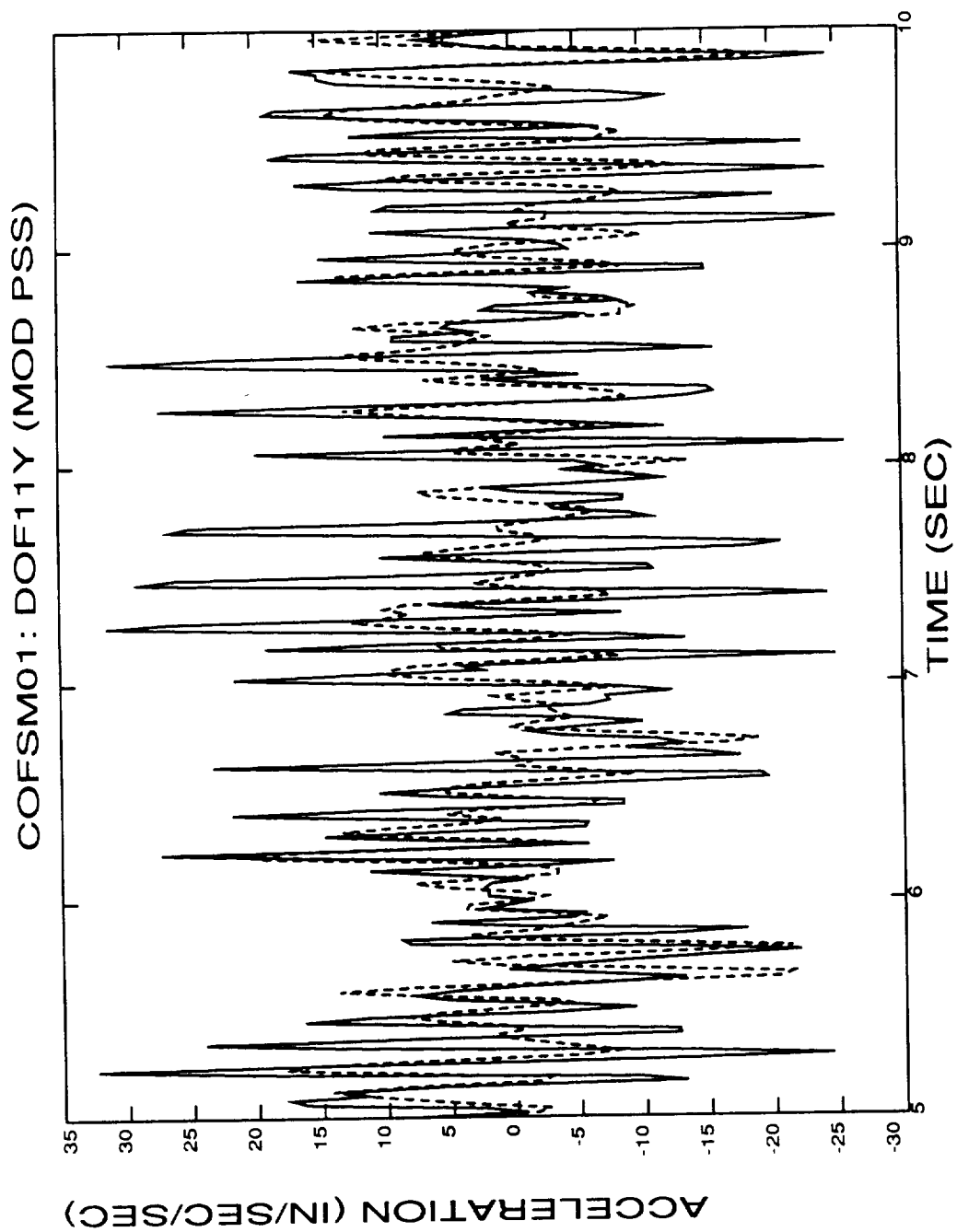
c) Node 14, y-direction, 0 to 20 seconds.

Figure 5.4 (continued)



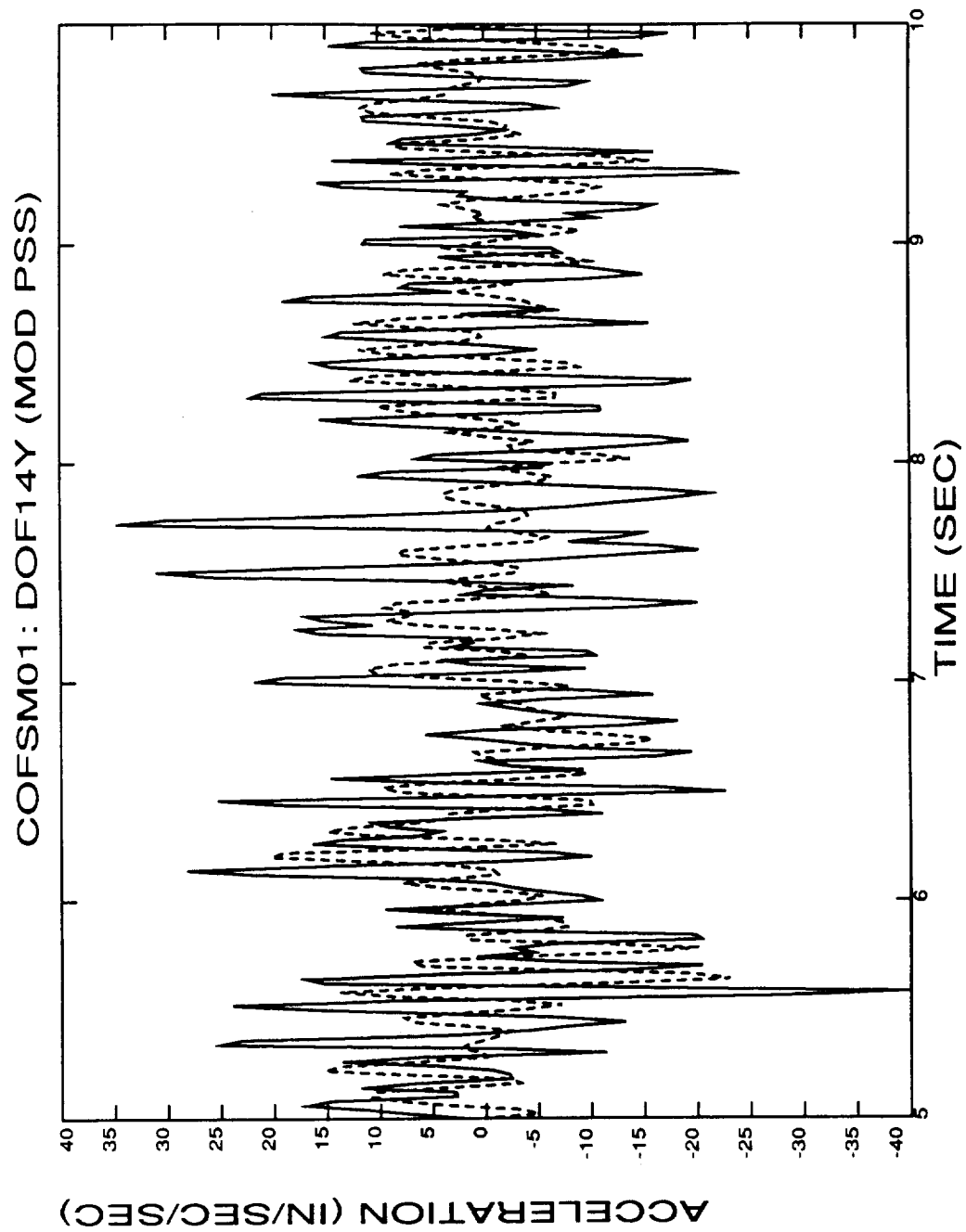
d) Node 14, y-direction, 5 to 10 seconds.

Figure 5.4 (concluded)



a) Node 11, y-direction.

Figure 5.5: Comparison of Module Pseudostatic Response for Identified and Actual Pseudostatic Influence Matrices



b) Node 14, y-direction.

Figure 5.5 (concluded)

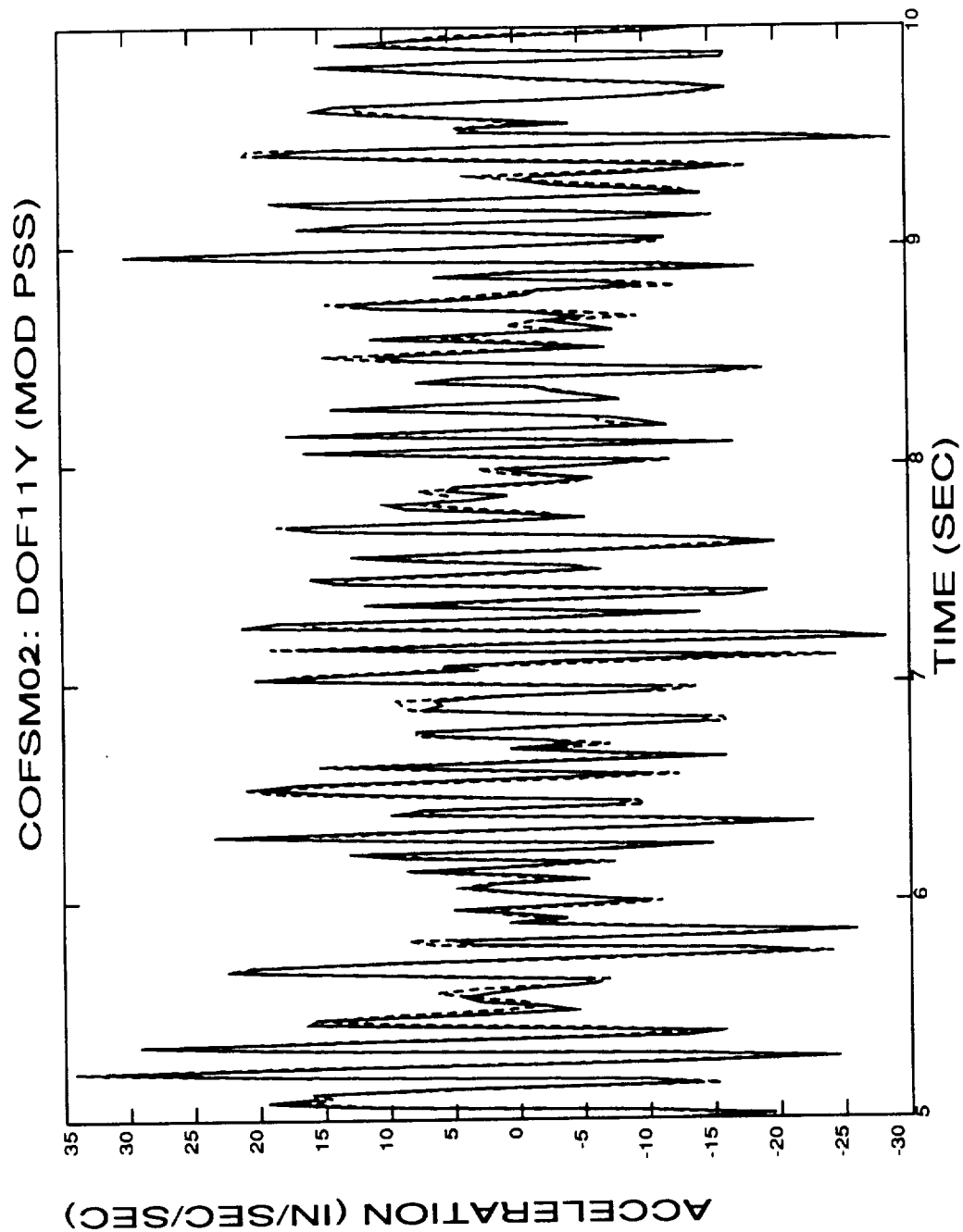
can be seen, the two pseudostatic responses are very different. What will tend to happen when this approach is used to identify modes of modules like the one being studied, is that because of the relationship of the motion of the many boundary points through the dynamics of the global system, the identified pseudostatic module response will be able to match the absolute response close enough so that the module modal properties will not be determinable. This is discussed further in Appendix F. Also, it is seen in the example problem below involving damage of the structure.

The global system was damaged only outside of the module. Then the structure was excited in exactly the same way as before. The module modal identification was performed using MODE-ID. Comparisons were made between the pseudostatic and absolute module responses as before (see Figure 5.6). The two responses were in good agreement, although not as closely as before, however, the module modal properties could not be determined because the identified "pseudostatic" response actually incorporated most of the module's dynamic response.

It should be pointed out that the module modal identification method implemented in MODE-ID works well for those cases where the modes to be identified have motions local to the module--the modes motion is contained largely within the module. The example presented in Appendix F fits into this category. Even though the global system was the earth down to bedrock and the bridge, the bridge elastic modes had their relative motion largely contained within the domain of the bridge.

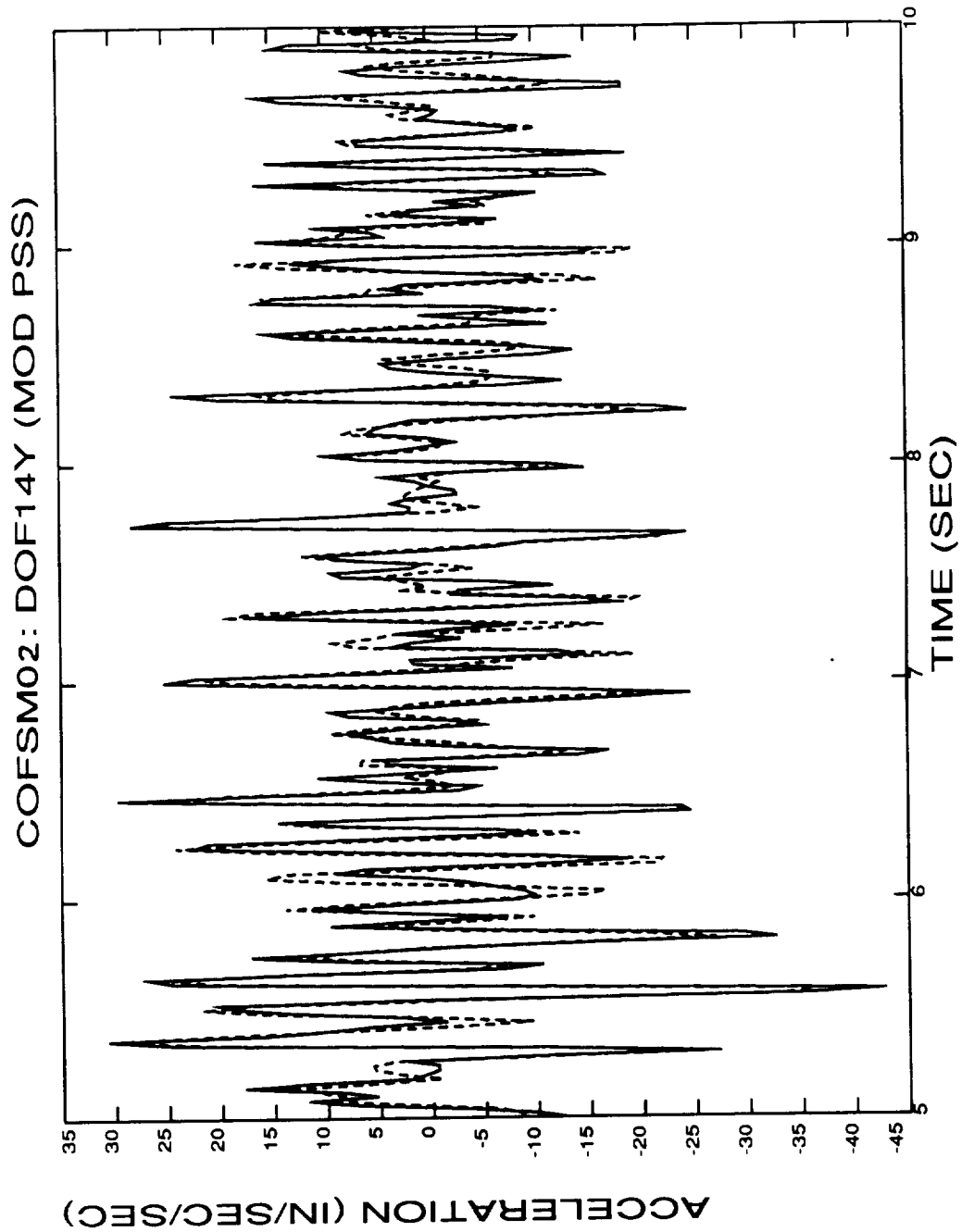
## 5.2 References

1. J.L. Beck, "Determining Models of Structures From Earthquake Records," Report No. EERL 78-01, Earthquake Engineering Research Laboratory, California Institute of Technology, Pasadena, California, 1978.
2. S.D. Werner, J.L. Beck and M.B. Levine, "Seismic Response Evaluation of Meloland Road Overpass Using 1979 Imperial Valley Earthquake Records," Earthquake Engineering and Structural Dynamics, Vol. 15, 249-274 (1987), John Wiley & Sons, Ltd., 1987.



a) Node 11, y-direction.

Figure 5.6: Comparison Between Absolute and Identified Pseudostatic Module Responses--Damaged Case



b) Node 14, y-direction.

Figure 5.6 (concluded)

## 6.0 MODAL STRAIN ENERGY DISTRIBUTION METHOD

One of the methods used to locate module damage, which was investigated and developed during the Phase I effort, is the "modal strain energy distribution method" (MSEDM) [1]. This method uses the previously developed damage indicators to establish which modes have been effected by the structural damage. Those modes which have not been effected very much or at all are used to establish where the damage can only be. The following material consists of 1) a review and discussion of the theoretical aspects of the method, 2) an example of the method, and 3) some conclusions.

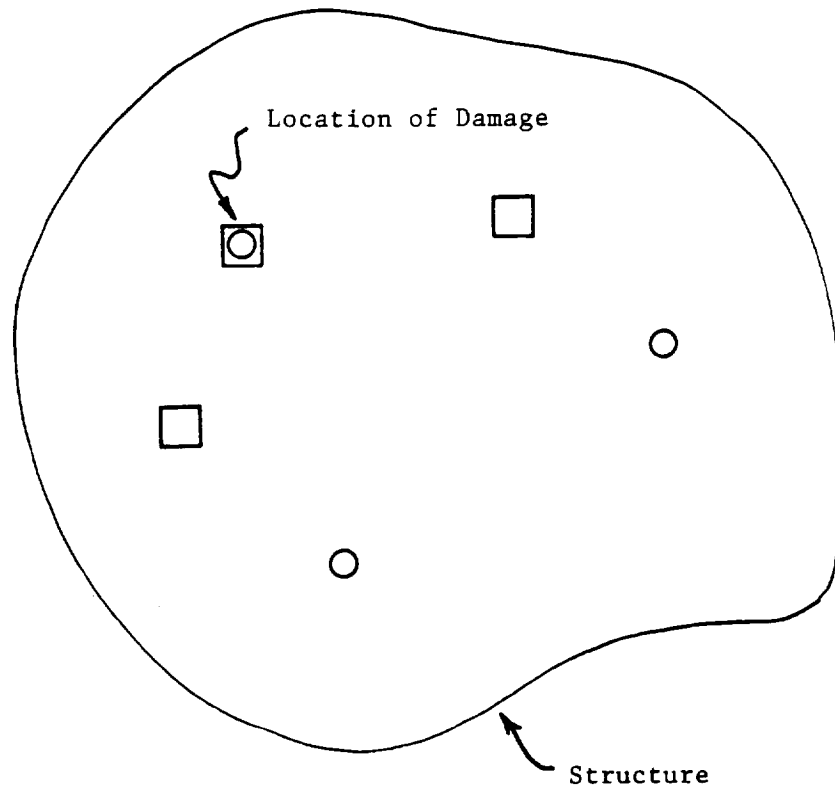
### 6.1 Theoretical Discussion

For this discussion assume that a damage indicator has been selected for determining which modes have been affected, and to what degree, by the damage. To look at the MSEDM, first look at a very simple example. Assume that the damage indicator shows that two modes, a and b, were totally unaffected by the damage. This means that the damage can only be at the locations of zero strain energy for Modes a and b (see Figure 6.1). Some of the points of zero strain energy are taken to be different for the two modes. For this example it is easy to determine the location of damage. For this simple example it was assumed that the two modes were global module modes--they involved motion throughout the module. If they had not, all that could have been said was that the only location the damage could be at in the domain of Modes a and b motion is at the single point indicated in Figure 6.1.

Continuing with this simple example, suppose that the damage indicator shows that Modes a and b have been changed only slightly by the damage. This indicates that there is not a great amount of damage at or near Modes a and b points of maximum strain energy. This is probably true for points of moderate levels of strain energy. However, there could be a sizable amount of damage near points of zero or low strain energy. For this case it is still possible to determine a subdomain which contains the damage somewhere within it (see Figure 6.2).

If the damage level is only "moderate" it is difficult to locate the damage by this method. This is because the damage indicator could have the same amplitude for a mode for moderate-level damage at a high strain energy



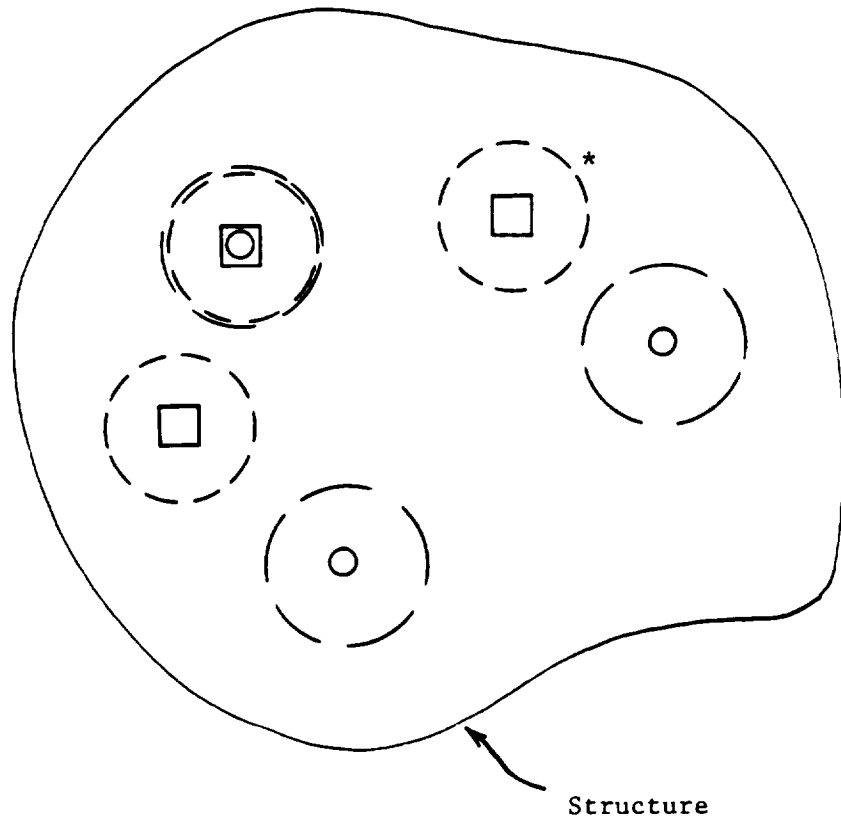


<u>Mode</u>	<u>Zero Strain Energy Point*</u>
a	○
b	□

---

\* The only locations where the damage can be is at the zero strain energy points.

Figure 6.1: Location of Damage Using Zero Strain Energy Points



<u>Mode</u>	<u>Zero Strain Energy Point</u>
a	○
b	□

\* The high-level damage can only be in the domains within the dashed closed curves.

Figure 6.2: Location of High-Level Damage Using Near Zero Strain Energy Points

point as for high-level damage at a point of medium-level strain energy. The analysis could be performed, but the best solution achieved might only be able to indicate a large number of locations, one of which is where the damage is. Because of this, it will be attempted to locate only "high-level" damage using the MSEDm.

Using the above ideas, it is possible to derive a simple expression for the location of high level damage within a module. It is necessary to determine the modal strain energy distribution (as a function of the spatial coordinates, i.e., x, y, z) for the modes of a structure. This can be done best using a finite element model. The procedure followed is to establish for each mode what its damage level is. If it is high-level, then all that can be said is that damage could be everywhere. If the damage indicated is low-level, then any high-level damage must be near or at the zero or low-level strain energy elements.

A low- and high-level cutoff,  $D_j^{c1}$  and  $D_j^{c2}$ , respectively, is defined for the  $j$ th mode. Based on this, the following is defined:

- 1) if  $D(\omega_j) \leq D_j^{c1}$ , all high-level damage is near low-level strain energy points; and
- 2) if  $D(\omega_j) > D_j^{c2}$ , high-level damage could be anywhere, where  $\omega_j$  is the  $j$ th natural frequency.

Next, a set is defined for Mode  $j$  of finite element numbers corresponding to all those elements where there may be high-level damage,  $W_j^d$ .

$$W_j^d = \{E_k | e_{kj} \leq f_j e_j^{\max}\} \quad (6-1)$$

where  $E_k$  = the  $k$ th element number ( $E_k = k$ ).

$e_{kj}$  = the element strain energy for the  $k$ th element and the  $j$ th mode.

$e_j^{\max}$  = the maximum element strain energy for the  $j$ th mode.

$$f_j = \begin{cases} g_j & , D(\omega_j) \leq D_j^{C1} \\ 1 & , D(\omega_j) > D_j^{C2} \end{cases}$$

$g_j$  = a constant factor for the  $j$ th mode.

The solution to the problem of where is the high-level damage located is found by determining the intersection of sets  $W_j^d$ . This can be seen from the following. The solution set,  $I^d$ , is a subset of  $W_j^d$ --

$$I^d \subseteq W_j^d \quad (6-2)$$

From this, it is seen that for the first two modes the solution must lie within the intersection of the two sets  $W_1^d$  and  $W_2^d$  (see Figure 6.3)--

$$I^d \subseteq W_1^d \cap W_2^d$$

The next set,  $W_3^d$ , can be combined with the intersection of the first two sets in the same way. Thus,

$$I^d \subseteq (W_1^d \cap W_2^d) \cap W_3^d$$

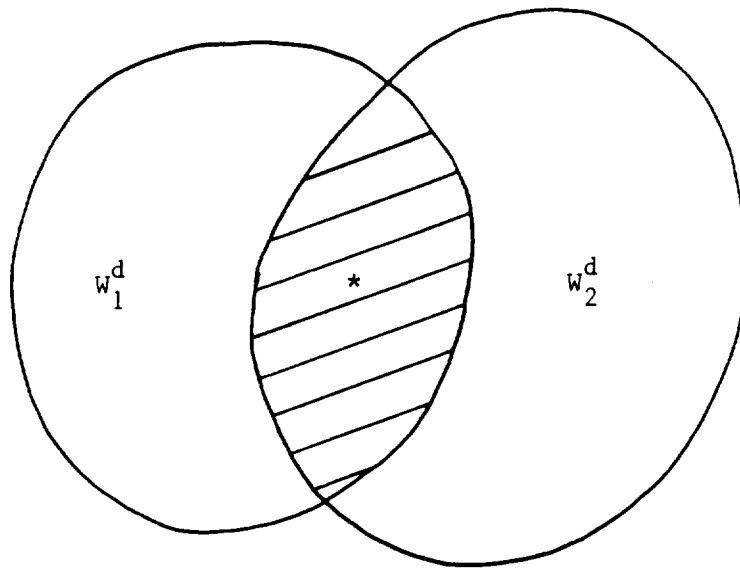
Finally, the solution is found to be

$$I^d = (\dots((W_1^d \cap W_2^d) \cap W_3^d) \cap \dots) \cap W_n^d$$

$$I^d = \bigcap_{j=1}^n W_j^d \quad (6-3)$$

where  $I^d$  = the set of element numbers corresponding to all the elements which were damaged to a high level.

Several things should be noted concerning the solution given by Equation 6-3. The set found will reference all the damaged elements. However, there may be element numbers in the set for which the corresponding elements are not damaged. This problem can be minimized by increasing the number of modes used. Another problem that can arise is when the module



---

\* The intersection of the sets is indicated by the cross-hatched portion.

Figure 6.3: The Intersection of the Sets for Modes One and Two

has a high degree of structural symmetry. This will be looked at in the case study presented herein. Lastly, the values for the  $g_j$  must be selected. This is not a straight forward task. As can be seen, the MSEDm is not purely quantitative. The threshold parameters  $D_j^{ci}$  must be selected in a qualitative/quantitative manner. Questions must be dealt with such as the following:

- 1) how high should the low-level cutoff be so that when the peak damage indicator value for a mode is less than it, that it can be assured that there is not any high-level damage at high-or moderate-level strain energy points for the mode;
- 2) how low should the high-level cut off be so that information is not lost by calling a "low-level peak" (one indicating no high-level damage at high-level strain energy points) a "high-level peak" (one indicating that the damage is so severe that it could be anywhere); and
- 3) how is local damage dealt with for a large variety of possible damage locations--how are the cutoffs dealt with? These issues were dealt with in a simple way for the case study.

## 6.2 Case Study

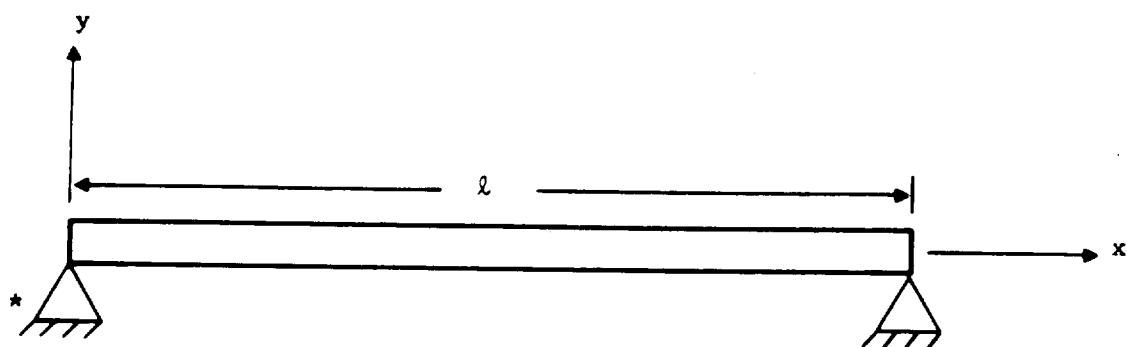
The study discussed in this section involves the numerical analysis of a simply supported uniform straight two-dimensional beam (see Figure 6.4). The modal strain energy distribution,  $e_i$ , for this beam was calculated analytically and is given by

$$e_i(x) = \frac{1}{2} EI \left( \frac{d^2 \phi_i(x)}{dx^2} \right)^2$$

where  $\phi_i(x)$  is the  $i$ th mode.

Once this was done, the beam was partitioned into segments of equal length and the strain energy computed for each one for each mode. These discrete modal energy distributions were used to locate the damage in the beam.

A computer code implementing the MSEDm was developed (described in Appendix G) and used to analyze this problem. The results for two of the damaged conditions are presented below. The first case involved having large damage within only Segment 22. Sixty beam segments were used to define the strain energy distribution (see Appendix H). Twelve modes



---

\* The pinned connection restrains translational motion at the pin, but allows rotational motion in the  $x$ - $y$  plane.

Figure 6.4: Simple Case Study--Uniform Pinned-Pinned Beam

SIMPLY SUPPORTED BEAM  
DAMAGE FILE USED : DAMOUT4.DD  
DAMAGE TITLE : DAMAGE AT N = 0.35 (LARGE)  
NUMBER OF MODES : 12  
NUMBER OF ELEMENTS : 60  
DAMAGE FRACTION : .3500

MODE NO.	MAXIMUM ELEMENT STRAIN ENERGY	ELEMENT NO.
1	1.000E+00	31
2	1.000E+00	45
3	1.000E+00	31
4	1.000E+00	38
5	1.000E+00	31
6	1.000E+00	45
7	1.000E+00	22
8	1.000E+00	34
9	1.000E+00	17
10	1.000E+00	45
11	1.000E+00	25
12	1.000E+00	38

Figure 6.5: MSEDm Applied to Simply Supported Beam--Damage in  
Segment 22, Damage Fraction is 0.35



SIMPLY SUPPORTED BEAM  
 DAMAGE FILE USED : DAMOUT4.DD  
 DAMAGE TITLE : DAMAGE AT N = 0.35 (LARGE)  
 NUMBER OF MODES : 12  
 NUMBER OF ELEMENTS : 60  
 DAMAGE FRACTION : .3500

ELEMENT DAMAGE SUMMARY

ELEMENT NO.	MODE NO.												POSSIBLE DAMAGE
	1	2	3	4	5	6	7	8	9	10	11	12	
1	x	x	x	x	x	x	x	x	x	x	x	x	YES
2	x	x	x	x	x	x	x			x		x	NO
3	x	x	x	x	x		x			x		x	NO
4	x	x	x	x	x		x			x		x	NO
5	x	x		x	x		x			x	x	x	NO
6	x	x		x	x		x		x	x	x	x	NO
7	x	x		x	x		x	x	x	x	x	x	NO
8	x	x		x	x		x	x	x	x		x	NO
9	x	x		x	x	x	x	x		x		x	NO
10	x	x		x	x	x	x			x		x	NO
11	x	x		x	x	x	x			x	x	x	NO
12	x	x		x	x	x	x			x	x	x	NO
13	x	x		x	x		x		x	x		x	NO
14	x	x		x	x		x		x	x		x	NO
15	x	x		x	x		x	x	x	x		x	NO
16	x	x		x	x		x	x		x	x	x	NO
17	x	x	x	x	x		x			x	x	x	NO
18	x	x	x	x	x		x			x		x	NO
19	x	x	x	x	x	x	x			x		x	NO
20	x	x	x	x	x	x	x		x	x		x	NO
21	x	x	x	x	x	x	x		x	x		x	NO
22	x	x	x	x	x	x	x	x		x	x	x	NO
23	x	x	x	x	x		x	x		x	x	x	NO
24	x	x	x	x	x		x	x		x		x	NO
25	x	x		x	x		x			x		x	NO
26	x	x		x	x		x		x	x		x	NO
27	x	x		x	x		x		x	x	x	x	NO
28	x	x		x	x		x		x	x	x	x	NO
29	x	x		x	x	x	x			x		x	NO
30	x	x		x	x	x	x	x		x		x	NO
31	x	x		x	x	x	x	x		x		x	NO
32	x	x		x	x	x	x			x		x	NO
33	x	x		x	x		x		x	x	x	x	NO
34	x	x		x	x		x		x	x	x	x	NO
35	x	x		x	x		x		x	x		x	NO
36	x	x		x	x		x			x		x	NO
37	x	x	x	x	x		x	x		x		x	NO
38	x	x	x	x	x		x	x		x	x	x	NO
39	x	x	x	x	x	x	x	x		x	x	x	NO
40	x	x	x	x	x	x	x		x	x		x	NO

x indicates possible modal element damage

Figure 6.5 (continued)

SIMPLY SUPPORTED BEAM  
 DAMAGE FILE USED : DAMOUT4.DD  
 DAMAGE TITLE : DAMAGE AT N = 0.35 (LARGE)  
 NUMBER OF MODES : 12  
 NUMBER OF ELEMENTS : 60  
 DAMAGE FRACTION : .3500

Page 3 of 3

# ELEMENT DAMAGE SUMMARY

ELEMENT NO.	MODE NO.												POSSIBLE DAMAGE
	1	2	3	4	5	6	7	8	9	10	11	12	
41	x	x	x	x	x	x	x		x	x		x	NO
42	x	x	x	x	x	x	x			x		x	NO
43	x	x	x	x	x		x			x		x	NO
44	x	x	x	x	x		x			x	x	x	NO
45	x	x		x	x		x	x		x	x	x	NO
46	x	x		x	x		x	x	x	x		x	NO
47	x	x		x	x		x		x	x		x	NO
48	x	x		x	x		x		x	x		x	NO
49	x	x		x	x	x	x			x	x	x	NO
50	x	x		x	x	x	x			x	x	x	NO
51	x	x		x	x	x	x			x		x	NO
52	x	x		x	x	x	x	x		x		x	NO
53	x	x		x	x		x	x	x	x		x	NO
54	x	x		x	x		x	x	x	x	x	x	NO
55	x	x		x	x		x		x	x	x	x	NO
56	x	x		x	x		x			x	x	x	NO
57	x	x	x	x	x		x			x		x	NO
58	x	x	x	x	x		x			x		x	NO
59	x	x	x	x	x	x	x			x		x	NO
60	x	x	x	x	x	x	x	x	x	x	x	x	YES

x indicates possible modal element damage

Figure 6.5 (concluded)

were used to represent the beam motion. Only one cutoff was used with the damage indicator--the low-and high-level cutoffs were taken to be equal. Also, the constant factor  $g_j$  was taken to be the same for all modes (called "damage fraction" in the computer code). Figure 6.5 is an output listing for a damage fraction of 0.35. It is indicated that there may be damage in Segments 1 and 60. This occurred because the beam end segments saw virtually no bending. This lead to there being essentially no strain energy in these segments for all the modes. Thus, these two element numbers appeared in all of the sets  $W_j^d$ . Thus, they were in the intersection of the sets  $W_j^d$ . This is a problem with the MSEDm--damage will always be predicted to be at locations where the modal strain energy is zero for all modes.

Eliminating the beam end segments from consideration, it is seen that no solution was determined for  $g_j = g = 0.35$ . It was decided to try to obtain a solution for  $g = 0.45$ . The results are given in Figure 6.6. As can be seen the solution indicates that there is damage in Segment 22. This result is correct, however, damage is also indicated to be in Element 39. This occurred because of the symmetry in the problem. There appears to be no resolution to this problem. For modules that are not highly symmetrical, this problem may not occur. Omitting the two problems just discussed, it appears that the MSEDm is reasonably accurate.

Another case was looked at with damage in two locations--damage in Segments 15 and 30. The results are given in Figure 6.7. The results are similar to those obtained for the previous case--the damage was located, however, undamaged locations were obtained also.

### 6.3 References

1. "Providing Structural Modules With Self-Integrity Monitoring," ANCO Engineers, Inc., final report to NASA, Number 1311.05, May 1985.

SIMPLY SUPPORTED BEAM  
DAMAGE FILE USED : DAMOUT4.DD  
DAMAGE TITLE : DAMAGE AT N = 0.35 (LARGE)  
NUMBER OF MODES : 12  
NUMBER OF ELEMENTS : 60  
DAMAGE FRACTION : .4500

Page 1 of 3

MODE NO.	MAXIMUM ELEMENT STRAIN ENERGY	ELEMENT NO.
1	1.000E+00	31
2	1.000E+00	45
3	1.000E+00	31
4	1.000E+00	38
5	1.000E+00	31
6	1.000E+00	45
7	1.000E+00	22
8	1.000E+00	34
9	1.000E+00	17
10	1.000E+00	45
11	1.000E+00	25
12	1.000E+00	38

Figure 6.6: MSDEM Applied to Simply Supported Beam--Damage in  
Section 22, Damage Fraction is 0.45

SIMPLY SUPPORTED BEAM  
 DAMAGE FILE USED : DAMOUT4.DD  
 DAMAGE TITLE : DAMAGE AT N = 0.35 (LARGE)  
 NUMBER OF MODES : 12  
 NUMBER OF ELEMENTS : 40  
 DAMAGE FRACTION : .4500

ELEMENT DAMAGE SUMMARY

ELEMENT NO.	MODE NO.												POSSIBLE DAMAGE
	1	2	3	4	5	6	7	8	9	10	11	12	
1	x	x	x	x	x	x	x	x	x	x	x	x	YES
2	x	x	x	x	x	x	x	x	x	x		x	NO
3	x	x	x	x	x		x			x		x	NO
4	x	x	x	x	x		x			x		x	NO
5	x	x	x	x	x		x			x	x	x	NO
6	x	x		x	x		x		x	x	x	x	NO
7	x	x		x	x		x	x	x	x	x	x	NO
8	x	x		x	x		x	x	x	x		x	NO
9	x	x		x	x	x	x	x		x		x	NO
10	x	x		x	x	x	x			x		x	NO
11	x	x		x	x	x	x			x	x	x	NO
12	x	x		x	x	x	x			x	x	x	NO
13	x	x		x	x		x		x	x		x	NO
14	x	x		x	x		x	x	x	x		x	NO
15	x	x		x	x		x	x	x	x		x	NO
16	x	x	x	x	x		x	x		x	x	x	NO
17	x	x	x	x	x		x	x		x	x	x	NO
18	x	x	x	x	x		x			x	x	x	NO
19	x	x	x	x	x	x	x		x	x		x	NO
20	x	x	x	x	x	x	x		x	x		x	NO
21	x	x	x	x	x	x	x		x	x		x	NO
22	x	x	x	x	x	x	x	x	x	x	x	x	YES
23	x	x	x	x	x		x	x		x	x	x	NO
24	x	x	x	x	x		x	x		x		x	NO
25	x	x	x	x	x		x			x		x	NO
26	x	x		x	x		x		x	x		x	NO
27	x	x		x	x		x		x	x	x	x	NO
28	x	x		x	x		x		x	x	x	x	NO
29	x	x		x	x	x	x	x		x	x	x	NO
30	x	x		x	x	x	x	x		x		x	NO
31	x	x		x	x	x	x	x		x		x	NO
32	x	x		x	x	x	x	x		x	x	x	NO
33	x	x		x	x		x		x	x	x	x	NO
34	x	x		x	x		x		x	x	x	x	NO
35	x	x		x	x		x		x	x		x	NO
36	x	x	x	x	x		x			x		x	NO
37	x	x	x	x	x		x	x		x		x	NO
38	x	x	x	x	x		x	x		x	x	x	NO
39	x	x	x	x	x	x	x	x	x	x	x	x	YES
40	x	x	x	x	x	x	x		x	x		x	NO

x indicates possible modal element damage

Figure 6.6 (continued)

SIMPLY SUPPORTED BEAM  
 DAMAGE FILE USED : DAMOUT4.DD  
 DAMAGE TITLE : DAMAGE AT N = 0.35 (LARGE)  
 NUMBER OF MODES : 12  
 NUMBER OF ELEMENTS : 60  
 DAMAGE FRACTION : .4500

ELEMENT DAMAGE SUMMARY

ELEMENT NO.	MODE NO.												POSSIBLE DAMAGE
	1	2	3	4	5	6	7	8	9	10	11	12	
41	x	x	x	x	x	x	x		x	x		x	NO
42	x	x	x	x	x	x	x		x	x		x	NO
43	x	x	x	x	x		x			x	x	x	NO
44	x	x	x	x	x		x	x		x	x	x	NO
45	x	x	x	x	x		x	x		x	x	x	NO
46	x	x		x	x		x	x	x	x		x	NO
47	x	x		x	x		x	x	x	x		x	NO
48	x	x		x	x		x		x	x		x	NO
49	x	x		x	x	x	x			x	x	x	NO
50	x	x		x	x	x	x			x	x	x	NO
51	x	x		x	x	x	x			x		x	NO
52	x	x		x	x	x	x	x		x		x	NO
53	x	x		x	x		x	x	x	x		x	NO
54	x	x		x	x		x	x	x	x	x	x	NO
55	x	x		x	x		x		x	x	x	x	NO
56	x	x	x	x	x		x			x	x	x	NO
57	x	x	x	x	x		x			x		x	NO
58	x	x	x	x	x		x			x		x	NO
59	x	x	x	x	x	x	x	x	x	x		x	NO
60	x	x	x	x	x	x	x	x	x	x	x	x	YES

x indicates possible modal element damage

Figure 6.6 (concluded)

## SIMPLY SUPPORTED BEAM

Page 1 of 3

DAMAGE FILE USED : DAMOUT3.DD

DAMAGE TITLE : DAMAGE AT N = 0.25 AND AT N = 0.5

NUMBER OF MODES : 12

NUMBER OF ELEMENTS : 60

DAMAGE FRACTION : .4000

MODE NO.	MAXIMUM ELEMENT STRAIN ENERGY	ELEMENT NO.
1	1.000E+00	31
2	1.000E+00	45
3	1.000E+00	31
4	1.000E+00	38
5	1.000E+00	31
6	1.000E+00	45
7	1.000E+00	22
8	1.000E+00	34
9	1.000E+00	17
10	1.000E+00	45
11	1.000E+00	25
12	1.000E+00	38

Figure 6.7: MSDEM Applied to Simply Supported Beam--Damage in Segments 15 and 30, Damage Fraction is 0.40

## SIMPLY SUPPORTED BEAM

Page 2 of 3

DAMAGE FILE USED : DAMOUT3.DD

DAMAGE TITLE : DAMAGE AT N = 0.25 AND AT N = 0.5

NUMBER OF MODES : 12

NUMBER OF ELEMENTS : 60

DAMAGE FRACTION : .4000

## ELEMENT DAMAGE SUMMARY

ELEMENT NO.	MODE NO.												POSSIBLE DAMAGE
	1	2	3	4	5	6	7	8	9	10	11	12	
1	x	x	x	x	x	x	x	x	x	x	x	x	YES
2	x	x	x	x	x	x	x	x	x	x	x		NO
3	x	x	x	x	x	x	x		x	x	x		NO
4	x	x	x		x	x	x		x	x	x		NO
5	x	x	x		x	x	x		x	x	x	x	NO
6	x	x	x		x	x	x		x	x	x	x	NO
7	x	x	x		x	x	x	x	x	x	x		NO
8	x	x	x		x	x	x	x	x	x	x		NO
9	x	x	x		x	x	x	x	x	x	x		NO
10	x	x	x		x	x	x		x	x	x	x	NO
11	x	x	x		x	x	x		x	x	x	x	NO
12	x	x	x		x	x	x		x	x	x		NO
13	x	x	x	x	x	x	x		x	x	x		NO
14	x	x	x	x	x	x	x	x	x	x	x		NO
15	x	x	x	x	x	x	x	x	x	x	x	x	YES
16	x	x	x	x	x	x	x	x	x	x	x	x	YES
17	x	x	x	x	x	x	x	x	x	x	x		NO
18	x	x	x	x	x	x	x		x	x	x		NO
19	x	x	x		x	x	x		x	x	x		NO
20	x	x	x		x	x	x		x	x	x	x	NO
21	x	x	x		x	x	x		x	x	x	x	NO
22	x	x	x		x	x	x	x	x	x	x		NO
23	x	x	x		x	x	x	x	x	x	x		NO
24	x	x	x		x	x	x	x	x	x	x		NO
25	x	x	x		x	x	x		x	x	x	x	NO
26	x	x	x		x	x	x		x	x	x	x	NO
27	x	x	x		x	x	x		x	x	x		NO
28	x	x	x	x	x	x	x		x	x	x		NO
29	x	x	x	x	x	x	x	x	x	x	x		NO
30	x	x	x	x	x	x	x	x	x	x	x	x	YES
31	x	x	x	x	x	x	x	x	x	x	x	x	YES
32	x	x	x	x	x	x	x	x	x	x	x		NO
33	x	x	x	x	x	x	x		x	x	x		NO
34	x	x	x		x	x	x		x	x	x		NO
35	x	x	x		x	x	x		x	x	x	x	NO
36	x	x	x		x	x	x		x	x	x	x	NO
37	x	x	x		x	x	x	x	x	x	x		NO
38	x	x	x		x	x	x	x	x	x	x		NO
39	x	x	x		x	x	x	x	x	x	x		NO
40	x	x	x		x	x	x		x	x	x	x	NO

\* indicates possible modal element damage

Figure 6.7 (continued)



SIMPLY SUPPORTED BEAM  
 DAMAGE FILE USED : DAMOUT3.DD  
 DAMAGE TITLE : DAMAGE AT N = 0.25 AND AT N = 0.5  
 NUMBER OF MODES : 12  
 NUMBER OF ELEMENTS : 60  
 DAMAGE FRACTION : .4000

Page 3 of 3

# ELEMENT DAMAGE SUMMARY

ELEMENT NO.	MODE NO.												POSSIBLE DAMAGE
	1	2	3	4	5	6	7	8	9	10	11	12	
41	x	x	x		x	x	x		x	x	x	x	NO
42	x	x	x		x	x	x		x	x	x		NO
43	x	x	x	x	x	x	x		x	x	x		NO
44	x	x	x	x	x	x	x	x	x	x	x		NO
45	x	x	x	x	x	x	x	x	x	x	x	x	YES
46	x	x	x	x	x	x	x	x	x	x	x	x	YES
47	x	x	x	x	x	x	x	x	x	x	x		NO
48	x	x	x	x	x	x	x		x	x	x		NO
49	x	x	x		x	x	x		x	x	x		NO
50	x	x	x		x	x	x		x	x	x	x	NO
51	x	x	x		x	x	x		x	x	x	x	NO
52	x	x	x		x	x	x	x	x	x	x		NO
53	x	x	x		x	x	x	x	x	x	x		NO
54	x	x	x		x	x	x	x	x	x	x		NO
55	x	x	x		x	x	x		x	x	x	x	NO
56	x	x	x		x	x	x		x	x	x	x	NO
57	x	x	x		x	x	x		x	x	x		NO
58	x	x	x	x	x	x	x		x	x	x		NO
59	x	x	x	x	x	x	x	x	x	x	x		NO
60	x	x	x	x	x	x	x	x	x	x	x	x	YES

x indicates possible modal element damage

Figure 6.7 (continued)

DAMAGE FILENAME : DAMOUT3.DD  
DAMAGE AT N = 0.25 AND AT N = 0.5  
NUMBER OF MODES : 12

MODE	D(W)	Dcrit(W)
1	100.000	10.000
2	100.000	10.000
3	100.000	10.000
4	1.000	10.000
5	100.000	10.000
6	100.000	10.000
7	100.000	10.000
8	1.000	10.000
9	100.000	10.000
10	100.000	10.000
11	100.000	10.000
12	1.000	10.000

Figure 6.7 (concluded)

## 7.0 SYSTEM IDENTIFICATION AS A METHOD OF LOCATING DAMAGE

System identification, SID, can be used as a tool to help determine if a structure has been damaged, and if so, where. The part of SID that is being referred to here is parameter estimation. In general, a parameter estimation method involves defining an objective function which expresses the difference between the predicted and experimental response of a system. The objective function is dependent only on the parameters ("constants") that are used to define the mathematical model of the system, e.g., thickness and density of plate components. The task is then to minimize the error in the prediction model. This is done by finding the model parameter values that correspond to a minimum extremum of the objective function. Different parameter estimation schemes use various types of objective functions and various methods for finding a minimum of objective function. Part of parameter estimation involves establishing the uncertainty in the experimental data and the uncertainty in the original estimates of the model parameters. Overall, system identification deals with identifying (characterizing) a physical system with a mathematical model using experimental data and one or more system identification analysis procedures [1].

In applying SID to the damage detection problem herein, the responses consist of the elements of the module transfer function matrix. (Of course, they could have been other variables such as the acceleration or strain at internal points of a structural module.) The model parameters are the constants which are used to define the element properties.

The good aspects of this type of approach are (1) the occurrence of damage, the determination of its location, and its extent (quantitative value) are determined, (2) for some cases the damage can be substantial and its quantitative value can still be determined with a reasonable degree of accuracy, and (3) the various basic numerical algorithms associated with this approach are well established and software implementing them can be written in a straight forward manner [2]. The drawbacks to using the method are 1) uniqueness of the solution cannot be assured--there can be other local minima besides the one which is sought, and one of these minima might be found, 2) the algorithms might work well for many different cases (i.e., different structures, damage situations), but for some others they may not

work well, and 3) a considerable amount of numerical effort (large computing times) can be required to find the solution.

The methods selected for implementation here are described in Reference 2. The objective function defined is based on Bayes Theorem. Hence, the method of SID used is called Bayesian Parameter Estimation. The algorithms developed for use in finding a minimum of the objective function is based on the Newton-Raphson minimization algorithm. Various modifications/enhancements can be made to these algorithms which would help in finding the desired minimum [3].

An important part of solving the SID problem is the determination of the sensitivity matrix, S. The elements of it are given by

$$S_{jk} = \partial R_j / \partial P_k \quad (7-1)$$

where  $R_j$  = the  $j$ th model response variable (i.e., an eigenvalue).

$P_k$  = the  $k$ th model parameter.

For this problem the model responses are elements of the module transfer function matrix (MTFM). There are two basic approaches for determining the MTFM; they are 1) "direct"--determine the matrix from the inversion of the power/cross-spectral matrix [4] and 2) "modal approach"--determine the matrix from the module modal parameters. If the former approach is used, the sensitivity matrix would have to be determined using finite differences--determine the MTFM corresponding to at least two different model parameter states and approximate the sensitivities using a finite difference approach to estimating a derivative (i.e., central difference). This method is very computation intensive.

It may be preferable to determine the MTFM from the module modal properties. Given an expression for the MTFM as an explicit function of the module modal properties, it is possible to differentiate it with respect to the model parameters.

$$H_{ij} = H_{ij}(\omega_k, \phi_k, \dots)$$

where  $H_{ij}$  = an element of the MTFM.

$\omega_k = \omega_k(P_l)$  is the  $k$ th module natural frequency.

$\phi_k = \phi_k(P_l)$  is the  $k$ th module mode (a vector).

$P_l$  = the  $l$ th model parameter.

$$\frac{\partial H_{ij}}{\partial P_l} = \sum_k \frac{\partial H_{ij}}{\partial \omega_k} \frac{\partial \omega_k}{\partial P_l} + \sum_{m,k} \frac{\partial H_{ij}}{\partial \phi_{mk}} \frac{\partial \phi_{mk}}{\partial P_l} + \dots \quad (7-2)$$

Also, it can be shown that [5]

$$\frac{\partial \omega_k}{\partial P_l} = \frac{1}{2\omega_k} \phi_k^T \left( \frac{\partial K}{\partial P_l} - \omega_k^2 \frac{\partial M}{\partial P_l} \right) \phi_k \quad (7-3)$$

and [6]

$$(M^{-1}K - \omega_k^2 I) \frac{\partial \phi_k}{\partial P_l} = - \left( \frac{\partial (M^{-1}K)}{\partial P_l} - \frac{\partial \omega_k^2}{\partial P_l} I \right) \phi_k \quad (7-4)$$

Equations 7-3 and 7-4 can be used along with Equation 7-2 to efficiently determine the required sensitivity matrix. In doing this, it is necessary to evaluate the derivative of the global stiffness and mass matrices with respect to each of the model parameters. This can be done using finite differences, perturbation techniques, or by developing an analytical expression for each element matrix and then assemble them to obtain the corresponding global matrix.

In preparation to performing the SID as described above, a simpler SID was performed using the system natural frequencies as the model responses. The system analyzed was a pinned-pinned straight two-dimensional beam. The SID to locate the damage was done using ASTRO/MOVE [5]\*. In its "undamaged" state, the model was a uniform beam. The model was "damaged" by changing the cross-section moment of inertia for a few beam elements. Natural

---

\* ASTRO/MOVE is a linear static and dynamic finite element computer code which can be used to perform nonlinear parameter estimation in an automated manner. It was developed by ANCO Engineers, Inc.

frequencies corresponding to the damaged state were determined--these were called "data". It was then determined, using SID, which elements had their moment of inertia changed ("damaged"). This worked well, as expected--the "damaged" elements were located. A few problems were encountered (it was not surprising), but they were easily dealt with. The kinds of problems encountered will be discussed in general in the recommendations in this section.

The next step taken was to include the system modes with the natural frequencies as making up the model responses. The same problem was rerun. However, even with a great deal of effort it was not possible to obtain any solution--the SID process never converged to a solution. It was concluded that ASTRO/MOVE probably has coding errors in it associated with the mode derivatives with respect to the beam element property constants. At this point the SID process was not investigated further.

Other SID projects have been performed by ANCO where the model responses included natural frequencies, mode components and acceleration response quantities, and the desired results obtained. This was done using a different ANCO SID computer code--NONBAY. However, this code uses the finite difference approach to calculating the response derivatives and is very laborious to use. For this reason, this code was not used to further the research.

Because this later code gave good results it is known that SID can be satisfactorily performed using all modal parameters as model responses. Thus, a SID process using the elements of the MTFM as model response should work well, as long as the usual problems encountered in performing SID can be dealt with adequately.

#### 7.1 A Few Recommendations for Performing System Identification To Detect Damage

There are a great number of recommendation/guidelines and things to be cautious about in performing system identification that could be discussed herein. Many of these are already documented in a variety of papers on SID. The only recommendations discussed herein are those which perhaps have a special bearing on damage detection for complex structures. They are discussed below.

It is important to minimize the number of model parameters. This is a sound practice that should be followed in performing any SID task. However, this is even more important when the structure is very complex, such as the space station. Even if the modular/substructure approach is used, many of the modules could be very complex themselves (hundreds of structural members). For this case it is necessary to use only a few module model parameters relative to the total number of parameters that could be used (hundreds of parameters corresponding to the truss cross-section properties).

One way this can be done is to "divide" a module into substructures. A single stiffness and mass parameter could be defined for each substructure. The stiffness and mass of a substructure would be modified by changing only their respective multiplicative factor, i.e.,

$$K^{(r)} = k_s^{(r)} K_u^{(r)}$$

$$M^{(r)} = k_m^{(r)} M_u^{(r)}$$

where  $K^{(r)}, M^{(r)}$  = the stiffness and mass matrix for the rth substructure, respectively.

$u$  = refers to the undamaged state.

$k_s^{(r)}, k_m^{(r)}$  = rth substructure model parameters corresponding to the stiffness and mass of the substructure, respectively.

Of course it is important to not make the substructures too small or too large.

When the damage level is high (a situation where it would be important to detect it), it may be difficult to find the solution to the problem using system identification--it may be difficult to find the correct local minima. Sometimes a solution may never be found. To minimize this type of problem it is important to have as much information about the module as possible (many natural frequencies as opposed to a few). Also, if any visual observations could be made and broken (badly damaged) members identified, this information could be used in obtaining a solution. Lastly, it may be helpful to extend the convergence domain to minimize any divergence problems [3].

## 7.2 References

1. B.J. Hsieh, C.A. Kot and M.G. Srinivasan, "Evaluation of System Identification Methodology and Application", ANL-83-38, Argonne National Laboratory, May 1983.
2. "Providing Structural Modules With Self-Integrity Monitoring", ANCO Engineers, Inc. Final Report 1311.05 prepared for NASA, May 1985.
3. M. Aoki, "Introduction to Optimization Techniques - Fundamentals And Applications of Nonlinear Programming", The MacMillan Co., New York, 1971.
4. R.K. Otnes and L. Enochson, "Digital Time Series Analysis", John Wiley and Sons, New York, 1972.
5. "ASTRO/MOVE User's Manual", ANCO Engineers, Inc., Culver City, California 90232.
6. R.B. Nelson, "Simplified Calculation of Eigenvector Derivatives", AIAA Journal, Vol. 14, No. 9, September 1976.



## 8.0 SELF-INTEGRITY MONITORING HARDWARE SYSTEM

### 8.1 Functional Requirements

The function of the Self-Integrity Monitoring System is to detect damage that may have occurred to the structure of the Space Station and report its extent and location.

This will be accomplished by sampling vibration signals sensed by accelerometers, comparing their characteristics to previously established parameters and analyzing and reporting differences.

The Data Acquisition and Processing System (DAPS) performs these sampling and analyzing tasks. Its major modules are:

- a. Host Processor System (HPS)
- b. Satellite Processor Systems (SPS)
- c. Inter-Processor Communication Loops (ICL)
- d. Data Acquisition-Signal Conditioning Modules (DASC)
- e. Sensors and Cables
- f. Software

The integration of these hardware and software modules forms the DAPS system. Reporting will be via communications link to an existing Space Station Computer (SSC) system that will provide the DAPS system with astronaut interactive capability. A simplified block diagram of the DAPS architecture is shown in Figure 8.1.

The frequency of the DAPS monitoring cycle has a marked influence on the functional requirements. In addition to data sampling frequency having a direct relationship to power consumption the cyclical heating and cooling of the various structural elements being monitored will dramatically impact the validity of data being received from the sensors unless adequate safeguards are adopted.

Ideally, monitoring should be conducted when the sensors and their associated structural members are exposed to the same environmental heating/cooling that prevailed when the "base-line" readings were obtained. This

# SELF-INTEGRITY MONITORING SYSTEM

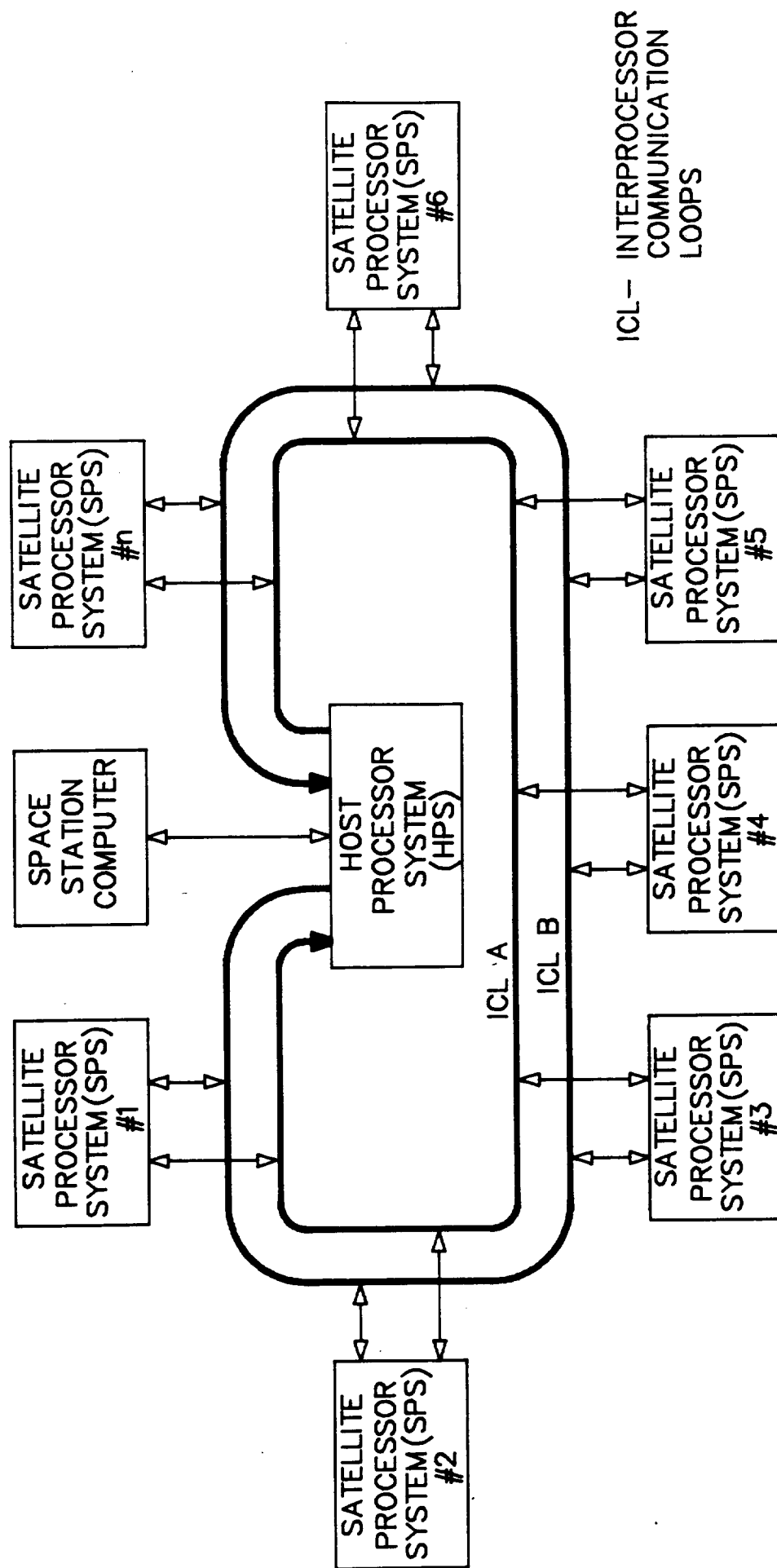


Figure 8.1: Basic DAPS Architecture

can be achieved by arranging for the monitoring cycle to coincide with the orbit and attitude of the Space Station.

Temperature stabilization requirements are examined in detail in Section 8.3.

It has been concluded that to obtain adequate transducer response the Space Station structure will require artificial excitation although initially it was considered possible that the DAPS system might be capable of detecting damage/degradation in the structure by sensing changes in responses to natural stimuli.

Experimentation will be conducted during the design phase to determine the optimum frequency and magnitude of structural excitation that meets both the DAPS requirements and constraints imposed by station operational considerations.

Excitation signals will be generated by the SPS systems and used to modulate power to vibrators mounted on the structure. A special output channel will be necessary in the DASC module to provide this capability.

## 8.2 DAPS Architecture

### 8.2.1 Hardware

Details of a typical HPS-SPS-ICL arrangement are shown in the simplified block diagram Figure 8.2. The basic system design allows one HPS system to support a quantity of SPS systems by multiplexing data over dual communication loops.

A loop configuration has been selected for the satellite communication network, to provide a high degree of reliability to this critical system element. Although a more complex arrangement both from a hardware and software standpoint than the "Star" arrangement originally proposed in the Phase I study, the need for redundancy throughout the DAPS system is manifest and the provision of duplicate hardware in this and other difficult to service system elements is mandatory.

This architecture permits satellites to be polled from either end of the loop so that the system may continue to operate effectively in the

# SELF-INTEGRITY MONITORING SYSTEM

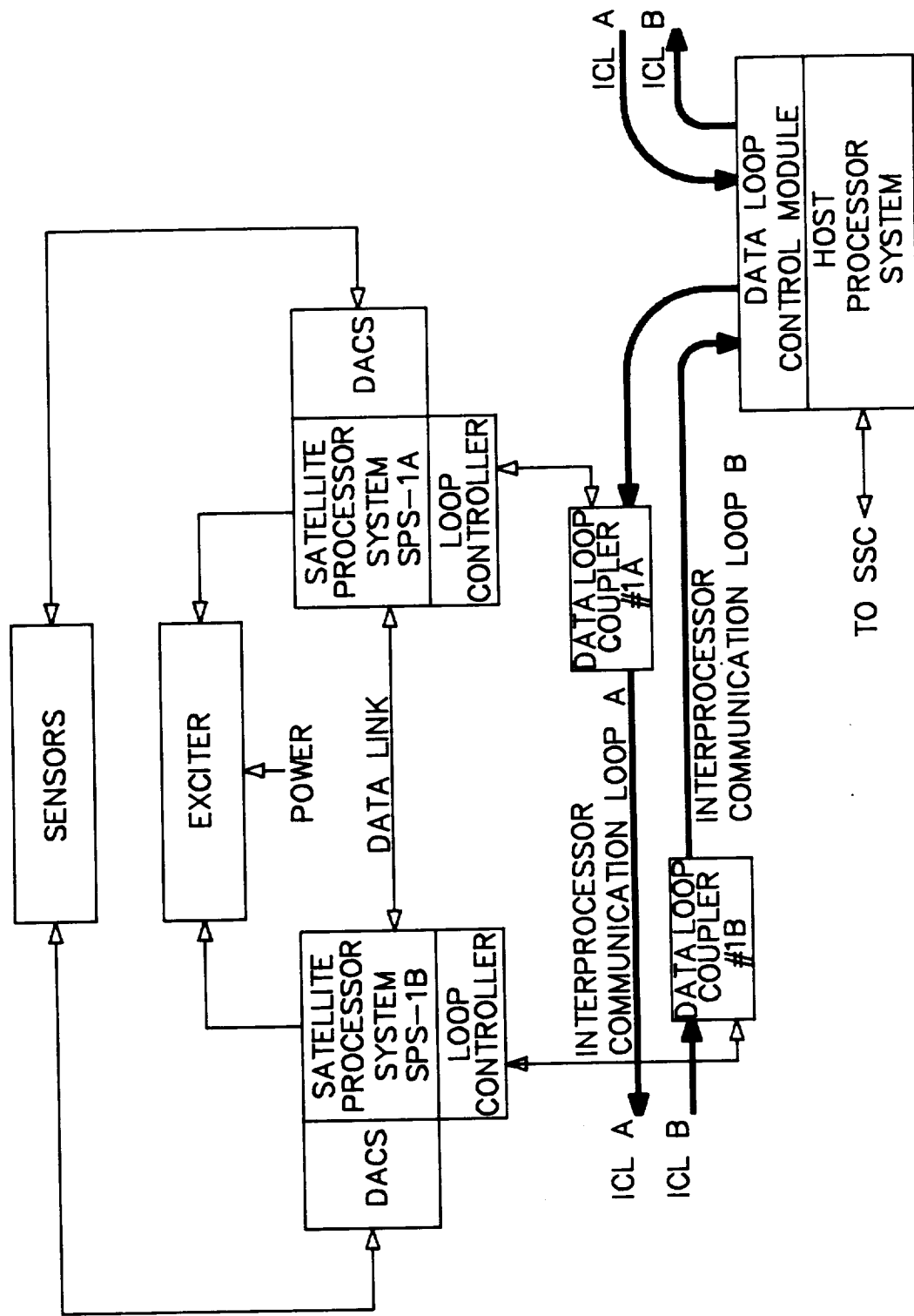


Figure 8.2: HPS-SPS-ICL Simplified Block Diagram

event of a communication link malfunction. The paired satellite processors will each be assigned to separate loops thereby permitting a processor disconnected by a loop hardware failure to be addressed via the healthy loop and the interprocessor link.

It is proposed to use fiber optic cables for HPS and SPS communications. These are in common usage in terrestrial distributed architecture data acquisition systems providing low loss, reliable, "noise" immune data links.

This choice will be reviewed during the detailed design phase when their suitability for use in a space environment, the availability of suitable Data Loop Couplers, and the practicality of using current optical cable termination techniques in a EVA environment will all require further evaluation.

If conventional cables are used for the data links, it is important that effective shielding and grounding techniques are used to ensure data is not compromised by noise or ground loops.

#### 8.2.1.1 Host Processor System

The Host subsystem is composed of the Processor Module and the Data Loop Controller Module.

A candidate microcomputer for both the Host and Satellite subsystems is the 8095, a member of the INTEL MCS-96 family. These are powerful single chip 16-bit processors that are tightly coupled with program and data memory. They support bit, byte, and word operations. Long word operations are also supported for a subset of the instruction set. With a 12 MHz clock frequency the device can perform a 16-bit addition in 1.0 micro-sec and 16 x 16 multiply or 32/16 divide in 6.25 micro-sec.

Also provided on-chip, are a serial port, a watchdog timer, and a pulse width modulated output signal. In addition, an optional on-chip A/D converter is available that will process up to eight 10-bit digital values.

These microcomputers are well suited to this type of application. Their 16-bit power, high speed math processing, high speed I/O and A/D conversion capability can all be fully utilized to enhance system performance.

At this time a space qualified version is not available, however, the manufacturer states that they will be released in the near future.

Both the Host Processor Module and Data Loop Controller Module will be installed within the Space Station structure and consequently their operating environment will be relatively benign by comparison with the balance of the system hardware.

For this reason and their resulting accessibility for corrective maintenance, redundant units have not been included in the HPS configuration. However, it is possible that when overall system reliability requirements are established and individual component performances are evaluated it will be determined that redundancy is also needed in the HPS system to meet overall Availability requirements.

#### 8.2.1.2 Satellite Processor System

The individual SPS systems are composed of a pair of INTEL 8095 microcomputers integrated together with their associated DACS modules. Each DACS module is an assembly of especially developed electronic units that perform signal conditioning, calibration, overvoltage protection and similar functions.

The sensor inputs from a structural module will be distributed between the paired units to provide continued integrity monitoring capability in the event of a partial DAPS hardware failure.

This will be achieved by strategically locating the sensors so that each structural "mode" is monitored by at least two transducers, ensuring that adequate data is still available for analysis under many possible hardware failure situations.

The 8095 microcomputer will accept eight channels of analog data and process them consecutively. The processor will execute one A to D conversion in 42 msec. (12 MHz clock) providing a 10-bit result (1 bit = 0.2%).

The microcomputer manufacturer states that the conversion accuracy is dependent upon the analog reference voltage and that "This can be advantageous if a ratiometric sensor is used since these sensors have an output that can be measured as a proportion of VREF."

Piezoelectric accelerometers are not ratiometric and consequently, to obtain accurate A/D conversions the satellite systems will each have an independent analog reference power source.

Both SPS processors will share the data common to their subsystem. After conditioning, processing and storage in the primary memory, the data will be copied in the memory of its paired back-up processor. Either of the processor pair may be designated as prime, its associate automatically becomes the back-up.

#### 8.2.1.2.1 DASC Module

All inputs from transducers will be routed to these modules that perform the data sampling and signal conditioning tasks.

A typical DASC-SPS arrangement is shown in Figure 8.3.

From each group of eight input channels seven can be used for accelerometers the eighth channel being dedicated to environmental temperature measurement for calibration purposes.

The signal conditioning capability of each input channel will be individually configurable, permitting it to be arranged to suit accelerometers with different output characteristics.

Configuration will be accomplished during system integration by the installation of a plug-in element appropriate for the target transducer. It will be possible, but difficult, to change the assignment of an input channel to a particular sensor model once the integration process is complete as the DASC modules will be hermetically sealed prior to their deployment.

The signal conditioning capabilities include:

- a. Low pass filters
- b. Charge amplifiers
- c. S & H circuit
- d. Temperature compensation for
  - sensors
  - electronics

# SELF-INTEGRITY MONITORING SYSTEM

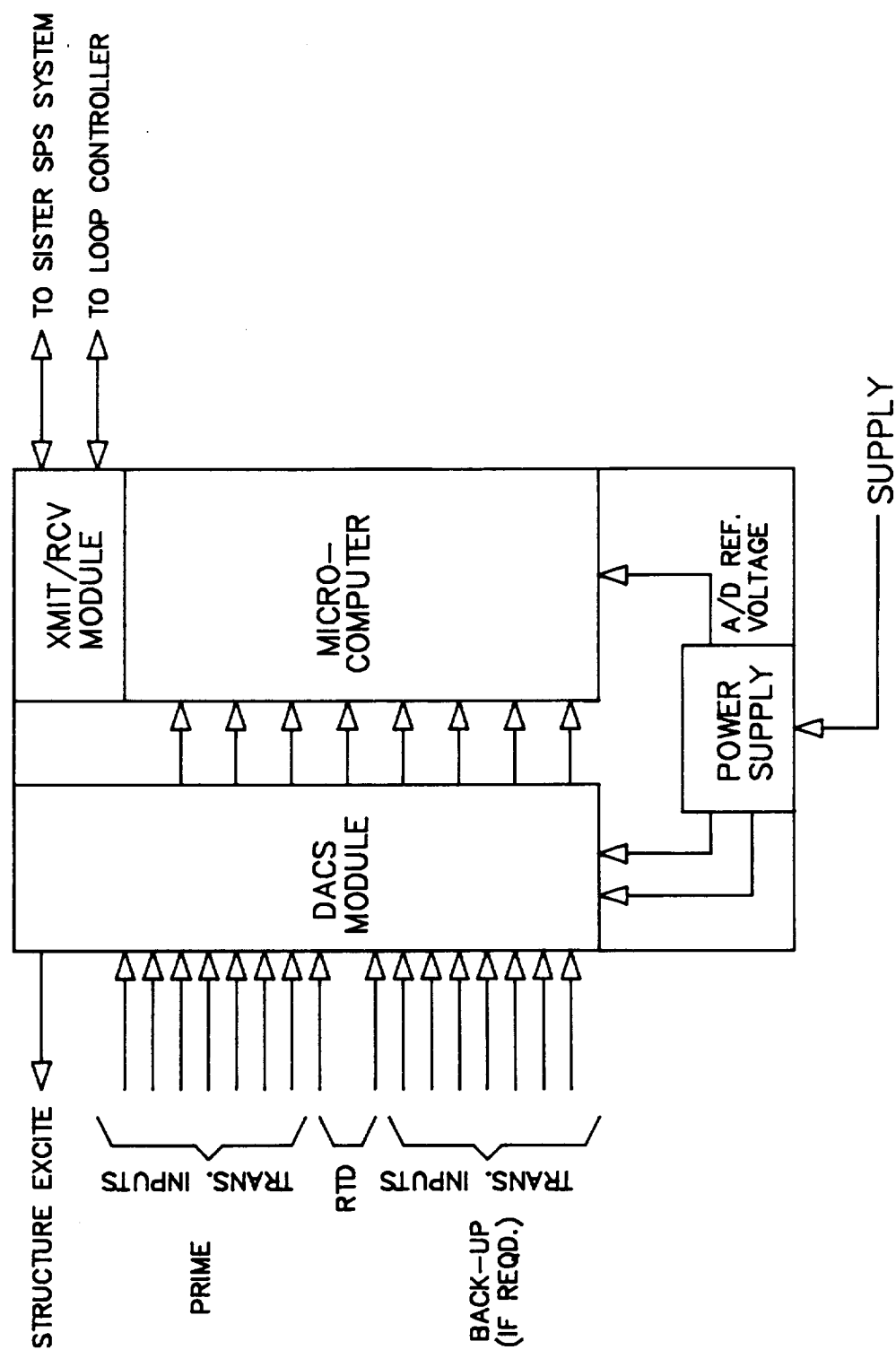


Figure 8.3: Typical DACS-SPC Configuration



Note: Techniques for obviating or compensating for temperature variations in sensors and electronic modules are presented in detail in Section 8.3. Selection of the optimum approach will be dependent upon analyses performed in the detailed design phase of the DAPS system development.

In addition to data acquisition control the DASC modules also provide for sensor excitation and calibration. Piezoelectric accelerometers only require excitation for "voltage insertion" calibration.

#### 8.2.1.2.2 Sensor Redundancy

The difficulty of replacing defective accelerometers under EVA conditions is not easy to quantify at this stage of the design process.

They will be mounted on the structure by threaded studs and their signal cables will be attached with plug and socket connectors, an arrangement that should facilitate their removal and replacement.

Therefore, to minimize system complexity and cost, the DAPS architecture has not been configured to provide redundant channels for these devices. However, this decision should be reassessed when the Availability requirements for these devices can be weighed against the difficulties of EVA maintenance.

Should back-up channels be deemed to be desirable, each DACS module will be equipped with a second set of eight channels to accommodate signals from back-up sensors which will be installed adjacent to the prime sensors at the time of their original placement.

The redundant channels will be furnished with their own signal conditioning circuits and then switched to the input of the common A/D converter. The switching will be via reed relays to ensure complete isolation of the primary/back-up channels.

Switchover from the primary to the back-up sensor for any particular node can be accomplished either manually or under software control.

To minimize astronaut involvement the SPS software routines would control the switchover procedure automatically. The HPS program will have the capability to manually overriding this.

### 8.2.1.3 Sensors and Cables

#### 8.2.1.3.1 Sensors

Piezoelectric accelerometers were selected for vibration measurement. When integrated into a system via a charge amplifier their sensitivity is independent of cable length (although long cables reduce the signal-to-noise ratio). The main disadvantage of charge amplifiers, slow recovery if saturated, is not anticipated to be a problem in this application.

A block diagram of a typical DASC input channel equipped with a Piezoelectric accelerometer is shown in Figure 8.4.

#### 8.2.1.3.2 Cables

Accelerometers will be connected with low noise co-axial cables. If voltage insertion is used for calibration purposes, two additional conductors will be required in the cable for this purpose.

All signal cables will be routed to avoid noise pick-up from electro-magnetic generating devices or power carrying conductors.

### 8.2.2 Software

Both the HPS and SPS systems will be equipped with the basic software modules necessary to perform tasks standard to most microcomputer-based systems. These functions include:

- a. Executive
- b. Data Management
- c. Communications
- d. Diagnostics and Health Testing

In addition, the HPS and SPS subsystem will have resident software programs developed specifically for this application.

- |                           |     |
|---------------------------|-----|
| e. DAPS data analysis     | HPS |
| f. HPS-SSC communications | HPS |

# SELF-INTEGRITY MONITORING SYSTEM

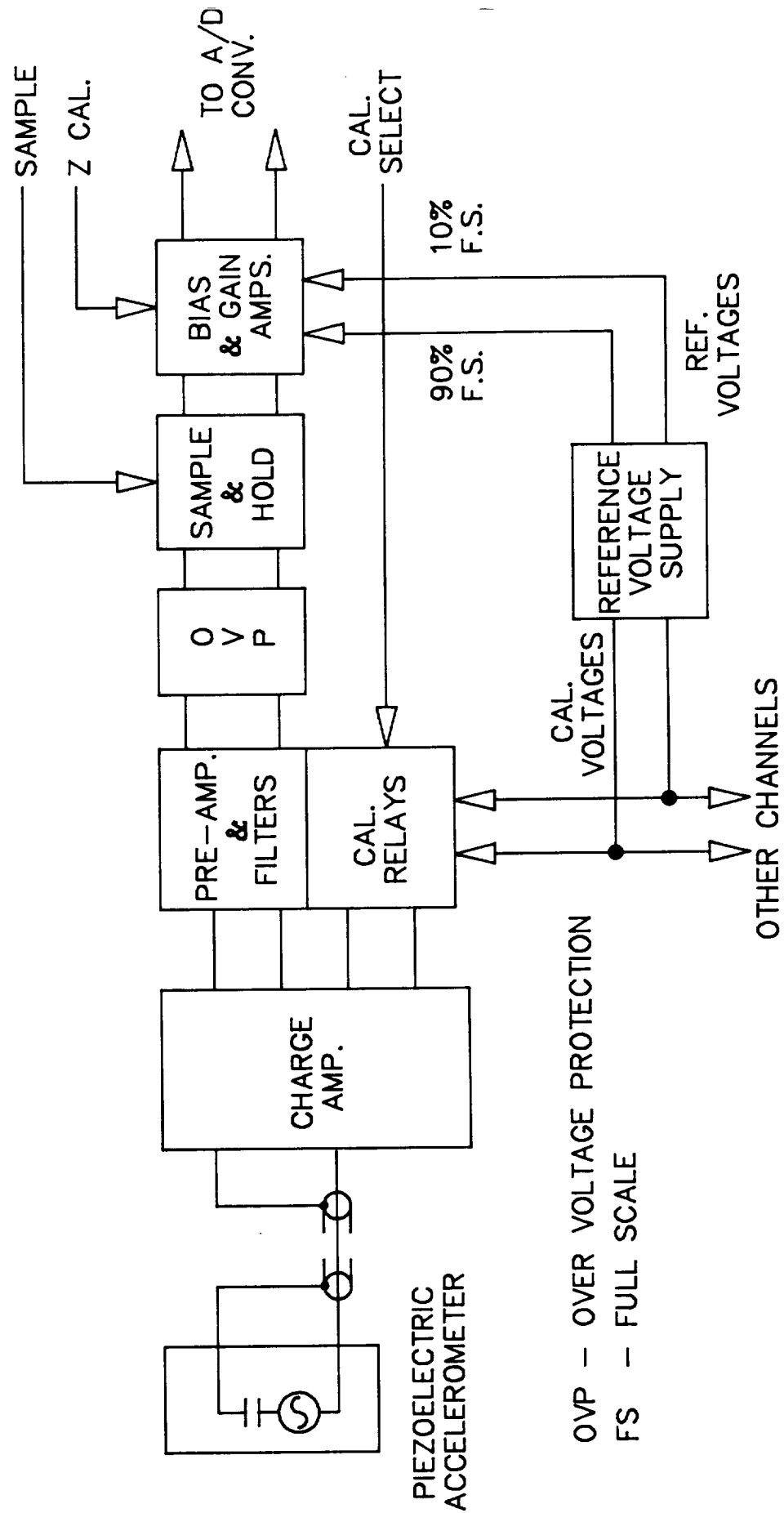


Figure 8.4: Typical DACS Input Channel

- g. SPS polling HPS
- h. Data acquisition SPS

and if redundant sensors/channels are installed

- j. Primary/redundant system selection SPS

#### 8.2.2.1 Executive

The Executive is responsible for controlling the orderly execution of the various software tasks. This control is performed on a time and event basis. In addition to this control function the Executive responds to interrupts by the system self-test routines performing a watchdog timer function.

#### 8.2.2.1 Data Manager

The Data Manager is used to store data sent from or received by the processor. It controls the input and output buffers and passes data to the appropriate destination within the sub-system.

#### 8.2.2.2 Communications

The Communications task has three major functions. They are:

##### a. Formatting

The primary function of the formatter is to assemble messages for transmission and to check and disassemble incoming messages. In the case of an error the message is ignored and the Executive is flagged. If an error is not detected the incoming data is accepted for use by the sub-system.

Formatting either adds or deletes protocol headers and trailers and either adds or verifies transmission error codes.

##### b. Loading

The HPS-SPS downline loading function will be controlled by the loader subtask. It performs the error checking and data store functions that are necessary to accomplish communications over fiber optic links.

### c. Transmit/Receiving

The Transmit/Receive function is basically an interrupt service routine that reacts to interrupts generated by the interface hardware.

### 8.2.2.3 Diagnostics and Health Checks

This task is responsible for monitoring the operational status of the system by conducting processor independent checks on data transfers and self-monitoring tests. The actions performed under the first category include the interrupts to the Executive in case of timeouts and communication error occurrences detected in the hardware.

For self-monitoring testing, two subtasks are provided. These are:

#### a. On-line Diagnostics

The Diagnostic subtask, executed following the network data scan, acquires the calibration data which is then processed to generate the parameters required by the Auto-Calibrate subtask. Two calibration points (10% and 90% full scale) are used to calculate compensation gains and offsets for the amplifiers and A/D converter.

#### b. Health Checks

The Heath Test subtask checks the validity of the RAM memory contents by check summing. Bus or I/O timeouts are detected by a hardware generated interrupt.

### 8.2.2.4 Data Analysis

The sensor signals in digital format will be transmitted to the HPS system from satellites and are used as parameters by the DAPS algorithm. The result of its analysis will be formatted and be continuously available to the SSC system on demand. The HPS system will store historical data for trend analysis. This data will be formatted and decimated periodically to minimize its demand for memory.

### 8.2.2.5 HPS-SSC Communications

Communications between the HPS and the Space Station computer will be initiated by the SSC system. A protocol and message format will be selected that is supported by the Space Station system and is compatible with the HPS hardware. As a minimum software tasks for

- communications,
- data display, and
- program reconfiguration and downloading

will be required to be installed in the Space Station computer.

#### 8.2.2.6 SPS Polling

Communications between the SPS and HPS systems are initiated by the Host. The transmission, reception, and retransmission tasks are under the direct control of the Loop Controller software (which is downloaded from the Host). The satellites will be polled for data periodically on an asynchronous basis.

#### 8.2.2.7 Data Acquisition

The Data Acquisition task resident in the SPS systems is responsible for acquiring data from the analog sensor points. Acquired data is placed in buffers and time tagged by SPS clocks which are synchronized by the Master Synchronizing Message from the Host. Data in these buffers is available for input signal processing and then transfer, on demand, to the Host.

Signal processing includes calibration, A/D conversion and compensation for environmental temperatures and sensor signal/temperature variations.

#### 8.2.2.8 Primary/Backup Selection

If redundant sensors/channels are installed, this special task resident in the SPS systems will monitor the health of the primary hardware. It will switch data acquisition from the primary to the backup device if sensor malfunctioning is detected.

### 8.3 Temperature Stabilization

The Data Acquisition/Signal Conditioning modules and the sensors, both of which are mounted externally on the Space Station structure, will be subjected to large temperature excursions as they are exposed to and then shaded from the sun. Heat will be transmitted primarily by radiation and conduction, convection heating being minimal.

The heating effects will be minimized by insulation and shielding, and temperature stability will be enhanced by the use of heat sinks.

#### 8.3.1 Electronic Modules

For accurate and reliable performance electronic modules require an operating temperature environment that is stable within defined limits.

Space qualified components will operate satisfactorily over a wide temperature range, but inaccuracies in data will arise if signals of identical strengths are processed at diverse temperatures, even if they are within the operating range specified for the electronic components.

The Satellite Processor modules and their associated signal conditioning electronics are the hardware items that will be subjected to the most extreme temperature variations, as they will be installed on the external structure and be exposed to thermal cycling from sun and shade.

In addition, in order to minimize power consumption it is planned to power the SPS systems only when a data sample is required. This will add to the temperature stability demands of the system.

Approaches to minimizing the deleterious effects of these influences on system performance are:

##### a. Insulation/Heat Sinking

This approach appears to be the most attractive.

It is anticipated that by insulating and heat sinking hardware, temperature fluctuations could be minimized to an acceptable level. When used in conjunction with a program of data acquisition timed to coincide with the Space Stations cyclical exposure to sun and shade, which will reduce temperature variations during sampling, this passive approach

would require the minimum of maintenance and would not consume Station power.

To establish the feasibility of this approach, analysis of the performance characteristics of all components will be necessary. Consultation with manufacturers to optimize the hardware selection process and a testing program with functioning prototypes to verify satisfactory performance, will also be required.

b. Heating/Refrigeration

Heating and cooling the modules would overcome the problem but at the expense of adding additional complexity to the system and power demands on the station. This approach is not planned unless reliable operation with a passive system cannot be attained.

c. Compensation

Compensation based on environmental temperature is a possibility but will be unreliable unless the temperature measurements are accurate. This appears to be the least desirable approach as it is questionable that accurate data would result.

8.3.2 Sensors

Sensors will be heated primarily by heat conducted from the structure to which they are attached, as they can be shielded from the majority of radiated energy by screening.

The output of accelerometers are directly influenced by environmental temperature.

The normal technique of measuring the transducer temperature and compensating its output accordingly would require each sensor to have its temperature monitored individually in this application, where sensors on the same DASC network may be in sun or shade simultaneously.

Such monitoring would require enlarging the system unduly. A feasible compromise is the siting of sensor groups to ensure uniform exposure to insolation or shade, and the dedication of one A/D input to measure their common temperature. This arrangement has been included in the system configuration.



## 8.4 Calibration and Compensation

### 8.4.1 DASC

The input channels will be calibrated "end to end" by a series of incremental routines.

Prior to a data measurement cycle the accuracy of the A/D converter will be checked with a reference voltage generated in the DASC module. The result stored in memory for data comparison purposes. The individual channels on the DASC module will be tested with routines that utilize:

- a. A shunt resistor [R cal]
- b. Shorting the inputs [Z cal]
- c. Applying (10% & 90%) F.S. voltage [V cal]

as appropriate for establishing their present response to these standard stimuli. Finally, the response of the sensors to calibration stimuli will be measured.

### 8.4.2 Accelerometers

- a. Chip accelerometers can be calibrated by exciting a separate element within the sensor. Requires additional conductors in the sensor cables for the excitation signal.
- b. Standard piezoelectric sensors can be calibrated by series (resistive) and shunt (capacitive) techniques using voltage insertion.

The voltage insertion technique assumes that there is no mechanical excitation of the transducer while the simulation voltage is being measured because of the difficulty of separating signals from concurrent stimuli. For this application, it is believed that excitation of the accelerometers arising from the natural vibrations of the structure will be minimal and consequently their effect on the system accuracy will be negligible. Additional conductors in the DASC--Charge Amplifier cable will also be required for the voltage insertion technique.

Unless the algorithm necessitates a very fast sampling rate that would utilize a significant amount of the processor capability, it is

planned that calibration routines will be performed every data acquisition cycle. Should this be impractical the routines will be performed less frequently and averaged. The calibration software will provide safeguards against abnormal calibration data being utilized without verification.

#### 8.4.3 Compensation

The possible influence of temperature fluctuations on sensor signal accuracy has been discussed in Subsection 8.3.2.

Each DASC module has one input channel dedicated to monitoring the environmental temperature of its associated sensors and compensating their signals accordingly.

### 8.5 System Power

#### 8.5.1 Limitations

The power available to run the DAPS system is limited and consequently a basic design requirement is to restrict system power consumption.

It is recommended that integrity monitoring will be performed during periods of reduced energy consumption of other Space Station systems. However, such intermittent operation introduces the need to ensure that all the electronic modules are thermally stabilized prior to operation. This requirement is addressed in detail in Section 8.3.

#### 8.5.2 Requirements

The format of a candidate power usage budget is shown in Table 8.1.

The budget presupposes that the HPS will be on-line constantly (100% duty cycle), but that the SPS sub-systems will each be powered intermittently. Each of the SPS modules will be energized in succession for a period that is sufficient to achieve temperature stability and collect data.

The duty cycle for these sub-systems can be approximated when the data needs of the software is defined. It can be optimized when hardware is available for functional testing.

TABLE 8.1: POWER USAGE BUDGET FOR THE TARGET SYSTEM

(Assumes 7 satellite subsystems - 5% duty cycle for electronics  
0.1% duty cycle for exciter [12 sec. on in 24 hours])

Equipment	Quantity		mw	mw	Total mw
<b>HPS system (100% Duty cycle)</b>					
- Host processor	1	@	5,000	=	5,000
- Communication link to SSC computer	1	@	1,000	=	1,000
- Data Memory	1	@	10,000	=	<u>10,000</u>
TOTAL HPS SYSTEM				16,000	16,000
<b>SPS system</b>					
- Satellite processor	2	@	5,000	=	10,000
- Communication loop controller	2	@	4,000	=	<u>8,000</u>
SUBTOTAL PER SYSTEM				18,000	
TOTAL 7 SPS SYSTEMS				5% of 7 @ 18,000 =	6,300
<b>ILC system</b>					
- Data loop couplers	7	@	2,000	=	28,000
TOTAL ILC SYSTEM				5% of 2 @ 28,000 =	2,800
<b>DACS system</b>					
- Charge amplifiers	7	@	800	=	5,600
- Signal conditioning modules	7	@	2,000	=	14,000
- Calibration channels	1	@	1,000	=	1,000
- Temp. compensation module	1	@	1,000	=	<u>1,000</u>
SUBTOTAL PER SYSTEM				21,600	
TOTAL 7 DASC SYSTEMS				5% of 7 @ 21,600 =	7,560
<b>Sensors</b>					
- Accelerometers (cal. only)	14	@	100	=	1,400
TOTAL 7 SPS SYSTEMS				5% of 7 @ 1,400 =	490
<b>Structure excitation</b>					
- Vibrators	1	@	600 x 10 <sup>3</sup>	=	600 x 10 <sup>3</sup>
TOTAL 7 SPS SYSTEMS 0.1% of 7 x 600 x 10 <sup>3</sup>				=	<u>4,200</u>
SYSTEM TOTAL					37,350
CONTINGENCY 20%					<u>7,470</u>
GRAND TOTAL					44,820

Continuous system power requirement assuming power conversion efficiency of 50% =  
2 x 44,820 mw = 100 watts.

## 8.6 System Installation and Integration

### 8.6.1 Installation

The system architecture is modular, allowing both the hardware and software to be expanded in incremental steps as the monitoring needs of the Station grow from the original basic kernel to the final arrangement.

As a necessary stage in the system development the final configuration of the entire system must be tested as an entity to ensure that all modules will function correctly when subjected to maximum performance demands. In addition, the various subsets of the final configuration that are planned to be operational entities during the Station erection phases must each also be tested for performance to ensure that they too will operate satisfactorily.

The most desirable site for these tests would be on a full scale "operational" mock-up of the station. At this stage in the system definition it is difficult to assess the amplification/attenuation effects of low gravity on the response that the structure exhibits to stimuli, and consequently it is quite likely that the data obtained in these tests will not be indicative of in-service use.

However, system testing under terrestrial conditions will eliminate many possible installation and integration problems prior to the systems deployment in space.

Modularity and standardization will simplify the system integration procedure and corrective maintenance activities.

Most data acquisition systems require adjustable signal conditioning circuits at the transducer interface for system set-up.

Resistance trimming is the most common technique to accomplish the adjustments. Circuits are arranged so that the altering of one or more resistances compensates for the particular characteristics of the attached sensor.

This approach will not be practical for this system for two reasons:

- a. All DAPS electronic hardware installed external to the Station will be hermetically sealed.
- b. Micro-electronic (hybrid) technology will be used for electronic fabrication wherever possible to enhance reliability and reduce size and weight.

Digital techniques for adjusting the resistance of a circuit under software control are available and may be applicable to set-up input channels for the DACS modules. This would permit replacement DACS modules to be substituted for installed units which have become defective, and the necessary circuit changes to customize them for the installed sensor to be downloaded from the SSC computer.

Sensors, cables, and SPS modules will all be installed on their associated Station structural members and then tested as an element of the entire system prior to the members being transported to space for incorporation in the structure.

The connections between sensors and the SPS modules will all be via hermetic type connectors. Optical communication links will only be utilized if the degree of difficulty for their termination and interconnection is comparable with the effort required for electrical cables.

### 8.7 Reliability

The inherent difficulty of performing EVA corrective maintenance on the Space Station structure mandates that the DAPS system have a high degree of reliability, and in addition, function effectively in a degraded mode.

Some EVA corrective work will be unavoidable and therefore hardware design must emphasize modularity so that it may be quickly and simply executed.

During detailed system design an evaluation will be necessary to establish the required DAPS Availability, and from that, the level of redundancy in installed hardware necessary to achieve it.

The measure of Availability is

$$\text{Availability} = \frac{\text{MTBF} - \text{MTTR}}{\text{MTBF}}$$

MTBF = Mean time between failures.

MTTR = Mean time to repair.

The use of redundant hardware and the implementation of automatic failover routines under software control increases system Availability dramatically, permitting many corrective tasks to be conducted concurrent with planned routine preventative maintenance activities, thereby reducing the need for emergency responses to failures.

There are trade-offs to be made in this regard. The added costs and complexity of the system elements necessary to achieve high Availability must be compared to the criticality of the DAPS to the safe operation of the Space Station.

In addition, the strategically siting of sensors that provides the system with the inherent ability to function effectively in a degraded mode will also enhance the Availability to a large extent.

It is not possible to make these trade-offs until the criticality of the system is established and the detailed design process has commenced. Statistical analysis of the components will yield their individual probability of failure and a model can be developed to postulate the MTBF for subsystems and the entire system.

Performance of the DAPS system under degraded operation (as opposed to failure) of the subsystems and major elements will also be assessed. The items that will be evaluated are:

- a. Host Processor System
- b. Satellite Processors System
- c. Interprocessor Communication Loops
- d. DASC modules comprising:
  - Charge Amplifier
  - Active filters
  - Calibration circuits
  - Sample and Hold [S&H]
- e. Sensors

## 8.8 Maintenance

The need to minimize astronaut activities associated with hardware installation and system integration mandates that the hardware modules be simple to install and inter-connect and be interchangeable wherever possible.

Such design criteria will also simplify the corrective maintenance tasks.

It is envisaged that the system hardware installed on the Station will be elements of a complete system that has been integrated and tested as an entity on earth. It is also expected that concurrent with the manufacture, adjustment and testing of the primary modules a quantity of backup elements will be built so that they have the same characteristics as the primary modules and consequently are interchangeable with them.

The availability of these interchangeable tested system elements will permit hardware corrective maintenance on the Station to be accomplished by substitution, the defective module being returned to earth for repair if appropriate.

System maintenance will also be aided by the availability of a functioning duplicate system on the earth which will allow:

- a. Development of duplicate modules as needed.
- b. Simulation of possible hardware and software malfunctions that may arise on the primary system.
- c. Testing of structure additions/modifications after the primary system is in operation.

## 9.0 CONCLUSIONS AND COMMENTS

The research described in this report deals with many topics; they are listed as follows:

- module/substructure transfer function matrix--the definition and computation of it;
- damage indicators--they are used to help observe changes in the module transfer function matrix;
- time domain system (module) identification--identify module modal properties;
- modal strain energy distribution method--locate damage by determining which modes have not been affected by the damage;
- general system identification; and possible damage detection hardware system.

The conclusions are broken into subsections corresponding to the above topics.

### 9.1 Module Transfer Function Matrix

The module transfer function matrix (MTFM) relates the module response at its interior points to the module inputs made up of its boundary motions and forces applied to its interior points. It was shown that the MTFM exists for a general structural system. Then, it was calculated for a variety of simple systems. It was relatively simple to calculate for modules with one degree-of-freedom (DOF) at their boundary. For modules with two or more DOF at their boundary it was impossible to calculate it in a robust manner using a standard multi-input multi-output (MIMO) transfer function computation method (a method involving the inversion of the MIMO power and cross-spectra matrix). A method of calculating it using force appropriation was developed. However, this method is not robust because it involves locating/placing forces within and without a module to generate no boundary motion within a desired frequency domain. Also, it is possible to use a method which involves determining those frequency domains whose corresponding motion is due only to global/local modes.



## 9.2 Damage Indicators

Scalar functions of part of or the entire MTFM were developed as a means of more easily observing/detecting changes in it. An unlimited number of functions could be defined to do this. However, a few functions were selected which it was hoped would be very sensitive to small changes in the matrix. These "indicators" were then used to determine if a given mode had been affected by the damage.

## 9.3 Time Domain Module Modal Identification

The time domain module modal identification method developed by Beck works well for those global modes which have their motion largely local to the physical domain of the module. The method does not work satisfactorily for those global modes which involve motion of the entire global system, and where there are a large number of module boundary degrees-of-freedom. What happens here is that the pseudostatic module response is close enough to the absolute response that the relative response is very small. This makes it impossible to determine the module modal properties.

## 9.4 Modal Strain Energy Distribution Method

The modal strain energy distribution method (MSEDM) for locating damage uses the fact that when a structure is damaged locally (i.e., at a single point) some modes will not be affected--the damage occurs at zero or near zero strain energy points. When this happens the damage indicators for those modes will indicate that they have not been affected. If enough unaffected modes can be found and good estimates of their strain energy distributions made, the location(s) of the damage can be determined with reasonable accuracy.

For this method to work it is necessary to have a reliable method of determining which modes were and were not affected. This is what the damage indicators were used for. However, to calculate them, a good estimate of the MTFM must be determined. As explained earlier, at the present time there is not a robust method for calculating it.

## 9.5 System Identification

Many system identification (SID) methods have been developed, some of which are usable for detecting damage in structural systems. The time domain method already described is one such example. The drawbacks to using SID for global systems are still drawbacks for its use with modules. However, there are additional problems associated with them when used with modules. However, they have the advantage that they can be implemented in a relatively straight forward manner and the damage can be both established (did it occur) and located with one method. Also, a great deal of research has been done on SID, particularly nonlinear parameter estimation, and many powerful methods developed. The normal cautions must be considered when implementing them.

## 9.6 Module Damage Detection Hardware System

A structural module damage detection system was designed with a fair amount of detail--a "second cut" design was made. The system could be used with various module damage detection methods.

**ANCO**

APPENDIX A

MODULE TRANSFER FUNCTION MATRIX--DERIVATION DETAILS

This appendix contains some of the hand calculations that were done as a part of the effort to establish the existence of the module (substructure) transfer function matrix. They are provided for the reader who is interested in the details of the various derivations discussed in the main body of this report. There are four sets of calculations provided. They are listed as follows:

1. Determine Substructure Transfer Function (multi-input multi-output problem);
2. Eigenvalues for Substructure With Clamped (fixed) Boundary;
3. Substructure Transfer Function--Relative Responses; and
4. Defining Two Different Substructure Input Vectors Corresponding to the Boundary Motions.

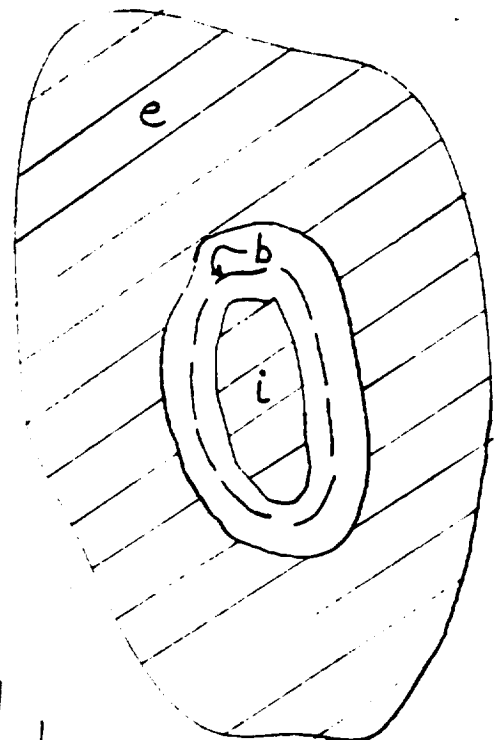
DETERMINE SUBSTRUCTURE TRANSFER FUNCTION  
(multi-input multi-output problem)

Determine Substructure Transfer Function  
(Multi-Input Multi-Output Problem)

Define regions of a global structure as follows:

Region	Description
e	Refers to portion of structure which is <u>external</u> to the module including its boundary (module consists of regions i and b)

b	Refers to the <u>boundary</u> of the module. The boundary of the module is also the boundary of the <u>other</u> substructure.
---	--



Region	Description
--------	-------------

i	Refers to portion of structure which is <u>internal</u> -- it is the module less its boundary
---	---

Dynamic equilibrium equations for entire structure (linear system) -

$$[M]\{\ddot{x}(t)\} + [C]\{\dot{x}(t)\} + [K]\{x(t)\} = \{f(t)\}$$

This matrix equation is for the physical domain.

Do work in the frequency domain. Thus, Fourier Transform the above system of eqs; replace  $[M]$  and  $\{x(t)\}$  with  $M$  and  $x$ , respectively.

$$f(M\ddot{x} + C\dot{x} + Kx) = f(f)$$

MADE BY WOW DATE 4/27/87CHECKED BY GIY DATE 9/3/87JOB NUMBER 1311.05 PAGE 3 OF 12DESCRIPTION Substructure Transfer Function  
NASA II

$$M\ddot{f}(x) + C\dot{f}(x) + Kf(x) = f(t)$$

$$M(-\omega^2 X(\omega)) + C(i\omega X(\omega)) + KX(\omega) = F(\omega)$$

Where  $i = \sqrt{-1}$  and this is a matrix equation.

$$(-\omega^2 M + i\omega C + K) X(\omega) = F(\omega)$$

$$\tilde{K}(\omega) X(\omega) = F(\omega) \quad \underline{\text{or}} \quad [\tilde{K}]\{X(\omega)\} = \{F(\omega)\}$$

Partition this equation as follows:

$$\begin{bmatrix} \tilde{K}_{ee} & \tilde{K}_{eb} & \tilde{K}_{ei} \\ \tilde{K}_{be} & \tilde{K}_{bb} & \tilde{K}_{bi} \\ \tilde{K}_{ie} & \tilde{K}_{ib} & \tilde{K}_{ii} \end{bmatrix} \begin{Bmatrix} X_e(\omega) \\ X_b(\omega) \\ X_i(\omega) \end{Bmatrix} = \begin{Bmatrix} F_e(\omega) \\ F_b(\omega) \\ F_i(\omega) \end{Bmatrix}$$



MADE BY UBW DATE 4/27/87CHECKED BY GIY DATE 9/3/87JOB NUMBER 1311.05 PAGE 4 OF 12DESCRIPTION Substructure Transfer Function  
WASH II

Expand this equation as follows:

$$\begin{cases} \tilde{K}_{ee} X_e + \tilde{K}_{eb} X_b + \tilde{K}_{ei} X_i = F_e \\ \tilde{K}_{be} X_e + \tilde{K}_{bb} X_b + \tilde{K}_{bi} X_i = F_b \\ \tilde{K}_{ie} X_e + \tilde{K}_{ib} X_b + \tilde{K}_{ii} X_i = F_i \end{cases}$$

It should be noted that for the above partitioning,  $X_e$ ,  $X_b$  and  $X_i$  are vectors of displacement (Fourier transform of) for the degrees-of-freedom corresponding to the external structure (less boundary), boundary and internal structure (less boundary), respectively.

It is now desired to determine the substructure transfer function matrix. This is done from the third equation from the above set of equations. This can be done because  $\tilde{K}_{ie} = 0$ .

$\tilde{K}_{ie}$  can be shown to be zero by using the concept of the influence coefficient. The static problem is looked at first. All displacements are constrained to be zero except for one of the displacements in the external structure (less the boundary). Thus,

$$[K_{ie}] \begin{Bmatrix} 0 \\ \vdots \\ 0 \\ x_e^{(j)} \\ 0 \\ \vdots \\ 0 \end{Bmatrix} = \{f_i\}, \quad \{x_b\} = 0, \quad \{x_i\} = 0$$

With the boundary displacements being zero, the applied force vector  $\{f_i\}$  necessary to keep the internal structure (less boundary) from deforming/displacing, due to a nonzero  $x_e^{(j)}$ , is zero. Thus,

$$K_{ie}^{(kj)} x_e^{(j)} = f_i^{(k)} = 0 \Rightarrow K_{ie}^{(kj)} = 0$$

Using somewhat similar reasoning for the mass matrix, it is found that  $M_{ie}^{(kj)} = 0$ . If the damping matrix is taken to be proportional to the mass and stiffness matrix, then it can be shown that  $C_{ie}^{(kj)} = 0$ . Note that this is for

$$C = \alpha M + \beta K$$

Thus, it is seen that  $\tilde{K}_{ie} = 0$ . Using the third equation in the set of equations for the partitioned system, the following is found:

$$\tilde{K}_{ib} X_b + \tilde{K}_{ii} X_i = F_i$$

$$\tilde{K}_{ii}^{-1} \tilde{K}_{ib} X_b + \tilde{K}_{ii}^{-1} \tilde{K}_{ii} X_i = \tilde{K}_{ii}^{-1} F_i$$

$$\tilde{K}_{ii}^{-1} \tilde{K}_{ib} X_b + X_i = \tilde{K}_{ii}^{-1} F_i$$

$$X_i = \tilde{K}_{ii}^{-1} F_i - \tilde{K}_{ii}^{-1} \tilde{K}_{ib} X_b$$

$$= \tilde{K}_{ii}^{-1} (F_i - \tilde{K}_{ib} X_b)$$

$$= \tilde{K}_{ii}^{-1} [I \mid -\tilde{K}_{ib}] \begin{Bmatrix} F_i \\ X_b \end{Bmatrix}$$

$$X_i = T_{ii} [I \mid -\tilde{K}_{ib}] \begin{Bmatrix} F_i \\ X_b \end{Bmatrix}$$

Given that all the possible inputs and outputs are considered, the substructure transfer function matrix is given by

$$T_{ii} [I \mid -\tilde{K}_{ib}]$$

If all the boundary motions are zero, the substructure transfer function matrix is given by

$$\tilde{K}_{ii}^{-1}$$

when considering all possible applied loads.

If all the applied substructure loads are zero, the substructure transfer function matrix is given by

$$-\tilde{K}_{ii}^{-1} \tilde{K}_{ib}$$

when considering all possible boundary motions.

In determining a transfer function matrix from experiment or an analytical model (i.e., finite element), the only inputs and outputs which are used are those which are nonzero. Thus, this is what is done below. The input and output vectors are partitioned into parts (block vectors) corresponding to variables which are and are not used.

$$X_b = \begin{Bmatrix} X_b^{u_b} \\ X_b^{n_b} \end{Bmatrix} = \begin{Bmatrix} X_b^{u_b} \\ 0 \end{Bmatrix}$$

$$F_i = \begin{Bmatrix} F_i^{u_f} \\ F_i^{n_f} \end{Bmatrix} = \begin{Bmatrix} F_i^{u_f} \\ 0 \end{Bmatrix}$$

$$X_i = \begin{Bmatrix} X_i^{u_i} \\ X_i^{n_i} \end{Bmatrix}$$

where the superscripts  $u$  and  $n$  refer to variables which are used and not used, respectively. The input variables which are not used must be zero, i.e., no applied force component. The response components which are not used are not necessarily zero, they are just not used in the transfer function calculations.

The equation relating the substructure internal motions,  $X_i$ , to the substructure excitations,  $X_b$  and  $F_f$ , is partitioned as follows:

$$\begin{Bmatrix} X_i^{u_i} \\ X_i^{n_i} \end{Bmatrix} = \begin{bmatrix} T_{ii}^{u_i u_f} & T_{ii}^{u_i n_f} \\ T_{ii}^{n_i u_f} & T_{ii}^{n_i n_f} \end{bmatrix} \left( \begin{Bmatrix} F_i^{u_f} \\ 0 \end{Bmatrix} - \right.$$

$$\left. \begin{bmatrix} \tilde{K}_{ib}^{u_f u_b} & \tilde{K}_{ib}^{u_f n_b} \\ \tilde{K}_{ib}^{n_f u_b} & \tilde{K}_{ib}^{n_f n_b} \end{bmatrix} \begin{Bmatrix} X_b^{u_b} \\ 0 \end{Bmatrix} \right)$$

The equation for the substructure responses which are used is given as follows:

$$X_i^{u_i} = T_{ii}^{u_i u_f} (F_i^{u_f} - \tilde{K}_{ib}^{u_f u_b} X_b^{u_b}) + T_{ii}^{u_i n_f} (-\tilde{K}_{ib}^{n_f u_b} X_b^{u_b})$$

$$X_i^{u_i} = T_{ii}^{u_i u_f} F_i^{u_f} - (T_{ii}^{u_i u_f} \tilde{K}_{ib}^{u_f u_b} + T_{ii}^{u_i n_f} \tilde{K}_{ib}^{n_f u_b}) X_b^{u_b}$$

This is the desired result for the substructure.

The next task is to look at the poles of the substructure transfer function matrix. The substructure transfer function matrix for all possible inputs and outputs,

$$T_{ii} [I \mid -\tilde{K}_{ib}]$$

where  $T_{ii} = \tilde{K}_{ii}^{-1} = \frac{1}{\det(\tilde{K}_{ii})} [A_{ij}]^T$ , in general has poles which correspond to the frequencies where  $\det(\tilde{K}_{ii}) = 0$  for the case of no damping. When there is damping, the poles correspond to minima of  $\det(\tilde{K}_{ii})$ . There can be fewer poles for  $T_{ii} \tilde{K}_{ib}$  than for  $T_{ii}$ . This is because some of the zeros of  $\tilde{K}_{ib}$  could correspond to some of the poles of  $T_{ii}$ . However, the set of poles of  $T_{ii} \tilde{K}_{ib}$  is always a subset of the set of poles of  $T_{ii}$ .



Similar reasoning can be used for the case of some of the inputs and outputs not being considered.

$$\begin{bmatrix} T_{ii}^{uu} & T_{ii}^{un} \\ T_{ii}^{nu} & T_{ii}^{nn} \end{bmatrix} = \tilde{K}_{ii}^{-1} = \frac{1}{\text{Det}(\tilde{K}_{ii})} [A_{ij}]^T$$

Thus, each block matrix within the partitioned matrix  $T_{ii}$  has a scalar multiplier of  $1/\text{Det}(\tilde{K}_{ii})$ .

This can be factored outside of all the terms in the equation for  $X_i^u$ . Thus, the poles for this case correspond to some or all of the poles for the case of using all possible inputs and outputs for the substructure.

EIGENVALUES FOR SUBSTRUCTURE WITH CLAMPED (fixed) BOUNDARY

WSW

5/13/87

GTY

9/13/87

1311.05

1

3

Fixed Boundary Substructure  
Eigenvalue Problem

## Eigenvalues for Substructure With Clamped (Fixed) Boundary

This problem is straight forward; however, for completeness it is discussed below. In Section 3.0 the dynamic system equations were partitioned into three zones, eg., exterior, boundary and interior. The third equation resulting from the partitioning (Equation 3.5c) is given as follows:

$$\bar{K}_{ie} X_e + \bar{K}_{ib} X_b + \bar{K}_{ii} X_i = F_i$$

Of course  $\bar{K}_{ie} = 0$ . For the substructure, defined by the boundary and interior, having a fixed boundary,  $X_b = 0$ . Thus, the resulting equation for the substructure

WPK

5/13/87

GTY

9/2/87

131105

2

3

Fixed Boundary Substructure  
Eigenvalue Problem

is

$$\tilde{K}_{ii} X_i = F_i$$

This equation was arrived at from the total system and fixing the boundary. Thus, it represents the fixed boundary substructure problem. The mass and stiffness matrices which correspond to  $\tilde{K}_{ii}$  are  $M_{ii}$  and  $K_{ii}$ , respectively -- these correspond to the fixed boundary problem. Thus, the eigenvalue problem

$$[-\omega^2 M_{ii} + i\omega C_{ii} + K_{ii}]\{\phi\} = 0$$

corresponds to the fixed boundary substructure problem. This can be written as

$$[\tilde{K}_{ii}]\{\phi\} = 0$$

The eigenvalues are found from

MADE BY

WBW

DATE

5/13/87

CHECKED BY

GIT

DATE

9/3/87

JOB NUMBER

1311.05

PAGE

3

OF

3

DESCRIPTION

Fixed Boundary Substructure  
Eigenvalue Problem

$$\{\phi\} = [\tilde{K}_{ii}]^{-1} \{0\} = \frac{1}{\text{Det}([\tilde{K}_{ii}])} [A_{ij}]^T \{0\}$$

Thus, for a nontrivial solution

$$\text{Det}([\tilde{K}_{ii}]) = 0$$

This is the desired result.

SUBSTRUCTURE TRANSFER FUNCTION--RELATIVE RESPONSES

## Substructure Transfer Function -- Relative Responses

This material uses the concept of the substructure transfer function matrix developed in the notes "Substructure Transfer Function - NASA II" of 4/24/89 by WSW. The starting point here is with the following equation:

$$\tilde{K}_{ib} X_b(\omega) + \tilde{K}_{ij} X_i(\omega) = F_i(\omega)$$

Where the various terms, i.e.,  $X_i(\omega)$ , are either vectors or matrices and are defined in the above referenced document.

From this point it is desired to develop the expression for the substructure transfer function

matrix for relative responses of the substructure interior degrees-of-freedom. This is done using the so called "pseudostatic method" for nonuniform base enforced motion\*. The substructure response,  $X_i$ , is absolute. It can be expressed as follows:

$$X_i = S_i(\omega) + R_i(\omega)$$

where

$S_i(\omega)$  = Fourier transform of the "pseudostatic component" of the structural response (which represents the "static" effects of the multiple support movements on the response of the structure)

\*1) See "Dynamics of Structures" by R.W. Clough & J. Penzien, McGraw - Hill, Inc., 1975.

2) "Seismic Response Characterization of Meloland Road Overpass During 1979 Imperial Valley Earthquake", AA report, March 1985.



$R_i(\omega)$  = vector of Fourier Transform of components of  
 the fixed boundary dynamic response  
 of the substructure interior; these are  
 relative responses

$\omega$  = transform variable

The vector  $S_i$  is given by the following:

$$S_i = P X_b$$

where

$$P = -K_{ii}^{-1} K_{ib}$$

From these equations, the following is found:

$$\tilde{K}_{ii} (S_i + R_i) = F_i - \tilde{K}_{ib} X_b$$

$$\tilde{K}_{ii} S_i + \tilde{K}_{ii} R_i = F_i - \tilde{K}_{ib} X_b$$

$$\tilde{K}_{ii} R_i = F_i - \tilde{K}_{ib} X_b - \tilde{K}_{ii} S_i$$

$$= F_i - \tilde{K}_{ib} X_b - \tilde{K}_{ii} P X_b$$

$$= F_i - (\tilde{K}_{ib} + \tilde{K}_{ii} P) X_b$$

(Assume lumped mass system and neglect damping terms related to the effective boundary forces; thus  $C_{ib} = 0$  and  $M_{ib} = 0$ .)

$$\tilde{K}_{ib} = -\omega^2 M_{ib} + i\omega C_{ib} + K_{ib} \approx K_{ib}$$

$$\begin{aligned} \tilde{K}_{ii} P &= -(-\omega^2 M_{ii} + i\omega C_{ii} + K_{ii}) K_{ii}^{-1} K_{ib} \\ &= -(-\omega^2 M_{ii} K_{ii}^{-1} K_{ib} + i\omega C_{ii} K_{ii}^{-1} K_{ib} + K_{ib}) \end{aligned}$$

MADE BY W3W DATE 6/29/87  
 CHECKED BY G I Y DATE 9/3/87

 JOB NUMBER 1311.05 PAGE 5 OF 6  
 DESCRIPTION Substructure Transfer  
Function For Relative Responses  
NASA II

$$\tilde{K}_{ii} R_i = F_i - (\tilde{K}_{ib} - (-\omega^2 M_{ii} \tilde{K}_{ii}^{-1} K_{ib} + i\omega C_{ii} \tilde{K}_{ii}^{-1} K_{ib} + K_{ib})) X_b$$

$$\cong F_i + (-\omega^2 M_{ii} \tilde{K}_{ii}^{-1} K_{ib} + i\omega C_{ii} \tilde{K}_{ii}^{-1} K_{ib}) X_b$$

$$\cong F_i + (-\omega^2 M_{ii} \tilde{K}_{ii}^{-1} K_{ib}) X_b$$

$$\tilde{K}_{ii} R_i = F_i + (-\omega^2 M_{ii} \tilde{K}_{ii}^{-1} K_{ib}) X_b$$

This equation can be inverse transformed as follows:

$$(-\omega^2 M_{ii} + i\omega C_{ii} + K_{ii}) R_i(\omega) = F_i(\omega) + (-\omega^2 M_{ii} \tilde{K}_{ii}^{-1} K_{ib}) X_b(\omega)$$

$$M_{ii} \ddot{r}_i(t) + C_{ii} \dot{r}_i(t) + K_{ii} r_i(t) = f_i(t) + M_{ii} \tilde{K}_{ii}^{-1} K_{ib} \ddot{x}_b(t)$$

WBA

6/29/87

GIY

9/3/87

1311.05

6

6

Substructure Transfer

For Relative Responses

This equation is identical to that for the relative structural response for the multi-base input problem using the pseudostatic approach, except that it is for the substructure problem and includes the possibility of applied forces.

It is possible to obtain an expression for the transfer function matrix from an earlier equation. This is done as follows:

$$\tilde{K}_{ii}^{-1} \tilde{K}_{ii} R_i = \tilde{K}_{ii}^{-1} (F_i + (-\omega^2 M_{ii} \tilde{K}_{ii}^{-1} K_{ib}) X_b)$$

$$R_i(\omega) = \tilde{K}_{ii}^{-1} (F_i(\omega) + (-\omega^2 M_{ii} \tilde{K}_{ii}^{-1} K_{ib}) X_b(\omega))$$

$$= \tilde{K}_{ii}^{-1} \begin{bmatrix} I & -\omega^2 M_{ii} \tilde{K}_{ii}^{-1} K_{ib} \end{bmatrix} \begin{Bmatrix} F_i(\omega) \\ X_b(\omega) \end{Bmatrix}$$

This equation is similar to one of the transfer function equations already derived.

DEFINING TWO DIFFERENT SUBSTRUCTURE INPUT  
VECTORS CORRESPONDING TO THE BOUNDARY MOTIONS

## Defining Two Different Substructure Input Vectors Corresponding to the Boundary Motions

In the preceding calculations involving the development of the substructure transfer function matrix, the input vector was taken to be

$$\begin{Bmatrix} F_i \\ X_b \end{Bmatrix}.$$

For this case the transfer function matrix was

$$T_{ii} [I \mid -\tilde{K}_{ib}].$$

The purpose of this note is to point out that

it is possible to define a second/different input vector. This can be done simply by looking at the equation written just prior to defining the transfer function.

$$X_i = \tilde{K}_{ii}^{-1} (F_i - \tilde{K}_{ib} X_b)$$

Instead of taking  $X_b$  as some of the inputs, take  $-\tilde{K}_{ib} X_b$  as some of them. Let

$$X'_b = -\tilde{K}_{ib} X_b$$

$$X_i = \tilde{K}_{ii}^{-1} (F_i + X'_b)$$

$$= \tilde{K}_{ii}^{-1} \begin{bmatrix} I & I \end{bmatrix} \begin{Bmatrix} F_i \\ X'_b \end{Bmatrix}$$

When the input vector is defined using  $X_b'$ , it is necessary to know the matrix  $\tilde{K}_{ib}$ . This makes determining the transfer function matrix more difficult. However, the transfer function obtained is

$$\tilde{K}_{ii}^{-1} [I \mid I].$$

Its poles correspond to the eigenvalues of the substructure with its boundaries fixed.

If the other input vector is used, it is not necessary to determine  $\tilde{K}_{ib}$  explicitly.

However, the transfer function determined will involve  $\tilde{K}_{ib}$ . There are advantages and disadvantages to both approaches.



**ANCO**

APPENDIX B

THEORETICAL BASIS OF MAC/RAN IV MULTI-INPUT  
SINGLE-OUTPUT TRANSFER FUNCTION COMPUTATIONS

This appendix contains a brief discussion of some of the theoretical aspects of the multi-input single-output transfer function computations performed by MAC/RAN IV [1,2]. The material is taken from Reference 1. Also, some of the MAC/RAN IV input data listings that were used to perform this type of computation is presented. Finally, a brief discussion of the ANCO computer program/macro used to perform multi-input multi-output transfer function computations, MIMO, is presented.

#### References

1. R.K. Otnes and L. Enochson, "Digital Time Series Analysis," John Wiley and Sons, New York, New York, 1972.
2. "MAC/RAN IV, Time Series Data Analysis System," University Software Systems, El Segundo, California, 1973.

THEORY OF MULTI-INPUT SINGLE-OUTPUT TRANSFER  
FUNCTION COMPUTATIONS PERFORMED BY MAC/RAN IV

## CHAPTER 9

### TRANSFER FUNCTION AND COHERENCE FUNCTION COMPUTATIONS

#### 9.1 PROPERTIES OF FREQUENCY RESPONSE FUNCTIONS

A discussion of linear systems and the computational procedures necessary for obtaining estimates of them from measured time histories is presented in this chapter. The simplest case, which has a single input and a single output, is discussed first. A generalization to the multiple-input, single-output system is then presented. Computational requirements and procedures for confidence limit evaluations are given in Sections 9.4 to 9.9. Extensions to other ideas of multivariate statistics are given in Section 9.10.

#### 9.3 SPECTRAL RELATIONSHIPS FOR MULTIPLE-INPUT LINEAR SYSTEMS

A model of a linear system responding to multiple inputs will now be considered. It will be assumed that

#### MULTIPLE-INPUT LINEAR SYSTEMS

333

$p$  inputs exist, and a single output is measured. Three types of coherence functions, ordinary, multiple, and partial, play an important role in this analysis, and their evaluation is discussed.

Consider a linear system with time-invariant parameters and  $p$  inputs  $x_\ell(t)$ ,  $\ell = 1, 2, \dots, p$ . That is

$$y(t) = \sum_{\ell=1}^p y_\ell(t) \quad (9.21)$$

where  $y_\ell(t)$  is defined as that part of the output produced by the  $i$ th input,  $x_\ell(t)$ , when all the other inputs are zero (see Figure 9.2). The function  $h_{\ell y}$  in Figure 9.2 is defined as the weighting function associated with the linear system between the input  $x_\ell(t)$  and the partial output  $y_\ell(t)$ . Hence,  $y_\ell(t)$  is given as follows:

$$y_\ell(t) = \int_{-\infty}^{\infty} h_{\ell y}(\tau) x_\ell(t - \tau) d\tau \quad (9.22)$$

The Fourier transform of (9.22) gives

$$Y_\ell(f) = H_{\ell y}(f) X_\ell(f) \quad (9.23)$$

where  $Y(f)$  and  $X(f)$  are the Fourier transforms of  $Y(t)$  and  $x(t)$ , respectively. Then the Fourier transform  $Y(f)$  for the total output is

$$Y(f) = \sum_{\ell=1}^P Y_\ell(f) = \sum_{\ell=1}^P H_{\ell y}(f) X_\ell(f) \quad (9.24)$$

The statistician reading this material should immediately note that (9.24) is a regression equation for zero mean variables. The dependent variable is  $Y$ , the independent variables are  $X_\ell$ , and the regression coefficients are  $H_{\ell y}$ . Thus, electrical or mechanical engineering frequency domain transfer function concepts

### 334 TRANSFER AND COHERENCE FUNCTION COMPUTATIONS

can be interpreted by the statistician via regression analysis of complex random variables. This concept is delved into in considerable detail by (Akaike, 1965). The gist of it is that we can treat each frequency band independently, and by accomplishing many complex variable regression analyses (one for each frequency band) we will obtain the entire frequency domain functions.

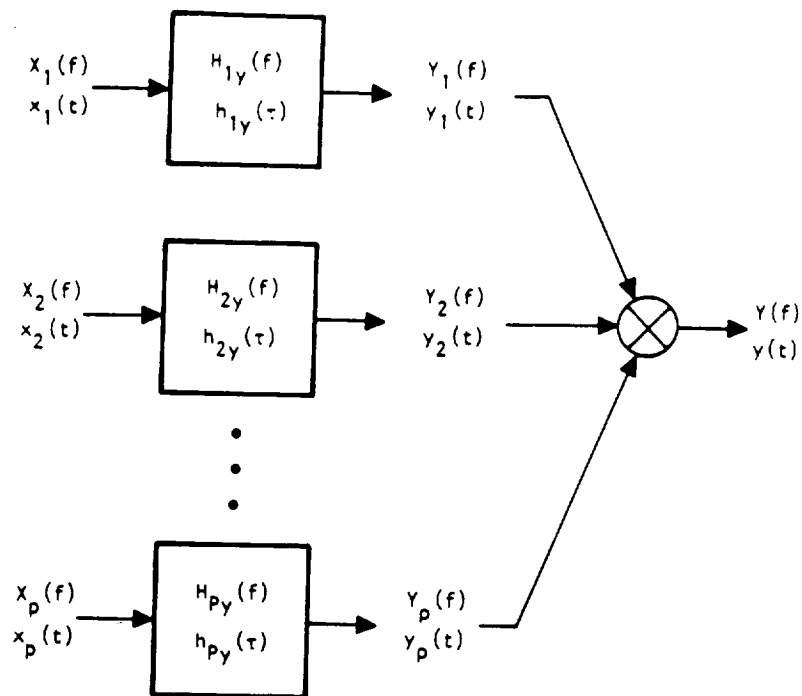


Fig. 9.2 Multiple-input linear system.

As in multiple regression analysis, the preceding relations can be expressed more concisely in matrix notation, and many results become more readily apparent. First, define a  $p$ -dimensional input column vector [the prime (') denotes transpose]

$$X(t) = [x_1(t), x_2(t), \dots, x_p(t)]' \quad (9.25)$$

## MULTIPLE-INPUT LINEAR SYSTEMS

335

Also define a  $p$ -dimensional transfer function vector

$$H(f) = [H_{1y}(f), H_{2y}(f), \dots, H_{py}(f)]' \quad (9.26)$$

Next, define a  $p$ -dimensional cross power spectrum vector of the output  $y(t)$  with the inputs  $x_i(t)$ ,

$$G_{xy}(f) = [G_{1y}(f), G_{2y}(f), \dots, G_{py}(f)]' \quad (9.27)$$

where

$$G_{ly}(f) \equiv G_{x_ly}(f) \quad l = 1, 2, \dots, p \quad (9.28)$$

Finally, define the  $(p \times p)$  matrix of the power and cross spectra of all the inputs  $x_i(t)$  by

$$G_{xx}(f) = \begin{bmatrix} G_{11}(f) & G_{12}(f) & \dots & G_{1p}(f) \\ G_{21}(f) & G_{22}(f) & \dots & G_{2p}(f) \\ \vdots & \vdots & & \vdots \\ G_{p1}(f) & G_{p2}(f) & \dots & G_{pp}(f) \end{bmatrix} \quad (9.29)$$

where for simplicity we adopt the notation

$$G_{ij}(f) = G_{x_i x_j}(f) \quad i, j = 1, 2, \dots, p \quad (9.30)$$

The matrix  $G_{xx}(f)$  is Hermitian, since it equals its conjugate transpose. This implies, for example, that the eigenvalues of  $G_{xx}(f)$  are real numbers, should these parameters be of interest in an application.

The system of linear equations to obtain a least squares solution for the  $H_{ly}(f)$  of (9.23) is the matrix equation

### 336 TRANSFER AND COHERENCE FUNCTION COMPUTATIONS

$$G_{xy}(f) = G_{xx}(f) H(f) \quad (9.31)$$

This is equivalent to

$$\begin{bmatrix} G_{1y}(f) \\ G_{2y}(f) \\ \vdots \\ G_{py}(f) \end{bmatrix} = \begin{bmatrix} G_{11}(f) & G_{12}(f) & \dots & G_{1p}(f) \\ G_{21}(f) & G_{22}(f) & \dots & G_{2p}(f) \\ \vdots & \vdots & & \vdots \\ G_{p1}(f) & G_{p2}(f) & \dots & G_{pp}(f) \end{bmatrix} \begin{bmatrix} H_{1y}(f) \\ H_{2y}(f) \\ \vdots \\ H_{py}(f) \end{bmatrix} \quad (9.32)$$

The solution to this system of equations is

$$H(f) = G_{xx}^{-1}(f) G_{xy}(f) \quad (9.33)$$

For the practical situation, we estimate the spectra and cross spectra in (9.32) with the procedures described in Chapters 6, 7, and 8.

EXAMPLE OF MAC/RAN IV MULTI-INPUT SINGLE-OUTPUT TRANSFER  
FUNCTION COMPUTATION INPUT DATA CARD IMAGE LISTINGS



RELATIVE MODULE TRANSFER FUNCTION MATRIX COMPUTATION  
USING PSD AND TRANS PROCESSORS IN MAC/RAN IV

```

JBHEAD REL.SIMP.TRANS.FUNCT.- PSD,J4F457U ACC(4MODES-2MODES), F6=0
FILIN J4F457U2.SDF
C* ACCEL. RESP.S      TIME      A4(IN1)      A5(OUT1)      A6(OUT2)
FILIN CCHAN           1.        2.        3.        4.
C* ACCEL. RESP.S      A7(IN2)
FILIN CCHAN           5.
FILIN J4F457U4.SDF
C* ACCEL. RESP.S      A4(IN1)      A5(OUT1)      A6(OUT2)      A7(IN2)
FILIN CCHAN           2.        3.        4.        5.
FILIN RANTRNC1.SDF
C* APPL. FORCES      F5
FILIN CCHAN           2.
PREP
PREP  SRCE RPSD-SISO,
PREP  TYPEJ4F457URTF60
PLUG
PLUG  WIRE TIME, SEC.      1      1
PLUG  SUB RELACC5          7      3      -2
PLUG  WIRE RELACC5        -2      2
PLUG  WIRE ABSACC4         2      3
PLUG  WIRE ABSACC7         5      4
PLUG  MULC F5X50.         10     -10 50.
PLUG  WIRE FORCEF5        -10      5
PLOT
PLOT  SCALE      0.0      24.0
FILOUT RELPSDAS.SDF
PSD  TRANS      1024.0      6.0      0.12
PSD  TOUTMTFC
PSD  RETAIN      0.0
PSD  FOUT33333
PSD  PLOT
PSD  SCALPSD      0.0      8.0
PSD  SCALCSD      0.0      8.0
PSD  SCALCOH      0.0      8.0
PSD  SCALTFF      0.0      8.0      0.0      100.
FILIN J4F457U2.SDF
C* ACCEL. RESP.S      TIME      A4(IN1)      A5(OUT1)      A6(OUT2)
FILIN CCHAN           1.        2.        3.        4.
C* ACCEL. RESP.S      A7(IN2)
FILIN CCHAN           5.
FILIN J4F457U4.SDF
C* ACCEL. RESP.S      A4(IN1)      A5(OUT1)      A6(OUT2)      A7(IN2)
FILIN CCHAN           2.        3.        4.        5.
FILIN RANTRNC1.SDF
C* APPL. FORCES      F5
FILIN CCHAN           2.
PREP
PREP  SRCE RPSD-SISO,
PREP  TYPEJ4F457URTF60
PLUG
PLUG  WIRE TIME, SEC.      1      1
PLUG  SUB RELACC6          8      4      -2
PLUG  WIRE RELACC6        -2      2
PLUG  WIRE ABSACC4         2      3
PLUG  WIRE ABSACC7         5      4
PLUG  MULC F5X50.         10     -10 50.

```

PLUG	WIRE FORCEFS		-10	5		
PLOT	PLOT					
PLOT	SCALE	0.0	24.0			
FILEOUT	RELPSDA6.SDF					
PSD	TRANS	1024.0		6.0		0.12
PSD	TOUTMTFC					
PSD	RETAIN	0.0				
PSD	POUT33333					
PSD	PLOT					
PSD	SCALPSD	0.0	8.0			
PSD	SCALCSD	0.0	8.0			
PSD	SCALCOH	0.0	8.0			
PSD	SCALTFF	0.0	8.0	0.0		100.
END						

JBHEAD REL.MISO TRANS.FUNCT.FROM TRANS, J4F2F3 ACC(D1S4-D1S2)MODES, F3=0  
FILIN RELPSDA5.SDF  
FILOUT JUNKRA5.SDF  
TRANS TAPE  
FILIN RELPSDA6.SDF  
FILOUT JUNKRA6.SDF  
TRANS TAPE  
END

ABSOLUTE MODULE TRANSFER FUNCTION MATRIX COMPUTATION  
USING PSD AND TRANS PROCESSORS IN MAC/RAN IV

```

FILIN J4F470U4.SDF
C* ACCEL. RESP.S
FILIN CCHAN
C* ACCEL. RESP.S
FILIN CCHAN
FILIN RANTRNC1.SDF
C* APPL. FORCES
FILIN CCHAN

```

FILIN	TIME	A4 (IN1)	A5 (OUT1)	A6 (OUT2)
C* ACCEL. RESP.S	1.	2.	3.	4.
FILIN CCHAN				
C* ACCEL. RESP.S	A7 (IN2)			
FILIN CCHAN	5.			
FILIN RANTRNC1.SDF				
C* APPL. FORCES	F5			
FILIN CCHAN	2.			

B-14

PSD	PLOT					
PSD	SCALPSD	0.0	8.0			
PSD	SCALCSD	0.0	8.0			
PSD	SCALCOH	0.0	8.0			
PSD	SCALTFF	0.0	8.0	0.0		.06
END						

JBHEAD MIMO TRANSFER FUNCTION FROM TRANS, J8F5F6 MODEL RANTR IN., F6=0  
FILIN ABSPSDA5.SDF  
FILOUT JUNKAA5.SDF  
TRANS TAPE  
FILIN ABSPSDA6.SDF  
FILOUT JUNKAA6.SDF  
TRANS TAPE  
END



BRIEF DISCUSSION OF ANCO COMPUTER CODE MIMO FOR  
COMPUTING MULTI-INPUT MULTI-OUTPUT TRANSFER  
FUNCTIONS USING MAC/RAN IV

**USE OF THE TRANS PROCESSOR AND  
VERIFICATION OF TRANSFER FUNCTIONS**

**June 1987**

**ANCO Contract No. 1311.05C (NASA)  
P.O. No. 2461**

**Prepared for**

**ANCO ENGINEERS, INC.  
9937 Jefferson Blvd.  
Culver City, California 90232**

**Prepared by**

**UNIVERSITY SOFTWARE SYSTEMS  
El Segundo, California**

## Table of Contents

1	OVERVIEW OF WORK DONE .....	1
2	COMPUTING AUTO AND CROSS SPECTRA .....	1
2.1	Degrees of Freedom .....	1
2.2	Segmentation .....	2
2.3	Distinction Between Effective Resolution Bandwidth and Computational Bandwidth, and the RETAIN Option. ....	2
3	THE LINEAR SYSTEMS PROCESSOR (TRANS) .....	3
3.1	Spectral Matrix Prepared by PSD .....	3
3.2	Ordinary, Multiple, and Partial Coherence .....	3
4	COMPUTATION PROCEDURE SUMMARY .....	4
4.1	ANCO's Automatic Control File Generator .....	4
4.1.1	Adjustable RETAIN Option .....	4
4.1.2	Using TRANS for Plotting .....	4
4.1.3	Confidence Limits .....	5
4.1.4	Frequency Bounds, and Instabilities in Computations .....	5
4.2	Plotted and Printed Results .....	5

## 1 OVERVIEW OF WORK DONE

The primary task of this job was to confirm the automatic control file generation for Micro-MAC/RAN and Micro-MAC/RAN:TRANS processing of finite element model results. The basic problem was to isolate a linear substructure from the finite element model and simulate a multi input / multi output linear system whose transfer functions could be effectively computed by a combination of the MAC/RAN PSD and TRANS processors. The two endpoints of the substructure were treated as the input points and the interior nodes the outputs. Transfer functions were computed between all input/output pairs, but not between outputs or between inputs. Two cases were processed by ANCO. Each case used a different base excitation for the large model, therefore the resulting endpoints of the substructure were different. Additionally, the first case processed 4095 data points with a 50 sps sampling rate, while the second case processed 1024 points with a 16.667 sps sampling rate. USS was to duplicate ANCO's results if possible, and to make recommendations on the procedures used to obtain these results. In particular, to determine whether the automatic control file generator was setting up the proper control file for MAC/RAN. In making these conclusions, various procedural issues were discussed. The following sections briefly describe these issues. The last section makes some recommendations as to control procedures.

## 2 COMPUTING AUTO AND CROSS SPECTRA

### 2.1 Degrees of Freedom

The PSD processor uses a technique that combines segment and frequency averaging to obtain statistically meaningful auto and cross spectra. By statistically meaningful, we mean that the resultant spectra has enough degrees of freedom (d.o.f.) to be considered a reasonable expectation of the mean power present in the data, as a function of frequency. By definition, the d.o.f. in a spectrum computation is

$$n = \frac{2BN}{f_s}$$

where

B is the bandwidth  
N is the number of points  
 $f_s$  is the sampling rate

If the data is too large to fit in core as one segment, we need to distinguish between the number of points per segment,  $N_s$ , and the number of points,  $N$ .

By default, PSD will try to make the proper decisions for what segment length the data needs to be broken down into and the number of frequency averages necessary to achieve a default d.o.f. of 30. This happens when the user leaves the field for Bandwidth on the first PSD controller blank or zero.

If PSD has enough core memory available, it will try to process data as one segment, and do frequency wise averaging to obtain the desired d.o.f.

In this case, the bandwidth becomes

$$\frac{15f_s}{N_s}$$

## 2.2 Segmentation

If PSD does not have enough memory to process the data as one segment, it breaks the data down into the minimum number of equal length segments that will fit into available memory. Zeros are padded to achieve a transformable length. Since segments will be averaged, if the bandwidth of each segment is  $B_s$ , then the d.o.f. will be

$$n = \frac{2N}{f_s} \frac{15f_s}{N_s} = 30 \times (\text{the number of segments})$$

If we had left the Bandwidth field blank or equal to zero, then PSD would need to modify the bandwidth for each segment to achieve the proper d.o.f. after averaging the segments. Also, if trailing zeros were padded in the segment(s), a weighting factor is used to compensate for the diminished magnitude of each segments Fourier transform. Refer to the MAC/RAN Reference Manual, Chapter 8 (D.3)

## 2.3 Distinction Between Effective Resolution Bandwidth and Computational Bandwidth, and the RETAIN Option.

Generally, if points of a spectral function are computed at the Effective Resolution Bandwidth, then the spectral values are approximately statistically independent. If a finer spacing is used, by way of PSD's RETAIN option, more points will be computed, however with little if any statistical significance. That is, there will be overlap between the estimates computed.

If more points are desired, to match with other functions, or for finer resolution of plots, then making the computational bandwidth smaller than the resolution bandwidth will achieve this at the expense of increased computation time and larger listings and plot files. By default, PSD tries to use a computation bandwidth equal to the desired resolution bandwidth, since that is the minimum spacing that gives

approximately non-overlapping, independent frequency values. This is also directly related to the d.o.f. in the computation. That is, if a very few d.o.f. are selected because the user specified a very narrow resolution bandwidth, then the frequency values will not be at all orthogonal, since the variance in each estimate would be very high (little or no frequency averaging was done).

### **3 THE LINEAR SYSTEMS PROCESSOR (TRANS)**

#### **3.1 Spectral Matrix Prepared by PSD**

A PSD option is to create a spectral matrix for the TRANS processor using the aforementioned techniques. This matrix contains the auto spectra of the output and all inputs, plus the cross spectra between inputs and output and the cross spectra between all pairs of inputs. This is because TRANS will try to determine the effect of each input on the output's composite response, so that individual transfer functions can be computed that "subtract out" the effects of the inputs that are not involved in the path for the particular transfer function. This concept is tied directly with the three types of coherence that are computed.

#### **3.2 Ordinary, Multiple, and Partial Coherence**

The idea of coherence is directly related to the linearity of the considered system or systems. TRANS computes the three coherencies automatically. The ordinary coherence is also computed by PSD but for a multiple input system, it is useful primarily for comparison purposes with the partial coherence. It is, however, the only coherence computed between inputs, as the inputs are assumed to be independent of each other. (Note that this does not mean they need be statistically independent; only that we assume they will "move" in the same way regardless of how many of them are present or where they are in the system. They are the "givens" in our set of equations). TRANS computes ordinary coherence between input pairs as an option, and we do not need this option for the problem considered here, since we know that the inputs to the substructure are really responses due to a base motion in the global system.

The partial coherence tells us how much of the computed response is due to a particular input. That is, if input 7 has a strong effect on output 5 and input 4 has a secondary effect on output 5, the partial coherence between 7 and 5 should be close to 1.0 since the response is almost completely due to the input at 7. Similarly, the partial coherence between 4 and 5 would be low, as the response at 5 would "feel" a strong presence from another point in the structure, namely input 7. The ordinary coherence ignores any distinc-

tion between other inputs and the input used in the computation. It does not condition the coherence computation on any other input. Thus, the ordinary coherence between 7 and 5, for example, might be high if the effect of 4 and other inputs is relatively minor. If multiple inputs contribute equally to an output motion, the ordinary coherence computation is usually off the mark, as it senses what it considers to be non-linearities in the transfer function. That is, there are unaccountable components in the response given the information that the ordinary coherence has to make its computation.

The multiple coherence plays the part of the ordinary coherence for a multi input system. It assumes that it has the information from all the inputs considered and computes a composite coherence. For linear systems with known inputs and low noise, the multiple coherence function is usually very close to 1.0 across the spectrum. If there is a drop in multiple coherence, this is an indication that a source of motion has been ignored, or that noise was introduced (incoherent components), or that the system is in fact somewhat nonlinear.

#### **4 COMPUTATION PROCEDURE SUMMARY**

##### **4.1 ANCO's Automatic Control File Generator**

USS's replication of the preliminary ANCO computations show that the automatic control file generator computed a good set of instructions for the PSD and TRANS processors. However, certain recommendations are made. These are:

###### **4.1.1 Adjustable RETAIN Option**

In light of the above discussion (Section 2), USS recommends that the automatic generation program allows the RETAIN decimation factor to be entered as a variable, since blindly retaining all points can be misleading as well as highly costly for large or many computations.

###### **4.1.2 Using TRANS for Plotting**

ANCO writes a Standard Data File (SDF) of the real and imaginary parts of the computed transfer functions using the TRANS TAPE option. They then use the PLUG and PLOT processors to plot the magnitude and phase of these transfer functions. TRANS directly plots the transfer functions along with the various coherence functions. USS matched the ANCO plots using only the TRANS processor. This eliminated some computation time and complexity that are introduced by the PLUG and PLOT processes. Additionally, the coherence functions should not be ignored, since for production runs,

they will verify that the transfer functions are meaningful. The concepts of coherence are directly related to multiple input transfer functions due to their statistical nature.

#### **4.1.3 Confidence Limits**

Another reminder of the statistical nature of spectrum computations is that upper and lower bounds are printed and optionally overlayed on the TRANS plots. USS recommends that this concept is noted, even if confidence limits are not plotted during the course of the production runs. By default, TRANS computes response functions with a 95% confidence that the results are between the upper and lower confidence levels. Note that if the difference between the upper and lower confidence levels is very large compared to the magnitude of the 95% value computed, then the transfer function may still be suspect. (For example, being 95% certain that the actual transfer function lies between 0 and infinity is quite meaningless).

#### **4.1.4 Frequency Bounds, and Instabilities in Computations**

A new TRANS controller allows printing and plotting of results between frequency start and stop values. This is useful if there is a problem computing the inverse of the spectral matrix or computation of transfer functions by dividing two statistically insignificant values, e.g. noise into noise when very little energy is present in the input or output in a frequency range. Also, for situations where a great deal of oversampling was done in the time histories, one does not want to deal with values of response or coherence well above a frequency where energy is known not to exist in appreciable amount. The TRANS FREQ and TRANS SCAL controllers allow plotting of the points of interest without spikes or glitches due to the aforementioned phenomena. The TRANS listing file will inform the user if there were any instabilities in the computation and at what frequencies they occurred.

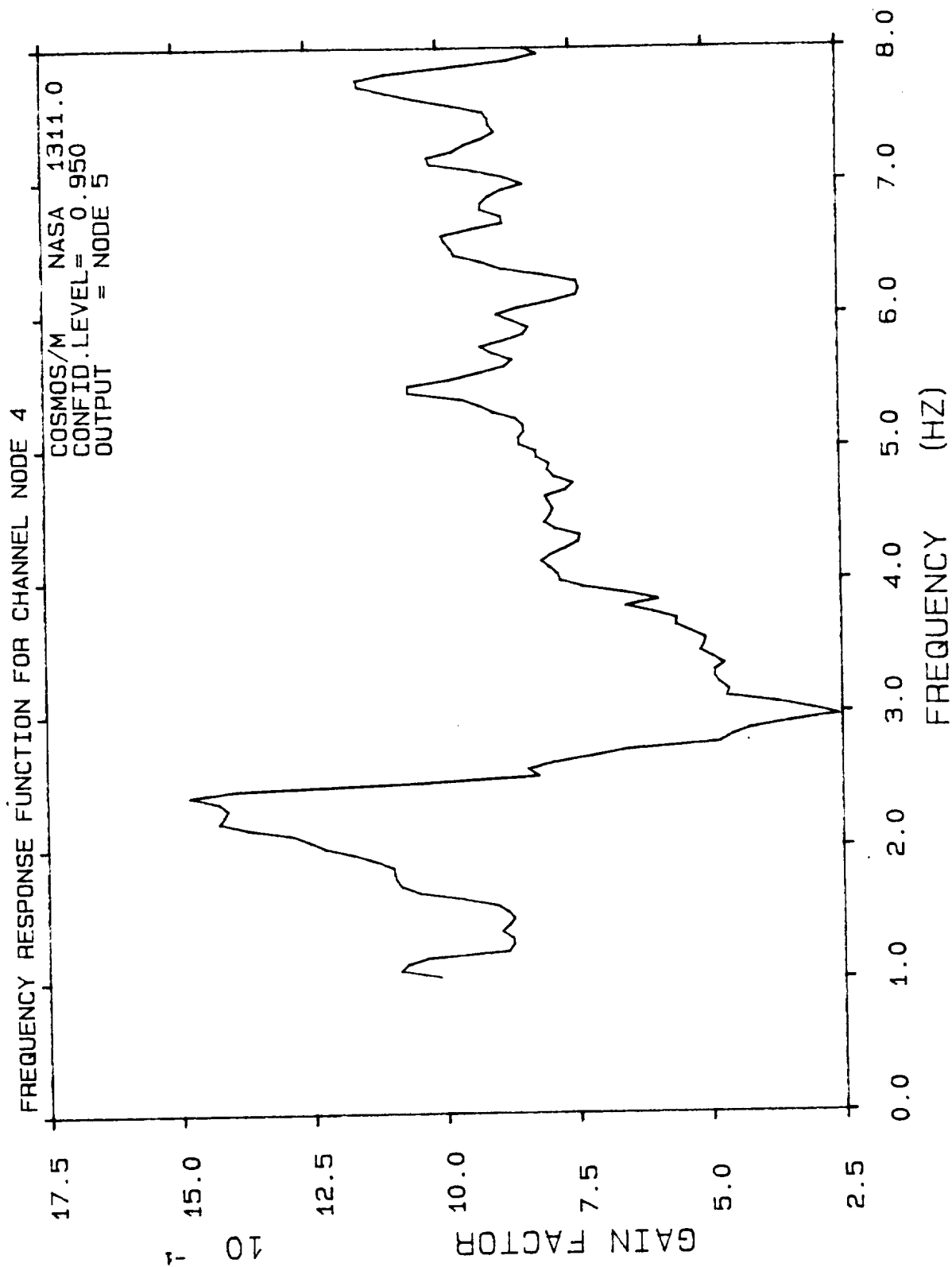
#### **4.2 Plotted and Printed Results**

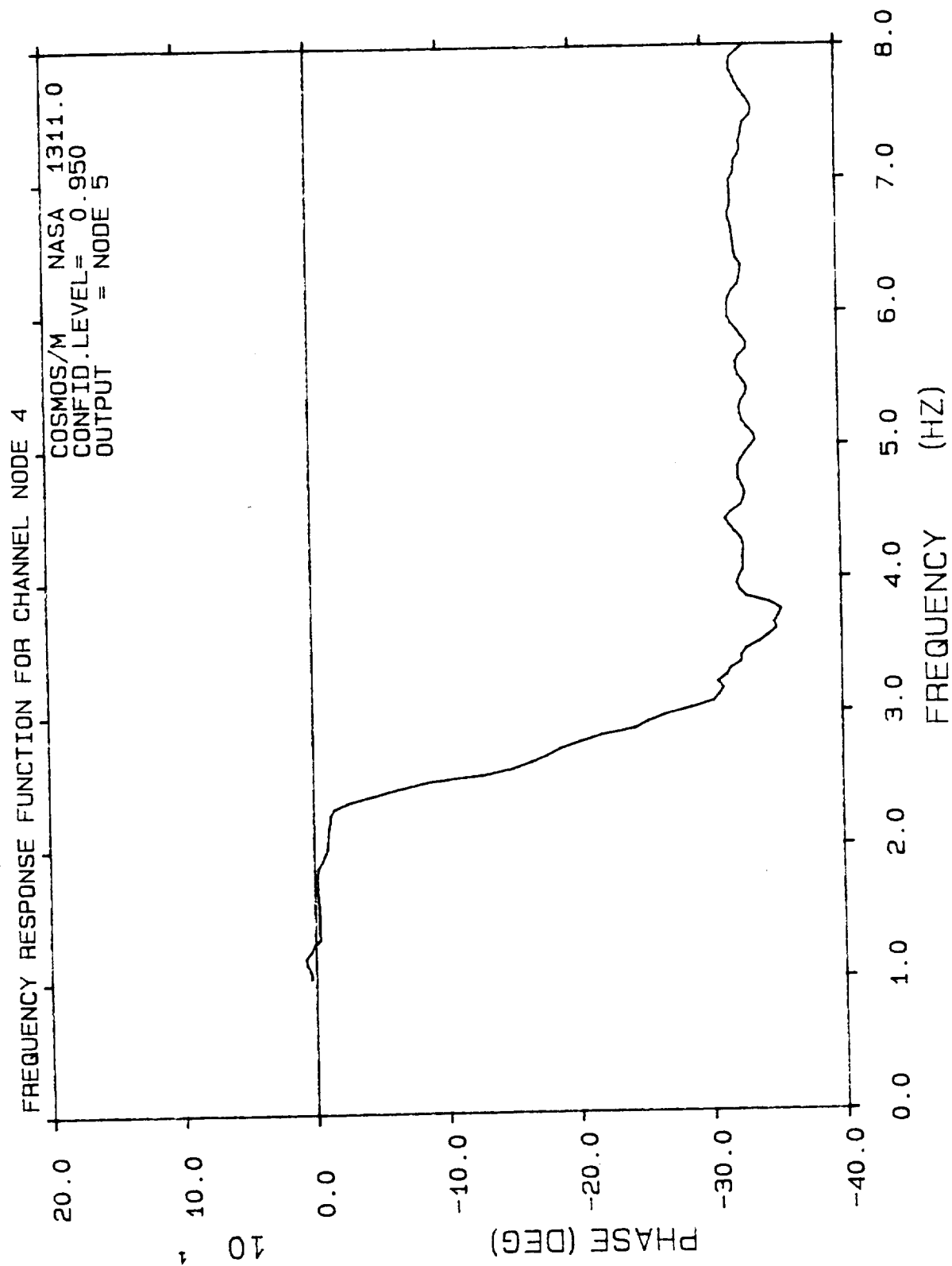
Delivered with this report are two sets of plots and listings that illustrate the matching of ANCO's results by USS. The first set (Set 1) correspond to phase 1 of the test runs and are designated by Source and Type annotation "COSMOS/M NASA 1311.0." Set 2 is annotated "NASA PHASE II" and corresponds to phase 2 of the test runs.

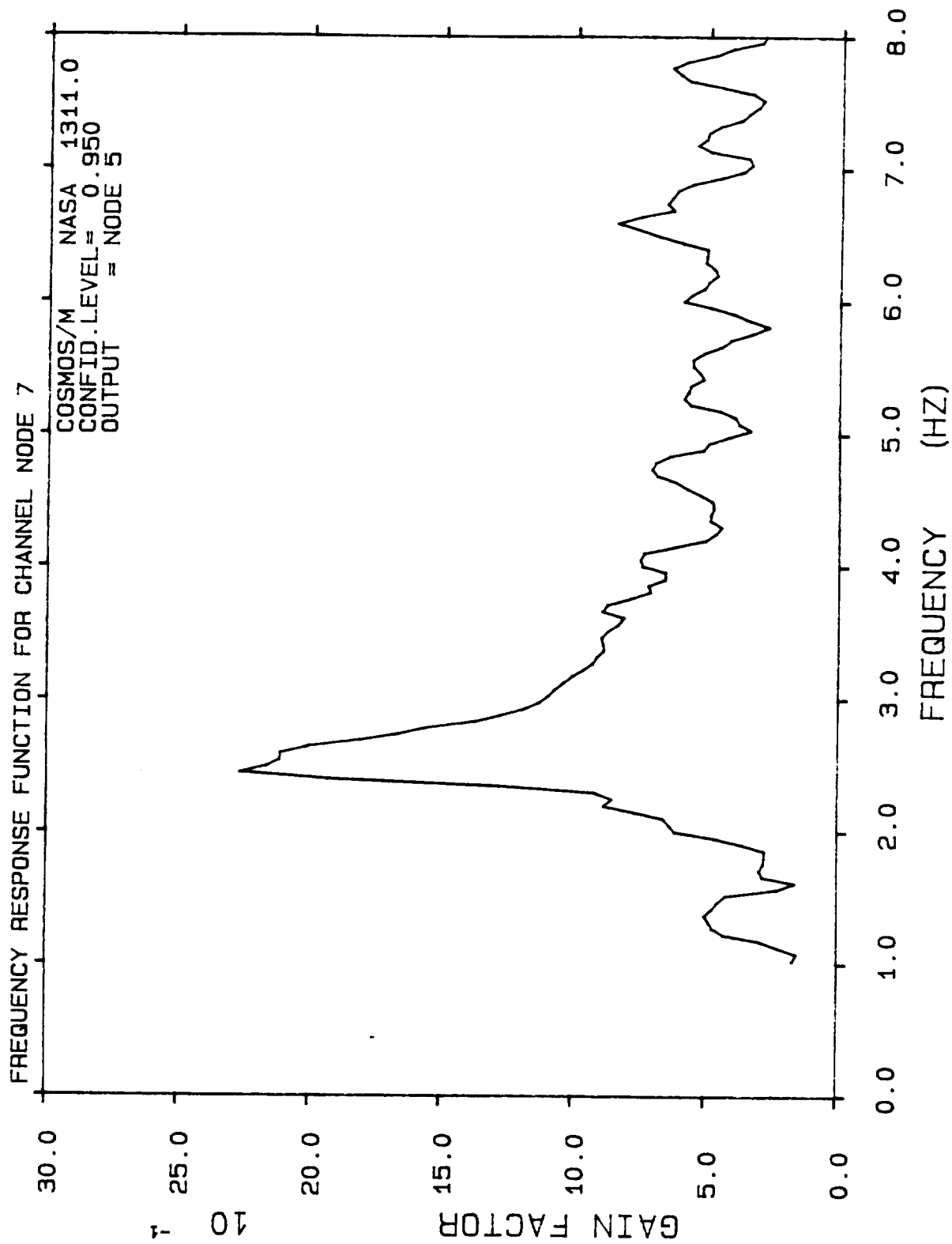
Note that the PSD plot and print suppress option was invoked to eliminate the display of unwanted information (TRANS will provide the relevant plots and print in the second step), however, on occasion it is instructive to view the spectra of the inputs and the outputs from PSD to see where the greater

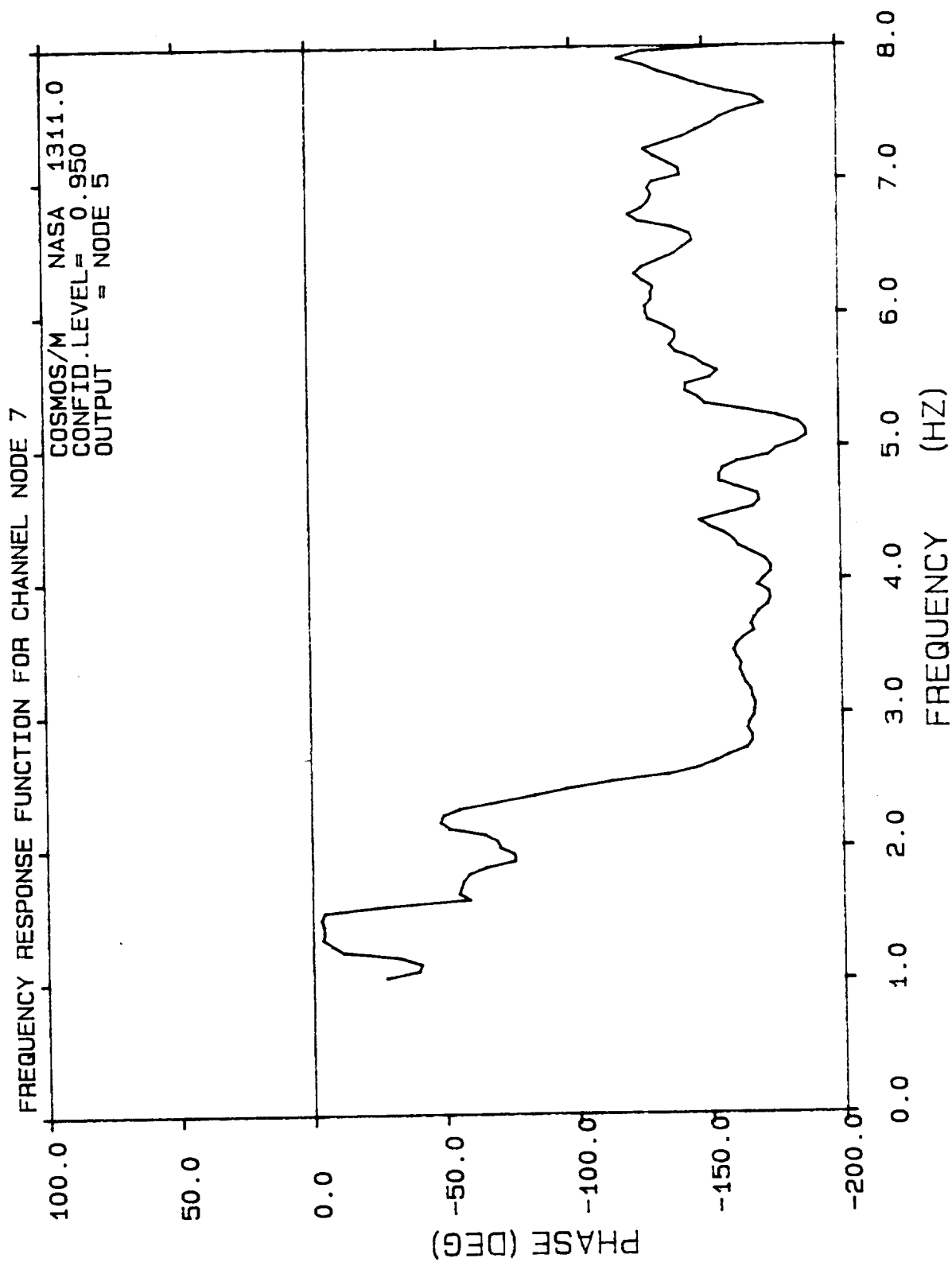


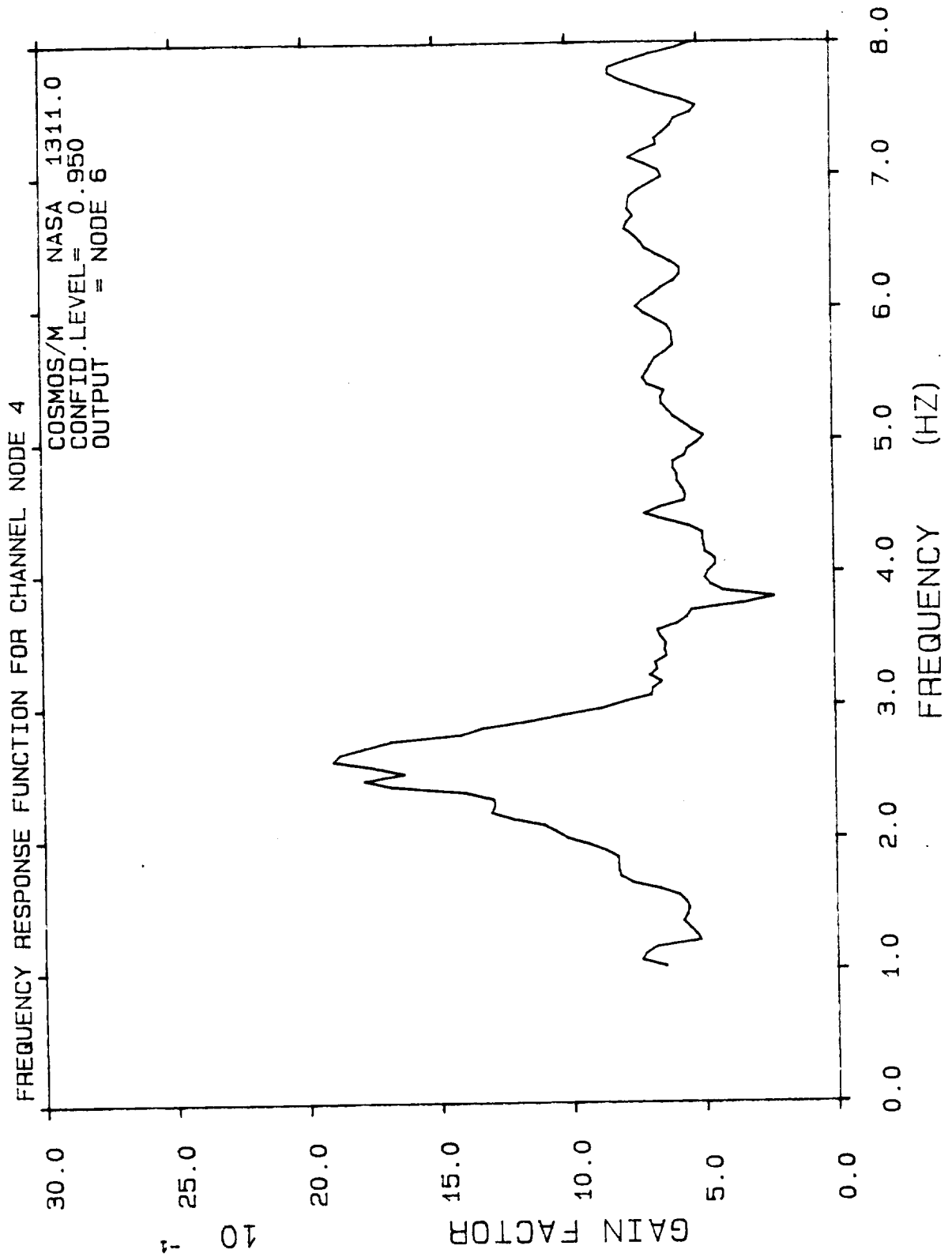
part of energy lies in the spectrum, and to get an idea about the signal to noise ratio in the transfer function computations.

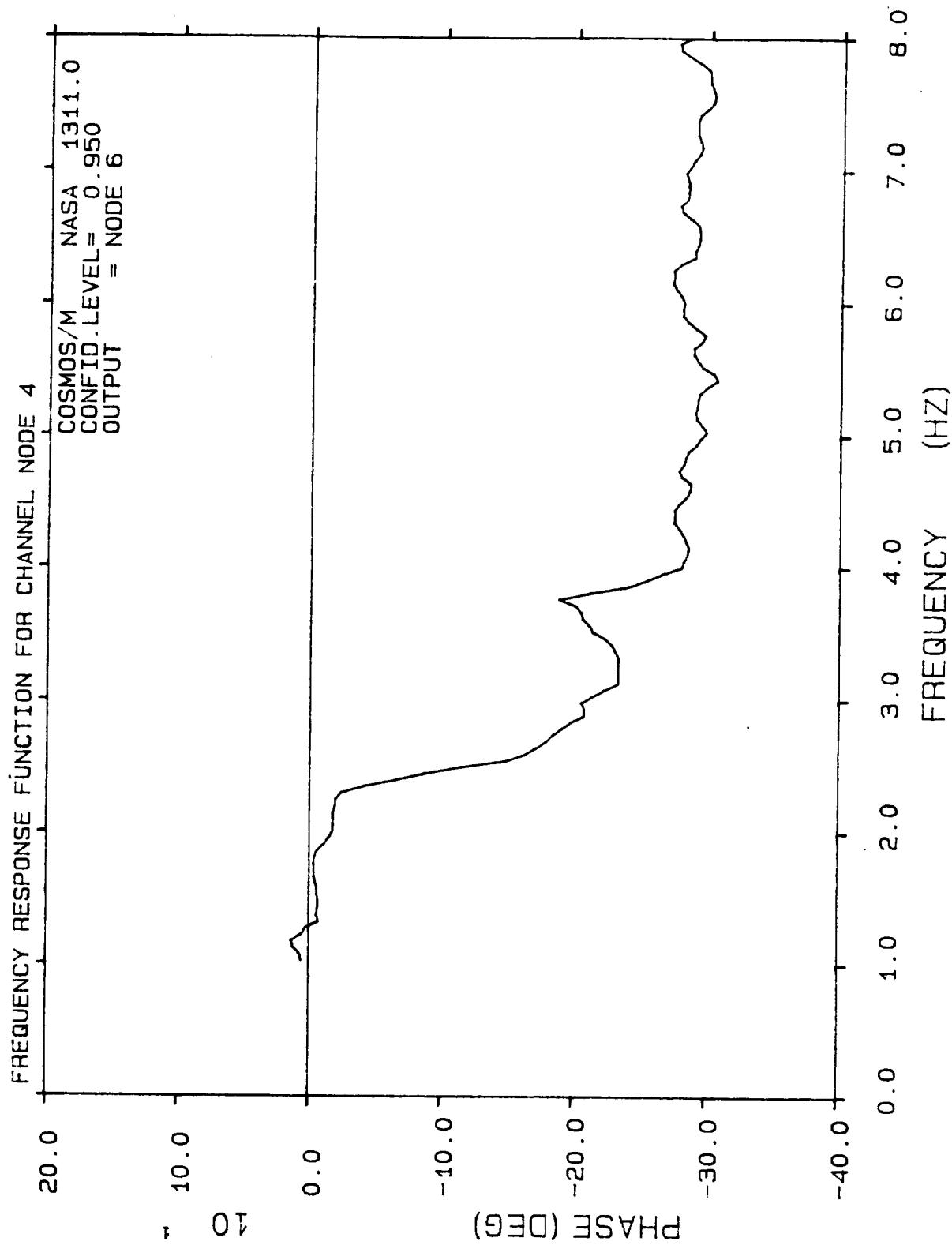


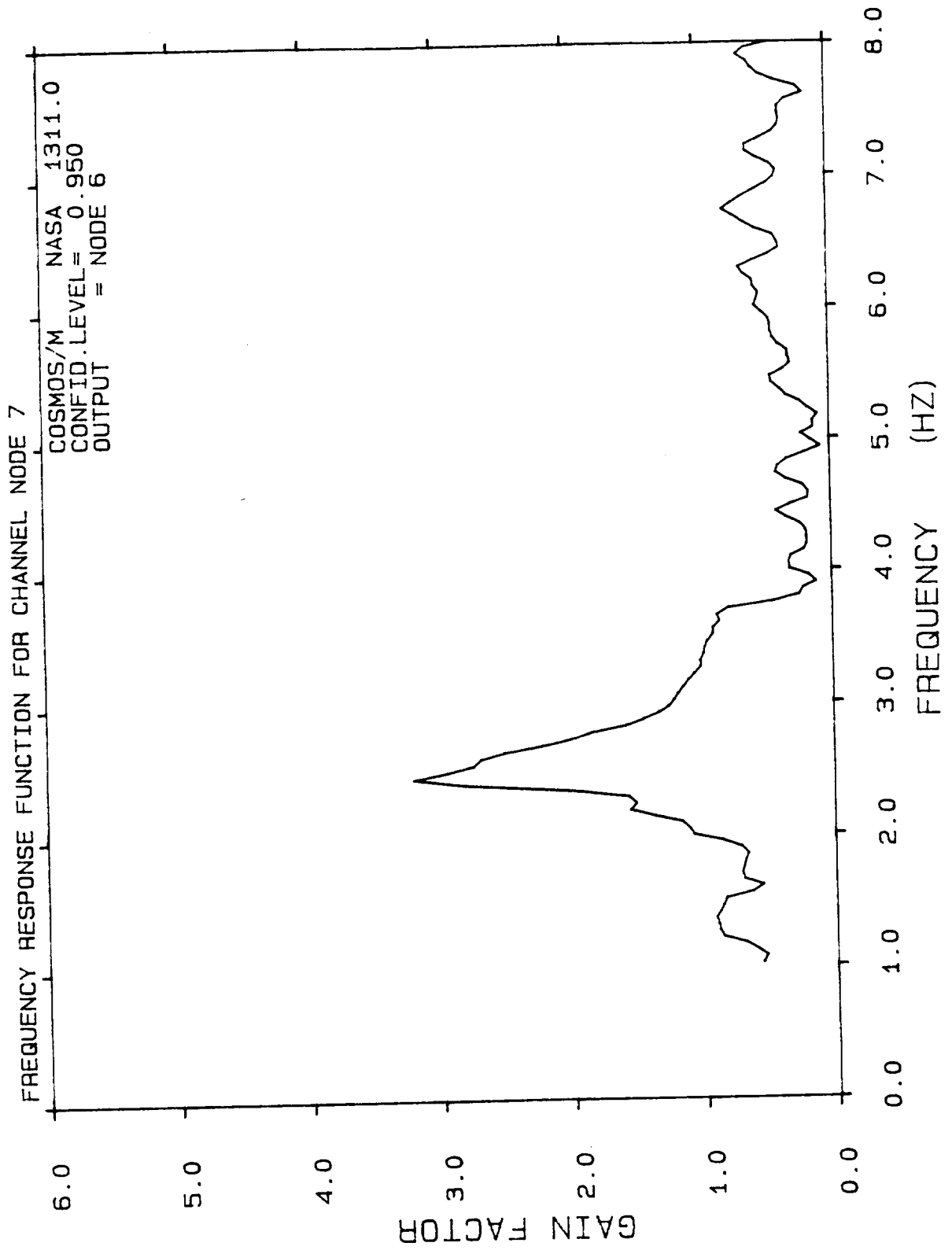




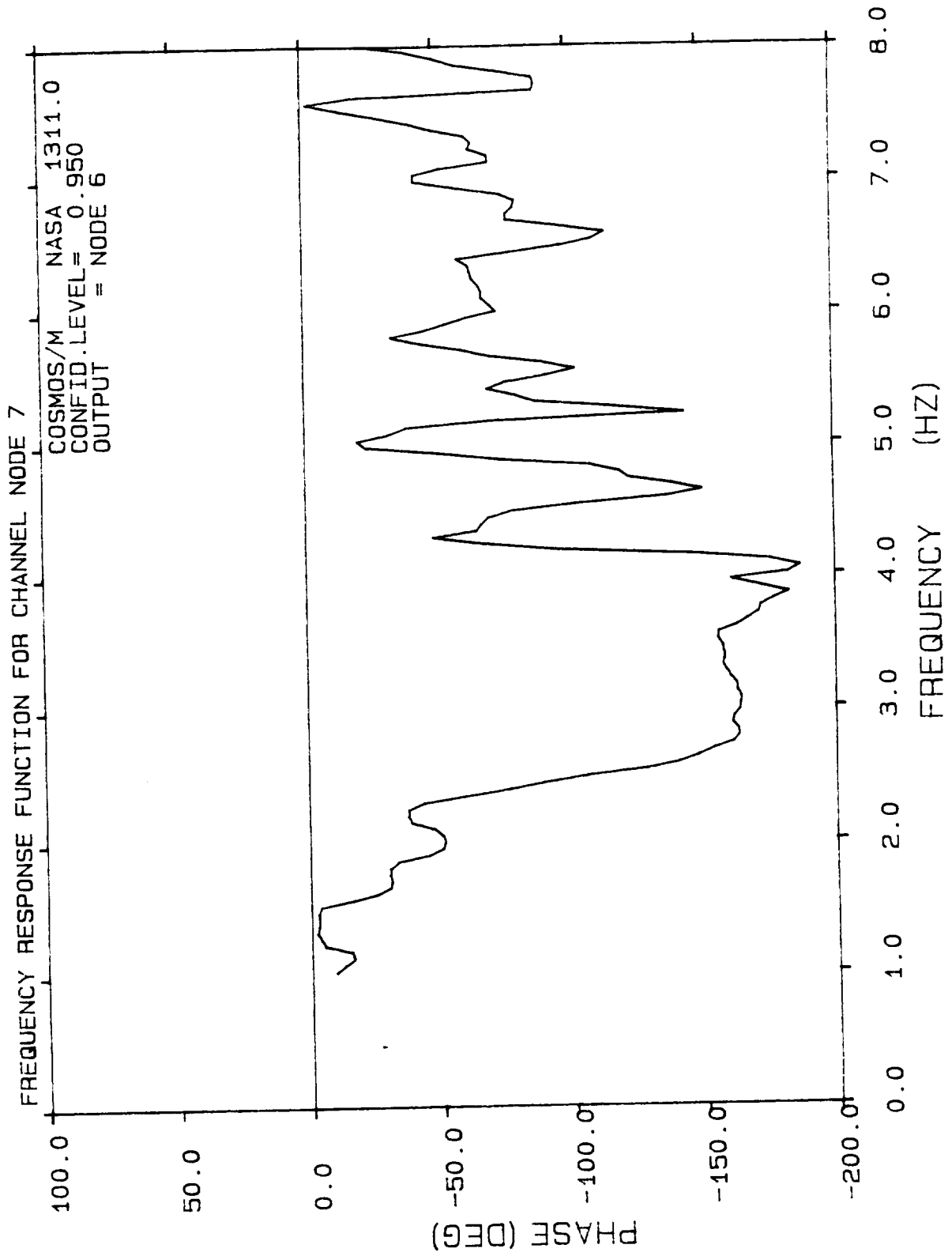


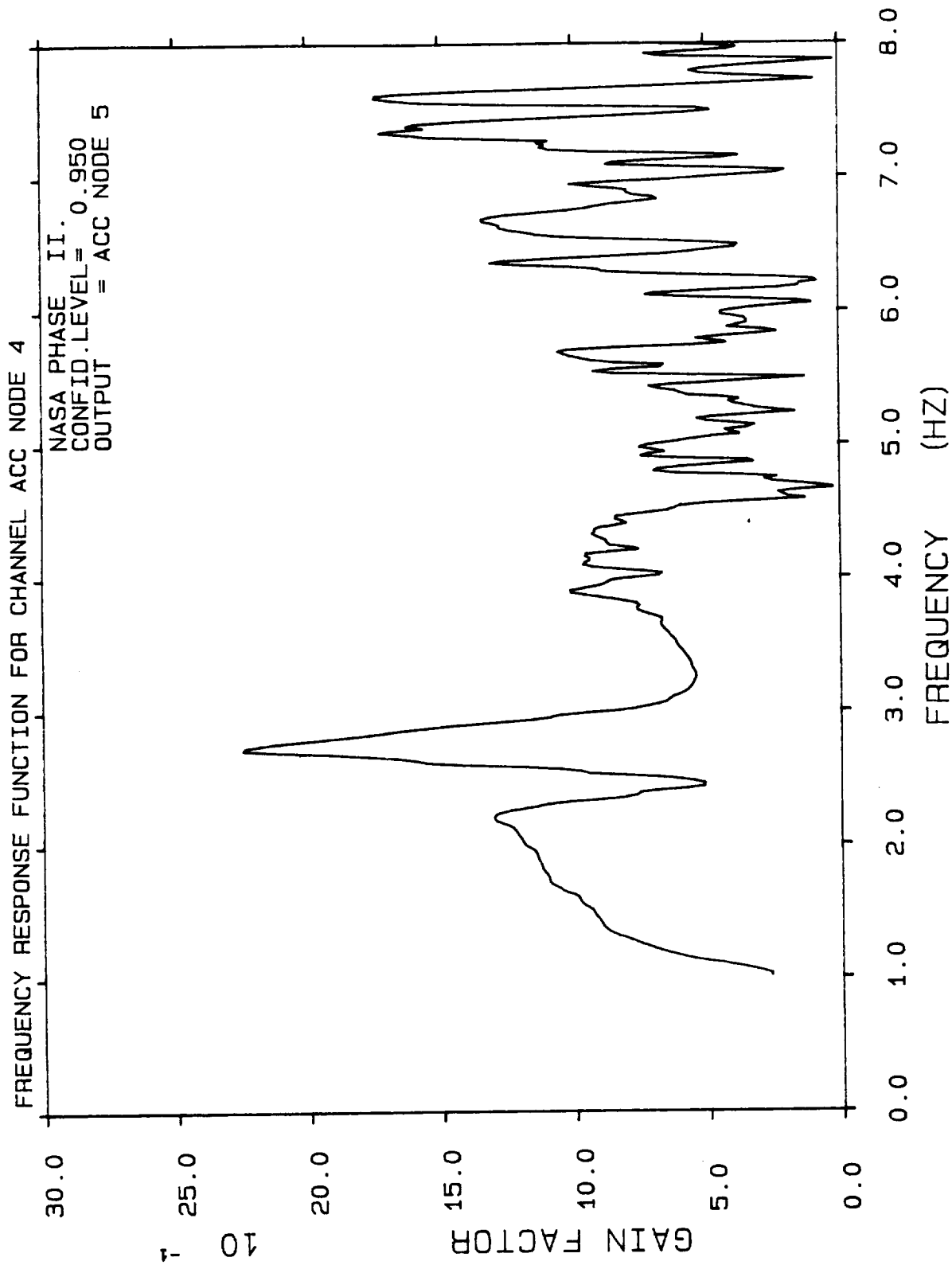


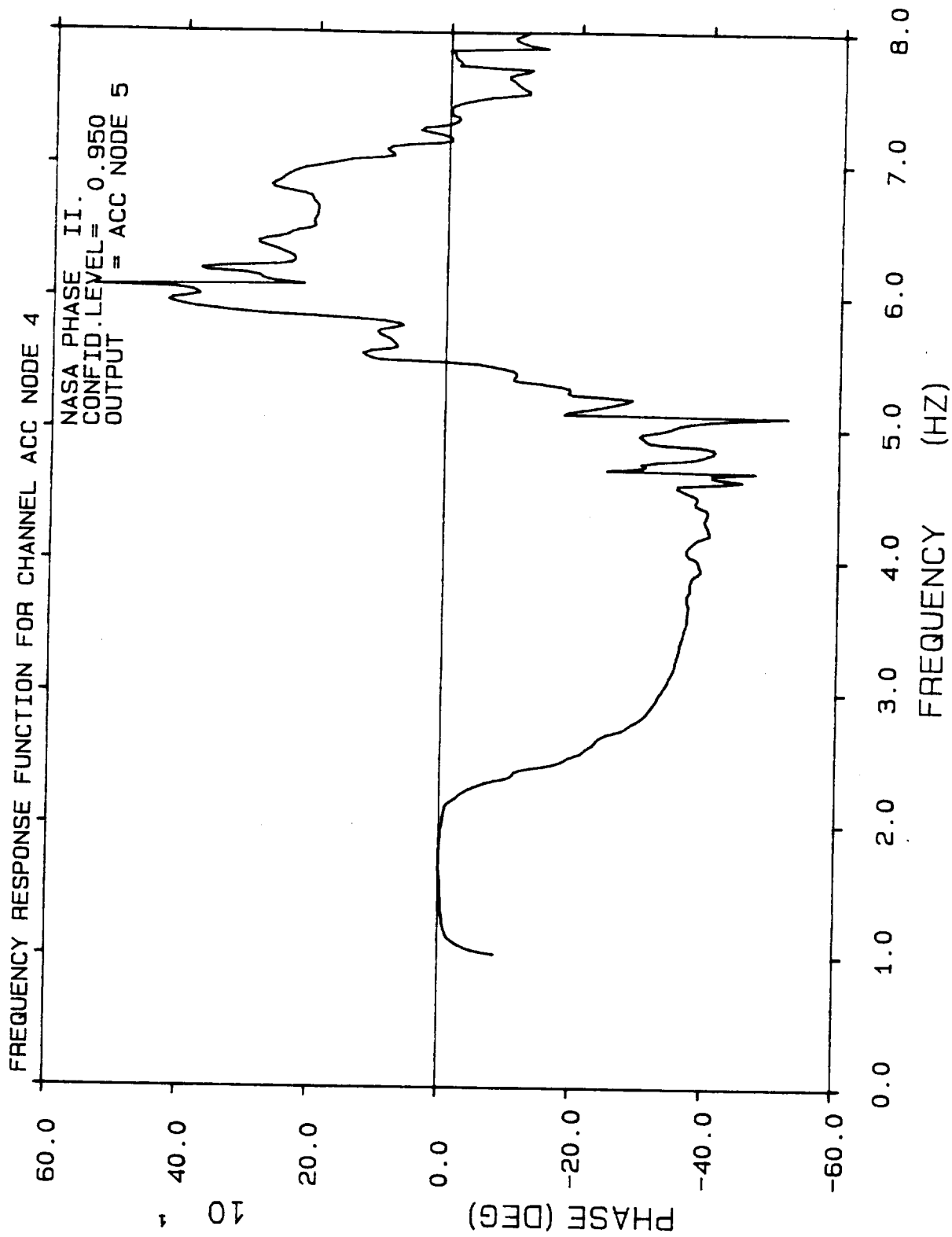


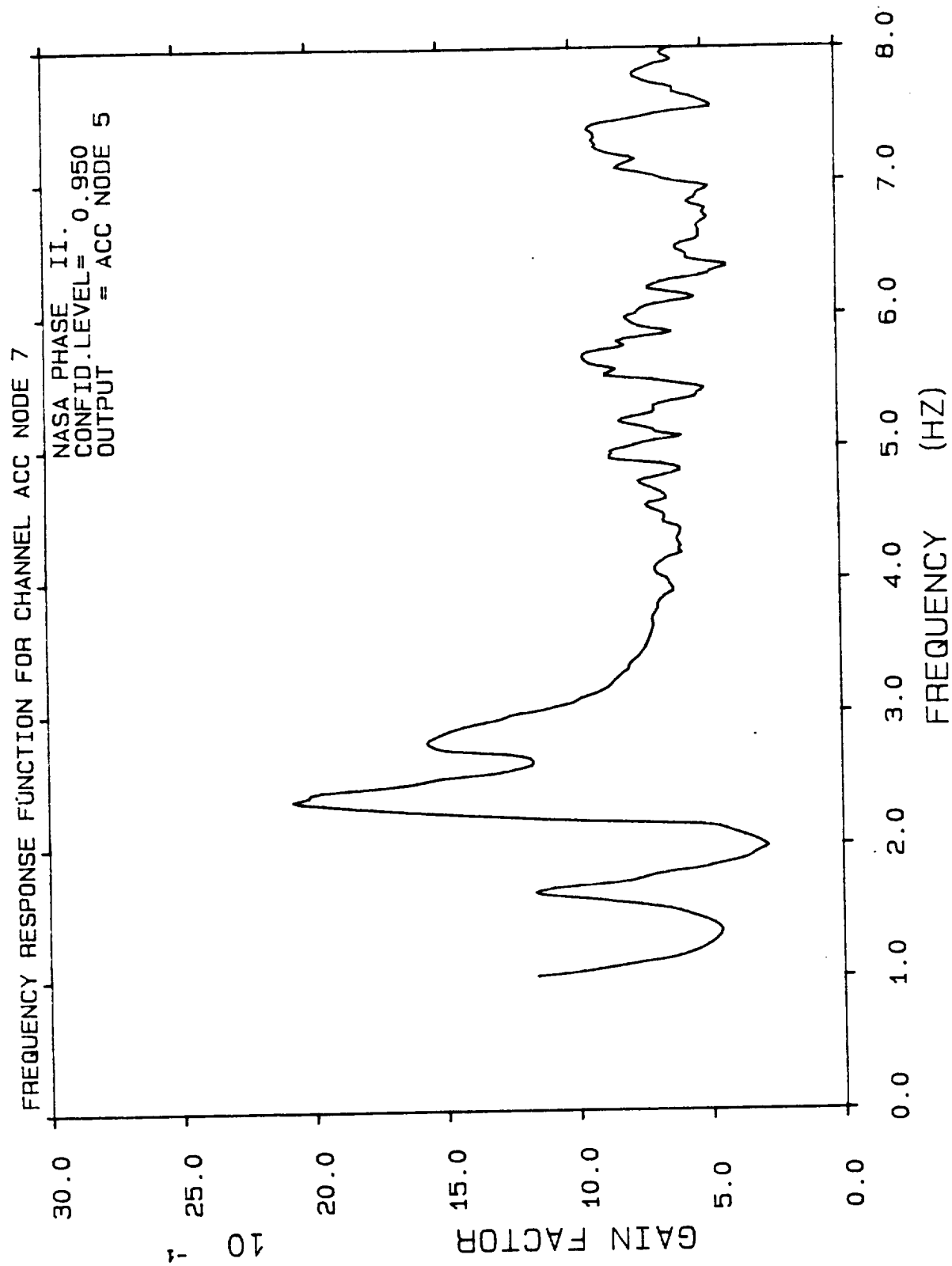


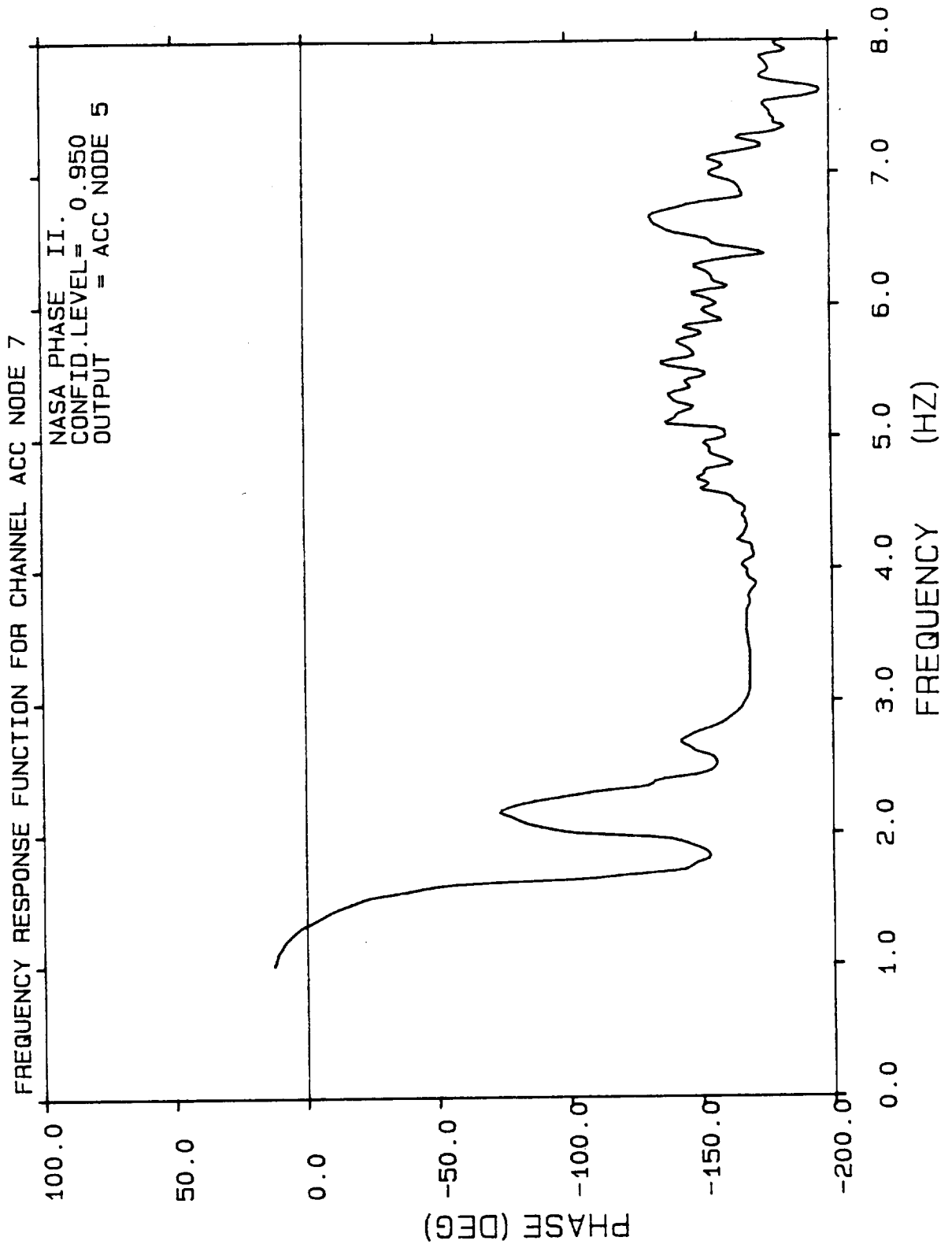


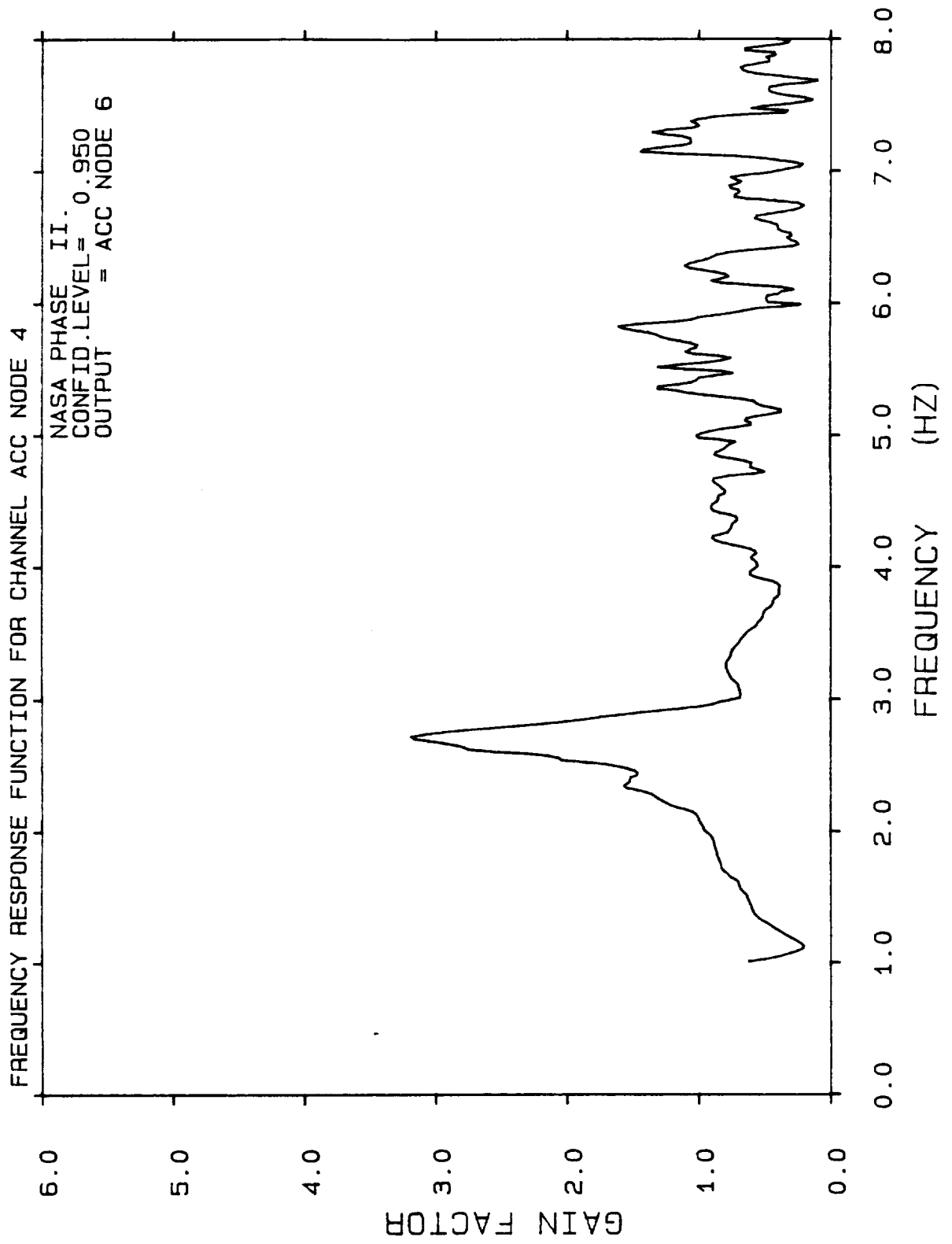


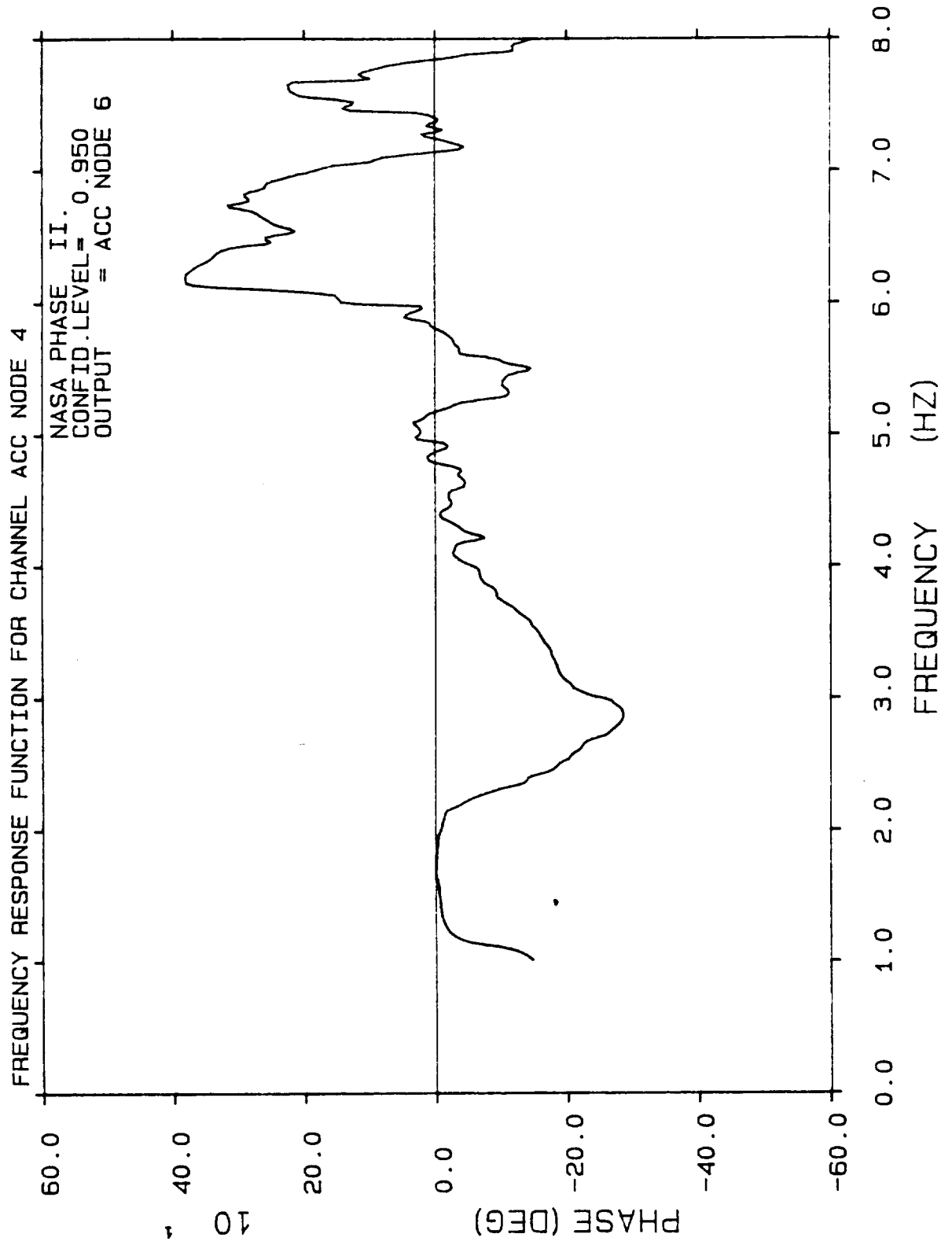


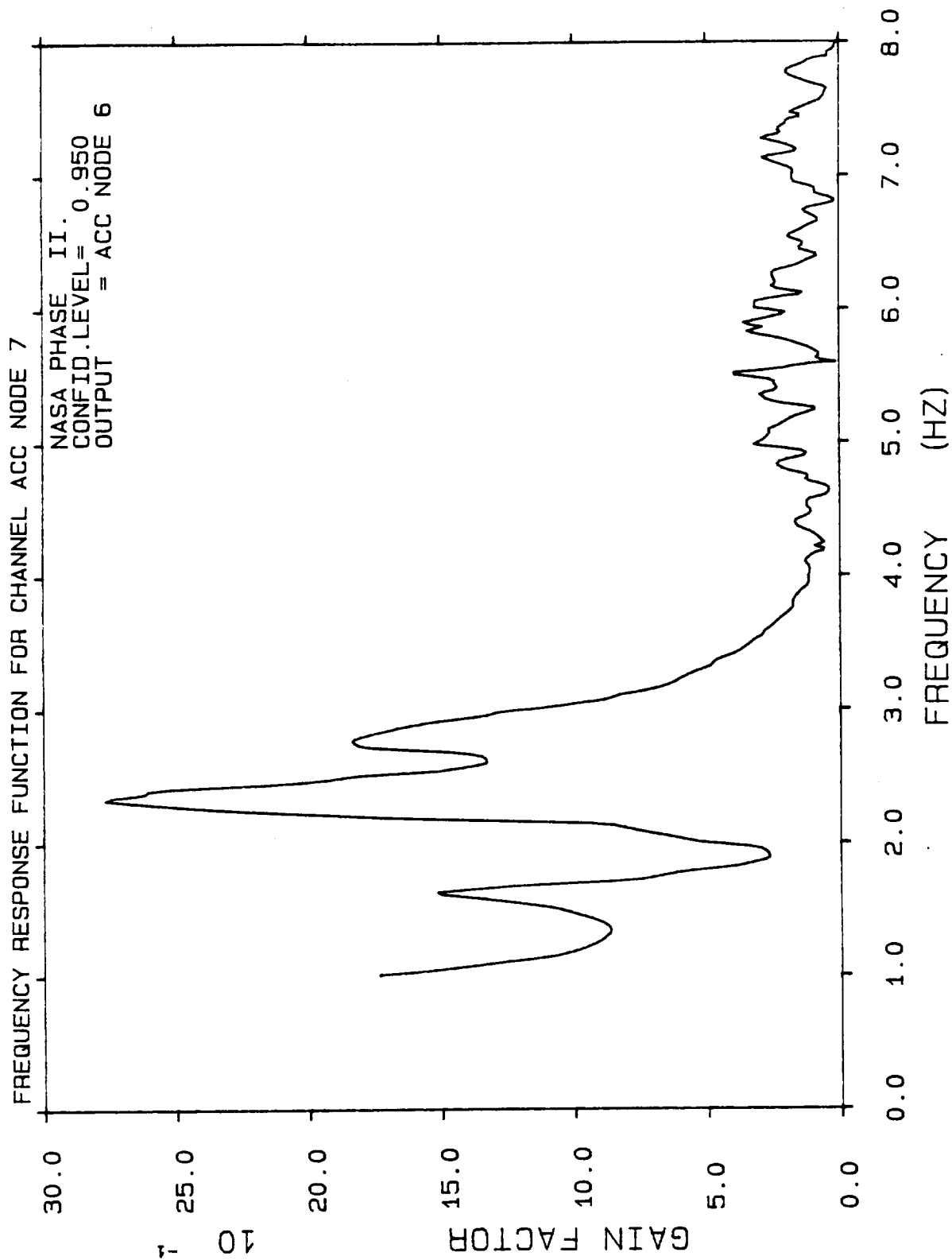




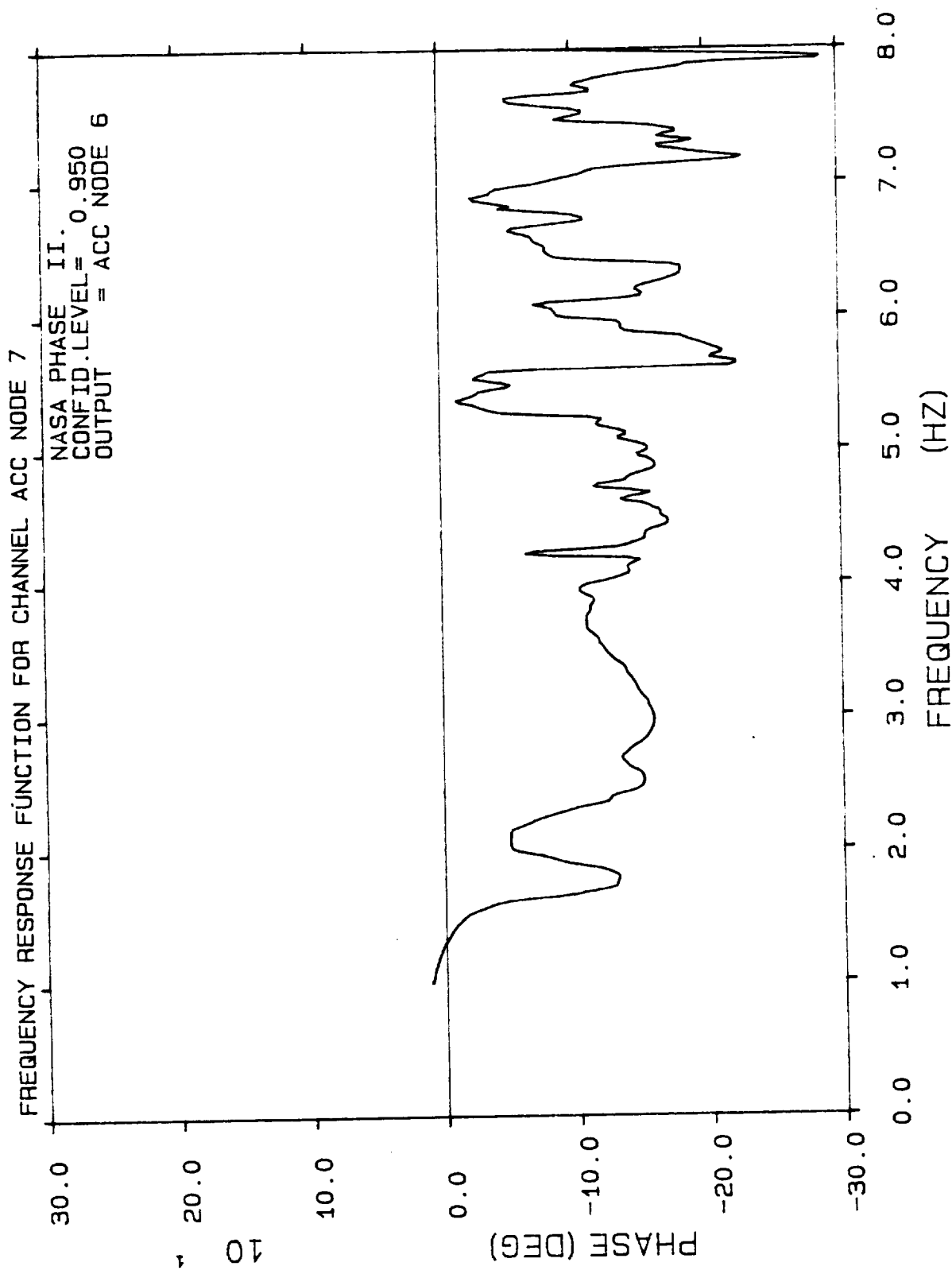












SOURCE CODE LISTING FOR  
MIMO TRANSFER FUNCTION AND  
DAMAGE INDICATOR COMPUTATION

Volume in drive A has no label  
Directory of A:\

FILAD		222	9-02-86	2:03p
FILBD		364	10-27-86	3:05p
FILECH		544	8-29-86	4:33p
FILEM		360	8-28-86	11:56a
FILEX		466	1-06-87	10:22a
FILMAP		557	8-28-86	2:21p
MACDAM		2507	1-06-87	9:35a
MACRD1		1156	4-17-87	10:11a
MACRD2		299	9-03-86	9:13a
MACRD3		271	10-22-86	3:49p
NASA		6408	4-17-87	10:10a
DAMAGE	FOR	2857	1-27-87	2:03p
DAMCOM	FOR	1096	1-27-87	2:04p
MACWRT	FOR	1575	1-07-87	9:58a

14 File(s) 1191424 bytes free

```

C
C SUBROUTINE FILAD(FILOT,IFLEN)
C
      SUBROUTINE FILAD(FILOT,IFLEN)
      IMPLICIT INTEGER*2 (I-N)
      CHARACTER*1 FILOT(6)
      IFL = IFLEN + 1
      DO 10 I=IFL,6
        FILOT(I) = 'O'
10      CONTINUE
      RETURN
      END

```

#NOFLOATCALLS

CHARACTER\*80 KEY

CHARACTER\*14 FLNAME

C  
C  
C

CALL VCLEAR

CALL VCURXY(0,0)

KEY = 'ENTER FILENAME TO DISPLAY : #'

CALL KEYBD(KEY,R,I,FLNAME,3,(14),0,5)

OPEN(7,FILE=FLNAME,FORM='UNFORMATTED')

10

CONTINUE

READ(7) FTR,FTI

WRITE(\*,8000) FTR,FTI

8000 FORMAT(2X,1PE10.3,5X,1PE10.3)

GO TO 10

STOP

END

```

C
C SUBROUTINE FILECH - PURPOSE TO SEE IF A .SDF EXTENSION IS ON
C
      SUBROUTINE FILECH(FIL1,IER)
      IMPLICIT INTEGER*2 (I-N)
      CHARACTER*1 FIL1(12)
      LOGICAL*2 IER
C
C FIRST LOOK FOR A .
C
      IER = .FALSE.
      DO 10 I=1,12
        IF(FIL1(I).EQ.'.') GO TO 20
10      CONTINUE
      RETURN
20      CONTINUE
      ILEN = I
      IF(FIL1(ILEN+1).NE.'S' .AND. FIL1(ILEN+1).NE.'s') RETURN
      IF(FIL1(ILEN+2).NE.'D' .AND. FIL1(ILEN+2).NE.'d') RETURN
      IF(FIL1(ILEN+3).NE.'F' .AND. FIL1(ILEN+3).NE.'f') RETURN
      IER = .TRUE.
      RETURN
      END

```

```

C
C SUBROUTINE FILEM - TO CONSTRUCT A FILENAME
C
      SUBROUTINE FILEM(FIL1,FIL2,FX,INUM,ILEN)
      IMPLICIT INTEGER*2 (I-N)
      CHARACTER*1 FIL1(12),FIL2(12),FX(3)
      CHARACTER*2 ANUM
C
C WRITE OUT INUM TO ANUM
C
      WRITE(ANUM,900) INUM
900   FORMAT(I2)
C
C CALL FILCHG TO GET FILENAME
C
      CALL FILMAP(FIL1,FIL2,FX,ANUM,ILEN)
      RETURN
      END

```

```

C
C SUBROUTINE TO CHECK ON FILE AND ITS LENGTH
C
      SUBROUTINE FILEX(FIL1,ILEN)
      IMPLICIT INTEGER*2 (I-N)
      CHARACTER*1 FIL1(20)
C
C GET LENGTH OF FILE
C
      DO 5 I=1,ILEN
        IF(FIL1(I).EQ.' ') GO TO 7
      5  CONTINUE
        GO TO 8
      7  CONTINUE
        ILEN = I-1
C
C NOW SEE IF AN EXTENSION WAS ADDED
C
      8  CONTINUE
        DO 10 I=1,ILEN
          IF(FIL1(I).EQ.'.') GO TO 20
      10  CONTINUE
        RETURN
      20  CONTINUE
        ILEN = ILEN-1
        RETURN
      END

```



```

C
C SUBROUTINE FILMAP - TO CONSTRUCT A FILENAME
C CALLED FORM FILEM
C
      SUBROUTINE FILMAP(FIL1,FIL2,FX,ANUM,ILEN)
      IMPLICIT INTEGER*2 (I-N)
      CHARACTER*1 ANUM(2),FX(3),FIL1(12),FIL2(12)
C
C
C
      DO 10 I=1,ILEN
        FIL2(I) = FIL1(I)
10      CONTINUE
      DO 15 I=1,2
        FIL2(ILEN+I) = ANUM(I)
15      CONTINUE
      FIL2(ILEN+3) = '.'
      DO 20 I=1,3
        FIL2(ILEN+3+I) = FX(I)
20      CONTINUE
C
C CHANGE BLANKS TO ZEROES
C
      NLEN = ILEN + 6
      DO 30 I=1,NLEN
        IF(FIL2(I).EQ.' ') FIL2(I) = '0'
30      CONTINUE
      RETURN
      END

```

ORIGINAL PAGE IS  
OF POOR QUALITY

C  
C SUBROUTINE MACDAM - MACRAN FFT CARD

C  
C       SUBROUTINE MACDAM(TITLE)  
C       IMPLICIT INTEGER\*2 (I-N)  
C       INTEGER\*2 ICHNI(10),ICHNO(14)  
C       CHARACTER\*12 FILIN(1)  
C       CHARACTER\*30 TITLE  
C       COMMON/NASADT/ICHNI,ICHNO,NINPUT,NOUTPT,FILIN,NFNTS

C  
C WRITE OUT STUFF

C       WRITE(10,8003) TITLE  
8003   FORMAT('JBHEAD ',A30,5X,' INPUT CHANNEL FOURIER TRANSFORMS')  
C       WRITE(10,8010) FILIN  
8010   FORMAT('FILIN',2X,A12)

C  
C HERE FOR INPUT CHANNELS TO BE FFT BY FOUR

C       IF(NINPUT.GT.3) GO TO 50  
C       WRITE(10,9030) (ICHNI(IL),IL=1,NINPUT)  
C       GO TO 100  
50       CONTINUE  
C       WRITE(10,9030) (ICHNI(IL),IL=1,3)  
C       NLines = (NINPUT+1)/4  
C       DO 60 IJ=1,NLines  
C         IL = 4 + 4 \* (IJ-1)  
C         IK = IL + 3  
C         IF(IK.GT.NINPUT) IK = NINPUT  
C         WRITE(10,9040) (ICHNI(IM),IM=IL,IK)  
60       CONTINUE  
100       CONTINUE

C  
C WRITE OUT FILOUT STUFF FOR MACRAN

C       WRITE(10,8020)  
C       WRITE(10,8030)  
C       WRITE(10,8040)  
C       WRITE(10,8050)  
C       WRITE(10,8060)

C  
C WRITE OUT MACRAN STUFF FOR OUTPUT CHANNEL FFT

C       WRITE(10,8007) TITLE  
8007   FORMAT('JBHEAD ',A30,5X,' OUTPUT CHANNEL FOURIER TRANSFORMS')  
C       WRITE(10,8010) FILIN

C  
C HERE FOR OUT CHANNELS TO BE FFT BY FOUR

C       NOPT = NOUTPT  
C       IF(NOPT.GT.12) NOPT = 12  
C       IF(NOPT.GT.3) GO TO 150  
C       WRITE(10,9030) (ICHNO(IL),IL=1,NOPT)  
C       GO TO 200  
150       CONTINUE  
C       WRITE(10,9030) (ICHNO(IL),IL=1,3)

```

      NLINES = (NOPT+1)/4
      DO 160 IJ=1,NLINES
        IL = 4 + 4 * (IJ-1)
        IK = IL + 3
        IF (IK.GT.NOPT) IK = NOPT
        WRITE(10,9040) (ICHNO(IM),IM=IL,IK)
160    CONTINUE
200    CONTINUE
      WRITE(10,8070)
      WRITE(10,8030)
      WRITE(10,8080)
      WRITE(10,8090)
      WRITE(10,8060)
C
C HERE IF MORE THAN 12 OUTPUT CHANNELS
C
      IF (NOUTPT.LE.12) GO TO 300
      WRITE(10,8010) FILIN
      WRITE(10,9030) (ICHNO(IL),IL=13,NOUTPT)
      WRITE(10,7020)
      WRITE(10,8030)
      WRITE(10,7040)
      WRITE(10,7050)
      WRITE(10,8060)
300    CONTINUE
      WRITE(10,7070)
      RETURN
C
C FORMAT SECTION
C
9030  FORMAT('FILIN',1X,'CCHAN',14X,'1.',1X,3(9X,I2,'.'))
9040  FORMAT('FILIN',1X,'CCHAN',5X,4(9X,I2,'.'))
8020  FORMAT('FILOUT FORDI.SDF')
8030  FORMAT('FOUR')
8040  FORMAT('FILIN',2X,'FORDI.SDF')
8050  FORMAT('FILOUT',1X,'FORDI.DAT')
8060  FORMAT('CTAPE',52X,'-1.')
8070  FORMAT('FILOUT FORD01.SDF')
8080  FORMAT('FILIN FORD01.SDF')
8090  FORMAT('FILOUT FORD01.DAT')
7020  FORMAT('FILOUT FORD02.SDF')
7040  FORMAT('FILIN FORD02.SDF')
7050  FORMAT('FILOUT FORD02.DAT')
7070  FORMAT('END')
      RETURN
      END

```

```

C
C SUBROUTINE MACCRD1 - PURPOSE TO WRITE OUT FIRST MACRAN CARD
C
      SUBROUTINE MACRD1(FILIN,NINPUT,ICHNI,ICHNO,TITLE,NPNTS)
      IMPLICIT INTEGER*2 (I-N)
      DIMENSION ICHNI(10)
      CHARACTER*12 FILIN
      CHARACTER*30 TITLE
C
C WRITE OUT FIRST COUPLE OF COMMENT CARDS
C
      WRITE(10,9010) TITLE
9010  FORMAT('JBHEAD ',A30,5X,'TRANSFER FUNCTIONS')
      WRITE(10,9020) FILIN
9020  FORMAT('FILIN',2X,A12)
C
C NOW WRITE OUT CHANNEL NUMBERS
C
      IF(NINPUT.GT.2) GO TO 50
      WRITE(10,9030) ICHNO,(ICHNI(IL),IL=1,NINPUT)
      GO TO 100
50    CONTINUE
      WRITE(10,9030) ICHNO,(ICHNI(IL),IL=1,2)
      NLINES = (NINPUT+1)/4
      DO 60 IJ=1,NLINES
        IL = 3 + 4 * (IJ-1)
        IK = IL + 3
        IF(IK.GT.NINPUT) IK = NINPUT
        WRITE(10,9040) (ICHNI(IM),IM=IL,IK)
60    CONTINUE
9030  FORMAT('FILIN',1X,'CCHAN',14X,'1.',1X,3(9X,I2,'.'))
9040  FORMAT('FILIN',1X,'CCHAN',5X,4(9X,I2,'.'))
C
C HERE FOR REST OF DATA
C
100   CONTINUE
      WRITE(10,9050) NPNTS
9050  FORMAT(
      1 'FILOUT MATRXD2.SDF'
      2/'PSD   TRANS',11X,I4,'.',19X,'6.',
      3/'PSD   TOUTMTEC'
      4/'PSD   RETAIN'
      5/'END'
      6/)
      RETURN
      END

```

```

C
C SUBROUTINE MACCRD2 - PURPOSE TO WRITE OUT 2ND MACRAN CARD
C
      SUBROUTINE MACRD2
      IMPLICIT INTEGER*2 (I-N)
C
C WRITE OUT STUFF
C
      WRITE(10,9010)
9010  FORMAT('FILIN  MATRXD2.SDF'
1      /'FILOUT TRNSMD2.SDF'
2      /'TRANS  TAPE'
3      /'END'
4      /)
      RETURN
      END

```

```
C
C SUBROUTINE MACCRD3 - PURPOSE TO WRITE OUT 3RD MACRAN CARD
C
```

```
      SUBROUTINE MACRD3
      IMPLICIT INTEGER*2 (I-N)
      WRITE(10,9010)
9010  FORMAT('FILIN  TRNSMD2.SDF'
1     /'FILOUT HD2.DAT'
2     /'CTAPE',52X,'-1'
3     /'END'
4     /)
      RETURN
      END
```

```

C
C PROGRAM NASA - PURPOSE : TO CREATE A BATCH FILE
C WHICH WILL EXECUTE MACRAN SEVERAL TIMES
C
      IMPLICIT INTEGER*2 (I-N)
      DIMENSION ICHNI(10),ICHNO(14)
      CHARACTER*80 KEY
      CHARACTER*30 TITLE
      CHARACTER*12 MFIL1I,MFIL1O,MFIL2I,MFIL2O
      CHARACTER*12 MFIL3I,MFIL3O,MFIL4I,MFIL4O
      CHARACTER*12 FILIN,FILOT1,FILOT2
      CHARACTER*6 MFIL1,MFIL2,MFIL3,MFIL4,FILOT
      CHARACTER*3 FX1,FX2,FX3,FX4,AYN
      CHARACTER*1 ATYPE,FILET(12)
      LOGICAL*2 EXISTS,IER
      COMMON/NASADT/ICHNI,ICHNO,NINFUT,NOUTPT,FILIN,NPNTS
      EQUIVALENCE (FILOT2,FILET(1))

C
C
      CALL VCLEAR
      CALL VCURXY(0,0)
C
C DISPLAY PROGRAM NAME TO USER
C
      KEY = 'PROGRAM NASA - TO GENERATE A MACRAN BATCH FILE$'
      CALL PRMPT(KEY,1.10)
C
C BEGIN HERE
C
C
C OPEN UP FILE CONTAINING NPTS
C
      OPEN(31,FILE='INTRFS.DAT')
      READ(31,8831) NPTS
8831  FORMAT(I4)
      NPNTS = (NPTS+3)/4
      IR = 7
10    CONTINUE
      KEY = 'ENTER INPUT MACRAN FILENAME (INCLUDING .SDF) : $'
      CALL KEYBD(KEY,R,I,FILIN,3,(12),0,IR)
C
C SEE IF FILE EXISTS
C
      INQUIRE(FILE=FILIN,EXIST=EXISTS)
      IF(EXISTS) GO TO 15
      IR = IR + 1
      CALL VCURXY(0,IR)
      WRITE(*,9010)
9010  FORMAT(1X,'FILE DOES NOT EXISTS - PROGRAM ABORT!!!')
      STOP
C
C MAKE SURE IT HAS A .SDF EXTENSION
C
15    CONTINUE
      IR = IR + 1
      CALL VCURXY(0,IR)

```

```

        WRITE(*,8543) NPPTS,NPNTS
8543  FORMAT(1X,'NUMBER OF POINTS : ',I4,
1    /1X,'NUMBER OF POINTS/SEGMENT ; ',I4\ )
        CALL VCURXY(0,IR)
        CALL FILECH(FILIN,IER)
        IF(IER) GO TO 20
        IR = IR + 2
        CALL VCURXY(0,IR)
        WRITE(*,9002)
9002  FORMAT(1X,'NO .SDF EXTENSION - PROGRAM ABORT!!!')
        STOP

C
C HERE IF OK
C
20      CONTINUE
        IR = IR + 2
        KEY = 'ENTER OUTPUT FILENAME - NO FILE EXTENSIONS PLEASE :$'
        CALL KEYBD(KEY,R,I,FILOT,3,(6),0,IR)

C
C VERIFY NO EXTENSION AND GET CURRENT LENGTH
C
        IFLEN = 6
        CALL FILEX(FILOT,IFLEN)
        NFLEN = IFLEN + 6

C
C NOW GET INPUT/OUTPUT CHANNELS
C
30      CONTINUE
        IR = IR + 2
        CALL VCURXY(0,IR)
        KEY = 'ENTER THE NUMBER OF INPUT CHANNELS ( <= 10 ) :$'
        CALL KEYBD(KEY,R,NINPUT,A,2,(2),0,IR)
        IF(NINPUT.LE.10) GO TO 40
        IR = IR + 1
        CALL VCURXY(0,IR)
        WRITE(*,9030)
9030  FORMAT(1X,'TOO MANY INPUT CHANNELS SPECIFIED\')
        GO TO 30
40      CONTINUE
        IR = IR + 2
        CALL VCURXY(0,IR)
        WRITE(*,9031)
9031  FORMAT(1X,'SPECIFY MACRAN CHANNEL TO USE FOR EACH INPUT\')
        IR = IR + 1
        CALL VCURXY(0,IR)
        KEY = '--> $'
        DO 45 IC=1,NINPUT
            IR = IR + 1
            CALL KEYBD(KEY,R,ICHNI(IC),A,2,(2),0,IR)
45      CONTINUE

C
C NOW GET OUTPUT CHANNELS
C
48      CONTINUE
        CALL VCLEAR
        IR = 2

```



```

      CALL VCURXY(0,IR)
      KEY = 'ENTER THE NUMBER OF OUTPUT CHANNELS ( <= 14 ) :$'
      CALL KEYBD(KEY,R,NOUTPT,A,2,(2),0,IR)
      IF(NOUTPT.LE.14) GO TO 50
      IR = IR + 1
      CALL VCURXY(0,IR)
      WRITE(*,9040)
9040  FORMAT(1X,'TOO MANY OUTPUT CHANNELS SPECIFIED\')
      GO TO 48
C
C NOW GET OUTPUT CHANNELS
C
50    CONTINUE
      IR = IR + 2
      CALL VCURXY(0,IR)
      WRITE(*,9041)
9041  FORMAT(1X,'SPECIFY MACRAN CHANNEL FOR EACH OUTPUT\')
      IR = IR + 1
      CALL VCURXY(0,IR)
      KEY = '--> $'
      DO 55 IC = 1,NOUTPT
        IR = IR + 1
        CALL KEYBD(KEY,R,ICHNO(IC),A,2,(2),0,IR)
55    CONTINUE
C
C SEE IF A DAMAGED OR UNDAMAGED CASE
C
      IR = IR + 2
      CALL VCURXY(0,IR)
54    CONTINUE
      KEY = 'IS THIS A (D)AMAGED OR (U)NDAMAGED RUN? :$'
      CALL KEYBD(KEY,R,I,ATYPE,3,(1),0,IR)
      IF(ATYPE.EQ.'D' .OR. ATYPE.EQ.'d') GO TO 56
      IF(ATYPE.EQ.'U' .OR. ATYPE.EQ.'u') GO TO 56
      GO TO 54
56    CONTINUE
C
C GET TITLE FOR THIS RUN
C
      KEY = 'ENTER A DESCRIPTIVE TITLE FOR THIS RUN : $'
      IR = IR + 2
      CALL KEYBD(KEY,R,I,TITLE,3,(30),0,IR)
C
C NOW START CREATING THE BATCH FILE
C
      OPEN(6,FILE='NASAD.BAT',STATUS='NEW')
      OPEN(7,FILE='NASAREN.BAT',STATUS='NEW')
      OPEN(8,FILE='MATRX.DAT',STATUS='NEW')
      WRITE(8,4010) NINPUT,NOUTPT,ATYPE,TITLE
4010  FORMAT(I5,2X,I5,2X,A1/A30)
C
C ASSIGN GENERIC FILENAMES TO MACRAN FILES
C
      MFIL1 = 'TRNSD1'
      MFIL2 = 'TRNSD2'
      MFIL3 = 'TRNSD3'

```

```

MFIL4 = 'TRNSD4'
FX1 = 'INF'
FX2 = 'OUT'
FX3 = 'SDF'
FX4 = 'DAT'
IL = 6

C
C NOW LOOP OVER THE NUMBER OF OUTPUT CHANNELS TO PROCESS
C
      DO 100 ICHN=1,NOUTPT
C
C GET FIRST MACRAN FILENAME
C
      CALL FILEM(MFIL1,MFIL1I,FX1,ICHN,IL)
      OPEN(10,FILE=MFIL1I,STATUS='NEW')
C
C NOW WRITE OUT FIRST MACRAN CARD
C
      CALL MACRD1(FILIN,NINPUT,ICHNI,ICHNO(ICHN),TITLE,NPNTS)
      CLOSE(10,STATUS='KEEP')
      CALL FILEM(MFIL1,MFIL1O,FX2,ICHN,IL)
C
C GET SECOND MACRAN FILENAME
C
      CALL FILEM(MFIL2,MFIL2I,FX1,ICHN,IL)
      OPEN(10,FILE=MFIL2I,STATUS='NEW')
C
C WRITE OUT SECOND CARD
C
      CALL MACRD2
      CLOSE(10,STATUS='KEEP')
      CALL FILEM(MFIL2,MFIL2O,FX2,ICHN,IL)
C
C GET THIRD MACRAN FILENAME
C
      CALL FILEM(MFIL3,MFIL3I,FX1,ICHN,IL)
      OPEN(10,FILE=MFIL3I,STATUS='NEW')
C
C WRITE OUT THIRD MACRAN CARD
C
      CALL MACRD3
      CLOSE(10,STATUS='KEEP')
      CALL FILEM(MFIL3,MFIL3O,FX2,ICHN,IL)
C
C NOW ADD TO THE NASAD.BAT FILE
C
      WRITE(6,6010) MFIL1I,MFIL1O
      WRITE(6,6060) MFIL2I,MFIL2O
      WRITE(6,6010) MFIL3I,MFIL3O
C
C GET OUTPUT FILENAME
C
      CALL FILEM(FILOT,FILOT1,FX3,ICHN,IFLEN)
      CALL FILEM(FILOT,FILOT2,FX4,ICHN,IFLEN)
C
C WRITE OUT BATCH COMMANDS

```

```

C
      WRITE(6,6020) FILOT1,FILOT1
      WRITE(6,6030) FILOT2,FILOT2
      WRITE(8,4020) (FILET(IFM),IFM=1,NFLEN)
100    CONTINUE
4020  FORMAT(12A1)
C
      IF(IFLEN.EQ.6) GO TO 150
      CALL FILAD(FILOT,IFLEN)
150    CONTINUE
C
C FINISH OFF BATCH COMMANDS FOR NASA.BAT
C
      WRITE(6,6070)
C
      CLOSE(6,STATUS='KEEP')
C
C NOW ADD TO NASAREN.BAT
C
      WRITE(7,6050) FILOT,FILOT
      CLOSE(7,STATUS='KEEP')
C
C END IT ALL
C
      CLOSE(7,STATUS='KEEP')
      CALL VCURXY(0,23)
      STOP
C
C FORMAT SECTION
C
6010  FORMAT('MAC423 /R 10000 <',A12,' >',A12)
6020  FORMAT('DEL',1X,A12/'REN TRNSMD2.SDF',1X,A12)
6030  FORMAT('DEL',1X,A12/'REN HD2.DAT',1X,A12)
6040  FORMAT('DEL',1X,A6,'01.BFT'
1     /'REN FORDI.DAT',1X,A6,'01.BFT')
6045  FORMAT('DEL',1X,A6,'01.DFT'
1     /'REN FORD01.DAT',1X,A6,'01.DFT')
6046  FORMAT('DEL',1X,A6,'02.DFT'
1     /'REN FORD02.DAT',1X,A6,'02.DFT')
6050  FORMAT('DEL',1X,A6,'.BAT'
1     /'REN NASAD.BAT',1X,A6,'.BAT')
6060  FORMAT('MACTRN /R 10000 <',A12,' >',A12)
6070  FORMAT('TESTRD.EXE'/'NASAREN.BAT')
      END

```

#NOFLOATCALLS

```
IMPLICIT INTEGER*2 (I-N)
COMPLEX*8 TFU(14,10),TFD(14,10)
COMPLEX*8 DAM(7,2500)
DIMENSION ILMI(14),ILMO(14)
CHARACTER*80 KEY
CHARACTER*30 TITLE
CHARACTER*20 TFUF,TFDF
CHARACTER*1 ATYPE
COMMON/DAMC/TFU,TFD,DAM,ILMI,ILMO,NINPUT,NOUTPT
```

C  
C  
C

```
CALL VCLEAR
CALL VCURXY(0,0)
IR = 0
```

C

C GET EACH FILENAME, OPEN IT UP AND READ HEADER INFO

C

```
TFUF = 'HWUMAT.DAT'
OPEN(6,FILE=TFUF,FORM='UNFORMATTED')
READ(6) TITLE,NFREQ,NINPUT,NOUTPT,ATYPE,DELF
WRITE(*,9000) TITLE,NINPUT,NOUTPT,NFREQ,DELF
9000 FORMAT(1X,A30)
1 /1X,'NUMBER OF INPUT CHANNELS : ',I4
2 /1X,'NUMBER OF OUTPUT CHANNELS : ',I4
3 /1X,'NUMBER OF FREQUENCY POINTS : ',I4
4 /1X,'FREQUENCY STEP SIZE : ',1PE10.3,' HZ'\)
IR = IR + 6
CALL VCURXY(0,IR)
IF(ATYPE.EQ.'U'.OR. ATYPE.EQ.'u') WRITE(*,9010)
IF(ATYPE.EQ.'D'.OR. ATYPE.EQ.'d') WRITE(*,9015)
9010 FORMAT(1X,'UNDAMAGED'\)
9015 FORMAT(1X,'DAMAGED'\)
IR = IR + 2
CALL VCURXY(0,IR)
```

C

C GET DAMAGED TF FILENAME

C

```
TFDF = 'HWDMAT.DAT'
OPEN(7,FILE=TFDF,FORM='UNFORMATTED')
READ(7) TITLE,NFREQ,NINPUT,NOUTPT,ATYPE,DELF
WRITE(*,9000) TITLE,NINPUT,NOUTPT,NFREQ,DELF
IR = IR + 6
CALL VCURXY(0,IR)
IF(ATYPE.EQ.'U'.OR. ATYPE.EQ.'u') WRITE(*,9010)
IF(ATYPE.EQ.'D'.OR. ATYPE.EQ.'d') WRITE(*,9015)
IR = IR + 2
```

C

C SEE ABOUT ROW/COLUMN ELIMINATION

C

```
PAUSE
CALL VCLEAR
IR = 0
CALL VCURXY(0,IR)
DO 40 I=1,14
```

```

        ILMI(I) = 0
        ILMO(I) = 0
40      CONTINUE
        KEY = 'HOW MANY INPUT CHANNELS DO YOU WANT TO ELIMINATE? : $'
        CALL KEYBD(KEY,R,IELMI,A,2,(2),0,IR)
        IR = IR + 1
        IF (IELMI.EQ.0) GO TO 75
        CALL VCURXY(0,IR)
        WRITE(*,9200)
9200    FORMAT(1X,'ENTER CHANNELS TO ELIMINATE\')
        IR = IR + 1
        CALL VCURXY(0,IR)
        DO 50 I=1,IELMI
            KEY = '--> $'
            CALL KEYBD(KEY,R,ILMI(I),A,2,(2),0,IR)
            IR = IR + 1
50      CONTINUE
75      CONTINUE
        IR = IR + 1
        KEY = 'HOW MANY OUTPUT CAHNNELS DO YOU WANT TO ELIMINATE? : $'
        CALL KEYBD(KEY,R,IELMO,A,2,(2),0,IR)
        IF (IELMO.EQ.0) GO TO 100
        IR = IR + 1
        CALL VCURXY(0,IR)
        WRITE(*,9200)
        IR = IR + 1
        CALL VCURXY(0,IR)
        DO 80 I=1,IELMO
            KEY = '--> $'
            CALL KEYBD(KEY,R,ILMO(I),A,2,(2),0,IR)
            IR = IR + 1
80      CONTINUE
100     CONTINUE
C
C NOW READ IN ALL THE DATA, ONE FREQ POINT AT A TIME AND COMPUTE
C DAMAGE FOR THAT FREQ POINT
C
        NTOT = NINPUT + NOUTPT
        DO 150 IFQ=1,NFREQ
            DO 110 IO=1,NOUTPT
                READ(6) (TFU(IO,I),I=1,NINPUT)
                READ(7) (TFD(IO,I),I=1,NINPUT)
110     CONTINUE
            CALL DAMCOM(IFQ)
150     CONTINUE
C
C CALL MACWRT TO WRITE OUT DATA
C
        CALL MACWRT(DAM,NFREQ,DELF,TITLE)
C
C END IT ALL
C
        CALL GCURXY(IC,IR)
        IR = IR + 1
        CALL VCURXY(0,IR)
        STOP

```

END

#NOFLOATCALLS

```
SUBROUTINE DAMCOM(IFQ)
  IMPLICIT INTEGER*2 (I-N)
  COMPLEX*8 TFU(14,10),TFD(14,10)
  COMPLEX*8 DAM(7,2500),AUX1,AUX2,AUX3,AUX4,AUX5
  DIMENSION ILMI(14),ILMO(14)
  COMMON/DAMC/TFU,TFD,DAM,ILMI,ILMO,NINPUT,NOUTPT
```

C

C ZERO OUT AUX

C

```
AUX1 = (0.,0.)
AUX2 = (0.,0.)
AUX3 = (0.,0.)
AUX4 = (0.,0.)
AUX5 = (0.,0.)
```

C

C COMPUTE DAMAGE

C

```
DO 20 KK=1,NOUTPT
  DO 19 IK=1,NOUTPT
    IF(KK.EQ.ILMO(IK)) GO TO 20
19  CONTINUE
    DO 10 JJ=1,NINPUT
      DO 11 IJ=1,NINPUT
        IF(JJ.EQ.ILMI(IJ)) GO TO 10
```

19

11

C

C

```
CONTINUE
AUX1 = AUX1 + TFU(KK,JJ) * FTO(KK) * FTI(JJ)
AUX2 = AUX2 + TFD(KK,JJ) * FTO(KK) * FTI(JJ)
AUX3 = AUX3 + TFU(KK,JJ) * TFU(KK,JJ)
AUX4 = AUX4 + TFU(KK,JJ) * TFD(KK,JJ)
AUX5 = AUX5 + TFD(KK,JJ) * TFD(KK,JJ)
```

10

20

```
CONTINUE
DAM(1,IFQ) = (AUX5 + AUX4) / (AUX4 + AUX3)
DAM(2,IFQ) = (AUX4 + AUX3) / (AUX5 + AUX4)
DAM(3,IFQ) = AUX3/AUX4
DAM(4,IFQ) = AUX4 / AUX3
DAM(5,IFQ) = AUX4 / AUX5
DAM(6,IFQ) = AUX5 / AUX4
RETURN
END
```

PRECEDING PAGE BLANK NOT FILMED

```

#NOFLOATCALLS
      SUBROUTINE MACWRT(DAM,NFREQ,DELF,TITLE)
      IMPLICIT INTEGER*2 (I-N)
      COMPLEX DAM(7,2500),XDAM(7)
      REAL*4 RDAM(16)
      CHARACTER*4 ADAM(7)
      CHARACTER*30 TITLE
C
C  SET UP CHARACTER STRINGS
C
      ADAM(1) = 'DAM1'
      ADAM(2) = 'DAM2'
      ADAM(3) = 'DAM3'
      ADAM(4) = 'DAM4'
      ADAM(5) = 'DAM5'
      ADAM(6) = 'DAM6'
      ADAM(7) = 'DAM7'
C
C  OPEN UP OUTPUT DAMAGE.SCF FILE
C
      OPEN(20,FILE='DAMAGE.SCF',STATUS='NEW')
C
C  START WRITING OUT TO FILE
C
      WRITE(20,9090) TITLE
9090  FORMAT('JBHEAD',1X,'COMPUTED DAMAGE - ',A30)
      WRITE(20,9050)
      WRITE(20,9000)
      WRITE(20,9010)
      WRITE(20,9020)
      DO 20 I=1,6
        DO 10 IW=1,2
          WRITE(20,9030) ADAM(I)
10      CONTINUE
20      CONTINUE
      DO 30 I=1,16
        RDAM(I) = 0.0
30      CONTINUE
      CALL GCURXY(IC,IR)
      IR = IR + 1
      CALL VCURXY(O,IR)
      DO 100 IFQ=1,NFREQ
        RDAM(1) = FLOAT(IFQ-1) * DELF
        DO 40 I=1,6
          XDAM(I) = DAM(I,IFQ)
          RI = AIMAG(XDAM(I))
          RR = REAL(XDAM(I))
          RDAM(I*2) = RR
          RDAM(I*2+1) = RI
40      CONTINUE
      WRITE(20,9040) (RDAM(I),I=1,16)
100     CONTINUE
      WRITE(20,9060)
      CLOSE(20,STATUS='KEEP')
9000  FORMAT('CTAPE',2X,'NASA 1311.05')
9010  FORMAT('CTAPE',2X,'DAMAGE ',16X,'13')

```



```
9020  FORMAT('CTAPE',2X,'FREQUENCY')
9030  FORMAT('CTAPE',2X,A4)
9040  FORMAT('CTAPE',19X,4(E11.3,1X),
      1      /'CTAPE C',17X,4(E11.3,1X),
      2      /'CTAPE C',17X,4(E11.3,1X),
      3      /'CTAPE C',17X,4(E11.3,1X))
9050  FORMAT('FILOUT DAMAGE.SDF')
9060  FORMAT('END')
      RETURN
      END
```

**ANCO**

APPENDIX C

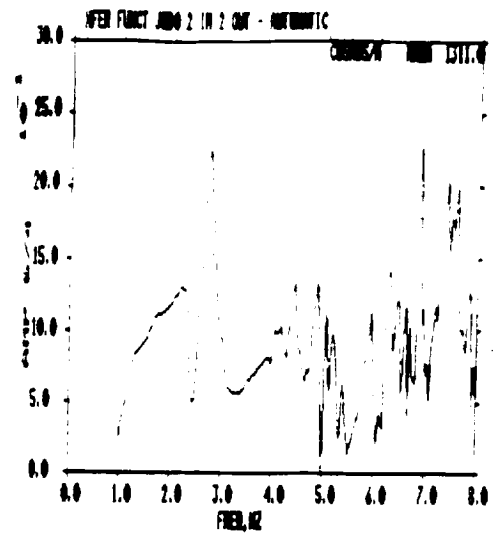
EXAMPLES OF MULTI-INPUT MULTI-OUTPUT MODULE  
TRANSFER FUNCTION MATRIX FOR NUMERICAL  
TWO BOUNDARY POINT PROBLEM

This appendix contains examples of multi-input multi-output (MIMO) module transfer function matrix computations for the numerical two boundary point problem. Three examples are provided. They are listed as follows:

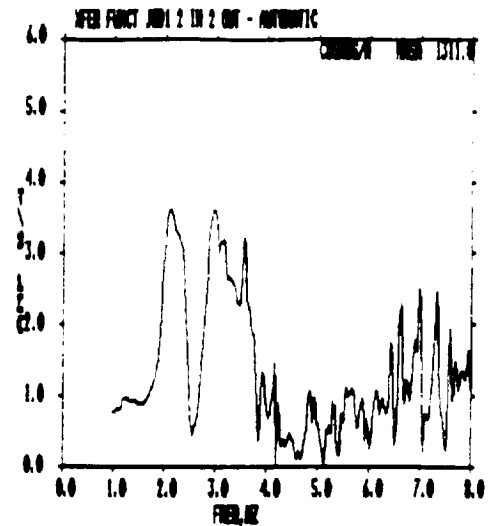
1. a comparison of MIMO module transfer function computation results for absolute responses is made; undamaged state and two damage levels are looked at; the damage is outside the module; the excitation of the global system is base motion;
2. a MIMO relative module transfer function matrix is presented for the numerical example without damage; also, corresponding time history gain [single-input single-output (SISO) transfer function modulus] and coherence (corresponding to the gain plots) plots are presented; the excitation of the global system is base motion; and
3. a MIMO relative module transfer function matrix is presented for the numerical example without damage; the excitation of the global system consists of a single force applied to Node Point 5.

MIMO ABSOLUTE MODULE TRANSFER FUNCTION MATRIX  
EXCITATION--BASE MOTION

a) Undamaged System (initial configuration)



b) System damaged outside of module--  
fundamental global natural frequency  
changed by -23.5%



c) System damaged outside of module--  
fundamental global natural frequency  
changed by 23.3%

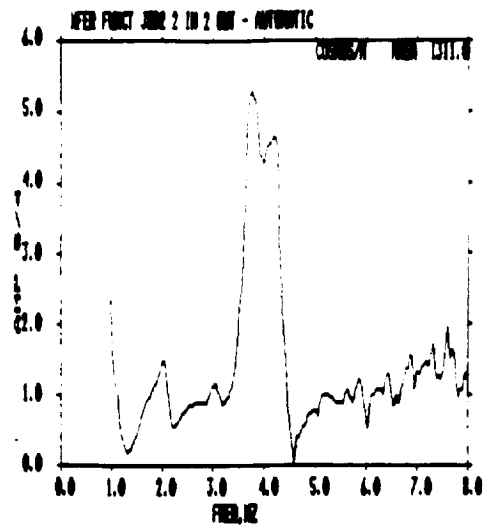
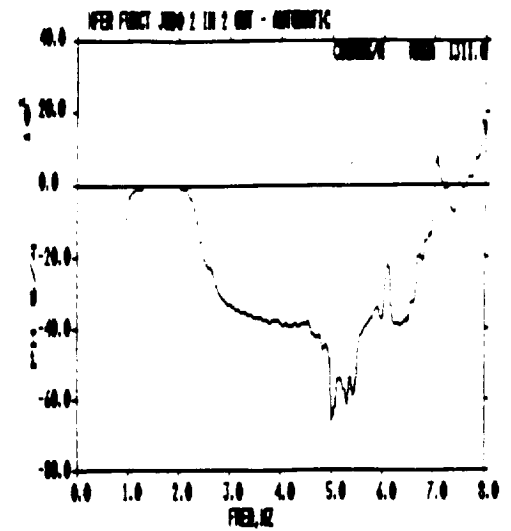
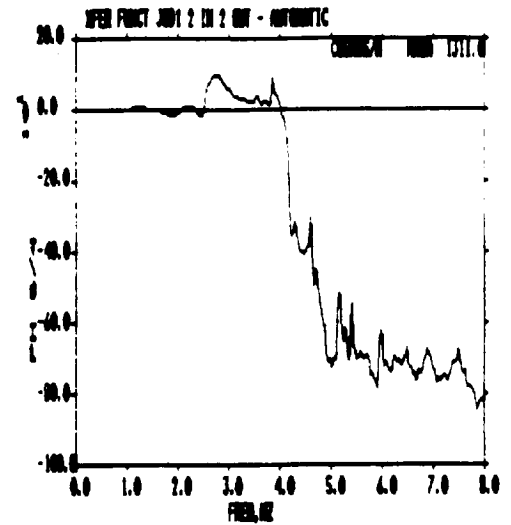


Figure C.1: Comparison of MIMO Transfer Function Modului for J8 Model;  
Element Output 5, Input 4

a) Undamaged system (initial configuration)



b) System damaged outside of module--  
fundamental global natural frequency  
changed by -23.5%



c) System damaged outside of module--  
fundamental global natural frequency  
changed by 23.3%

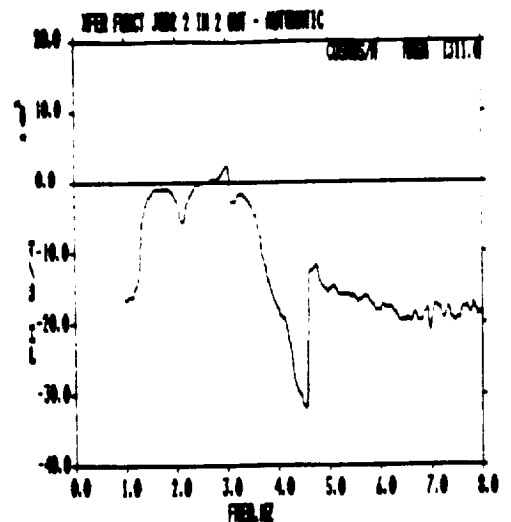
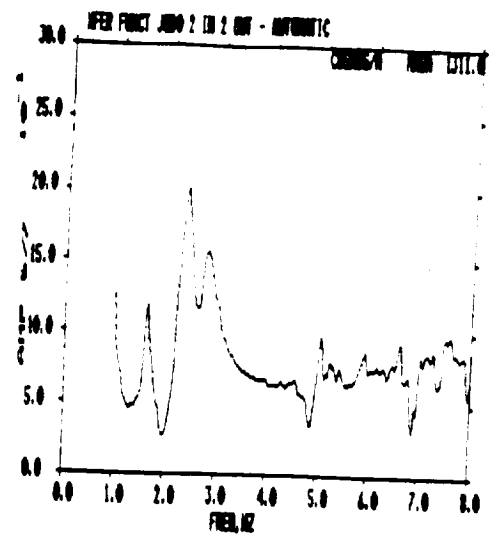


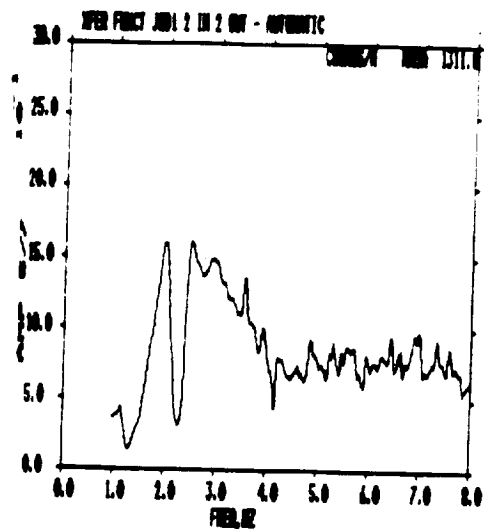
Figure C.2: Comparison of MIMO Transfer Function Phase for J8 Model;  
Element Output 5, Input 4

ORIGINAL DATE IS  
OF POOR QUALITY

a) Undamaged system (initial configuration)



b) System damaged outside of module--  
fundamental global natural frequency  
changed by -23.5%



c) System damaged outside of module--  
fundamental global natural frequency  
changed by 23.3%

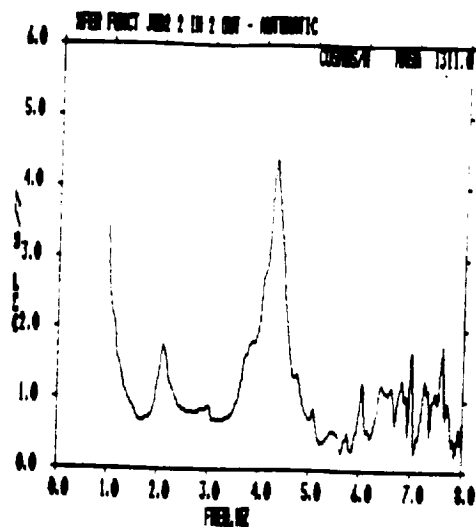
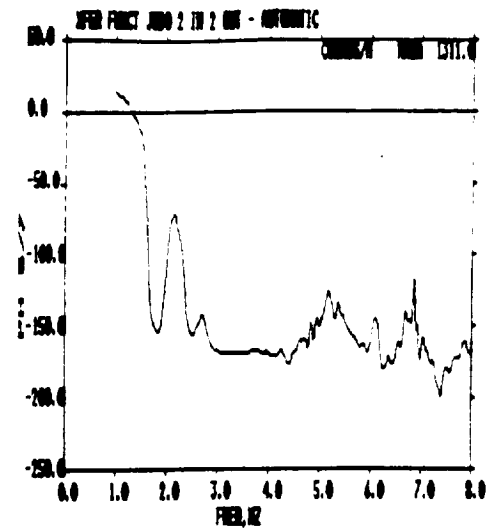
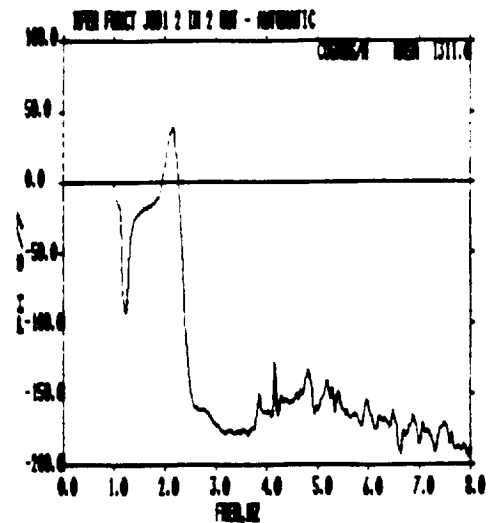


Figure C.3: Comparison of MIMO Transfer Function Modulul for J8 Model;  
Element Output 5, Input 7

a) Undamaged system (initial configuration)



b) System damaged outside of module--  
fundamental global natural frequency  
changed by -23.5%



c) System damaged outside of module--  
fundamental global natural frequency  
changed by 23.3%

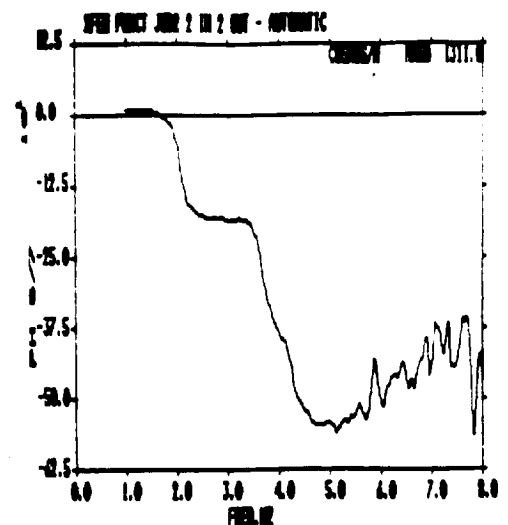


Figure C.4: Comparison of MIMO Transfer Function Phase For J8 Model;  
Element Output 5, Input 7

ORIGINAL PAGE IS  
OF POOR QUALITY



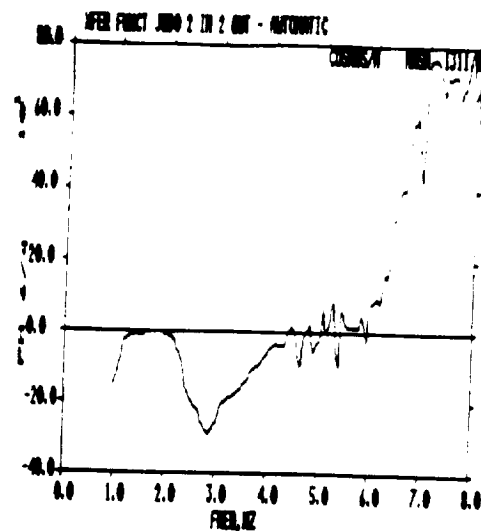
SFER PUNCH JUL 12 10 2 AM - AUTOMATIC

COUNT

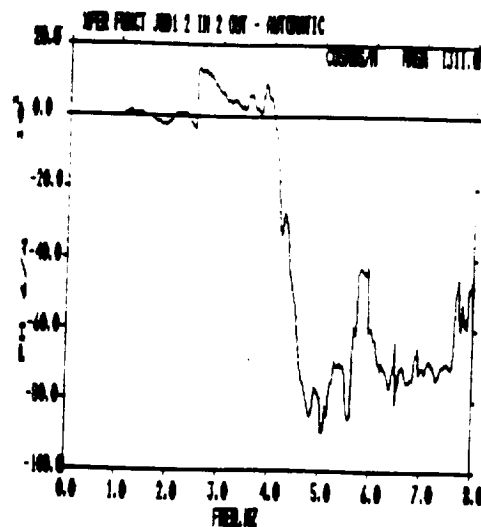
FREQUENCY

CHINA'S RICE IS  
OF POOR QUALITY

a) Undamaged system (initial configuration)



b) System damaged outside of module--  
fundamental global natural frequency  
changed by -23.5%



c) System damaged outside of module--  
fundamental global natural frequency  
changed by 23.3%

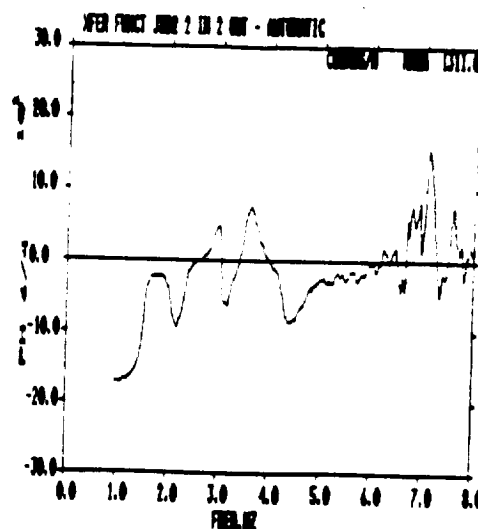
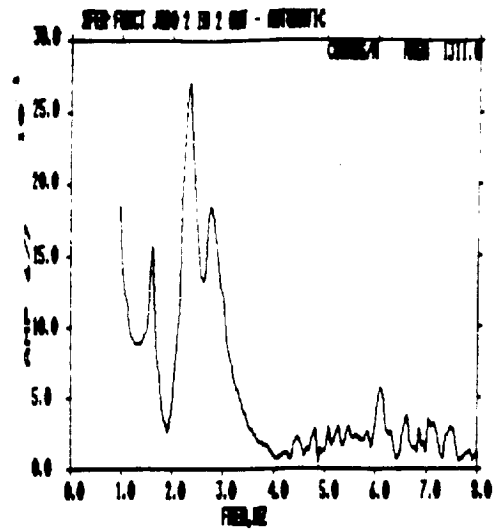
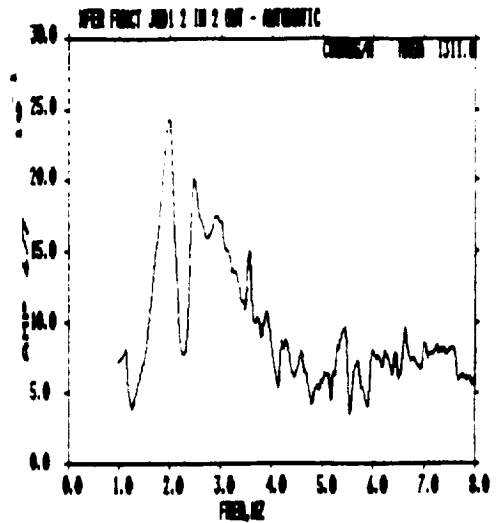


Figure C.6: Comparison of MIMO Transfer Function Phase for J8 Model;  
Element Output 6, Input 4

a) Undamaged system (initial configuration)



b) System damaged outside of module--  
fundamental global natural frequency  
changed by -23.5%



c) System damaged outside of module--  
fundamental global natural frequency  
changed by 23.3%

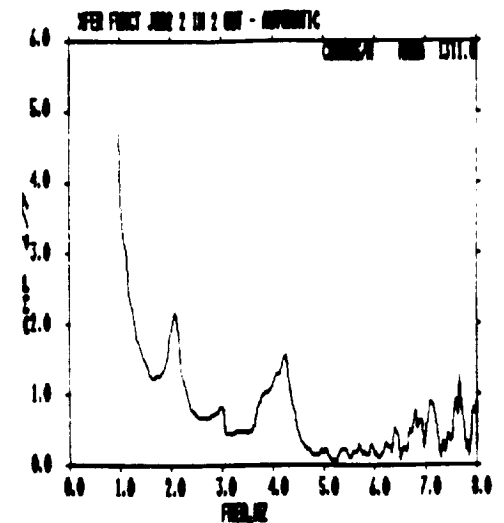
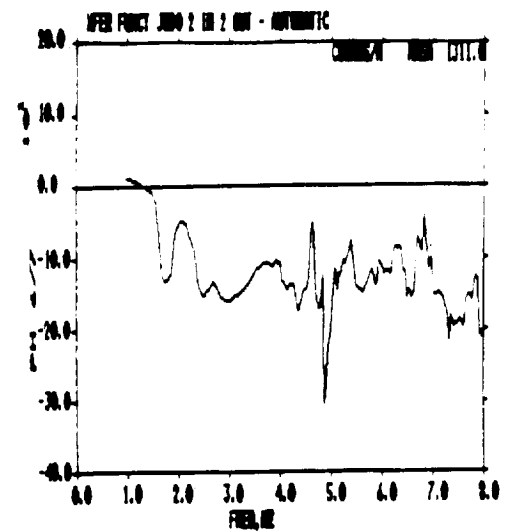
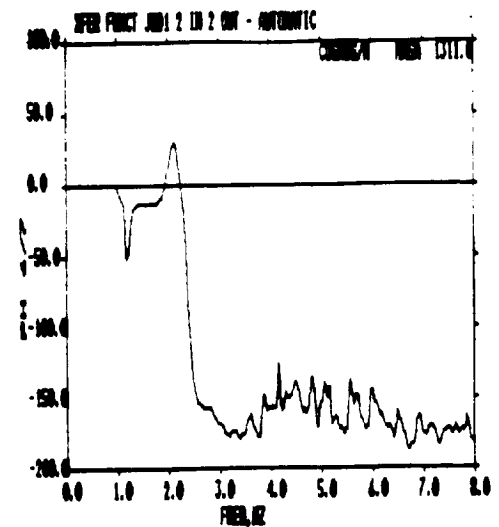


Figure C.7: Comparison of MIMO Transfer Function Modulus for J8 Model;  
Element Output 6, Input 7

a) Undamaged system (initial configuration)



b) System damaged outside of module--  
fundamental global natural frequency  
changed by -23.5%



c) System damaged outside of module--  
fundamental global natural frequency  
changed by 23.3%

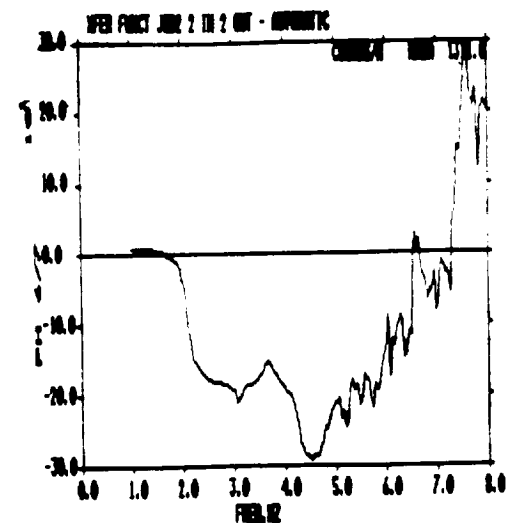
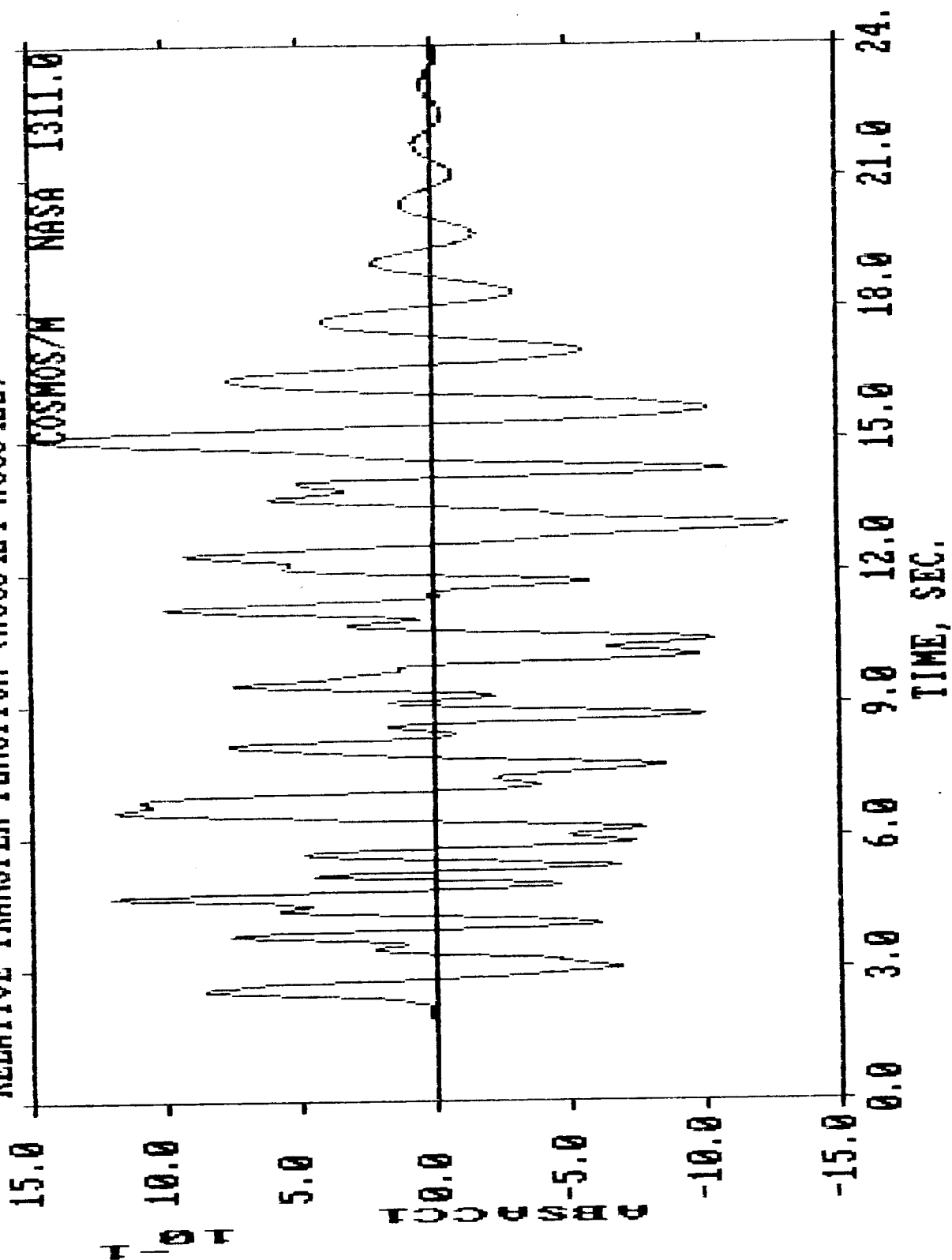


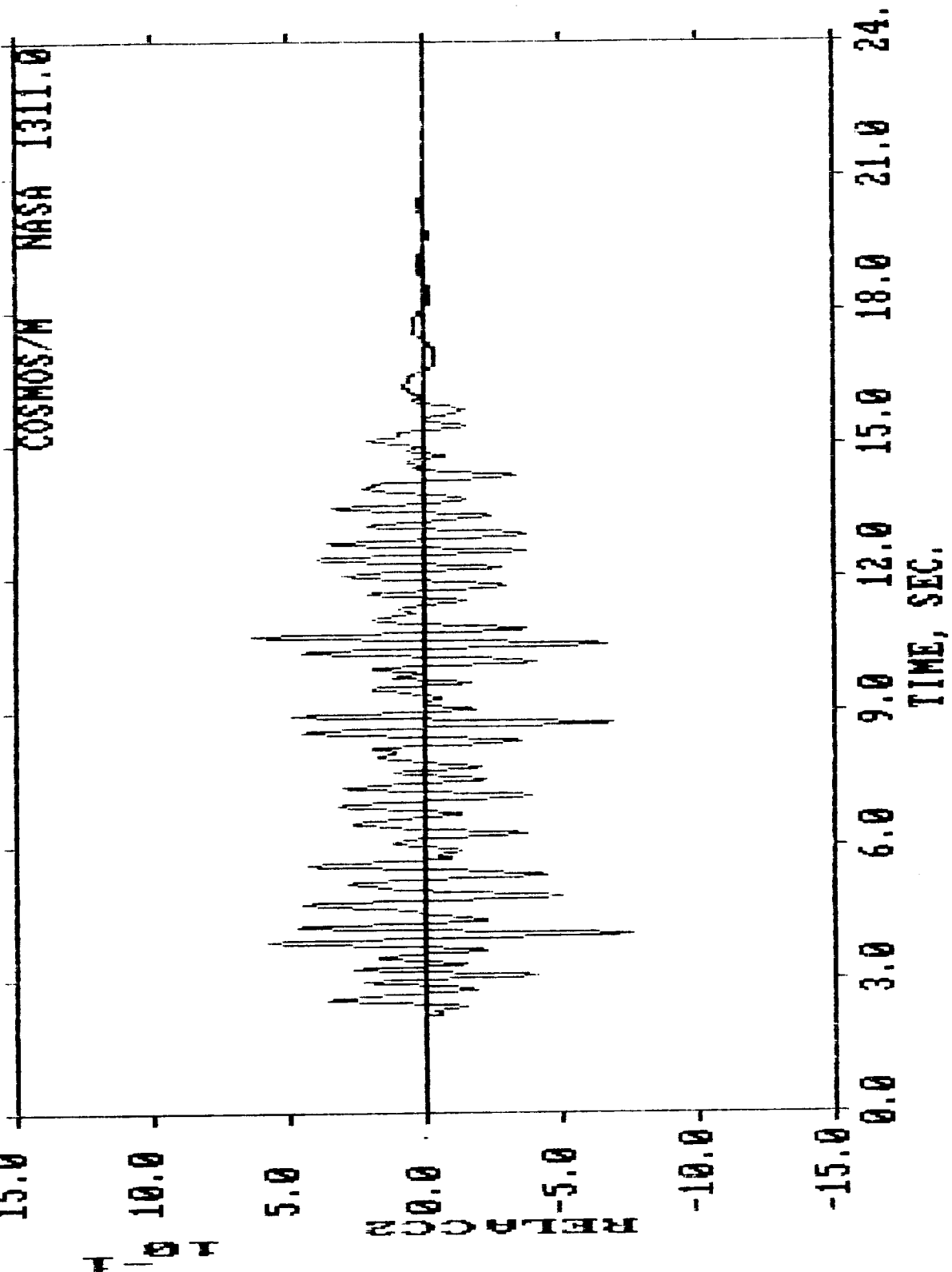
Figure C.8: Comparison of MIMO Transfer Function Phase for J8 Model;  
Element Output 6, Input 7

MIMO RELATIVE MODULE TRANSFER FUNCTION MATRIX  
EXCITATION--BASE MOTION

# RELATIVE TRANSFER FUNCTION (ACCJ4U4-ACCJ4U2)

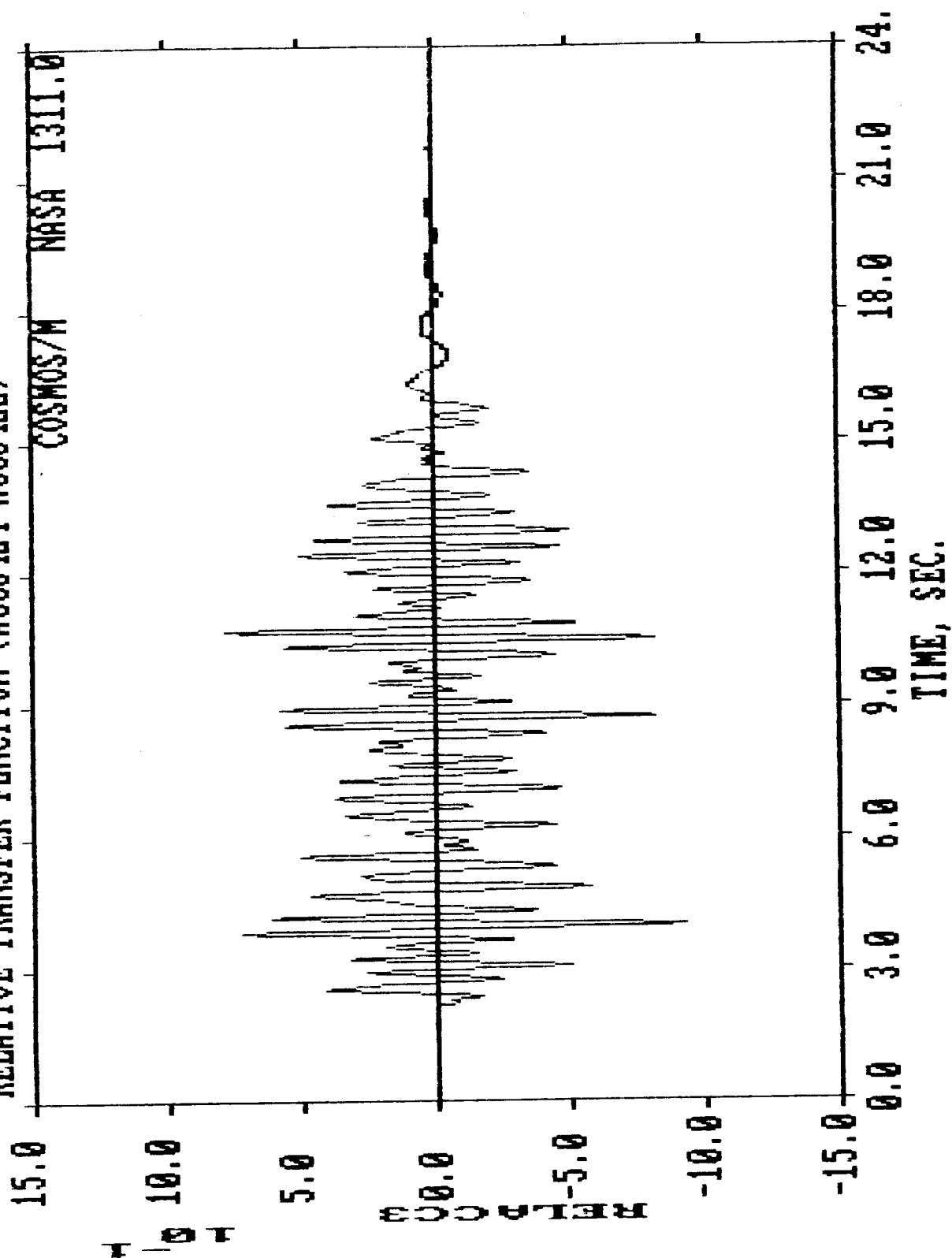


# RELATIVE TRANSFER FUNCTION (ACCJ4U4-ACCJ4U2)



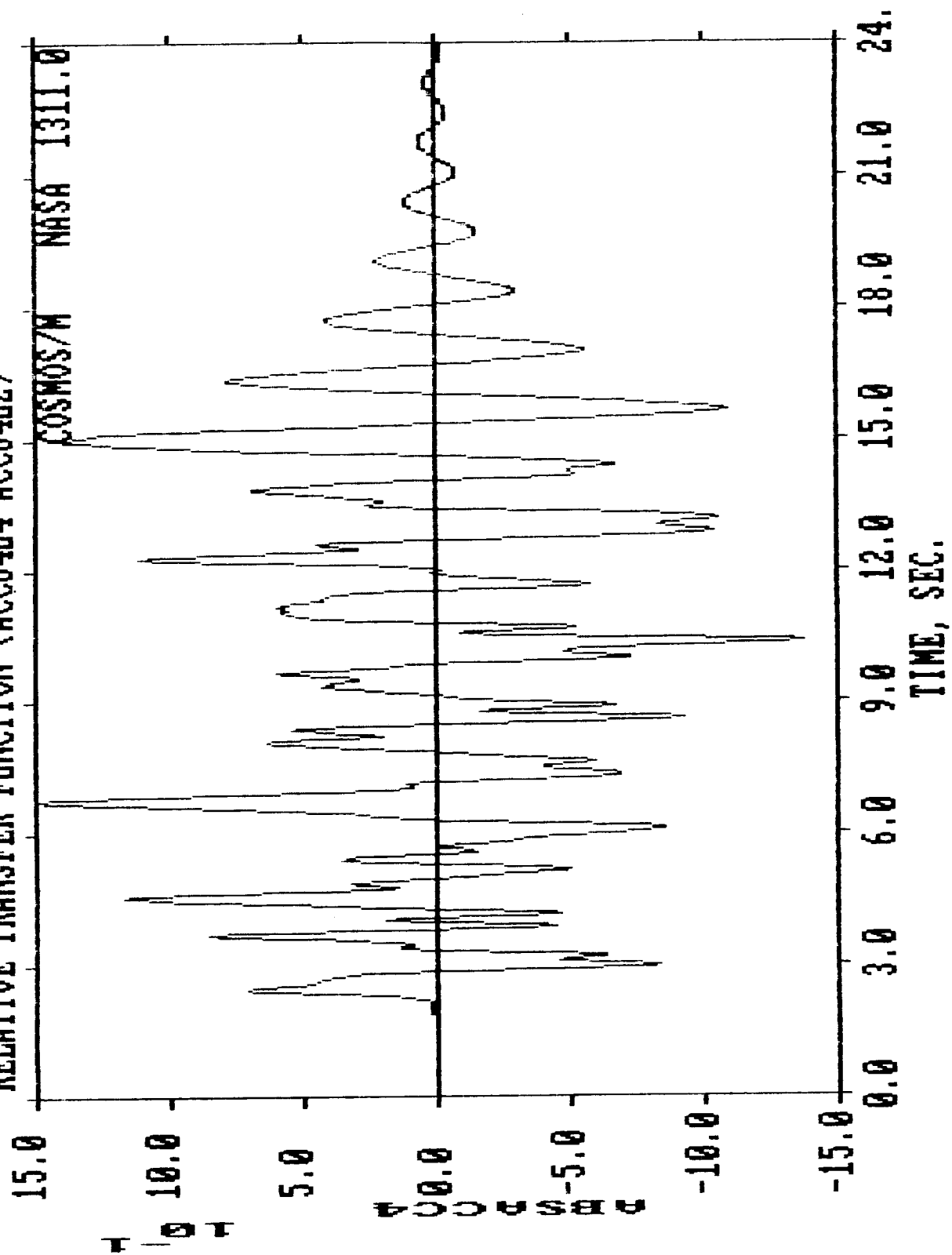
# RELATIVE TRANSFER FUNCTION (ACCJ4U4-ACCJ4U2)

COSMOS/M NASA 1311.0

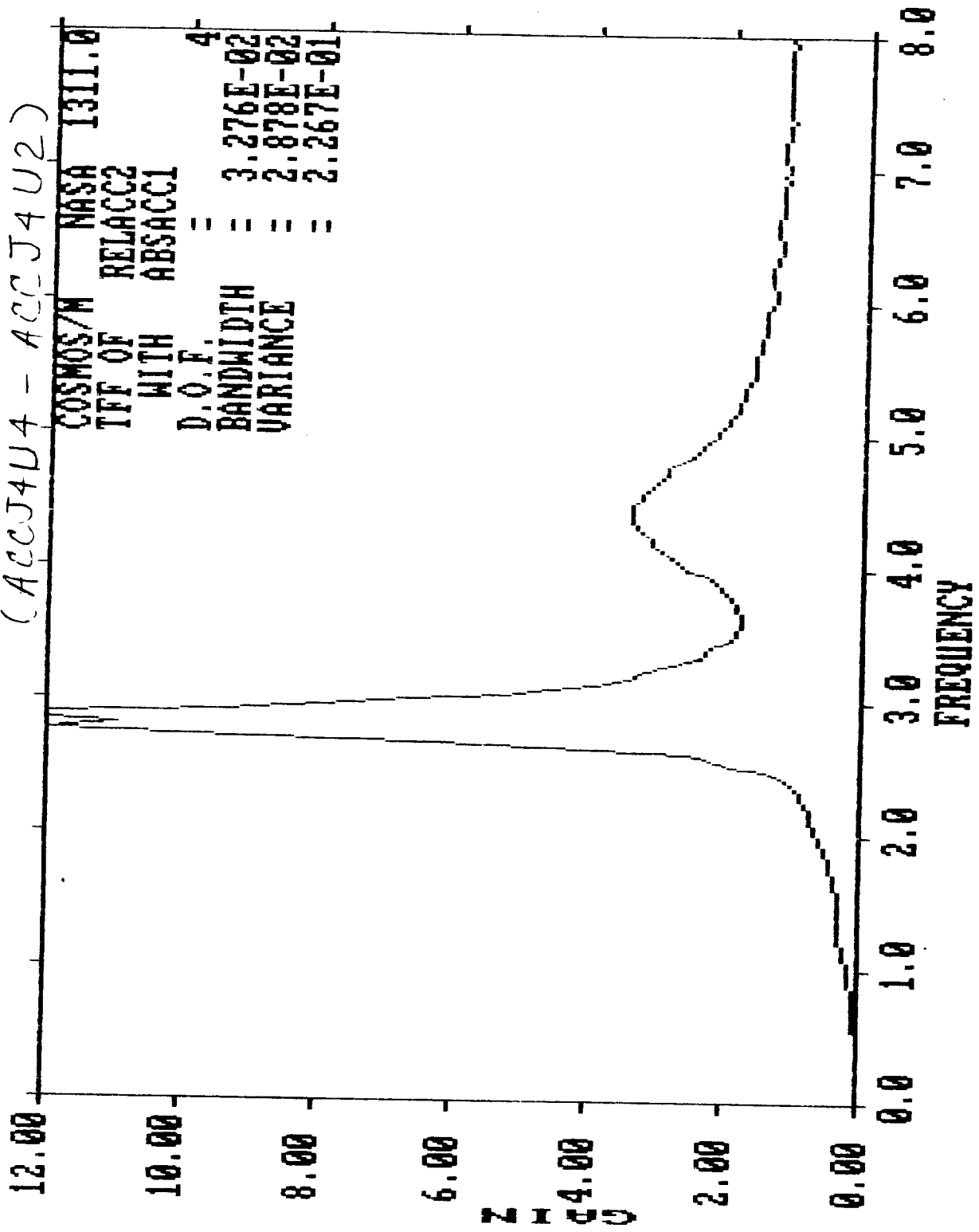




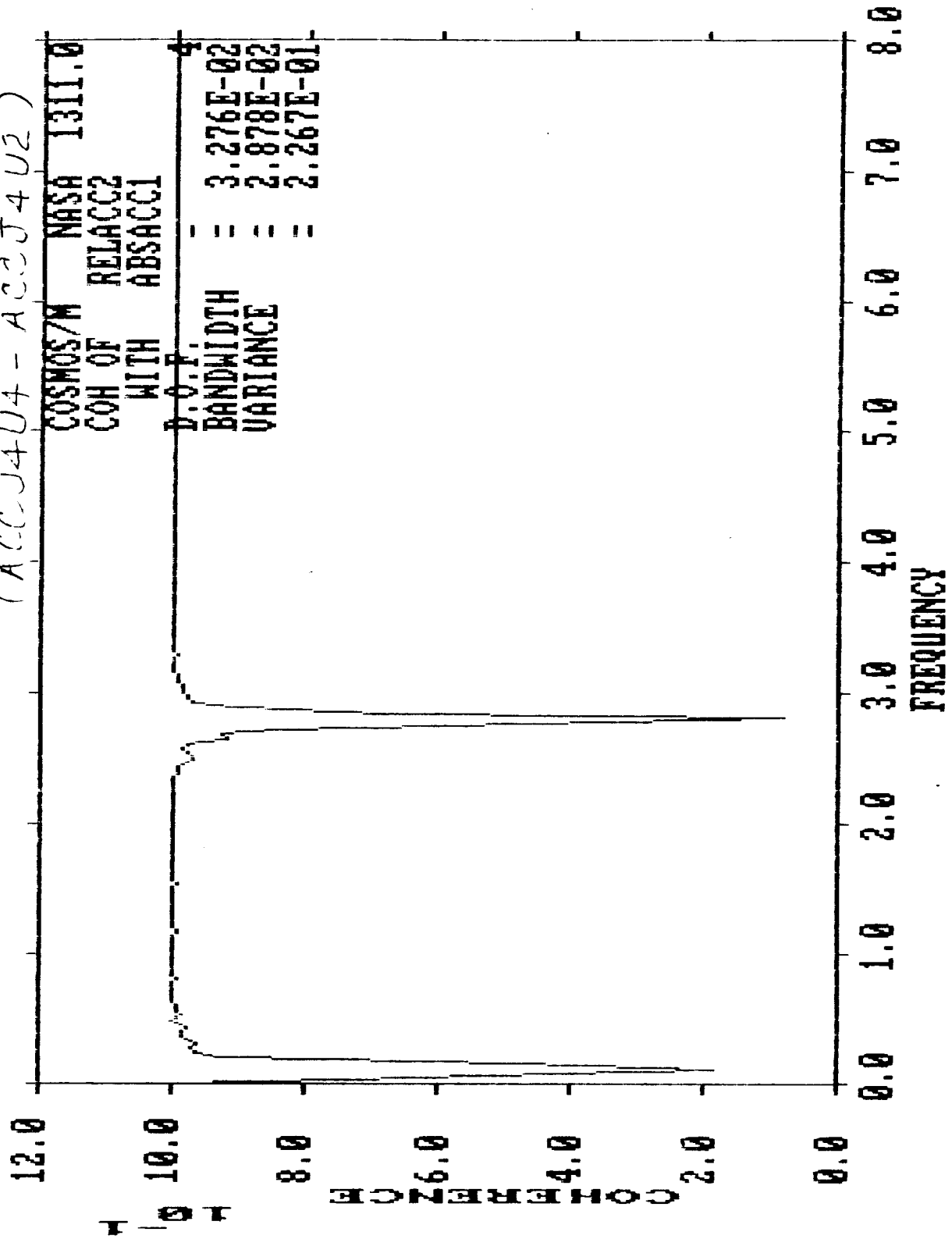
# RELATIVE TRANSFER FUNCTION (ACCJ4U4-ACCJ4U2)



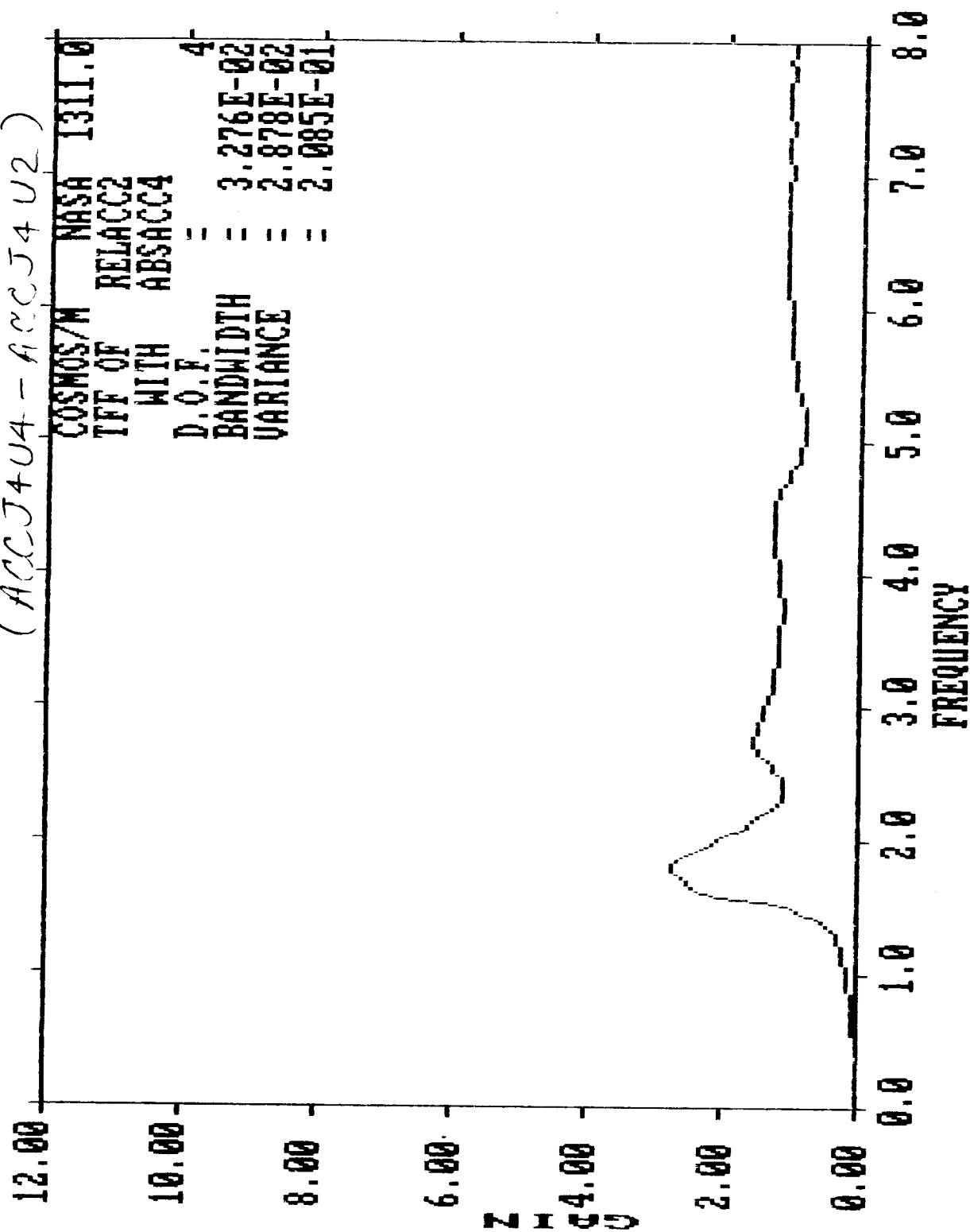
(ACCJ4U4 - ACCJ4U2)



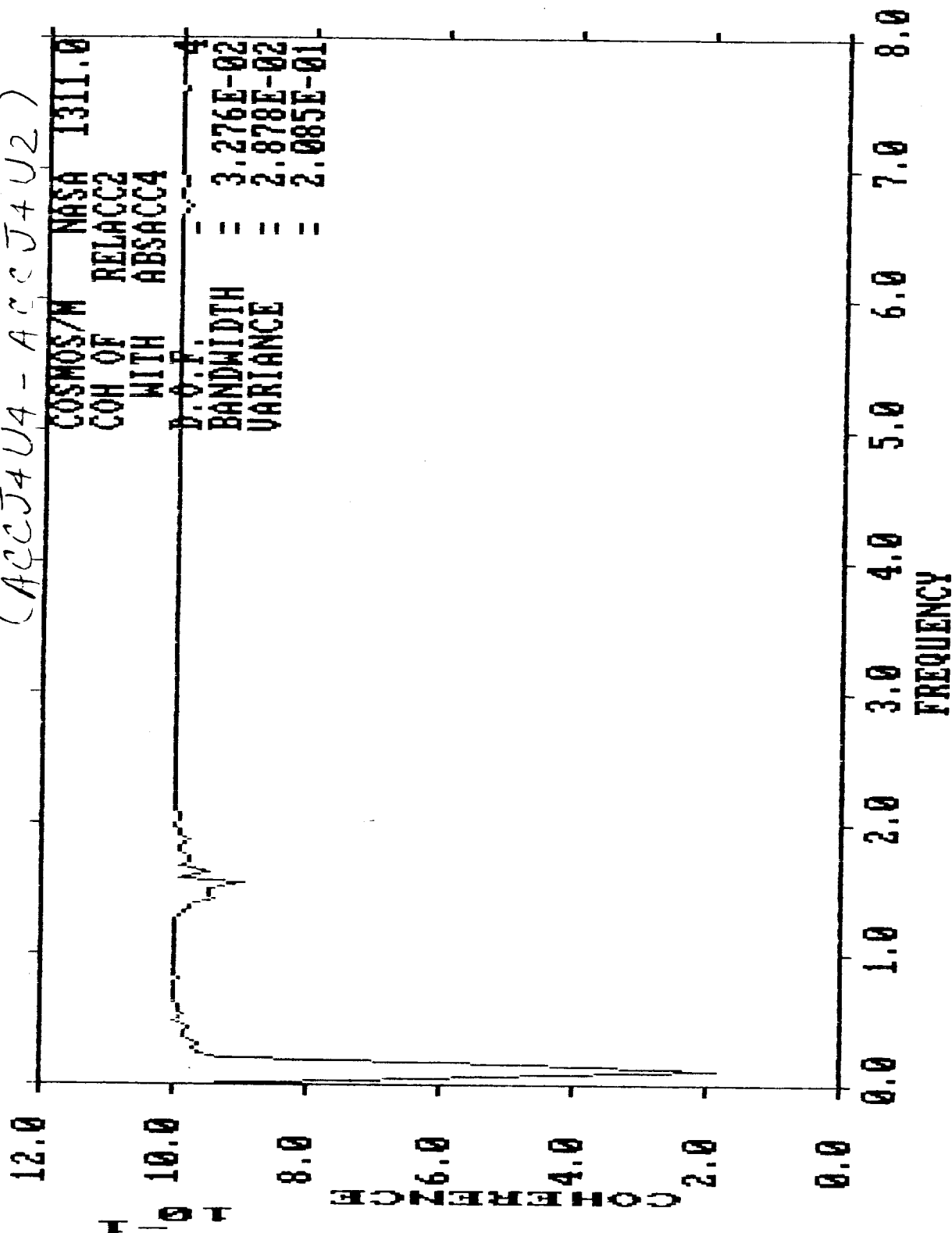
(ACCJ4U4 - ACCJ4U2)



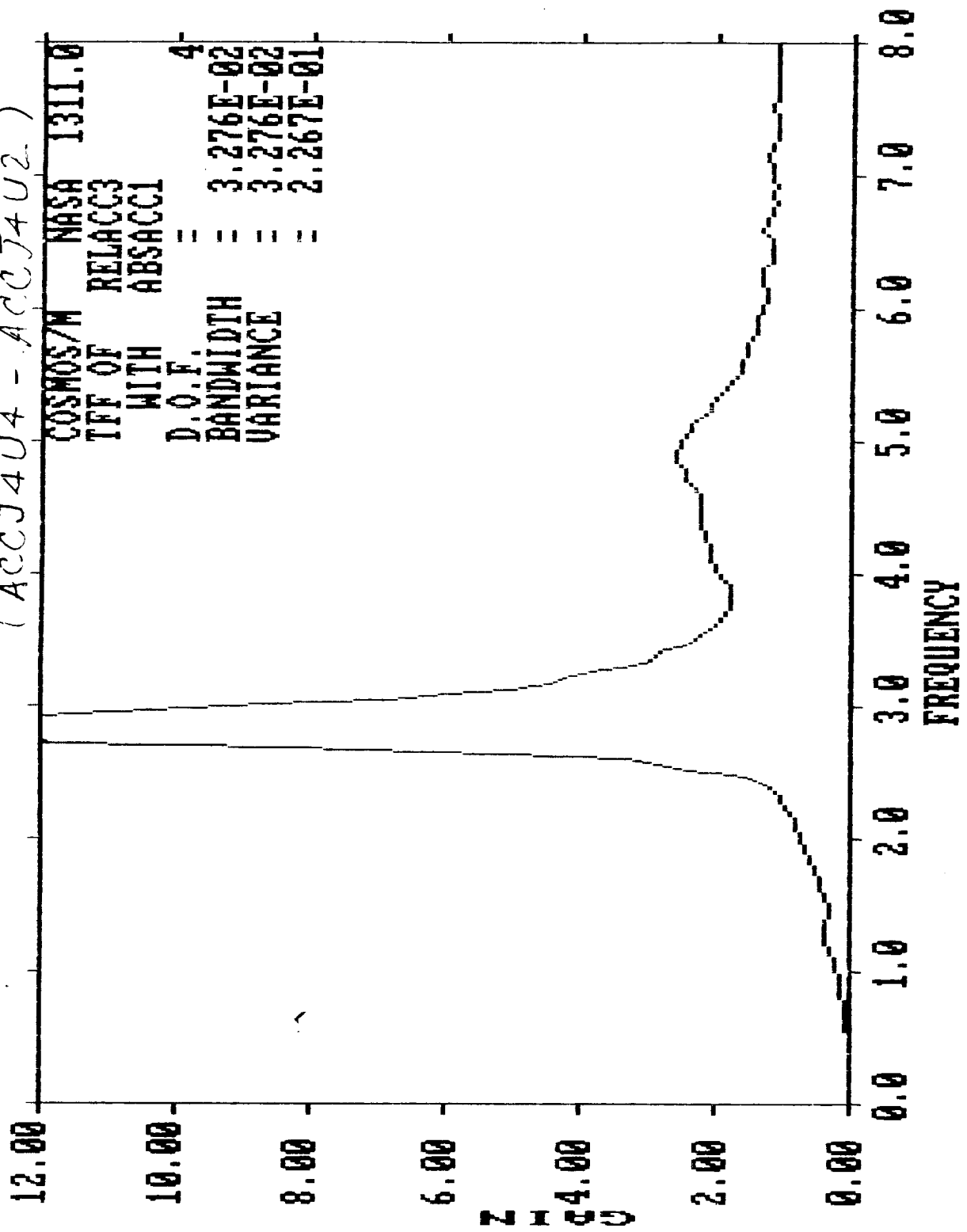
(ACCJ4U4-ACCJ4U2)



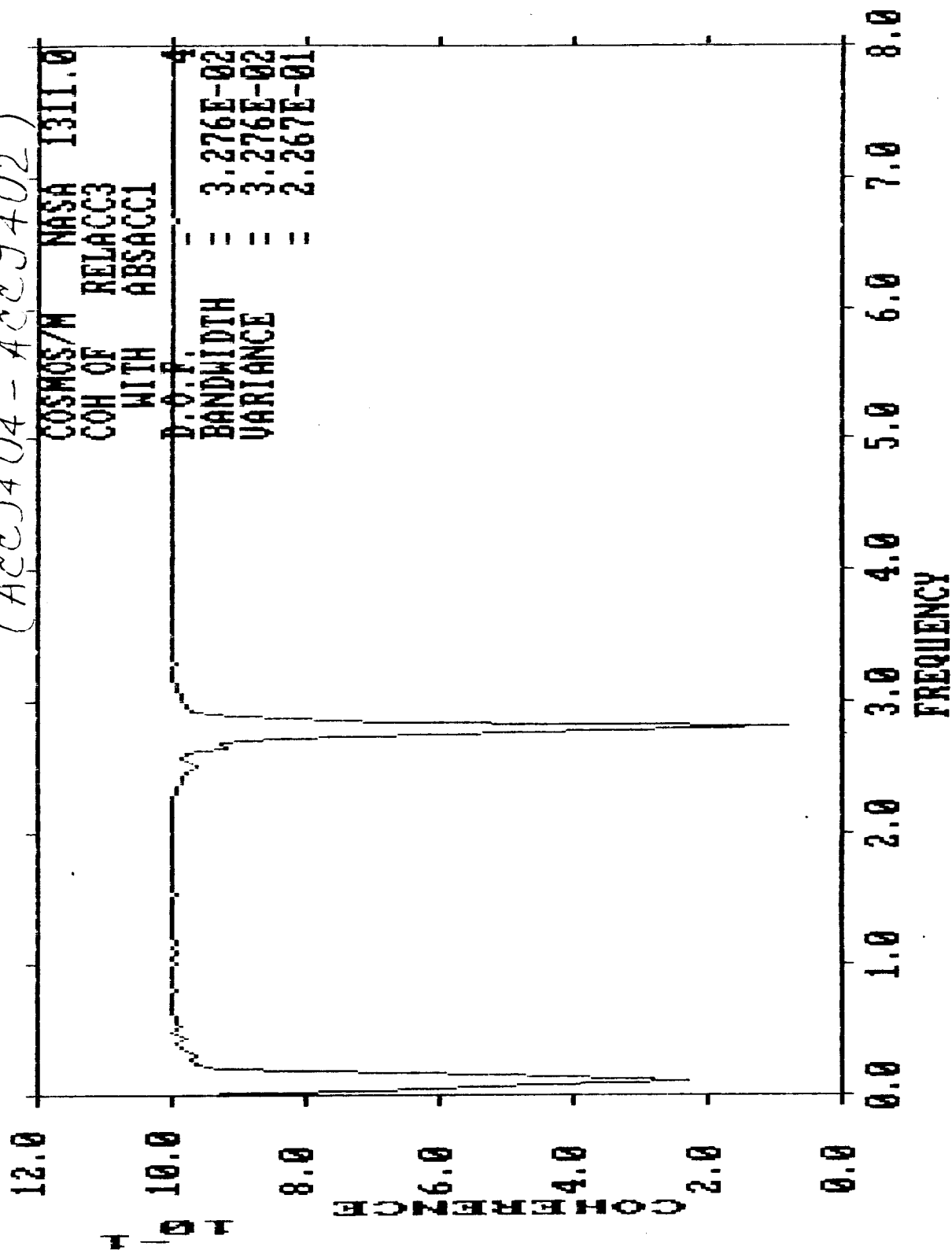
(ACCJ4U4 - ACCJ4U2)



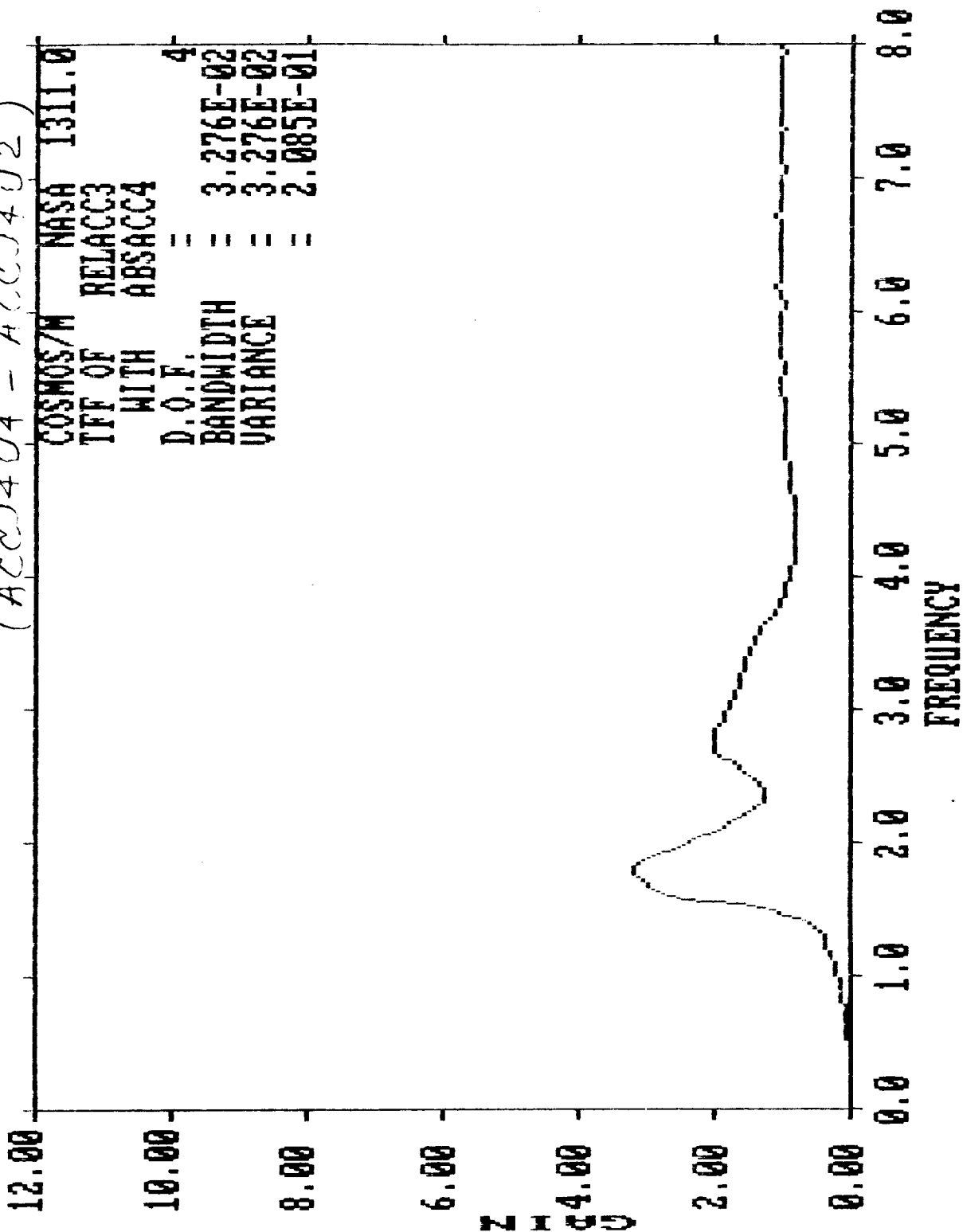
(ACCJ4U4 - ACCJ4U2)



(ACCJ4U4 - ACCJ4U2)

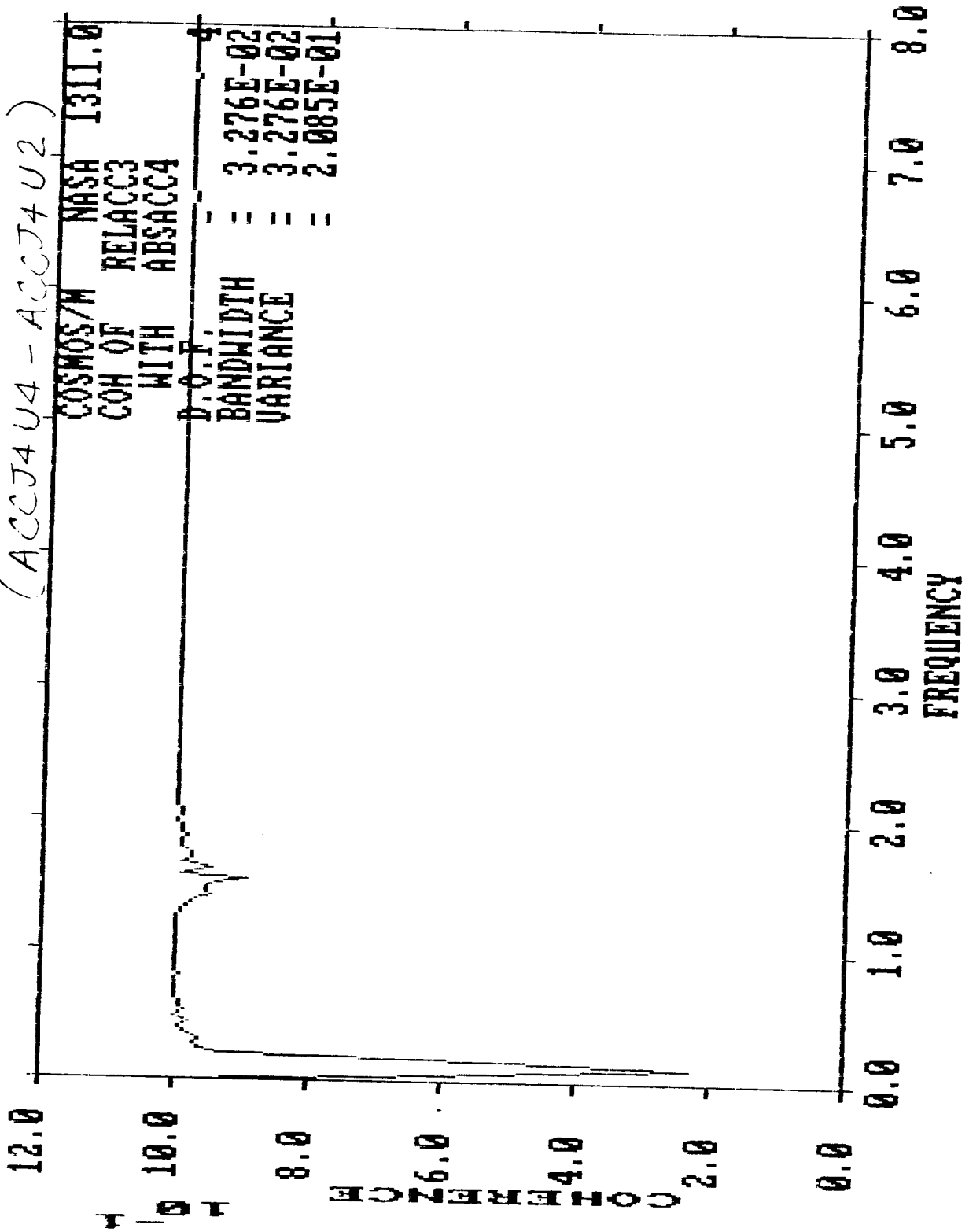


(ACCJ4U4 - ACCJ4U2)

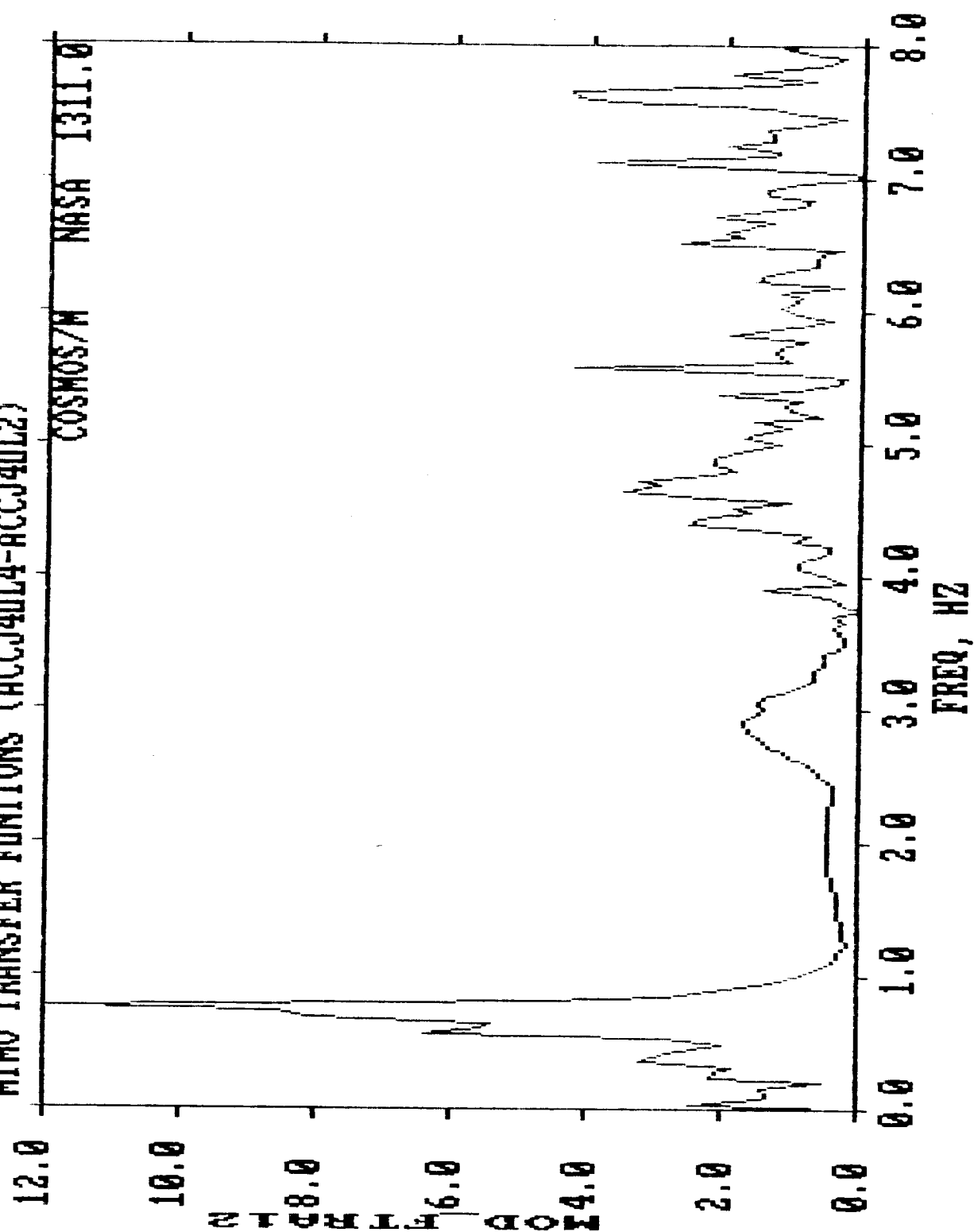




(ACCJ4U4 - ACCJ4U2)

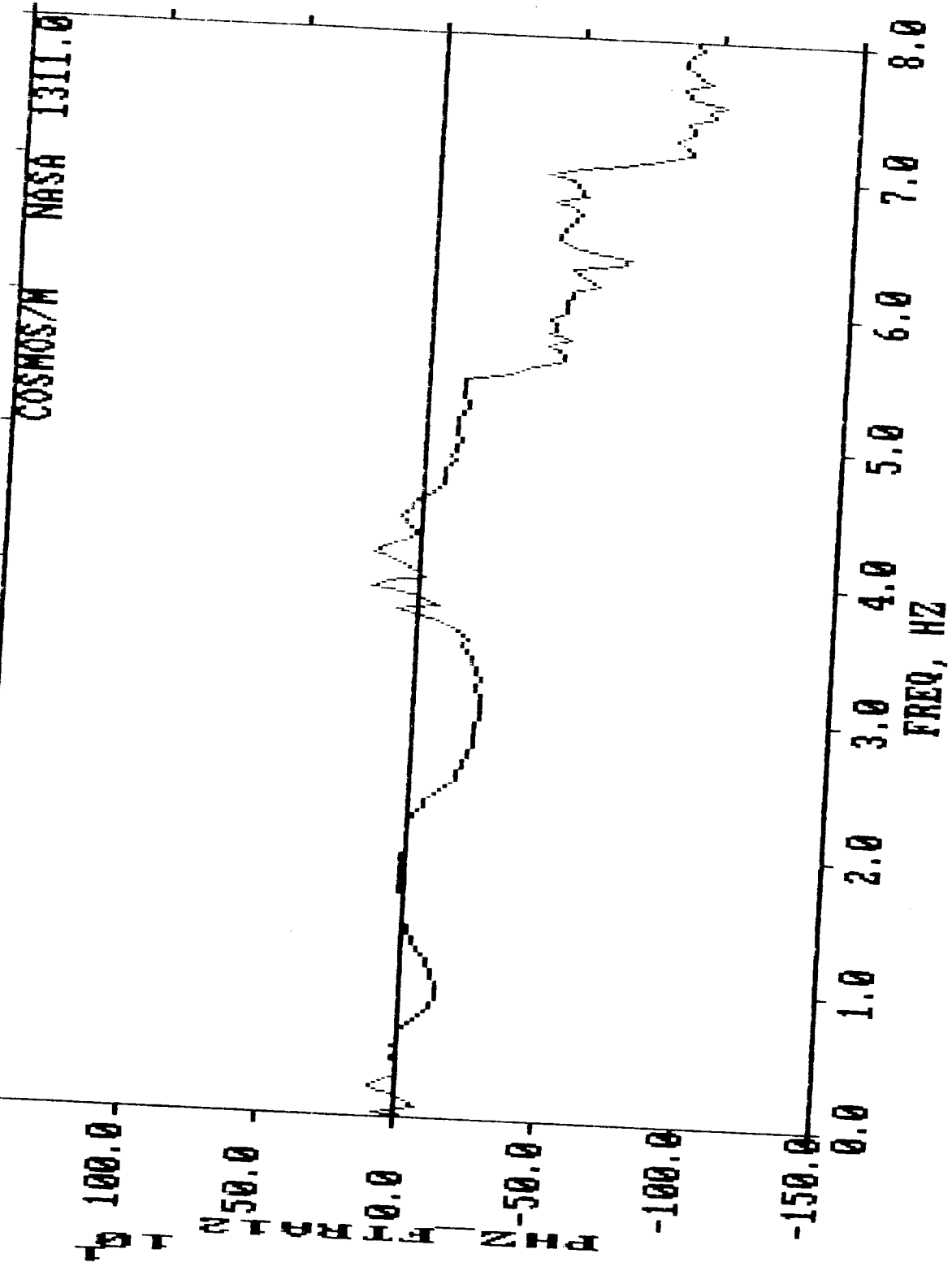


# MIMO TRANSFER FUNCTIONS (ACCJ4UL4-ACCJ4UL2)

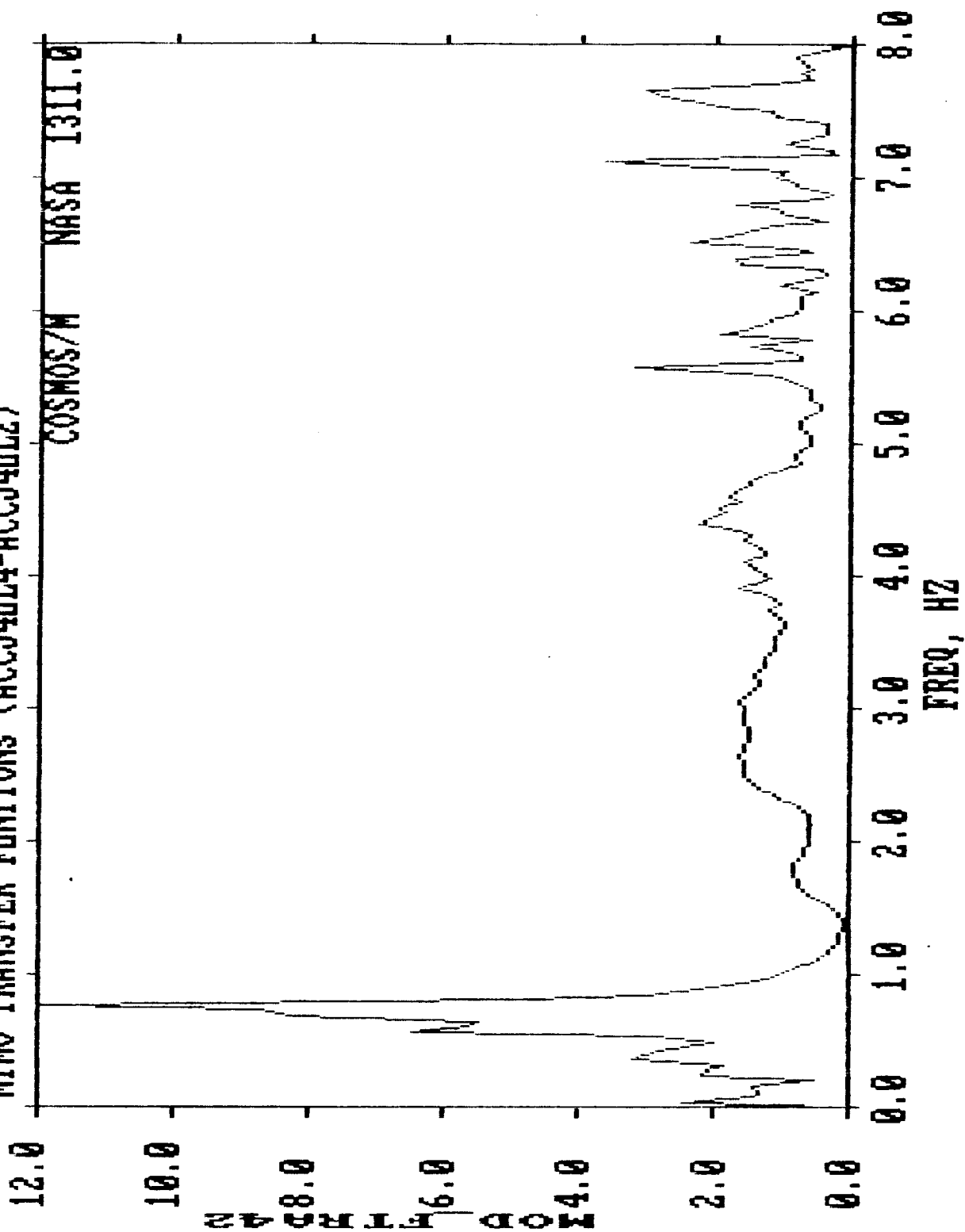


COSMOS/M NASA 1311.0

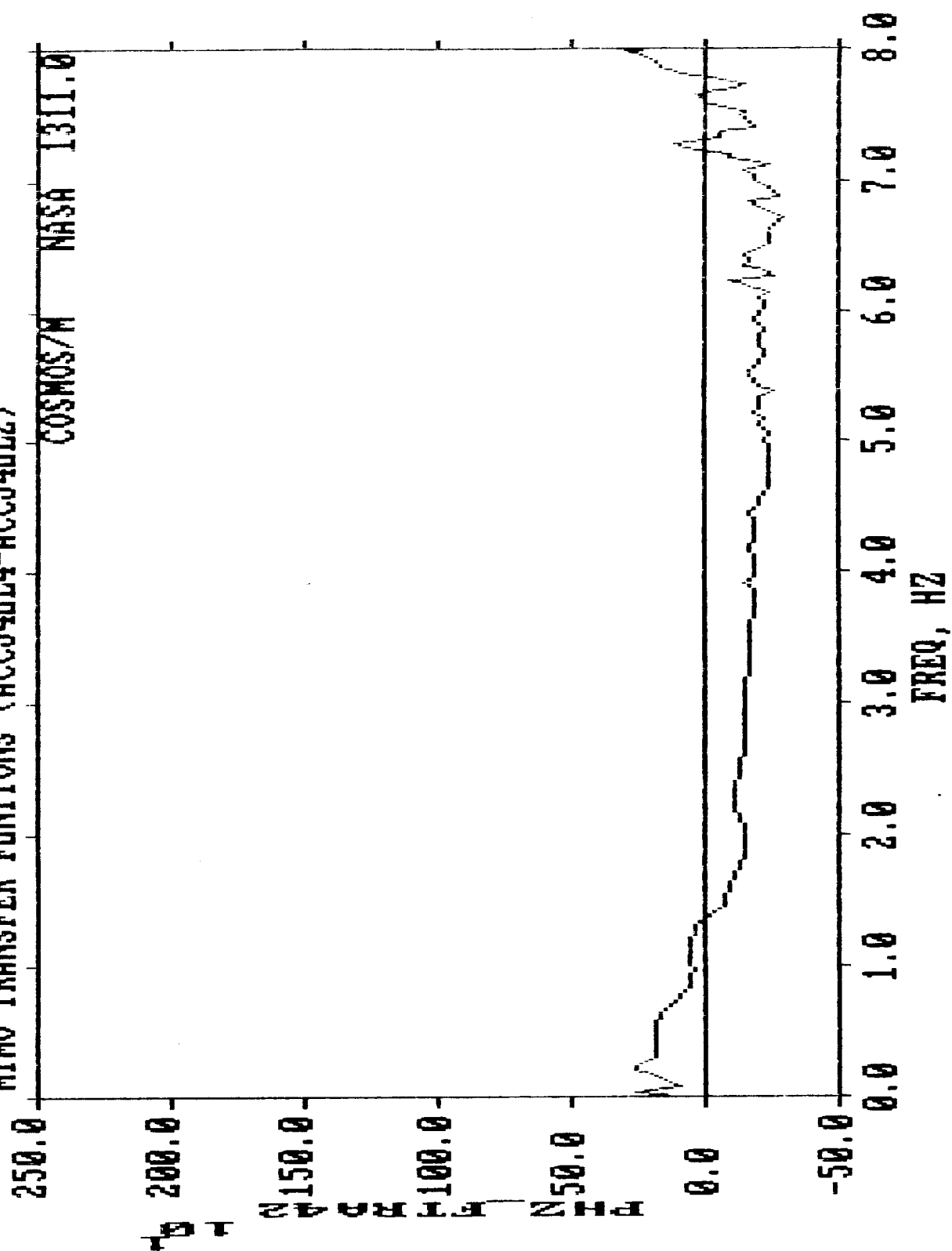
MIMO TRANSFER FUNCTIONS (ACCJ4UL4-ACCJ4UL2)



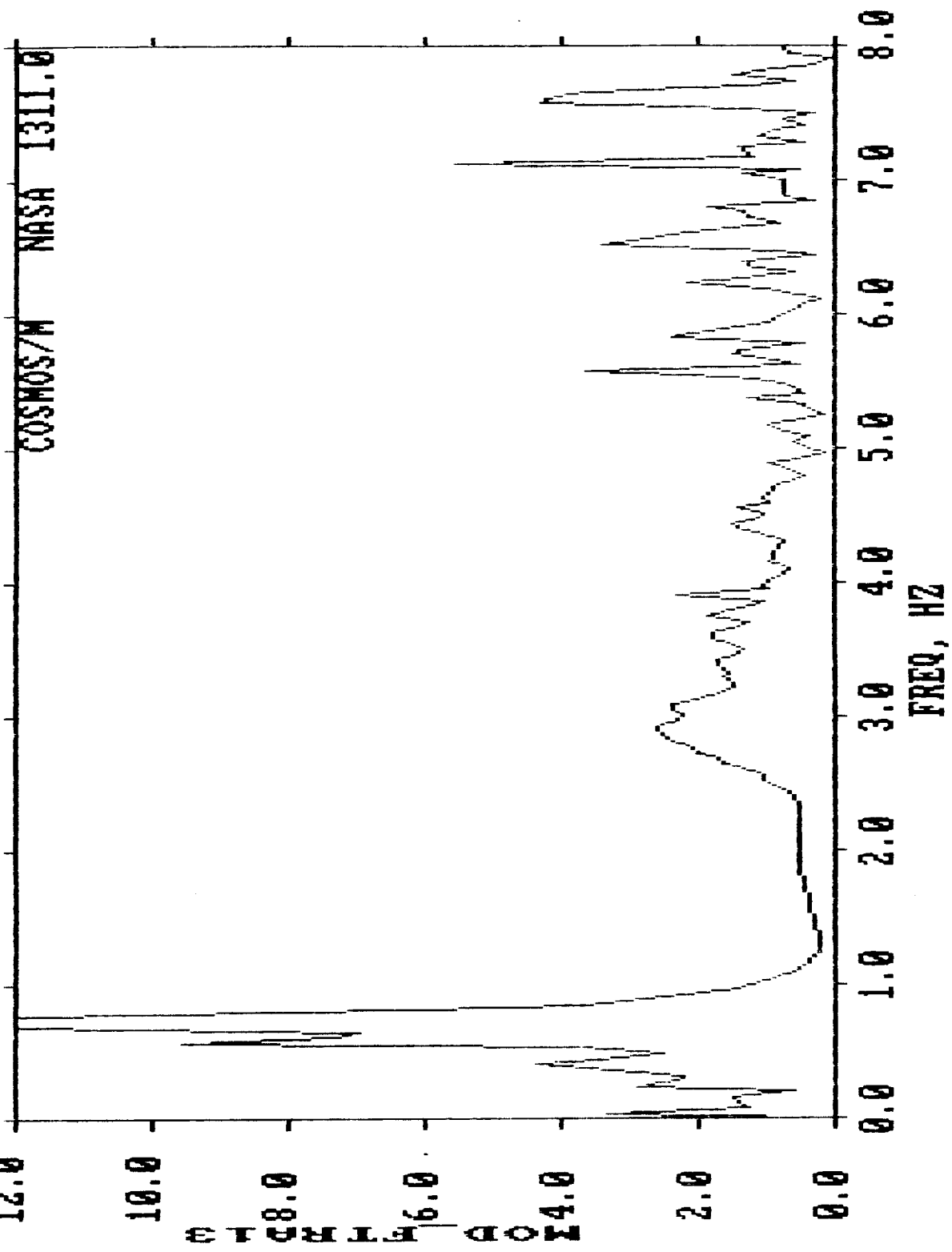
# MIMO TRANSFER FUNCTIONS (ACCJ4UL4-ACCJ4UL2)



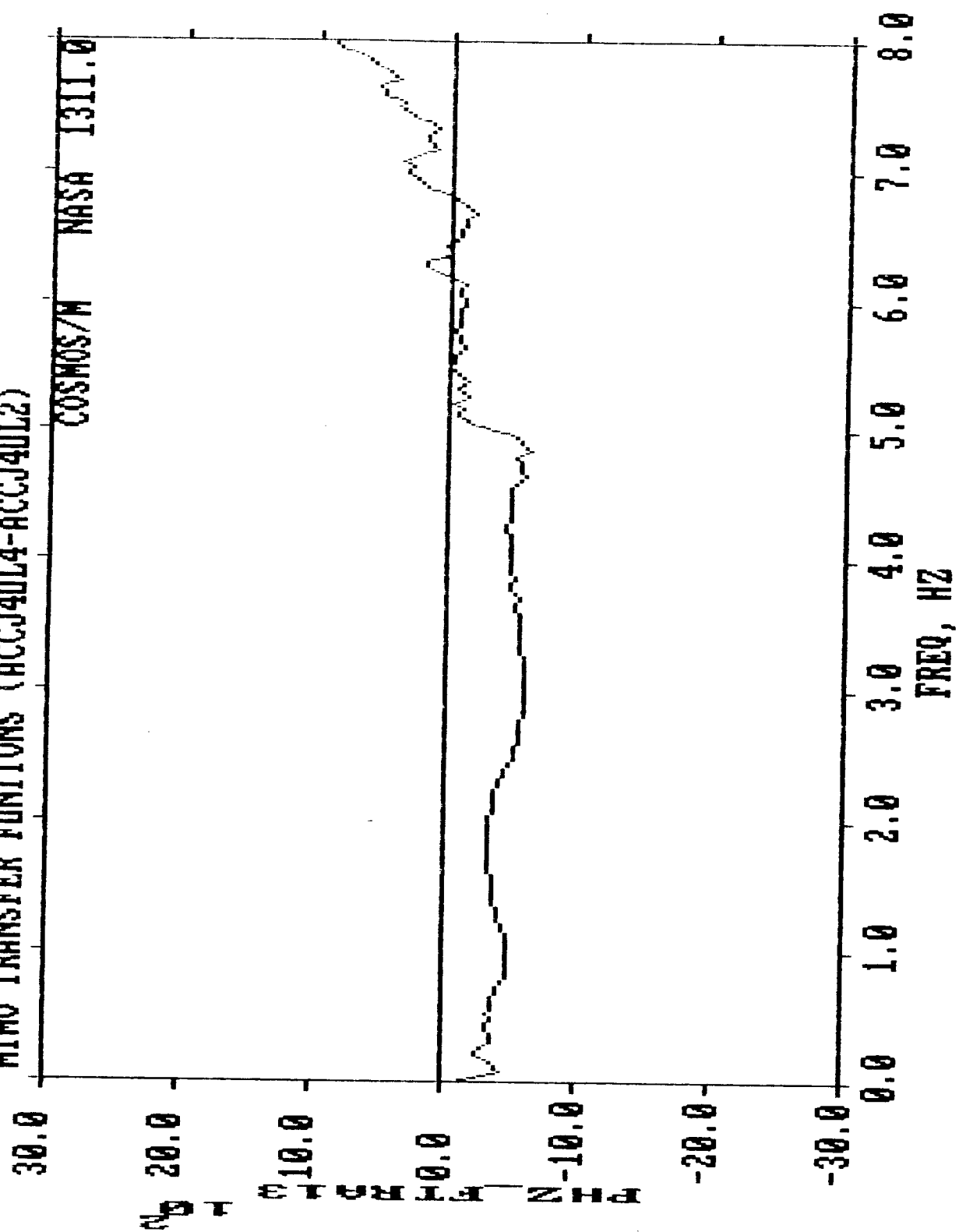
# MIMO TRANSFER FUNCTIONS (ACCJ4UL4-ACCJ4UL2)

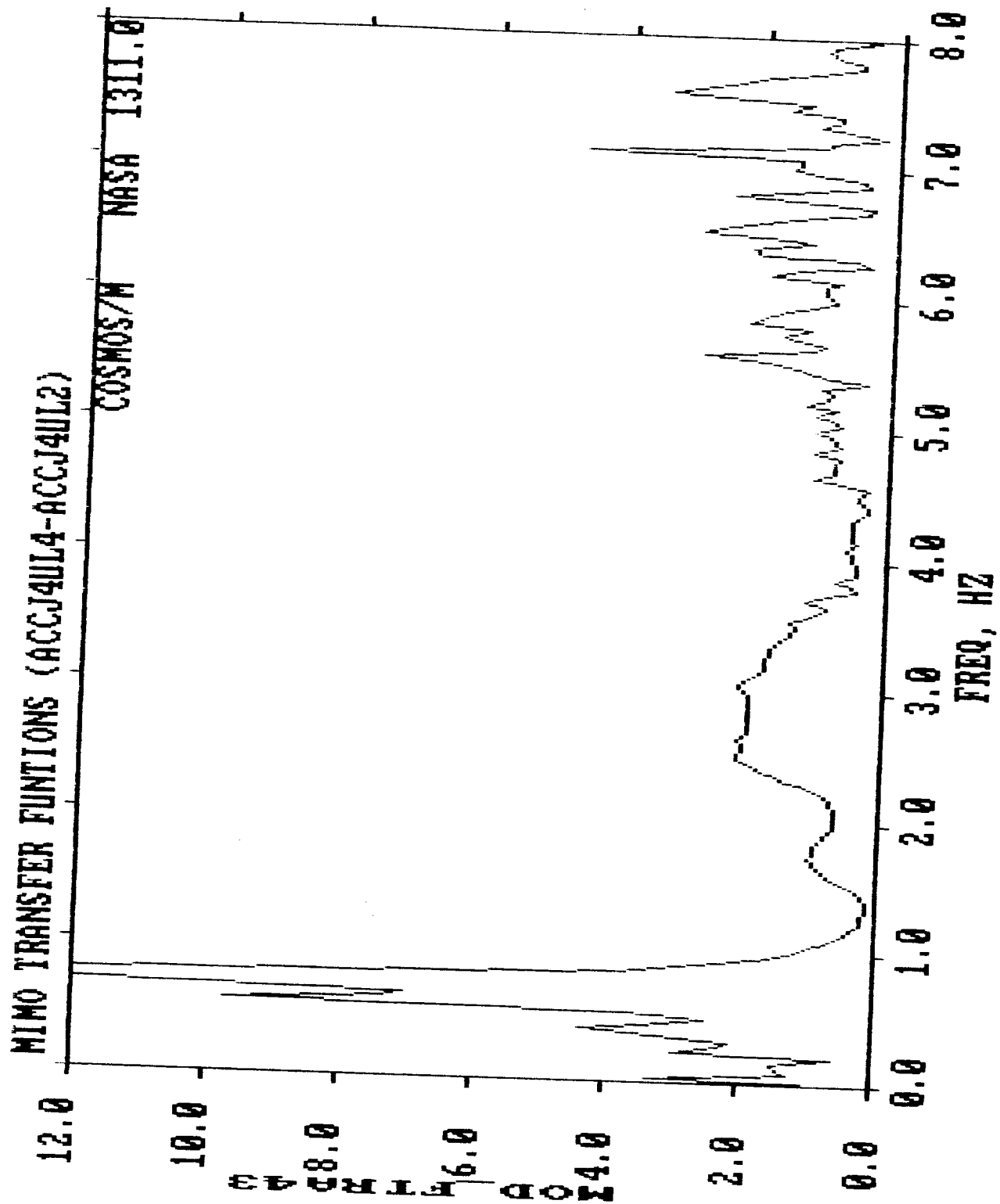


# MIMO TRANSFER FUNCTIONS (ACCJ4UL4-ACCJ4UL2)



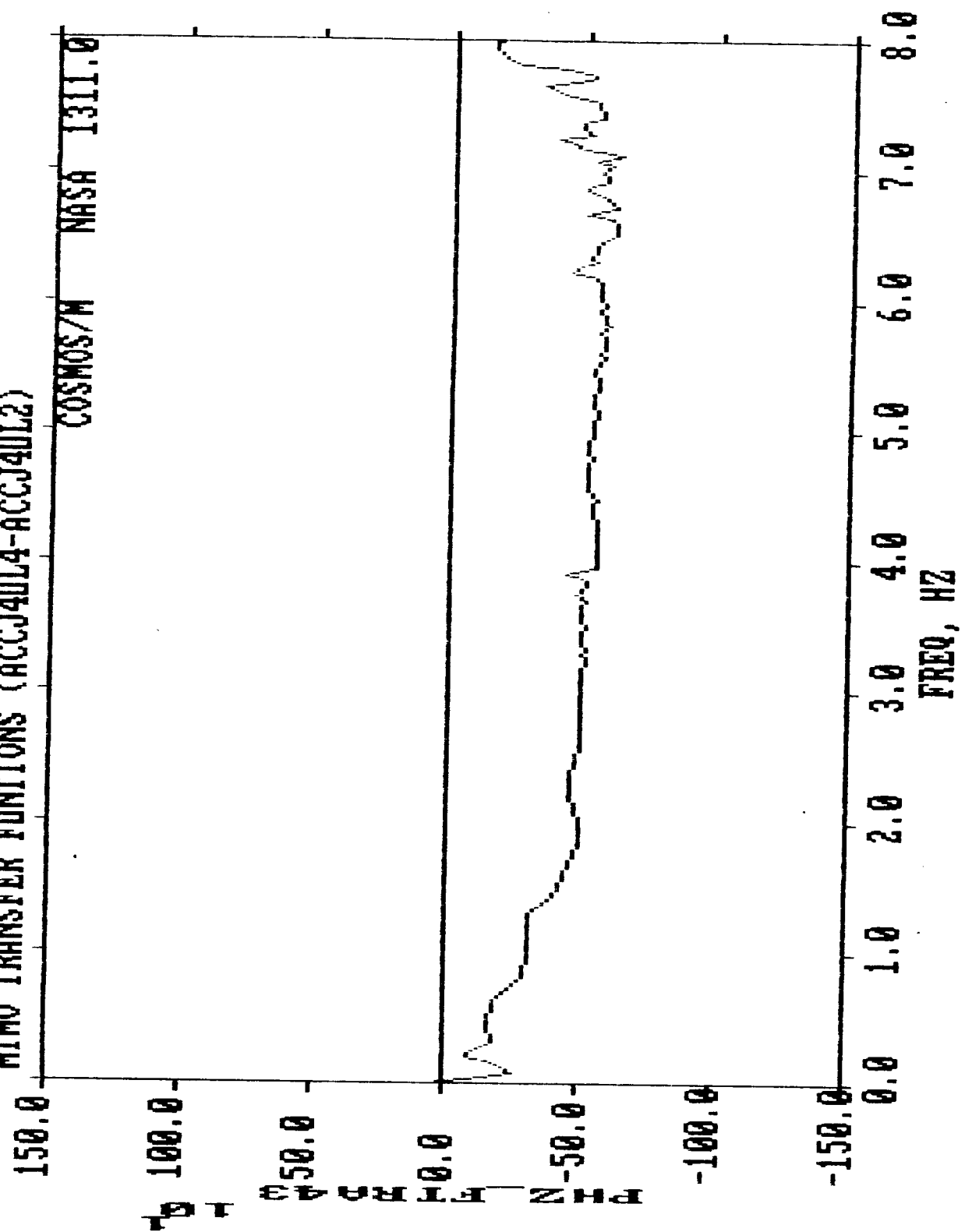
# MIMO TRANSFER FUNCTIONS (ACCJ4UL4-ACCJ4UL2)







# MIMO TRANSFER FUNCTIONS (ACCJ4UL4-ACCJ4UL2)



MIMO RELATIVE MODULE TRANSFER FUNCTION MATRIX  
EXCITATION--FORCE AT NODE POINT 5

MINO REL ACCEL TRANS FUN. - TRANS, J4F457U ACC(4M, 2HL), RT, R6=0

COSMOS7H NASA 13117.0

13.0

15.0

12.0

9.0

6.0

3.0

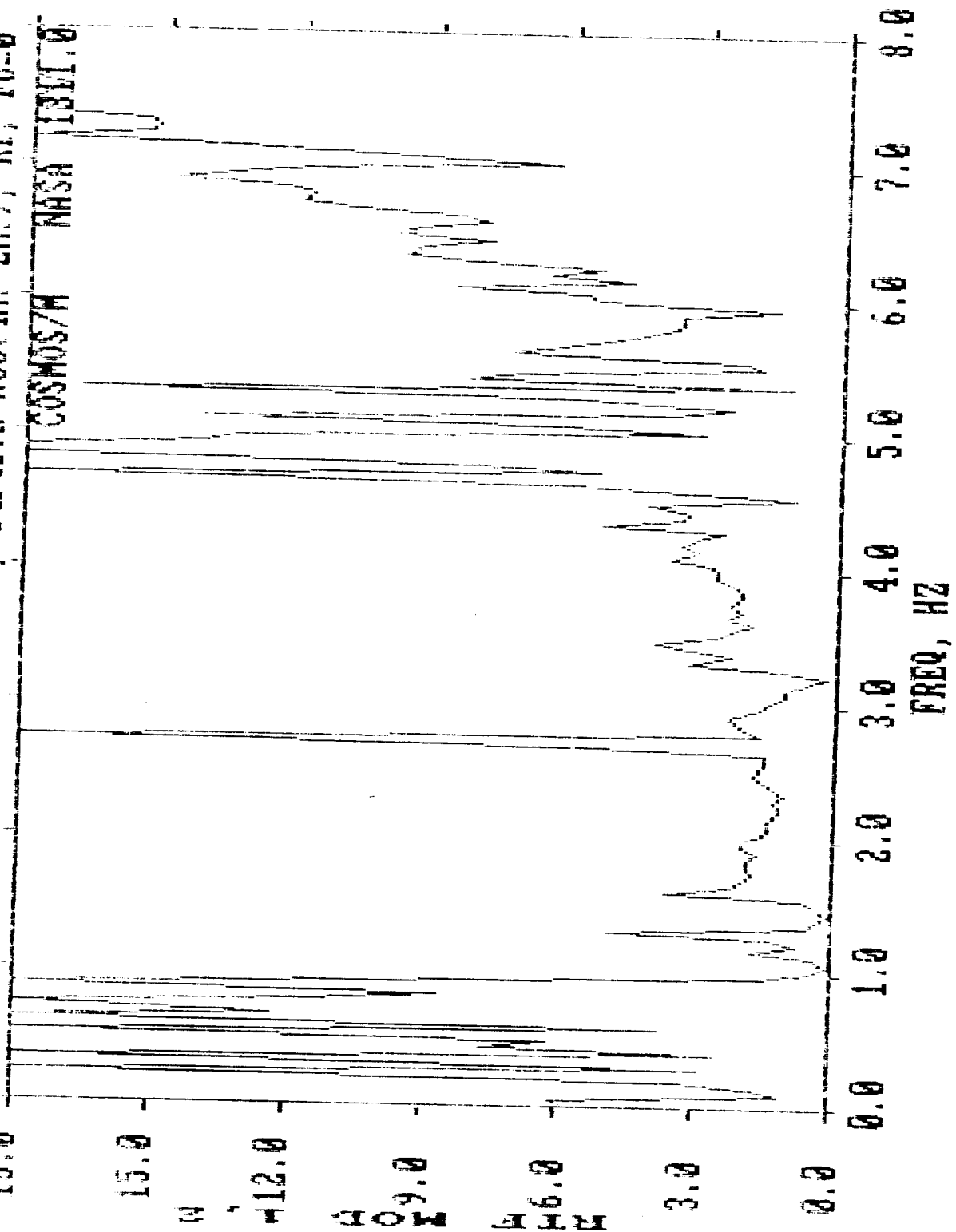
0.0

0.0 1.0 2.0 3.0 4.0 5.0 6.0 7.0 8.0

FREQ, HZ

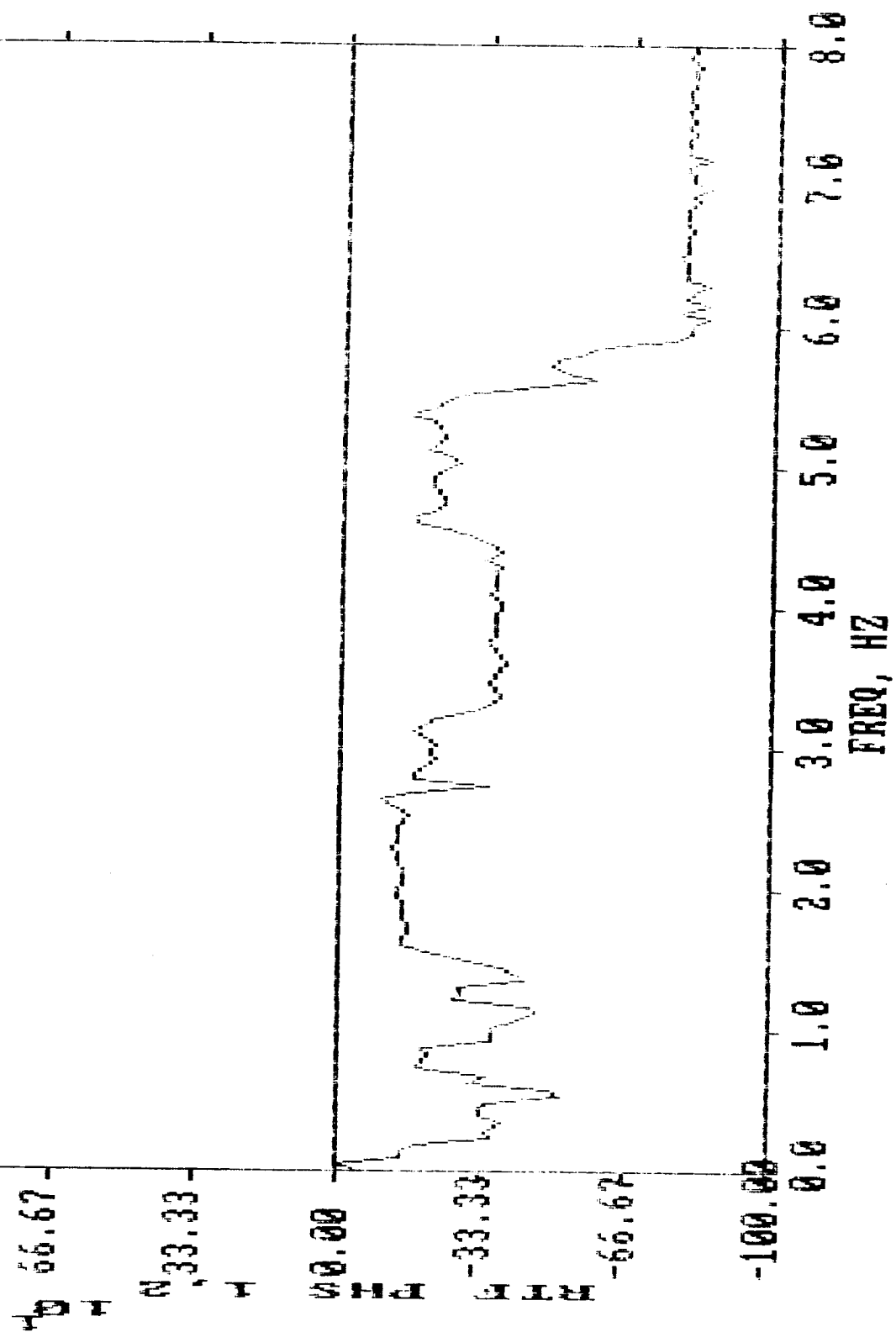
MINO REL ACCEL TRANS. FUN. - TRANS, J4F457H ACC(4M, -2M.), RT, F6=0

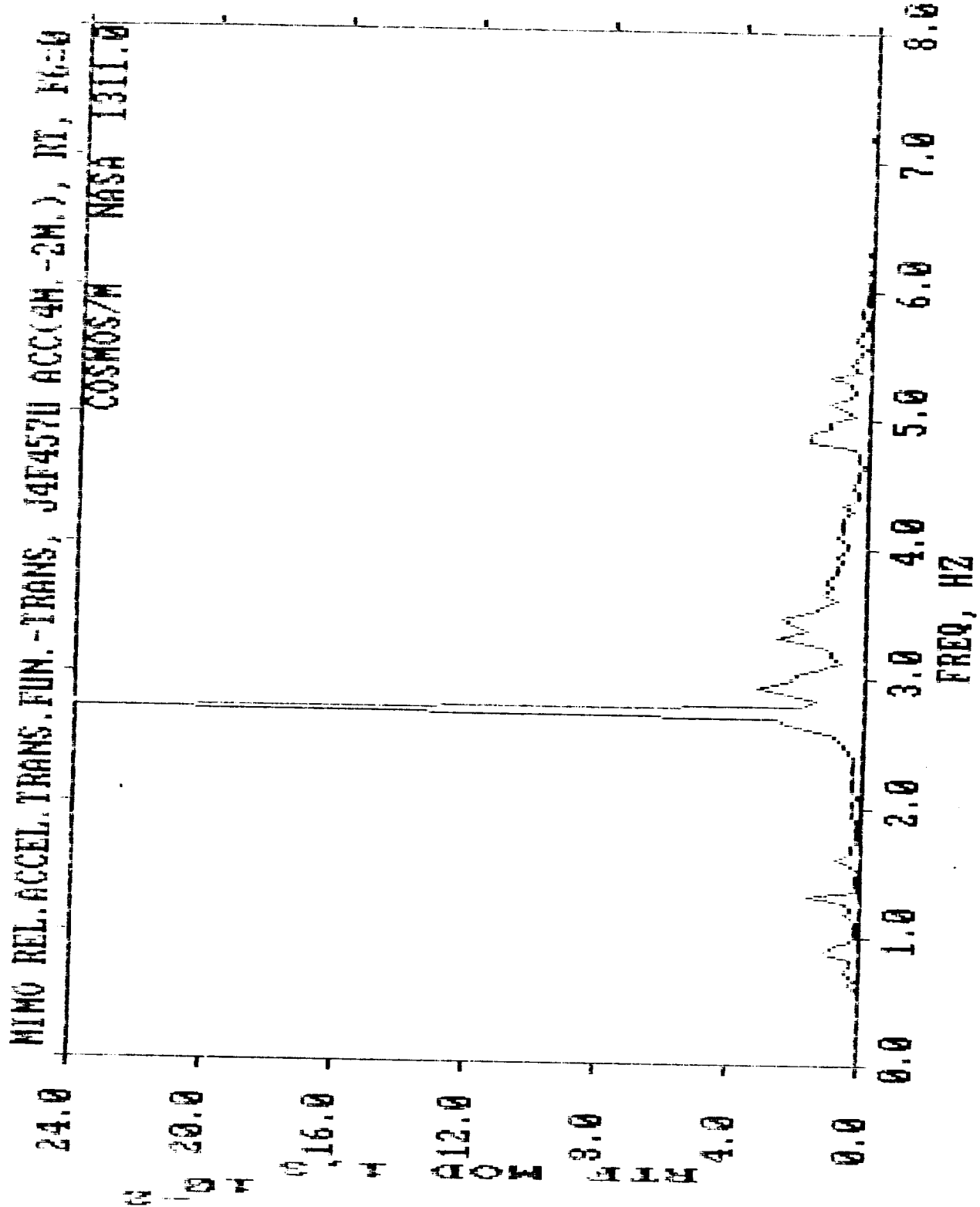
COSMOS/H NASA 1351.0



NIMO REL.ACCEL.TRANS.FUN.-TRANS, J4F457U ACC(4M-2H.), RT, P6=0

COSMO57M NASA 1311.0





HIHO REL ACCEL, TRANS, FUN, -TRANS, J4F437U ACC(4H, -2H.), RT, F6=0

COSMOS74 NASA 1311.0

25.0

0.0

-25.0

-50.0

-75.0

-100.0

-125.0

0.0

1.0

2.0

3.0

4.0

5.0

6.0

7.0

8.0

FREQ, HZ

MIMO REL.ACCEL TRANS.FUN.-TRANS, J4F457U ACC(4M.-2M.), RT, PG=0

COSMOS/M NASA 1311.0

12.0

10.0

8.0

6.0

4.0

2.0

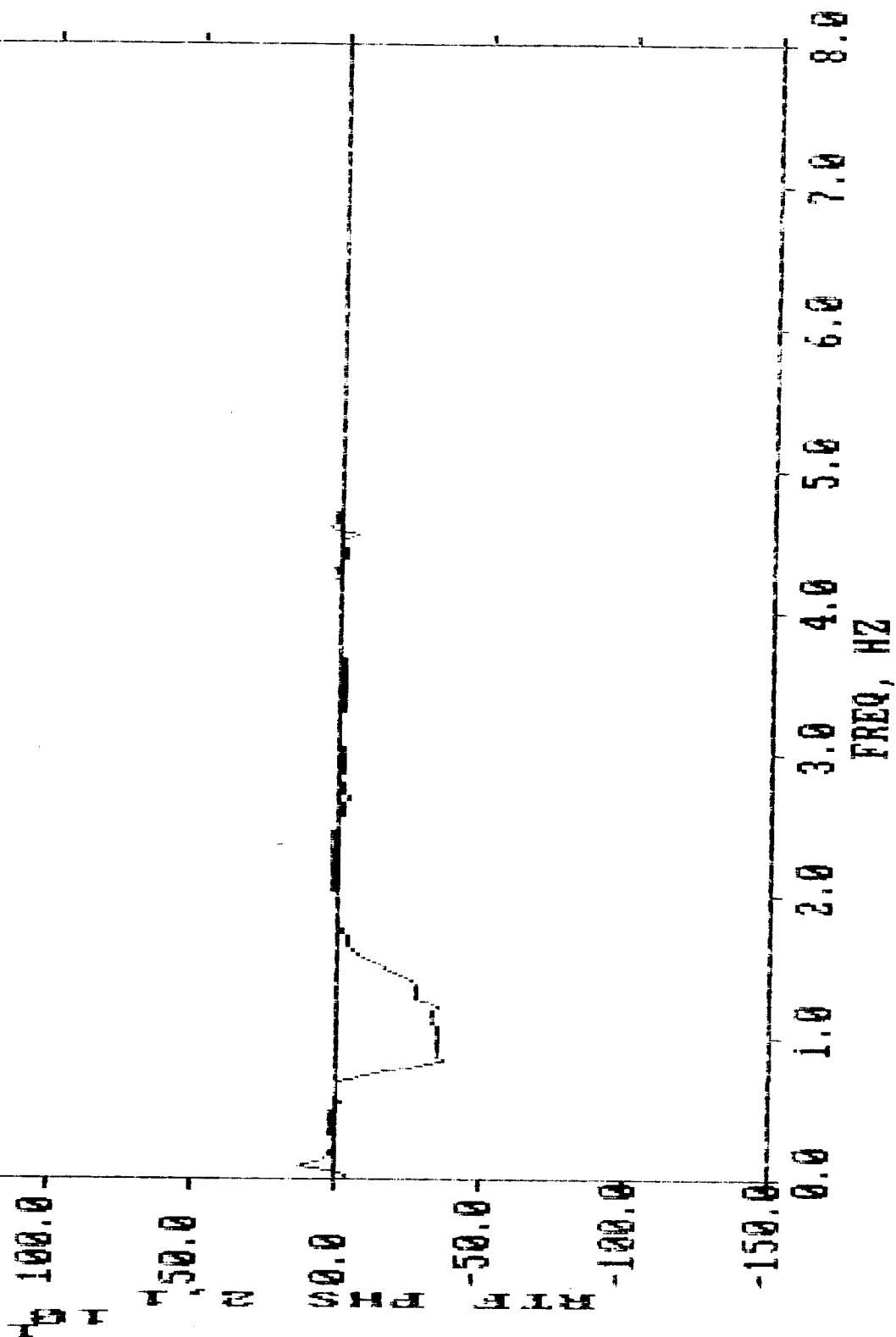
0.0

0.0 1.0 2.0 3.0 4.0 5.0 6.0 7.0 8.0  
FREQ, HZ



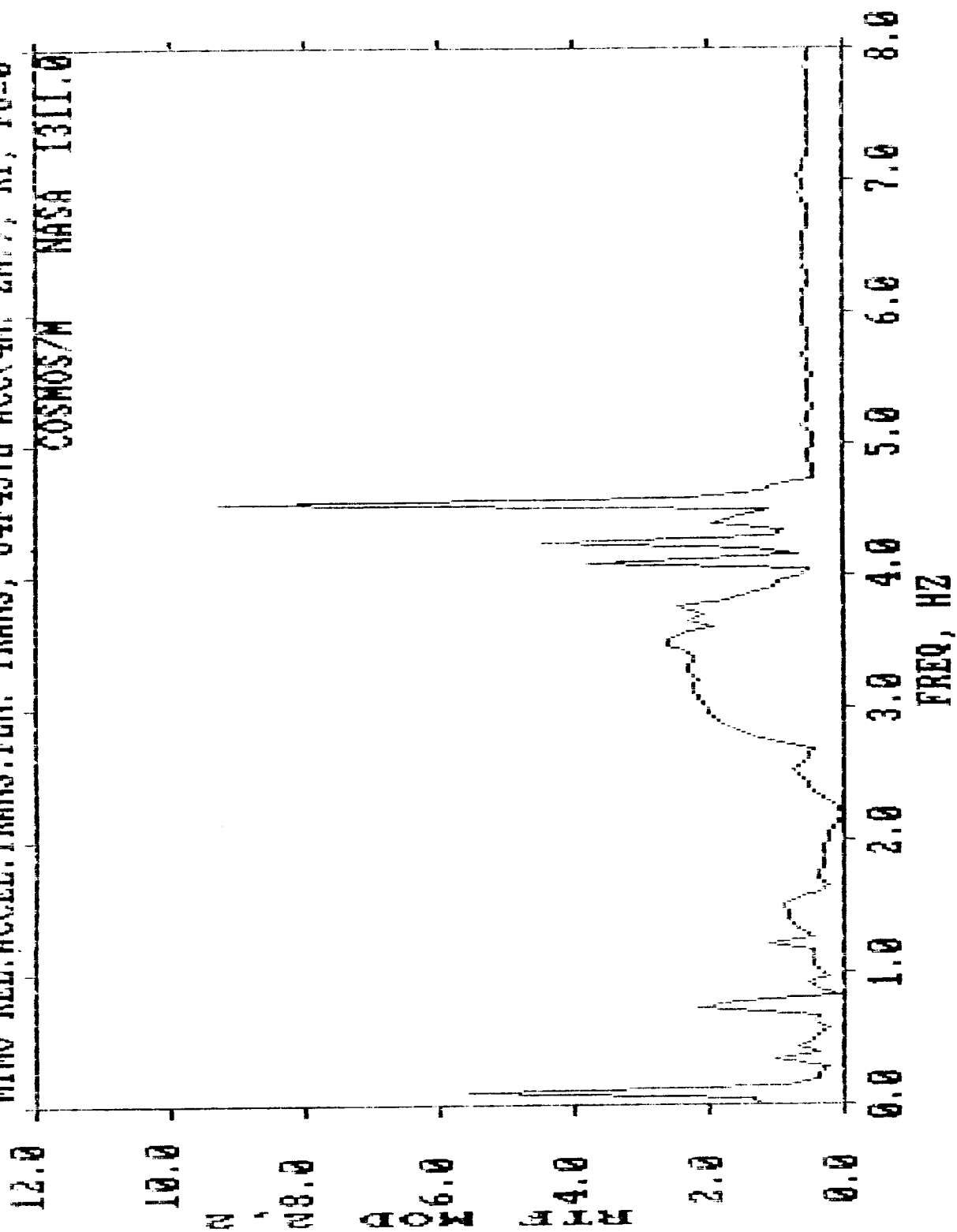
MINO REL. ACCEL. TRANS. FUN. - TRANS, J4F457U ACC(4M, 2H.), RT, P6=0

COSMOS/M NASA 1311.0



MIMO REL. ACCEL. TRANS. FUN. - TRANS, J4F457U ACC(4H, -2H.), RT, F6=0

COSMOS/M NASA 1311.0



MIMO REL.ACCEL.TRANS.FUN.-TRANS, J4F457U ACC(4M.-2M.), RT, F6=0

COSMOS/M NASA 1311.0

250.0

200.0

150.0

100.0

50.0

0.0

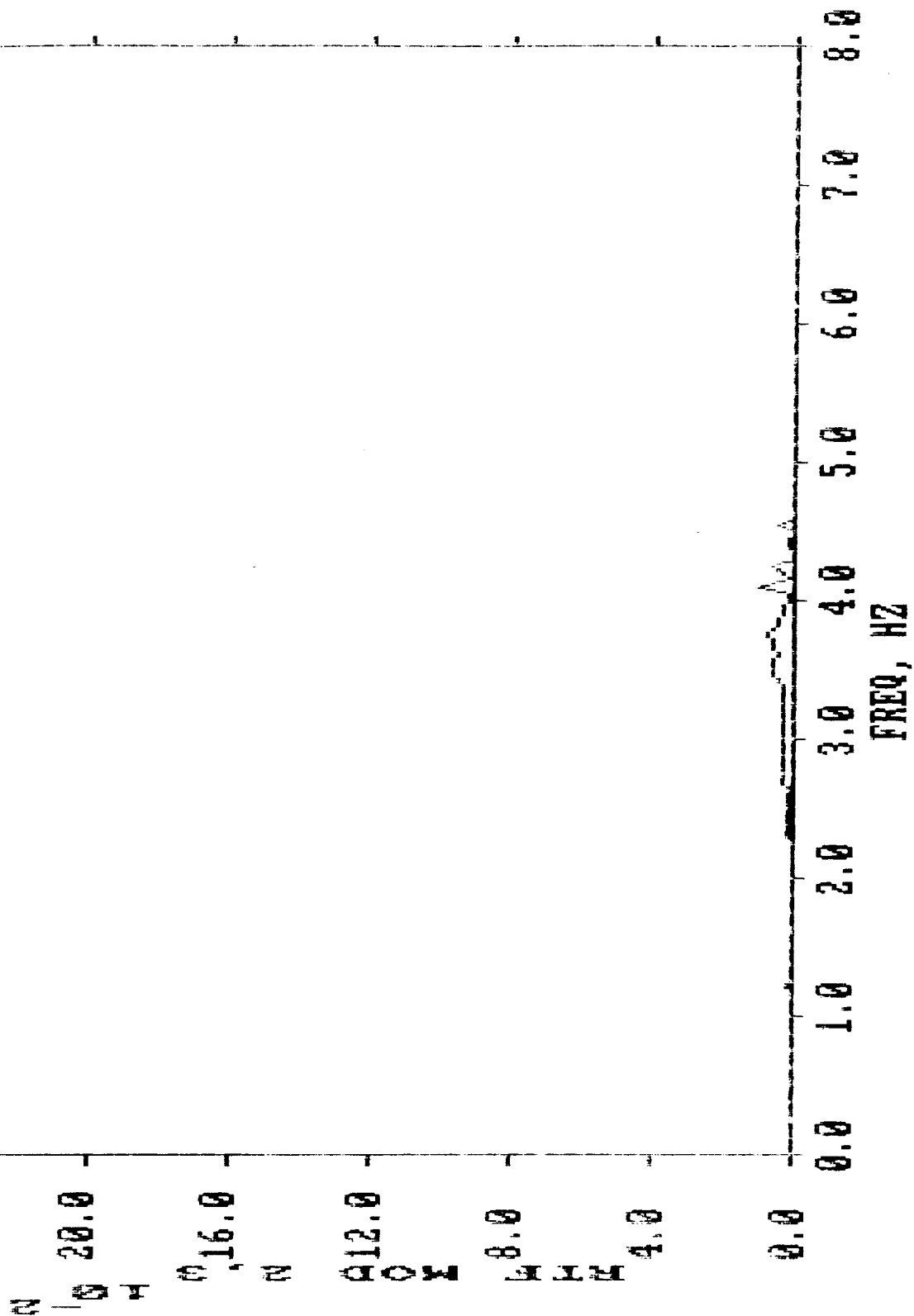
-50.0

0.0 1.0 2.0 3.0 4.0 5.0 6.0 7.0 8.0

FREQ, HZ

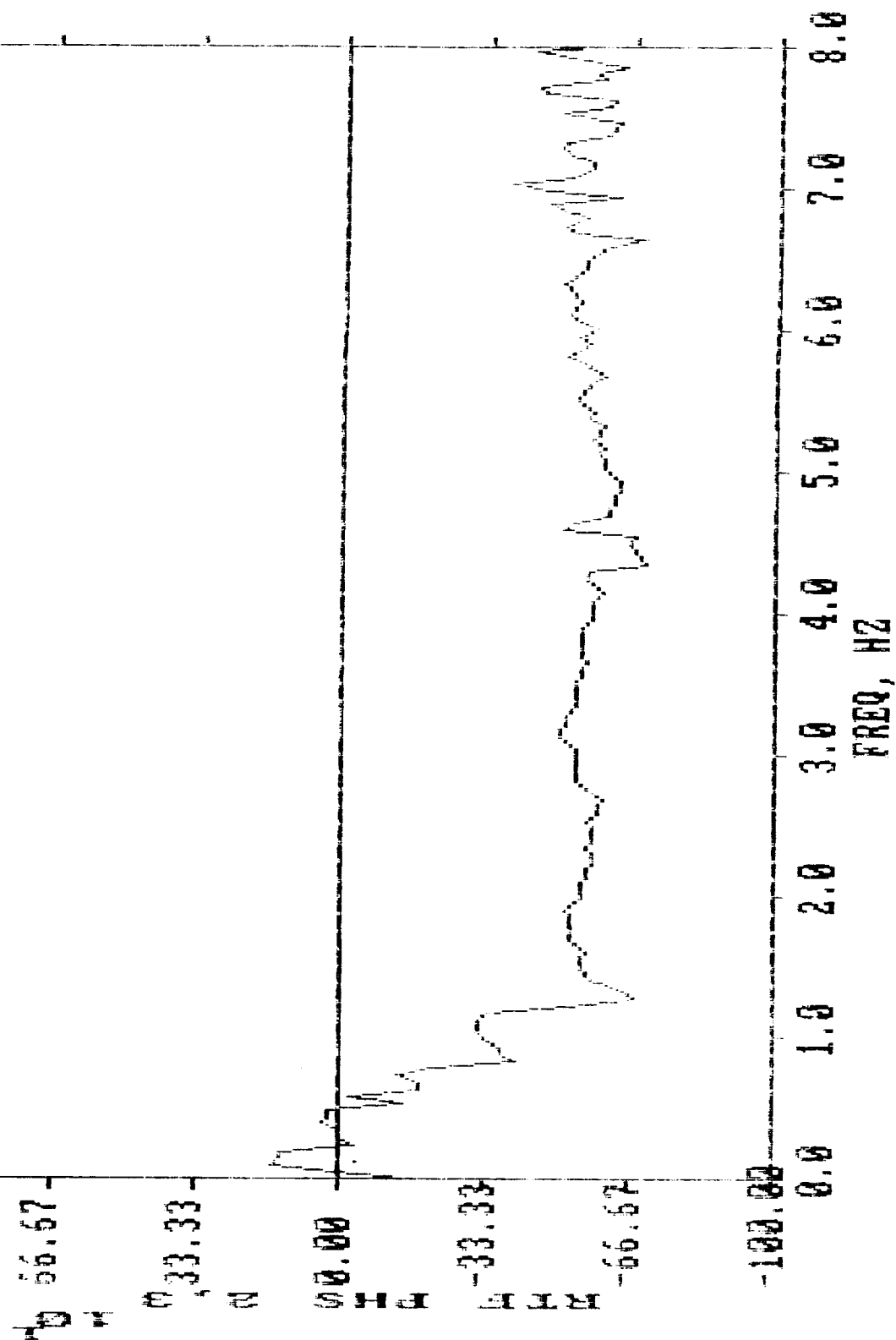
MIMO REL.ACCEL.TRANS.FUN.-TRANS, J4F457U ACC(4M.-2M.), RT, F6=0

COSMOS/M NASA 1311.0



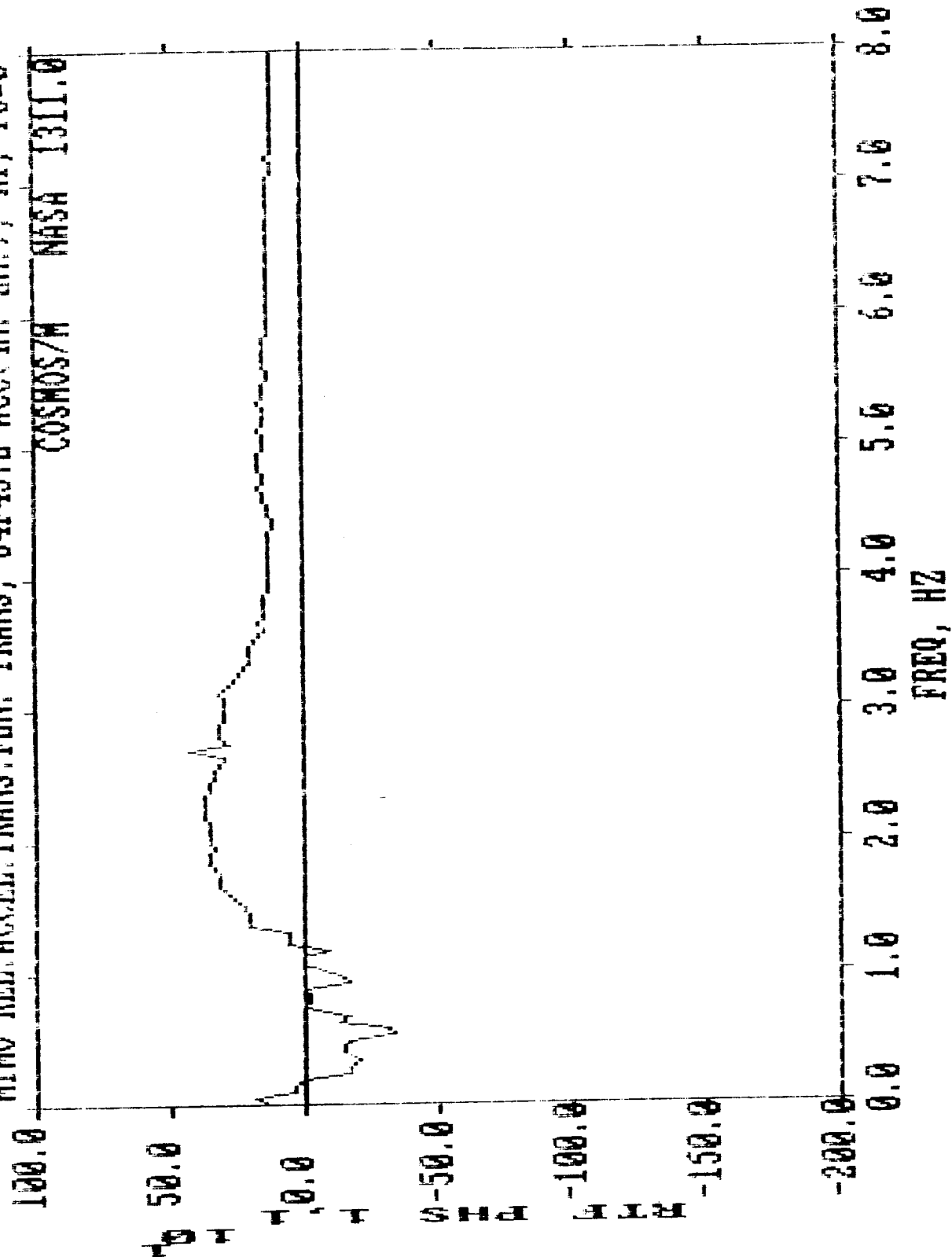
HIMO REL.ACCEL.TRANS.FUN.-TRANS, 34F457U ACC(2M.-2M.), RT, F6=0

COSMOS/M NASA 1311.0



MINO REL. ACCEL. TRANS. FUN. - TRANS, J4F457U ACC(4M, -2M.), RT, F6=0

COSMOS/M NASA 1311.0



**ANCO**

APPENDIX D

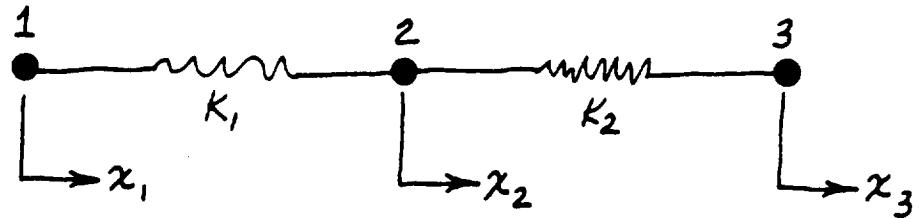
NONUNIFORM ENFORCED MOTION USING LARGE MASS METHOD

This appendix contains analytical calculations for the nonuniform enforced motion problem for a simple three degree-of-freedom system. Two of the mass points (at Nodes 1 and 3) have corresponding desired enforced accelerations. The third mass point (at Node 2) is between them and undergoes dynamic response. It is shown that the large mass method of nonuniform enforced motion work and that the fixed-base problem for the system can be solved.

ORIGINAL PAGE IS  
OF POOR QUALITY



Solve: Motion of free 3 degree of freedom system. Look at enforced motion compared to this problem.



Let  $M_1 = M_3 = M^*$ ,  $M_2 = M$

$$[M]\{\ddot{x}\} + [K]\{x\} = \{F\}$$

$$[M] = \begin{bmatrix} M^* & 0 & 0 \\ 0 & M & 0 \\ 0 & 0 & M^* \end{bmatrix}$$

$$[K] = \begin{bmatrix} K_1 & -K_1 & 0 \\ -K_1 & K_1 + K_2 & -K_2 \\ 0 & -K_2 & K_2 \end{bmatrix}$$

Let  $K_1 = K_2 = K$ , then

$$[K] = K \begin{bmatrix} 1 & -1 & 0 \\ -1 & 2 & -1 \\ 0 & -1 & 1 \end{bmatrix}$$

Eigenvalue problem is  $(-\omega^2[M] + [K])\{\phi\} = \{0\}$ .

$$\text{Det} \left( -\omega^2 \begin{bmatrix} M^* & 0 & 0 \\ 0 & M & 0 \\ 0 & 0 & M^* \end{bmatrix} + K \begin{bmatrix} 1 & -1 & 0 \\ -1 & 2 & -1 \\ 0 & -1 & 1 \end{bmatrix} \right) = 0$$

$$(K - \omega^2 M^*)(2K - \omega^2 M)(K - \omega^2 M^*) - [K^2(K - \omega^2 M^*) + K^2(K - \omega^2 M^*)]$$

$$= 0$$

$$(K - \omega^2 M^*)^2(2K - \omega^2 M) - 2K^2(K - \omega^2 M^*) = 0$$

$$(K - \omega^2 M^*)[(K - \omega^2 M^*)(2K - \omega^2 M) - 2K^2] = 0$$

$$\therefore K - \omega^2 M^* = 0, \quad \omega^2 = K/M^*$$

$$(K - \omega^2 M^*)(2K - \omega^2 M) - 2K^2 = 0$$

$$2K^2 - 2K\omega^2 M^* - K\omega^2 M + \omega^4 M M^* - 2K^2 = 0$$

$$\omega^2(-2KM^* - KM + \omega^2 M M^*) = 0$$

$$\therefore \omega^2 = 0 \quad (\text{rigid body mode})$$

$$-2KM^* - KM + \omega^2 M M^* = 0$$

$$\therefore \omega^2 = \frac{2K}{M} + \frac{K}{M^*}$$

Define:

$$\omega_1^2 = 0$$

$$\omega_2^2 = K/M^*$$

$$\omega_3^2 = 2K/M + K/M^*$$

Find  $\{\phi_1\}$ .

$$(-\omega^2[M] + [K])\{\phi_1\} = \{0\}$$

$$\begin{bmatrix} 1 & -1 & 0 \\ -1 & 2 & -1 \\ 0 & -1 & 1 \end{bmatrix} \begin{Bmatrix} \phi_{11} \\ \phi_{21} \\ \phi_{31} \end{Bmatrix} = \{0\}$$

Solve to get

$$\{\phi_1\} = \phi_{11} \begin{Bmatrix} 1 \\ 1 \\ 1 \end{Bmatrix}$$

Find  $\{\phi_2\}$ .

$$\left( -\frac{K}{M^*} \begin{bmatrix} M^* & 0 & 0 \\ 0 & M & 0 \\ 0 & 0 & M^* \end{bmatrix} + K \begin{bmatrix} 1 & -1 & 0 \\ -1 & 2 & -1 \\ 0 & -1 & 1 \end{bmatrix} \right) \begin{Bmatrix} \phi_{12} \\ \phi_{22} \\ \phi_{32} \end{Bmatrix} = \{0\}$$

$$K \begin{bmatrix} 0 & -1 & 0 \\ -1 & 2 - \frac{M}{M^*} & -1 \\ 0 & -1 & 0 \end{bmatrix} \begin{Bmatrix} \phi_{12} \\ \phi_{22} \\ \phi_{32} \end{Bmatrix} = \{0\}$$

MADE BY WBW DATE 3/16/88CHECKED BY GTY DATE 3/21/88JOB NUMBER \_\_\_\_\_ PAGE 4 OF 9DESCRIPTION Nonuniform Base Motion

Solve to get

$$\{\phi_2\} = \phi_{12} \begin{Bmatrix} 1 \\ 0 \\ -1 \end{Bmatrix}$$

Find  $\{\phi_3\}$ .

$$\left( -\left( \frac{2K}{M} + \frac{K}{M^*} \right) \begin{bmatrix} M^* & 0 & 0 \\ 0 & M & 0 \\ 0 & 0 & M^* \end{bmatrix} + K \begin{bmatrix} 1 & -1 & 0 \\ -1 & 2 & -1 \\ 0 & -1 & 1 \end{bmatrix} \right) \begin{Bmatrix} \phi_{13} \\ \phi_{23} \\ \phi_{33} \end{Bmatrix} = \{0\}$$

$$K \begin{bmatrix} -\frac{2M^*}{M} & -1 & 0 \\ -1 & -\frac{M}{M^*} & -1 \\ 0 & -1 & -\frac{2M^*}{M} \end{bmatrix} \begin{Bmatrix} \phi_{13} \\ \phi_{23} \\ \phi_{33} \end{Bmatrix} = \{0\}$$

Solve to get

$$\{\phi_3\} = \phi_{23} \begin{Bmatrix} -\frac{M}{2M^*} \\ 1 \\ -\frac{M}{2M^*} \end{Bmatrix}$$

Def. :

$$[\phi] = \left[ \begin{array}{c|c|c} 1 & 1 & -\frac{M}{2M^*} \\ 1 & 0 & 1 \\ 1 & -1 & -\frac{M}{2M^*} \end{array} \right]$$

$$[\phi]^T [M] [\phi] = \begin{bmatrix} M + 2M^* & 0 & 0 \\ 0 & 2M^* & 0 \\ 0 & 0 & M(1 + \frac{M}{2M^*}) \end{bmatrix} = [\tilde{M}]$$

$$[\phi]^T [K] [\phi] = K \begin{bmatrix} 0 & 0 & 0 \\ 0 & 2 & 0 \\ 0 & 0 & [\frac{M}{M^*}(2 + \frac{M}{2M^*}) + 2] \end{bmatrix} = [\tilde{K}]$$

$$[\tilde{M}] \{\ddot{\eta}\} + [\tilde{K}] \{\eta\} = [\phi]^T \{F\}$$

$$[\phi]^T \{F\} = \begin{bmatrix} 1 & 1 & 1 \\ 1 & 0 & -1 \\ -\frac{M}{2M^*} & 1 & -\frac{M}{2M^*} \end{bmatrix} \begin{Bmatrix} F_1 \\ F_2 \\ F_3 \end{Bmatrix} = \begin{Bmatrix} F_1 + F_2 + F_3 \\ F_1 - F_3 \\ -\frac{M}{2M^*}(F_1 + F_3) + F_2 \end{Bmatrix}$$

Note that  $\{\eta\} = [\eta_1 \quad \eta_2 \quad \eta_3]^T$

$$\left\{ \begin{array}{l} (M + 2M^*) \ddot{\eta}_1 = F_1 + F_2 + F_3 \\ 2M^* \ddot{\eta}_2 + 2K\eta_2 = F_1 - F_3 \\ M(1 + \frac{M}{2M^*}) \ddot{\eta}_3 + K[\frac{M}{M^*}(2 + \frac{M}{2M^*}) + 2] \eta_3 = -\frac{M}{2M^*}(F_1 + F_3) + F_2 \end{array} \right.$$

WBN

3/16/88

GIX

3/21/88

Nonuniform Base Motion

The above equations describe the motion (linear) of the system.

See what happens for  $F_2 = 0$  and

$$F_1 = M^* \ddot{X}_1(t) \quad , \quad F_3 = M^* \ddot{X}_3(t)$$

$$\text{Also } M^* \gg M$$

$$\ddot{\eta}_2 + \omega_2^2 \eta_2 = \frac{1}{2} (\ddot{X}_1 - \ddot{X}_3) = N_2(t)$$

$$\ddot{\eta}_3 + \omega_3^2 \eta_3 = - \frac{\ddot{X}_1 + \ddot{X}_3}{2(1 + \frac{M}{2M^*})} = M'(\ddot{X}_1 + \ddot{X}_3)$$

$$\text{Note that } \{x\} = [\phi] \{\eta\}$$

$$\therefore x_1 = \eta_1 + \eta_2 - \frac{M}{2M^*} \eta_3$$

$$x_2 = \eta_1 + \eta_3$$

$$x_3 = \eta_1 - \eta_2 - \frac{M}{2M^*} \eta_3$$

Now, determine  $x_1(t)$  and  $x_3(t)$  as functions of  $x_1(t)$  and  $x_3(t)$ . In the generalized coordinate equation for  $\eta_1(t)$  the term  $(M + 2M^*)$  appears. Note that it can be very well approximated by  $2M^*$  --

$$M + 2M^* \cong 2M^*$$

Thus,

$$2M^* \ddot{\eta}_1 = F_1 + F_3 = M^* \ddot{x}_1 + M^* \ddot{x}_3$$

$$\therefore \ddot{\eta}_1 = \frac{1}{2} (\ddot{x}_1 + \ddot{x}_3)$$

From the generalized coordinate equation for  $\eta_2(t)$  the following is found:

$$\ddot{\eta}_2 = \frac{1}{2} (\ddot{x}_1 - \ddot{x}_3) - \left(\frac{K}{M^*}\right) \eta_2$$

Note that  $K$  is finite and that  $M^*$  is to be rather large ( $M^* \gg M$ ). Thus, for the purpose of this discussion take  $M^* \rightarrow \infty$ . Thus,

$$\ddot{\eta}_2 \cong \frac{1}{2}(\ddot{X}_1 - \ddot{X}_3)$$

The generalized coordinate equation for  $\eta_3(t)$  becomes

$$M \ddot{\eta}_3 + 2K \eta_3 = -\frac{M}{2}(\ddot{X}_1 + \ddot{X}_3)$$

Thus, it is seen that for finite  $\ddot{X}_1$  and  $\ddot{X}_3$ ,  $\eta_3(t)$  is finite. Thus,

$$\ddot{x}_1(t) \cong \ddot{\eta}_1(t) + \ddot{\eta}_2(t) \cong \ddot{X}_1$$

$$\ddot{x}_3(t) \cong \ddot{\eta}_1(t) - \ddot{\eta}_2(t) \cong \ddot{X}_3$$



The last thing to be looked at is  $x_2(t)$ .

As previously determined

$$x_2(t) = \eta_1(t) + \eta_3(t)$$

The two generalized coordinates involved in this computation correspond to the following modes:

Generalized  
Coordinate

Mode

$\eta_1(t)$

$\begin{Bmatrix} 1 \\ 1 \\ 1 \end{Bmatrix}$ , rigid body

$\eta_3(t)$

$\begin{Bmatrix} 0 \\ 1 \\ 0 \end{Bmatrix}$ , fixed-base

If only the third mode is included, the motion  $x_2(t)$  determined will be a fixed-base motion.

**ANCO**

APPENDIX E

DERIVATION DETAILS FOR A DAMAGE INDICATOR

This appendix contains the derivation of one of the general damage indicators and an example of a specific case of it.

## Scalar Damage Indicator

This material consists of the steps followed in arriving at the basic scalar function used to observe changes in the module transfer function matrix. Other related scalar functions are presented.

$$X(\omega) = H(\omega) L(\omega)$$

Where  $X(\omega)$  = system response vector

$H(\omega)$  = system transfer function matrix

$L(\omega)$  = system input "load" vector

$\omega$  = transform variable

Let  $H = H^0 + \Delta H$  where  $H^0$  corresponds to a previously defined damage state (i.e., undamaged), and  $\Delta H$  is the change in the transfer function.

$$X = (H^0 + \Delta H) L = H^0 L + \Delta H L$$

Define an arbitrary vector  $Q$ .

$$\begin{aligned} Q^T X &= Q^T (H^0 L + \Delta H L) \\ &= Q^T H^0 L + Q^T \Delta H L \end{aligned}$$

$$\frac{Q^T X}{Q^T X} = \frac{Q^T H^0 L + Q^T \Delta H L}{Q^T X} = 1$$

$$\frac{\Phi^T H^0 L}{\Phi^T X} + D = 1$$

$$D = 1 - \frac{\Phi^T H^0 L}{\Phi^T X}$$

where

$$D = \frac{\Phi^T \Delta H L}{\Phi^T X}$$

$D$  is the scalar damage indicator.

One possible choice for  $\Phi$  is  $X$ . Thus, for

$$\Phi \equiv X$$

$$D = 1 - \frac{X^T H^0 L}{X^T X}$$

Another possible choice for  $\Phi$  is  $H^0 L$ . Thus,

$$\text{for } \Phi \equiv H^0 L$$

MADE BY

WBW

DATE

3/16/88

CHECKED BY

GTY

DATE

3/21/88

JOB NUMBER

1311.05

PAGE

4

OF

4

DESCRIPTION

Damage Indicator

$$D = 1 - \frac{(H^0 L)^T H^0 L}{(H^0 L)^T X}$$

$$= 1 - \frac{L^T H^0 T H^0 L}{L^T H^0 T X}$$

**ANCO**

APPENDIX F

CASE STUDY USING TIME  
DOMAIN SYSTEM IDENTIFICATION



This appendix contains excerpts from a published paper by Dr. J.L. Beck. It provides some of the details of the theoretical aspects of his time domain system identification approach to obtaining module modal properties. It also provides a case study where his method was successfully used to obtain the desired modal properties.

This appendix also contains material on the lack of identifiability in determining a pseudostatic matrix for a general module of a system.

# SEISMIC RESPONSE EVALUATION OF MELOLAND ROAD OVERPASS USING 1979 IMPERIAL VALLEY EARTHQUAKE RECORDS

S. D. WERNER

*Wiss, Janney, Elstner Associates, Inc., 2200 Powell Street, Suite 925, Emeryville, California, U.S.A.*

AND

J. L. BECK AND M. B. LEVINE

*Earthquake Engineering Research Laboratory, California Institute of Technology, Pasadena, California, U.S.A.*

## SUMMARY

During the 1979 Imperial Valley earthquake, an array of 26 strong-motion accelerometers produced records for the Meloland Road Overpass, a two-span reinforced concrete bridge structure located only 0.5 km away from the causative fault for this earthquake event. This paper describes the application of a new system identification methodology to the array of strong-motion measurements, in order to assess seismic response characteristics of this bridge. Results of this application show that (1) linear models provide an excellent fit to the measured motions of the bridge, despite the fact that it was subjected to very strong shaking; (2) the transverse response of the structure is controlled by its abutment motions, with no significant dynamic amplification in the deck; and (3) the vertical response of the bridge deck at the midlength of its spans is dominated by a single vertical translational mode whereas, above the central pier, the deck's vertical response is most affected by the vertical motions of the pier base and by torsion of the deck. Also, systematic estimates of modal damping ratios and qualitative assessments of states of stress developed in the bridge during the earthquake are provided.

## 1. INTRODUCTION

### 1.1. General background

Bridges are important elements of lifeline systems, providing for the transportation of people and materials across man-made and natural obstacles. It is important that bridges maintain this function following a major earthquake so that they do not impede either disaster relief or the long-term economic recovery of the affected area. The ability of bridges to withstand strong earthquakes is therefore a topic of considerable concern both to engineers and to public officials.

Past earthquakes have often caused extensive damage to bridges, resulting in significant economic loss, inconvenience and hardship to the surrounding communities.<sup>1-7</sup> Because of this, seismic design and retrofitting provisions for bridges in the United States have been substantially upgraded in recent years, particularly since the 1971 San Fernando earthquake.<sup>8-12</sup> In addition, there has been significant activity among earthquake engineers directed toward gaining further insight into the behaviour of bridges during earthquakes. These activities have entailed qualitative observations and interpretations of the behaviour of bridges during past earthquakes,<sup>13-15</sup> analytical research programmes that have investigated how the seismic response of bridges is influenced by non-linear response phenomena, travelling wave effects, skewness, soil/structure interaction, etc.,<sup>16-19</sup> and experimental research involving dynamic testing of bridge components,<sup>20-22</sup> shake table tests of bridge models,<sup>23</sup> ambient vibration measurements of actual bridge structures,<sup>24,25</sup> and full-scale forced vibration tests of bridges.<sup>26,27</sup>

In addition to the above research activities, it is clear that strong-motion measurements of actual bridge response, when obtained from a well-planned array of instruments and evaluated using established system

identification techniques, can also provide important quantitative information concerning the seismic response of bridges. However, to date, only five bridges in the United States (all in California) have been instrumented to record earthquake motions according to established guidelines and procedures.<sup>28-30</sup> Of these five bridges, three have yielded significant earthquake response data, but only two of these bridges have been studied using system identification techniques.<sup>28,31</sup> As shown in this paper, such data can indeed provide valuable insight into the seismic behaviour of bridges.

### 1.2. Bridge description and study overview

In October 1979, the Imperial Valley earthquake (magnitude 6.4) occurred along the Imperial fault, with rupture initiating just south of the United States-Mexico border and propagating in a north-westerly direction along the fault [Figure. 1(c)]. Significant shaking was produced throughout southeastern California and northcentral Mexico and numerous strong-motion records were obtained, particularly in the near field.<sup>32-34</sup>

Among the accelerograms obtained during this earthquake were those measured at the Meloland Road Overpass (MRO), a reinforced concrete bridge structure located east of El Centro, California. The MRO is comprised of two 104-ft spans with box girder construction, monolithic abutments and a single-column central pier [Figures 1(a) and 1(b)]. Because of its close proximity to the Imperial Fault [Figure. 1(c)], the MRO had previously been instrumented with an array of 26 strong-motion accelerometers along its deck, at its abutments and embankments, at the base of its central pier, and at a nearby free-field location (Figure. 2). All of these instruments were triggered during the Imperial Valley earthquake, providing the most extensive array of strong-motion measurements yet obtained for bridges in the United States. It is noted that the MRO was virtually undamaged by the earthquake,<sup>15,35</sup> despite the intense shaking to which it was subjected (0.51 *g* peak transverse acceleration measured on its deck).

This paper describes results of a study that evaluated this important array of data in order to obtain insights regarding the behaviour of bridges when subjected to strong seismic excitation. The study consisted of three main parts that entailed (1) a reprocessing of the original strong-motion data in order to circumvent certain recorder-induced distortions of the records; (2) development of a new system identification methodology suitable for evaluation of this extended array of bridge response data; and (3) application of the methodology to the reprocessed data in order to evaluate the seismic response characteristics of the MRO.<sup>31</sup>

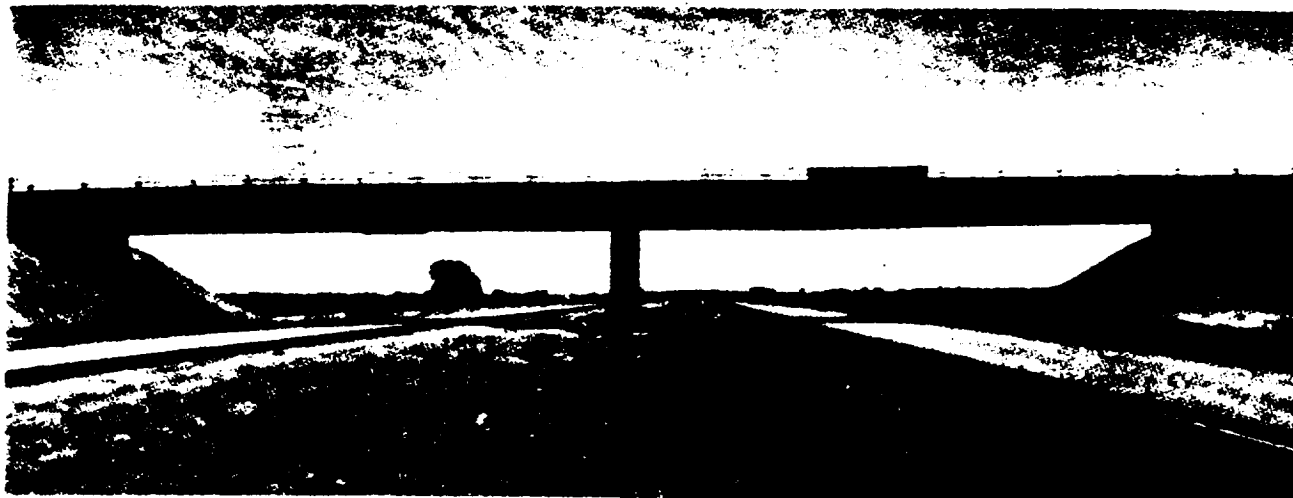
## 2. STRONG-MOTION DATA REPROCESSING

### 2.1. Instrumentation

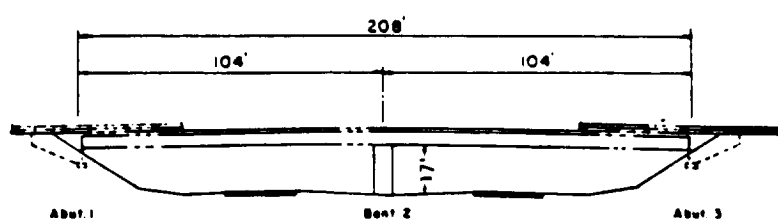
The MRO was instrumented in November 1978, about 11 months prior to the Imperial Valley earthquake. This instrumentation (Figure. 2) consists of two 13-channel remote-accelerometer central-recording systems. It comprises FBA-1 (single-axis) and FBA-3 (triaxial) force-balance accelerometer packages, two 13-channel central recording units interconnected for common timing and a triggering system. The recorders and trigger are located at the ground level next to the base of the central pier. The FBA accelerometers have a natural frequency of about 50 Hz and are designed to measure accelerations up to 1 *g* over a nominal frequency range of 0 to 50 Hz.<sup>35</sup> The bridge instrumentation system is maintained by the California Division of Mines and Geology, Office of Strong Motion Studies.

The MRO during the Imperial Valley earthquake are shown in Figure 3. The 13-channel accelerometer systems operated during the earthquake, in order for Channels 1-to-13, which led to data loss. The motions from the two recorders was reprocessing to correct for these

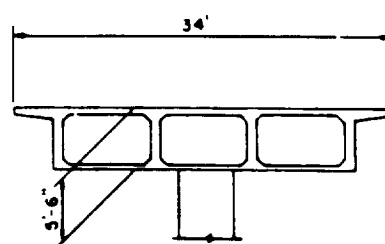
ORIGINAL PAGE IS  
OF POOR QUALITY



(a) View looking east

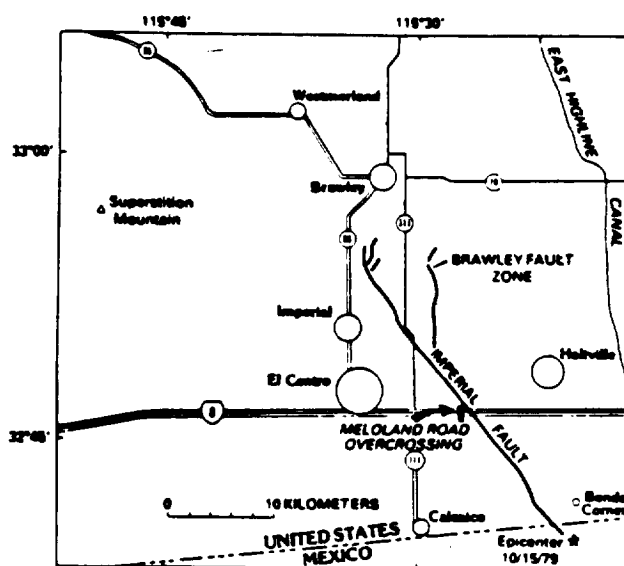


ELEVATION



TYPICAL SECTION

(b) Bridge dimensions



(c) Proximity to Imperial Fault

Figure 1. Bridge configuration and location

ORIGINAL PAGE IS  
OF POOR QUALITY

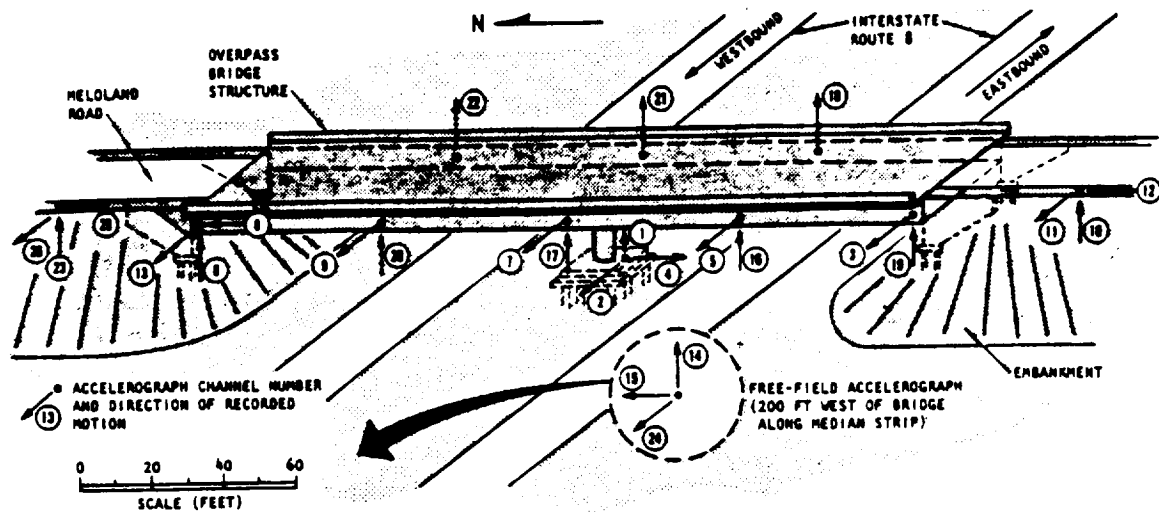


Figure 2. Meloland Road Overpass strong motion instruments

original film traces were reprocessed at the facilities of the University of Southern California. This reprocessing incorporated (1) new digitization techniques and software that were specially developed to correct the acceleration and time coordinates of the distorted traces; and (2) standard corrections for instrument frequency response and baseline adjustment.<sup>31</sup> The end result of this process was a set of uniformly processed time-history records, together with Fourier and response spectra from each of the 26 channels of data obtained at the MRO (e.g. Figure 4).

The recorder non-synchronization problem was identified by computing the cross correlation between several pairs of MRO acceleration records. The records that comprised each pair were typically each from a different recorder, and were measured at locations whose motions should be well correlated except for recorder-induced non-synchronization effects. Results of this assessment showed that the motion from the Channel 1-to-13 recorder consistently led the motions from the Channel 14-to-26 recorder by about 60 msec. This was corrected by an appropriate time shifting of the motions from Channels 1 to 13.

### 3. MODAL IDENTIFICATION METHODOLOGY

#### 3.1. Theoretical basis

To evaluate the array of records measured at the MRO, a new modal identification methodology was developed. This methodology, named MODE-ID, is applicable to an elastic system with an arbitrary configuration, with classical normal modes, and with motion measurements from any number of input and system response degrees of freedom. It is also assumed that the system is initially at an at-rest position.

The MODE-ID methodology considers a system whose equations of motion are

$$[M] \{\ddot{Y}\} + [C] \{\dot{Y}\} + [K] \{Y\} = -[C_{sf}] \{\dot{Z}\} - [K_{sf}] \{Z\} \quad (1)$$

where

- $[M], [C], [K]$  = mass, damping and stiffness matrices of the system
- $\{Y\}$  = vector of motions at  $N$  system degrees of freedom
- $\{Z\}$  = vector of input (support or 'foundation') motions at  $NS$  degrees of freedom
- $[C_{sf}], [K_{sf}]$  = damping and stiffness matrices that couple the system and 'foundation' response.

Following procedures described by Clough and Penzien,<sup>36</sup> the acceleration of the system is expressed as

$$\{\ddot{Y}\} = \{\ddot{S}\} + \{\ddot{X}\} \quad (2)$$

where  $\{\ddot{S}\}$  and  $\{\ddot{X}\}$  are the pseudostatic and dynamic components of acceleration respectively. In this, the pseudostatic component represents the 'static' contributions of the individual support motions to the system response (neglecting inertial and damping effects), and can be visualized as a time-dependent 'reference' position of the structure whose deformed shape at each instant of time is dependent on the instantaneous position of the structure's supports. This pseudostatic response is expressed as

$$\{\ddot{S}\} = [\ddot{R}] \{\ddot{Z}\} \quad (3)$$

where  $[\ddot{R}]$  is the pseudostatic matrix, given as

$$[\ddot{R}] = -[K]^{-1} [K_{sf}] \quad (4)$$

The dynamic component shown in equation (2) represents the contributions of the system's fixed-base modal vibrations about its pseudostatic reference position. The equations of motion for the dynamic response component are obtained by substituting equations (2) to (4) into equation (1) and neglecting the contributions of damping to the effective earthquake forces.<sup>36</sup> These equations take the form

$$[M] \{\ddot{X}\} + [C] \{\dot{X}\} + [K] \{X\} = -[M] [\ddot{R}] \{\ddot{Z}\} \quad (5)$$

In order to get a realistic spatially discrete model for the bridge of the form described in equations (1) to (5), the total number,  $N$ , of structural degrees of freedom would normally be chosen to be much greater than the number,  $NR$ , of structural degrees of freedom at which the response is actually measured. As a consequence, it is not possible to determine uniquely the elements of the stiffness and damping matrices from the measured seismic excitation and response, even if the mass matrix is assumed known.<sup>37</sup> Instead, an identifiable model in which the parameters are uniquely specified by knowing the excitation and response may be derived by assuming classical modes of vibration, as presented in the following discussion.

Let  $s_i$  and  $x_{ir}$ ,  $i = 1, 2, \dots, NR$ , denote the pseudostatic and dynamic components of the response at the  $NR$  degrees of freedom at which the system response is measured. The pseudostatic components  $s_i$  can be obtained from equation (3) using an  $NR \times NS$  submatrix  $[R]$  of the full  $N \times NS$  pseudostatic matrix  $[\ddot{R}]$ . Also, the dynamic components  $x_{ir}$  can be expressed as the superposition of the contributions of  $NM$  modes of vibration of the system which are significantly excited by the earthquake ( $NM \ll N$ ). This is expressed mathematically as

$$x_{ir}(t) = \sum_{r=1}^{NM} x_{ir}(t) \quad (6)$$

where  $x_{ir}$  is the  $r$ th mode response of the system at its  $i$ th degree of freedom. From a modal decomposition of equation (5) that incorporates orthogonality of the mode shapes, it can be shown that the modal contributions  $x_{ir}$ ,  $i = 1, 2, \dots, NR$ , satisfy the equation:

$$\{\ddot{x}_{ir}\} + a_r \{\dot{x}_{ir}\} + b_r \{x_{ir}\} = -[P^{(r)}] \{\ddot{Z}\} \quad (7)$$

where

$$a_r = 2\zeta_r \omega_r$$

$$b_r = \omega_r^2$$

$\zeta_r, \omega_r$  = damping ratio and natural frequency respectively of the  $r$ th mode,

and  $[P^{(r)}]$ , the effective participation factor matrix for the  $r$ th mode, is expressed as

$$[P^{(r)}] = [p_{ij}^{(r)}] = \begin{bmatrix} \phi_{1r} \gamma_{r1} & \phi_{1r} \gamma_{r2} & \dots & \phi_{1r} \gamma_{r,NS} \\ \phi_{2r} \gamma_{r1} & \phi_{2r} \gamma_{r2} & \dots & \phi_{2r} \gamma_{r,NS} \\ \vdots & \vdots & \ddots & \vdots \\ \phi_{NR,r} \gamma_{r1} & \phi_{NR,r} \gamma_{r2} & \dots & \phi_{NR,r} \gamma_{r,NS} \end{bmatrix} \quad (8)$$

In this,  $\phi_{ir}$  is the mode shape amplitude of the  $r$ th mode at the  $i$ th degree of freedom ( $i = 1, 2, \dots, NR$ ), and  $\gamma_{rj}$  is the conventional participation factor of the  $r$ th mode for the  $j$ th support degree of freedom ( $j = 1, 2, \dots, NS$ ).

The  $\gamma_{rj}$  are elements of the matrix.

$$[\Gamma] = [\gamma_{rj}] = [\phi]^T [M] [\tilde{R}] \quad (9)$$

where  $[\phi] = [\phi_{ir}]$  is the mode shape matrix. It is seen from equation (8) that the  $j$ th column of  $[P^{(r)}]$  contains the common factor  $\gamma_{rj}$ . Therefore, once  $[P^{(r)}]$  is obtained, the mode shape for the  $r$ th mode can in theory be readily calculated as the ratio of the elements in each row of any of the columns of  $[P^{(r)}]$ . However, these calculations are ill-conditioned when the various support motions are nearly identical, which is the case for the MRO.<sup>31</sup> Therefore, for such conditions, it is more desirable to obtain the mode shape from the ratios of sums of the rows of  $[P^{(r)}]$ . This ill-conditioning is discussed further in Section 3.3.

### 3.2. Identification procedure

The above discussion shows that the pseudostatic matrix  $[R]$ , and the normal mode parameters  $a_r$ ,  $b_r$ , and  $[P^{(r)}]$ , ( $r = 1, 2, \dots, NM$ ) represent the complete set of parameters needed to fully characterize the system's response as its measured degrees of freedom when it is subjected to the measured input motions. In MODE-ID, an optimization procedure is applied to estimate these parameters, in which the following error function is

minimized:

$$J(\theta) = \frac{1}{V} \sum_{i=1}^{NR} \sum_{n=0}^{NT} [\ddot{w}_i(n\Delta t) - \ddot{y}_i(n\Delta t; \theta)]^2 \quad (10)$$

where

- $\ddot{w}_i, \ddot{y}_i$  = measured acceleration and model acceleration at the  $i$ th measured response degree of freedom
- $\Delta t$  = sample interval of the digitized accelerograms
- $NT$  = total number of time samples (at interval  $\Delta t$ )
- $\theta$  = modal parameters to be estimated
- =  $\{[R]; a_r, b_r, [P^{(r)}]; r = 1, 2, \dots, NM\}$

and  $V$  is a normalizing factor given by

$$V = \sum_{i=1}^{NR} \sum_{n=0}^{NT} \ddot{w}_i^2(n\Delta t) \quad (11)$$

Therefore,  $J$  may be interpreted as the ratio of the mean-square error in the model acceleration to the mean-square of the measured acceleration.

The minimization of  $J$  with respect to the model parameters is implemented in MODE-ID using an iterative algorithm that is an adaptation of the modal-minimization method developed by Beck.<sup>37</sup> This algorithm consists of a series of modal sweeps in which, during each sweep, the estimates of the elements of the pseudostatic matrix  $[R]$  are first updated by minimizing  $J$  with respect to these elements only. Then, the estimates of the parameters of each mode ( $a_r, b_r, [P^{(r)}]$ ) are successively updated by a series of single-mode minimizations of  $J$ . This minimization for each mode actually corresponds to least-squares matching of a modified measured response in which the contributions of the pseudostatic response and the other modes are subtracted out; these contributions are computed from the new parameter estimates for those modes already treated in the sweep, and from the prior parameter estimates for those modes not yet treated. A single sweep is completed when the pseudostatic response and all significant modes have been treated in this manner. Successive modal sweeps are performed until the fractional decrease in  $J$  is less than a prescribed value, or until a prescribed maximum number of modal sweeps has been completed.

Usually only the first one or two of the strongest excited modes selected from the Fourier amplitude spectra of the records are initially included in the optimization process. Additional modes are then added, one at a time, by choosing appropriate initial estimates for the natural frequency and the damping ratio. Successive optimizations are performed until it is judged that all modes that significantly affect the response have been included. The modes are added successively in this manner so that it is easier to observe whether or not a mode has a significant effect on the match of the measured response.

In performing the minimization of  $J$  for each mode, the effective participation factors  $p_{ij}^{(r)}$  ( $i = 1, 2, \dots, NR$ ;  $j = 1, 2, \dots, NS$ ) are treated as being independent. This is not strictly correct since certain auxiliary conditions must be satisfied.<sup>31</sup> For example, the mode shapes derived from the effective participation factor matrices should satisfy the orthogonality conditions. These auxiliary conditions on the  $p_{ij}^{(r)}$  are not enforced since they involve the complete mode shape and pseudostatic matrices, whereas only those submatrices corresponding to the measured response degrees of freedom are actually estimated from the data. Therefore, the model used in the identification process may be viewed as being more general than the classical normal mode model described above. However, if the assumptions inherent in a classical normal mode model are sufficiently accurate, then the auxiliary conditions should be satisfied automatically by the estimated  $p_{ij}^{(r)}$ .

### 3.3. Effects of nearly identical support motions

The development provided in Sections 3.1 and 3.2 applies to the general case of any arbitrary input motions measured at each of the  $NS$  support degrees of freedom of the system. However, inspection of Figure 3 shows that the recorded 'support' motions of the MRO at the abutments, embankments and pier base in a given direction are nearly the same. Therefore, it is appropriate to consider the equations of motion for the limiting case where the support motions in a given direction are identical.

The vector of support accelerations may be expressed in this 'rigid-base' case as

$$\{\ddot{Z}(t)\} = \ddot{z}_T(t) \{I_T\} + \ddot{z}_V(t) \{I_V\} \quad (12)$$

where  $\ddot{z}_T$  and  $\ddot{z}_V$  are the common accelerations of the transverse and vertical support degrees of freedom respectively;  $\{I_T\}$  is an  $NS \times 1$  vector whose elements are unity and zero corresponding respectively to transverse and vertical support degrees of freedom; and  $\{I_V\}$  is an  $NS \times 1$  vector whose elements are unity and zero corresponding respectively to vertical and transverse support degrees of freedom.

Using equation (12), equation (3) becomes

$$\{\ddot{S}(t)\} = [\tilde{R}] \{I_T\} \ddot{z}_T(t) + [\tilde{R}] \{I_V\} \ddot{z}_V(t) \quad (13)$$

showing that the pseudostatic response is controlled by the two  $N \times 1$  vectors

$$\{s_T\} = [\tilde{R}] \{I_T\} \quad (14)$$

and

$$\{s_V\} = [\tilde{R}] \{I_V\}$$

and not by the values of the individual elements of the pseudostatic matrix  $[\tilde{R}]$ . From equation (14), each element of the vectors  $\{s_T\}$  and  $\{s_V\}$  is equal to the sum of the elements in the corresponding row of  $[\tilde{R}]$ , summed over the transverse and vertical support degrees of freedom respectively. Furthermore, because  $\{s_T\}$  represents the system's static response to unit rigid-body translation in the transverse direction, its elements are unity and zero, corresponding respectively to transverse and vertical response degrees of freedom. Similarly, since  $\{s_V\}$  represents the system's static response to unit vertical rigid-body translation, its elements are unity and zero, corresponding respectively to vertical and transverse response degrees of freedom.

In a similar manner, substituting equation (12) into the right-hand side of equation (7) leads to

$$- [P^{(r)}] \{\ddot{Z}\} = - [P^{(r)}] \{I_T\} \ddot{z}_T - [P^{(r)}] \{I_V\} \ddot{z}_V \quad (15)$$

showing that the excitation of the  $r$ th mode contribution to the system's dynamic response is controlled by the two  $NR \times 1$  vectors

$$\{p_T^{(r)}\} = [P^{(r)}] \{I_T\} \quad (16)$$

and

$$\{p_V^{(r)}\} = [P^{(r)}] \{I_V\}$$



and not by the values of the individual elements of the effective participation factor matrix  $[P^{(r)}]$ . From equation (16), each element of the vectors  $\{p_T^{(r)}\}$  and  $\{p_V^{(r)}\}$  is equal to the sum of the elements in the corresponding row of  $[P^{(r)}]$ , summed over the transverse and vertical support degrees of freedom respectively. From this, it can be shown that

$$\begin{aligned}\{p_T^{(r)}\} &= \gamma_T^{(r)} \{\phi^{(r)}\} \\ \text{and} \quad \{p_V^{(r)}\} &= \gamma_V^{(r)} \{\phi^{(r)}\}\end{aligned}\tag{17}$$

where  $\{\phi^{(r)}\}$  is the  $NR \times 1$  mode shape vector of the  $r$ th mode for the measured response degrees of freedom, and the scalars  $\gamma_T^{(r)}$  and  $\gamma_V^{(r)}$  are the conventional rigid-base participation factor for the  $r$ th mode in the transverse and vertical directions respectively.

The above discussion shows that the parameters controlling the response of the model when the support motions in a given direction are identical are  $\{s_T\}$ ,  $\{s_V\}$  and the parameters  $\{p_T^{(r)}\}$ ,  $\{p_V^{(r)}\}$ ,  $\omega_r$  and  $\zeta_r$  for each mode. It follows that it is only these parameters which can be determined uniquely during the application of system identification, using the measured common support motions  $\ddot{z}_T$  and  $\ddot{z}_V$  together with the measured response. The individual elements of the matrices  $[R]$  and  $[P^{(r)}]$  are not identifiable. If the support motions in each direction are nearly identical, as in the MRO, then the elements of these matrices might be identifiable in theory, but in practice the estimation process is ill-conditioned because of the presence of measurement noise and model error. The aforementioned parameters controlling the model response should, however, still be reliably estimated.

In view of this ill-conditioning, the mode shapes for MRO were evaluated using equations (16) and (17), that is, the elements in each row of the identified effective participation factor matrix were summed over the transverse and vertical support degrees of freedom separately. This gave the transverse and vertical components respectively of the scaled mode shape vector. Also, the elements in each row of the identified pseudostatic matrix were summed over the transverse and vertical support degrees of freedom separately to compute the vectors  $\{s_T\}$  and  $\{s_V\}$  in equations (14). These vectors were then checked to assure that their elements were close to the theoretical values of zero or unity.

As a final remark, if MODE-ID were applied to a long bridge with markedly different support motions because of travelling wave effects, then the above ill-conditioning would not occur. In this case, the individual elements of  $[R]$  and  $[P^{(r)}]$  should be estimated reliably by MODE-ID.

#### 4. OVERVIEW OF SEISMIC EVALUATION PROCESS

The evaluation of the MRO's seismic response was comprised of two main steps which involved (1) assessment of the MRO's modal and seismic response characteristics; and (2) application of the MRO's measured strong-motion records. In performing these steps, the essential element in the proper application of the system identification technique was more fully by Werner *et al.*<sup>31</sup>.

##### 4.1. Initial assessment process

An initial assessment of the MRO's seismic response characteristics was performed before the system identification process was applied.

## 5. BRIDGE RESPONSE CHARACTERISTICS

The above seismic evaluation process was applied to two subsets of the MRO's vertical and transverse strong-motion records, in order to assess dynamic response characteristics of two alternative subsystems of the bridge. Results of the MODE-ID application to these two subsets, denoted as Case 1 and Case 2, are summarized in the paragraphs that follow.

### 5.1. Case 1 results

The Case 1 subset of MRO records consists of input records which are the transverse and vertical motion measurements at the two abutments and the central-pier base, and response measurements which are the transverse and vertical motion measurements along the road deck (Figure 5). Therefore, this subset emphasizes the dynamic characteristics of a subsystem consisting of the road deck and central pier, whose contributions to the total bridge response are represented through the fixed-base normal modes that are identified. The pseudostatic matrix identified in the Case 1 application represents the additional 'quasi-static' contributions of the abutments, embankments, central-pier foundation, and underlying soil medium to the overall bridge response.

This Case 1 application resulted in the identification of a pseudostatic matrix  $[R]$ , and two normal modes. The identified matrix  $[R]$  is not reported here because of the ill-conditioning that arises from the near

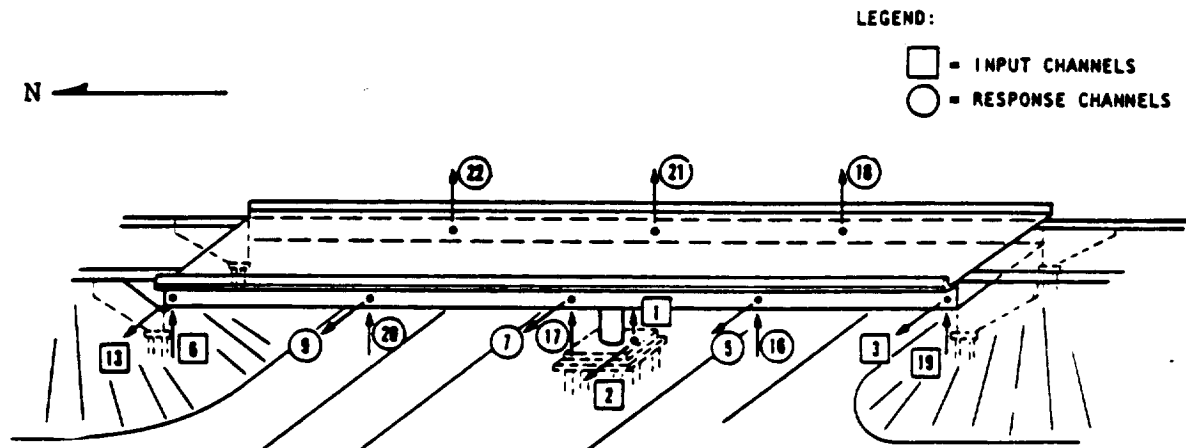


Figure 5. Case 1: input and response channels

coincidence of the MRO's support motions in a given direction (see Section 3.3). However, the sums of the elements in each row of  $[R]$  were close to their theoretical values of zero or unity.<sup>31</sup> It is these sums which control the pseudostatic response of the bridge because of the nearly identical support motions.

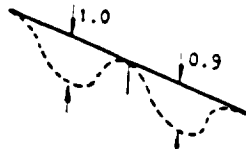

The two normal modes that were identified have the characteristics shown in Table I. The first of these modes, termed the deck vertical mode, has a natural frequency of 4.7 Hz, a damping ratio of 6½ per cent, and a mode shape consisting of vertical translations of the two deck spans that are nearly symmetric about the central pier. The other identified mode, termed the deck transverse mode, has a natural frequency of 3.7 Hz, a damping ratio of 6½ per cent that by coincidence is virtually the same as that of the deck vertical mode, and a mode shape consisting of transverse horizontal translations and torsional rotations of the bridge deck.

The degree to which the resulting bridge model, comprised of the above two modes and the pseudostatic matrix, represents the seismic response characteristics of the bridge is demonstrated by (1) the very low value of the measure-of-fit parameter ( $J = 0.056$ ) that was obtained; and (2) the very close comparisons that resulted between measured motion time histories at various channel locations and the time histories computed at these locations using the identified model (Figure 6). These show that the linear model that was identified has produced an excellent representation of the seismic response of the MRO, despite the fact that the MRO was subjected to very strong shaking.

Further insight into the nature of the MRO response is provided through a series of comparisons of measured and model motions at selected channels, as the contributions of each element of the model (i.e. the pseudostatic matrix and each normal mode) are successively incorporated into the computation of the model motions. Such comparisons are provided in Figure 7 for the transverse response at the midlength of the bridge (Channel 7), the vertical response at the midlength of one of the deck spans (Channel 16) and the vertical response of the deck face above the central pier (Channel 21). These comparisons show that each element of the MRO has affected its seismic response in a different way, as summarized below.

- (a) The pseudostatic response, by itself, provides an excellent fit with the measured transverse motions of the bridge; the additional contributions of the deck vertical mode and transverse mode to this fit are small [Figure 7(a)]. This shows that the transverse response of the MRO is controlled by the motions of the abutment and foundation supports. The structure provides only slight dynamic amplification of these transverse support motions.
- (b) For the vertical motions at the midlength of the deck spans, the principal contributor to the fit between measured and model motions is the deck vertical mode [Figure 7(b)]. This single mode dominates the bridge's vertical response at these span midlength locations, and the additional contributions to this response of the support motions (included through the pseudostatic matrix) and the torsional motions of the bridge deck (incorporated through the deck transverse mode) are small.

Table I. Case 1: significant modes of vibration

Mode	Frequency* (Hz)	Damping ratio	Mode shape
Deck vertical	4.74 (5.12)	0.066	
Deck transverse	3.72 (3.34)	0.066	

\* The values in parentheses are those obtained from a simple finite element model of MRO using equivalent rotational spring stiffnesses obtained from a simple bridge-foundation interaction model.<sup>38</sup>

- (c) For the vertical motions at a face of the bridge deck above the central pier, the deck vertical mode has a node. Therefore, as shown in Figure 7(c), the primary contributors to the deck vertical response at this central pier location are the vertical support motions at the central pier base (represented through the pseudostatic matrix) and the deck torsional motions (incorporated through the deck transverse mode).

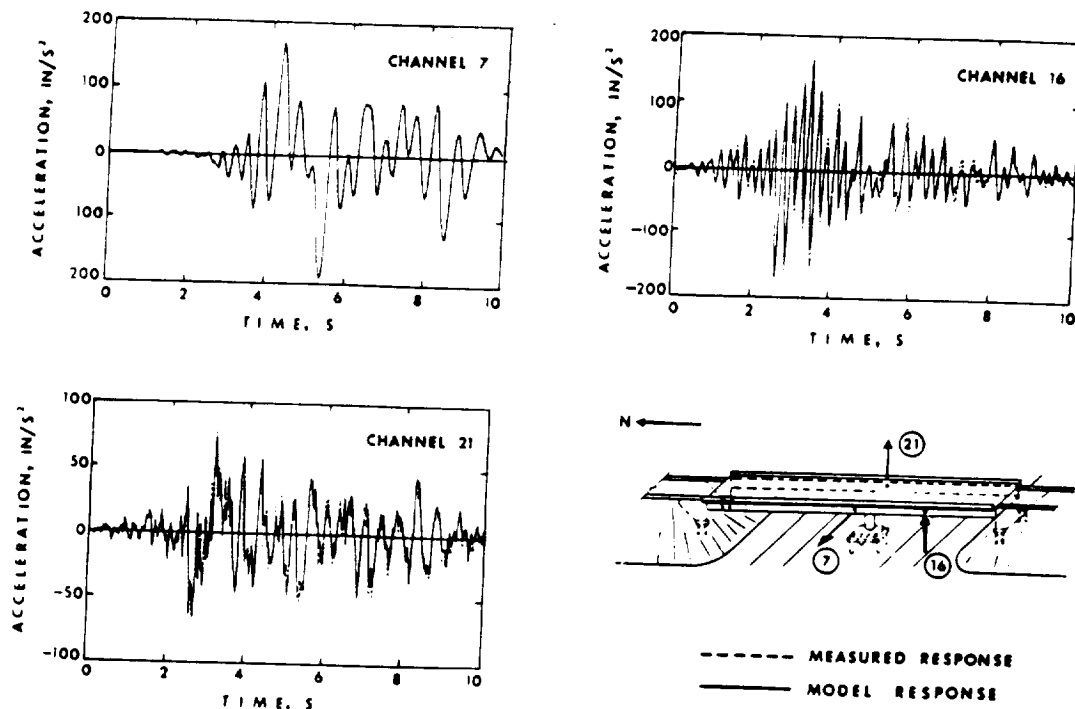


Figure 6. Case 1: fit of computed model response to measured response

It is also of interest to determine the state of bending stress developed within the MRO by the seismic excitations. However, these stresses cannot be estimated directly since it turns out that this requires the measurement of both the translational and rotational motions at each bridge support location, and the single accelerometer at each of the two abutments and at the central pier base is insufficient for this purpose. It is clear that the dynamic stresses developed in the MRO will be strongly dependent on the degree of restraint developed at the bridge supports. For example, the stresses developed at the base of the central pier will be strongly influenced by the degree of rotational restraint of the pier's footing/pile foundation; i.e. if the foundation is fixed against rotations the bending stresses at the base of the pier could be high whereas, if the foundation's rotational restraint is low (approaching a pinned condition), these bending stresses will be small. At the top of the central pier, it is anticipated that the bending stresses will be strongly dependent on how the abutments restrain the ends of the deck against torsional rotations. If this degree of torsional restraint by the abutments is low, the top of the pier will not be so restrained by the deck as the pier bends during transverse horizontal vibration of the bridge, and the bending stresses developed at the top of the central pier should be low. However, if the abutments restrain the torsional rotations at the ends of the deck, the bending rotations at the top of the central pier will be restrained by the deck during transverse horizontal vibration, and much higher bending stresses could result near the top of the central pier.

The above plausible trends were supported by dynamic analyses based on a simple finite element model of the MRO which showed that (1) the peak stresses developed within the deck were low and well within allowable values; and (2) the peak stresses developed within the central pier could have exceeded allowable values, depending on the degree of rotational constraint developed at the abutments and central pier foundation, as discussed above. This demonstrates the important effects that the abutments and central pier foundation could have on the MRO's seismic response above and beyond that indicated by the Case 1 assessments involving motions only. However, the stress calculations were not definitive because only nominal bounding values of the equivalent rotational spring stiffnesses at the supports were used. The stiffnesses could not be estimated uniquely from the current array of measured support motions which, as noted above, are insufficient to obtain the rotational components of foundation motion required for this purpose. This lack of uniqueness underscores the desirability of extending the existing array of accelerometers at the MRO, so that translations and rotations of the abutments and central pier foundation can be directly measured when future earthquakes occur.

## 6. CONCLUDING REMARKS

The results presented in this paper show that when seismic response measurements are obtained from a well-planned array of strong-motion instruments and are evaluated using proven system identification methods, significant insight into the behaviour of bridges during earthquakes can be obtained. The results also show that, despite the intense levels of shaking that were involved, the classical mode models identified from the MRO's strong-motion measurements have provided a good representation of its seismic response characteristics. Other important practical results that should be useful in enhancing the future seismic design of bridges include the following:

- (a) *Damping ratios.* The results presented herein represent one of the first times that modal damping levels attained in bridges during strong seismic excitation have been systematically estimated. Such damping ratios range from about 0.06 to about 0.08 for the various modes of vibration that were identified.
- (b) *Effects of bridge elements on seismic response.* The relative contributions of each of the various elements of the MRO (i.e. its abutments, deck, central pier, etc.) to its seismic response have been systematically isolated and evaluated. The abutments and embankments were seen to be the major contributors to the transverse response characteristics of the bridge, whereas the deck structure dominated the MRO's vertical response characteristics. The torsional response characteristics of the deck/abutment system and the bending response characteristics of the central pier also affected the transverse motions of the MRO.
- (c) *Dynamic stress levels.* Qualitative evaluations and dynamic analyses using simplified models were used to provide insights into the nature of the dynamic stresses developed in the MRO during the earthquake. These evaluations indicated that the central pier may well have been quite highly stressed, whereas the deck probably was not. They also show that the state of stress developed in the central pier is strongly influenced by the degree of rotational restraint provided by the abutments and the central-pier foundation. Unfortunately, the bridge stresses could not be estimated in a definitive manner because the earthquake-induced translational and rotational motions of the abutments and the central pier base could not be uniquely determined from the single set of instruments deployed at these support locations.

The results presented in this paper suggest additional investigations to further enhance the information that can be obtained from motions measured by this array of bridge instruments during future earthquakes. First of all, it has been shown that the abutments and pier foundations had a major effect on the behaviour of the MRO during the Imperial Valley earthquake. Therefore, effort should be directed toward obtaining further insight into the behaviour of these foundation elements. Such efforts should include (1) extending the array of accelerometers at the abutments and pier foundation so that their translations and rotations about three axes can be determined; (2) dynamic testing of the MRO abutment and pier foundation elements in order to determine appropriate impedances; and (3) careful measurement of static and dynamic properties of the soils in the embankments and underlying geologic layers in order to support interpretation of future strong-motion measurements and dynamic test results.

In addition to the above efforts directed toward increasing our understanding of the behaviour of the MRO's abutments, pier foundations and surrounding soil media, future investigation of the overall seismic response of the MRO using identification of extended bridge models should also prove to be valuable. The future use of non-classical mode models and certain classes of non-linear models should further extend the basic insights provided by the classical mode models used herein.

## ACKNOWLEDGEMENTS

This paper was prepared under a research project carried out at Agbabian Associates (AA) when the first and third authors were members of the AA staff. The project was funded through a grant by the National Science Foundation (Grant No. CEE-8111964), whose financial support is gratefully acknowledged.

The authors also acknowledge the contributions to various phases of the research of the following individuals: M. D. Trifunac, V. W. Lee and S. F. Masri of the University of Southern California; J. T. Ragsdale and N. A. Kaliakin, formerly of the California Division of Mines and Geology; R. M. Coppolino of MacNeal-Schwendler; R. F. Scott of the California Institute of Technology; and J. H. Gates of the California Department of Transportation.

# Lack of Identifiability in Determining Pseudostatic Matrix for a Module of a System

Let the system have  $N$  dof (degree-of-freedom) with

$x_i(t)$  = displacement at  $i^{\text{th}}$  dof

Let  $K$  = set of system dof at time  $t$  defining boundary motions of module, and

$I$  = set of system dof defining monitored output of module.

For each  $i \in I$ , we can write:

$$x_i(t) = S_i(t) + r_i(t)$$

where  $S_i(t)$  = pseudostatic response

$$= \sum_{k \in K} p_{ik} x_k(t)$$

where  $p = [p_{ik}]$  is the pseudostatic matrix and where

$r_i(t)$  = dynamic response due to fixed-boundary modes of module.

For identification of  $P$ , we would like to estimate the  $p_{ik}$  by least-squares matching of the monitored accelerations  $\ddot{x}_i(t)$ ,  $\forall i \in I$ , by the model pseudostatic acceleration  $\sum_{k \in I} p_{ik} \ddot{x}_k(t)$ . (Actually, this step is part of an iterative process in which the objective is to determine  $P$  and the modal parameters for the module.)

We now show that for sufficiently many inputs, this procedure will not work, primarily because the module boundary motions are not independently produced (i.e., produced by an agency external to the system) but instead are related through the dynamics of the system.

Suppose that only the system modes  $r \in R$  contribute significantly to the system response, then to a good approximation

$$\ddot{x}_i(t) = \sum_{r \in R} \phi_i^{(r)} \ddot{\eta}_r(t) \quad , \quad \forall i = 1, 2, \dots, N$$

where  $\ddot{\eta}_r(t)$  is the modal acceleration, and

$$\begin{aligned} \sum_{k \in K} p_{ik} \ddot{x}_k(t) &= \sum_{k \in K} p_{ik} \left( \sum_{r \in R} \phi_k^{(r)} \ddot{\eta}_r(t) \right) \\ &= \sum_{r \in R} \left( \sum_{k \in K} p_{ik} \phi_k^{(r)} \right) \ddot{\eta}_r(t) \end{aligned}$$

Suppose we can choose the  $p_{ik}$ ,  $i \in I$  and  $k \in K$ , so that

$$\phi_i^{(r)} = \sum_{k \in K} p_{ik} \phi_k^{(r)} \quad , \quad \forall i \in I \text{ and } \forall r \in R \quad (F-1)$$

Then,

$$\ddot{x}_i(t) = \sum_{k \in K} p_{ik} \ddot{x}_k(t) \quad , \quad \forall i \in I.$$

That is, when attempting to identify the pseudostatic parameters, erroneous values will be obtained which make  $\sum_{k \in K} p_{ik} \ddot{x}_k$  equal to the total response rather than just the pseudostatic response. But does a solution of Equation F-1 exist for the  $p_{ik}$ ?

Equation F-1 is a linear system of equations for the  $p_{ik}$  involving  $|I||K|$  unknowns and  $|I||R|$  equations, where  $|A|$  denotes the number of elements in set A. Thus, a solution (not necessarily unique) exists for the  $p_{ik}$  if  $|I||K| \geq |I||R|$  i.e.  $|K| \geq |R|$ . Thus, a solution exists if the number of inputs is not less than the number of modes which control the system response.

An alternative way of looking at this problem is that with  $|K|$  inputs to the module, it is possible to match exactly up to  $|K|$  modes in  $\ddot{x}_i(t)$  with an expression of the form  $\sum_{k \in K} p_{ik} \ddot{x}_k(t)$ , but, of course, the resulting estimate of the  $p_{ik}$ 's will in general be quite different from the true pseudostatic parameters. Thus, for the COFSMAST module with 12 boundary motions as input it is possible to match the contributions of 12 system modes to the module outputs by a suitable choice of the  $p_{ik}$ . It can be seen that from Equation F-1, if the system is damaged outside the module, the system mode shapes will change and so these "false" pseudostatic module parameters will change in general.



**ANCO**

APPENDIX G

MODAL STRAIN ENERGY DISTRIBUTION  
METHOD SOFTWARE

This appendix contains a note about the Modal Strain Energy Distribution Method Computer Code and the corresponding source code listings.

# MEMO

TO: WILLIAM WALTON  
FM: BLAKE JOHNSON  
DT: 27 FEB 87  
RE: NASA DAMAGE SOFTWARE--MSED

This is a written summary of the programs I have generated to date that allow assessment of damage using the MSED. I have included source listings of all the programs and a 1.2 Mb floppy diskette containing the source programs and the executables.

MODSTRN - This program computes element modal strain energies for a simply-supported beam due to bending deformation only. The user must input the number of elements and modes to use. The output element modal strain energies are contained in the file "MS.DD". This file is a binary file.

DAMIO - This program allows the user to input damage parameters to be used in damage assessment. Damage parameters are input on a mode-by-mode basis. The user also specifies the output file containing the damage parameters. This output file is an ASCII file.

MODSUM - This program performs the damage assessment based on the modal strain energies and the damage parameters. The user must input the file name containing the modal strain energies and the damage parameters. The user also specifies the damage fraction (g) used in assessing damage. Alternately, the user can select the option of summarizing the element strain energies for a given mode. In either case, output data is contained in the file "MODSUM.DD".

```

$NOFLOATCALLS
C
C PROGRAM MODSTRN - COMPUTE MODAL STRAIN ENERGY MODE BY MODE
C
      IMPLICIT INTEGER*2 (I-N)
      DIMENSION XTRN(200),XAVG(200)
      CHARACTER*80 KEY
      CHARACTER*40 TITLE
      COMMON/XDAT/XTRN,XAVG
C
C CLEAR SCREEN,DISPLAY PROGRAM
C
      KEY = 'MODSTRN - PROGRAM TO COMPUTE MODAL STRAIN ENERGY #'
      CALL VCLEAR
      CALL VCURXY(0,0)
      CALL PRMPT(KEY,1.00)
      CALL GCURXY(IC,IR)
      IR = IR + 1
C
C GET USER INPUTS
C
      KEY = 'ENTER DESCRIPTION OF RUN : #'
      CALL KEYBD(KEY,R,I,TITLE,3,(40),0,IR)
      IR = IR + 1
      KEY = 'ENTER THE NUMBER OF ELEMENTS TO USE : #'
      CALL KEYBD(KEY,R,NELM,A,2,(2),0,IR)
      IR = IR + 1
      KEY = 'ENTER THE NUMBER OF MODES TO USE : #'
      CALL KEYBD(KEY,R,NMODES,A,2,(2),0,IR)
      IR = IR + 1
      CALL VCURXY(0,IR)
C
C OPEN UP BINARY FILE CONTAINING DATA
C
      OPEN(6,FILE='MS.DD',STATUS='NEW',
1  FORM='UNFORMATTED')
      WRITE(6) TITLE,NELM,NMODES
C
C COMPUTE STRAIN ENERGY FOR 100 PTS FROM 0 TO 1
C
      XLM = 1.0 / NELM
      NELMP1 = NELM + 1
      XPI = 4.0 * ATAN(1.0)
C
C LOOP OVER NUMBER OF MODES
C
      DO 100 IMODE=1,NMODES
        XMV = 0.0
        XCOFF = 1.0
        DO 10 I=1,NELMP1
          XL = FLOAT(I-1) * XLM
          XS = FLOAT(IMODE) * XPI
          XSN = SIN(2*XS*XL)
          XTRN(I) = XCOFF * (XL/2 - XSN/(4.0 * XS))
10      CONTINUE
C
C COMPUTE ELEMENT STRAIN ENERGY
C
      DO 15 I=1,NELM

```

```

      XAVG(I) = (XTRN(I+1) - XTRN(I)) / 0.1
      IF (ABS(XAVG(I)) .GT. XMX) XMX = XAVG(I)
15      CONTINUE
C
C SCALE TO UNITY
C
      DO 20 I=1,NELM
        XAVG(I) = XAVG(I) / XMX
20      CONTINUE
C
C NOW WRITE IT OUT
C
      WRITE(6) (XAVG(I), I=1,NELM)
100     CONTINUE
      STOP
      END

```

```

*NOFLOATCALLS
      IMPLICIT INTEGER*2 (I-N)
      DIMENSION DAM(20),DAMCRT(20)
      CHARACTER*80 KEY
      CHARACTER*60 DAMTTL
      CHARACTER*20 DAMFIL
      CHARACTER*1 IEDCR

C
C CLEAR SCREEN, ETC
C
      CALL VCLEAR
      CALL VCURXY(0,0)
      KEY = 'DAMID - PROGRAM TO CREATE/EDIT DAMAGE PARAMETERS*'
      CALL PRMPT(KEY,1.00)
      IR = 6
      IR = IR + 1
      KEY = 'DO YOU WANT TO (C)REATE OR (E)DIT A DAMAGE FILE? : $'
      CALL KEYBD(KEY,R,I,IEDCR,3,(1),0,IR)

C
C HERE FOR FILE CREATION
C
      CALL VCLEAR
      IR = 0
      CALL VCURXY(0,IR)
      KEY = 'DAMAGE TITLE : $'
      CALL KEYBD(KEY,R,I,DAMTTL,3,(60),0,IR)
      IR = IR + 1
      KEY = 'NUMBER OF MODES USED : $'
      CALL KEYBD(KEY,R,NMODES,A,2,(2),0,IR)
      IR = IR + 2
      CALL VCURXY(0,IR)
      WRITE(*,9010)
9010  FORMAT(1X,'MODE',5X,'D(W)',10X,'Dcrit(W)')
      IR = IR + 1
      CALL VCURXY(0,IR)
      WRITE(*,9002)
9002  FORMAT(' NO. ')
      IR = IR + 1

C
C NOW READ IN DATA
C
      IST = IR
      IEND = IR + 9
      DO 20 IM=1,NMODES
      CALL VCURXY(0,IR)
        IF(IR.EQ.IST) WRITE(*,9200) IM
        IF(IR.NE.IST) WRITE(*,9201) IM
        KEY = ' $'
        CALL KEYBD(KEY,DAM(IM),I,A,1,(10),9,IR)
        CALL KEYBD(KEY,DAMCRT(IM),I,A,1,(10),23,IR)
        IR = IR + 1
        IF(IR.LE.IEND) GO TO 20
      DO 15 IER=IST,IEND
        CALL VCURXY(0,IER)
        WRITE(*,9000)
15      CONTINUE
        IR = IST
20      CONTINUE
        IR = 20

```

```

C
C GET OUTPUT FILENAME AND WRITE IT OUT
C
      KEY = 'ENTER OUTPUT DAMAGE FILENAME : '
      CALL KEYBD(KEY,R,I,DAMFIL,Z,(20),0,IR)
      OPEN(5,FILE=DAMFIL,STATUS='NEW')
      WRITE(5,8000) DAMFIL,DAMTTL,NMODES
      WRITE(5,8010)
      DO 30 I=1,NMODES
        WRITE(5,8020) I,DAM(I),DAMCRT(I)
30      CONTINUE
9201  FORMAT(1X,1X,I3\ )
9200  FORMAT(1X,I3\ )
9000  FORMAT(40X\ )
8000  FORMAT('DAMAGE FILENAME : ',A20/A60/'NUMBER OF MODES : ',I2)
8010  FORMAT('MODE ',5X,'D(W) ',10X,'DCRIT(W) ')
8020  FORMAT(1X,I2,5X,F7.2,7X,F7.2)
      STOP
      END

```

```

*NOFLOATCALLS
      IMPLICIT INTEGER*2 (I-N)
      DIMENSION ES(100,20),DAM(20),DAMCRT(20)
      CHARACTER*80 KEY
      CHARACTER*60 DAMTTL
      CHARACTER*40 TITLE
      CHARACTER*20 FLNME,DAMFIL
      CHARACTER*3 PDAM(100),ISM
      CHARACTER*27 FMT
      CHARACTER*2 FM
      CHARACTER*1 AES(100,20),FF,FMTM(27),FMM(2)
      DIMENSION ESMX(20),LESMX(20)
      COMMON/DAT/ES,AES,ESMX,LESMX,DAM,DAMCRT,PDAM
      EQUIVALENCE (FMT,FMTM(1)),(FM,FMM(1))

C
C  DEFINE FORMFEED
C
      FF = CHAR(12)
      FMT = '(7X,I2,5X, 1(A1,3X),10X,A3)'
      FM = ' 1'

C
C  DEISPLAY PROGRAM TO USER
C
      CALL VCLEAR
      CALL VCURXY(0,0)
      KEY = 'MODSUM - PROGRAM TO SUMMARIZE STRAIN ENERGY DATA$'
      CALL PRMPT(KEY,1.00)
      CALL GCURXY(IC,IR)
      IR = IR + 1

C
C  GET FILENAME CONTAINING DATA
C
      KEY = 'ENTER FILENAME CONTAINING MODAL STRAIN ENERGIES : $'
      CALL KEYBD(KEY,R,I,FLNME,3,(20),0,IR)
      OPEN(5,FILE=FLNME,FORM='UNFORMATTED')
      IR = IR + 1

C
C  SEE IF USER WISHES TO SUMMARIZE MODAL STRIN ENERGIES
C  FOR ALL ELEMENTS
C
      KEY='DO YOU WANT TO SUMMARIZE STRAIN ENERGIES FOR A MODE? : $'
      CALL KEYBD(KEY,R,I,ISM,4,(3),0,IR)
      IR = IR + 1
      IF(I.EQ.1) CALL MODSSUM

C
C  GET FILENAME CONTAINING DAMAGE INFO
C
      KEY = 'ENTER FILENAME CONTAINING DAMAGE DATA : $'
      CALL KEYBD(KEY,R,I,DAMFIL,3,(20),0,IR)
      IR = IR + 1
      OPEN(7,FILE=DAMFIL)

C
C  GET DAMAGE FRACTION
C
      KEY = 'ENTER DAMAGE FRACTION ( <= 1 ) : $'
      CALL KEYBD(KEY,FR,I,A,1,(10),0,IR)

C
C  READ IN DATA
C

```



```

      READ(5) TITLE,NELM,NMODES
      WRITE(FM,9111) NMODES
      FMTM(11) = FMM(1)
      FMTM(12) = FMM(2)
9111  FORMAT(I2)
      READ(7,7010) DAMTTL
7010  FORMAT(/A60/1X/1X)
      DO 10 I=1,NMODES
        READ(5) (ES(J,I),J=1,NELM)
        READ(7,7020) DAM(I),DAMCRT(I)
10    CONTINUE
7020  FORMAT(8X,F7.3,7X,F7.3)
C
C NOW DETERMINE MAX STRAIN ENERGIES FOR EACH MODE
C
      DO 30 I=1,NMODES
        XMJ = 0.0
        DO 20 J=1,NELM
          IF(ES(J,I).LE.XMJ) GO TO 20
          XMJ = ES(J,I)
          LMJ = J
20    CONTINUE
        ESMX(I) = XMJ
        LESMX(I) = LMJ
30    CONTINUE
C
C INITIATE AES
C
      DO 35 I=1,NMODES
        DO 34 J=1,NELM
          AES(J,I) = ' '
34    CONTINUE
35    CONTINUE
C
C NOW SORT IT ALL OUT
C
C BEGIN BY FINDING ELEMENTS WITH LOW STRAIN ENERGIES
C
      DO 100 I=1,NMODES
        IF(DAM(I).GT.DAMCRT(I)) GO TO 50
        ESMXL = FR * ESMX(I)
        DO 40 J=1,NELM
          IF(ES(J,I).LE.ESMXL) AES(J,I) = 'x'
40    CONTINUE
        GO TO 100
C
C HERE FOR ELEMENTS WITH HIGH STRAIN ENERGIES
C
      DO 50 CONTINUE
        DO 60 J=1,NELM
          AES(J,I) = 'x'
60    CONTINUE
100   CONTINUE
C
C NOW DETERMINE IF ANY ONE ELEMENT MIGHT HAVE DAMAGE
C
      DO 110 IL=1,NELM
        PDAM(IL) = 'YES'
      DO 120 IM=1,NMODES
        IF(AES(IL,IM).EQ.' ') PDAM(IL) = 'NO'
120   CONTINUE
110   CONTINUE
C
C NOW SUMMARIZE DATA
C
      OPEN(6,FILE='MODSUM.DD',STATUS='NEW')

```

```

      NPG = (NELM + 39) / 40 + 1
      IPAGE = 1
      WRITE(6,9000) TITLE,IPAGE,NPG,DAMFIL,DAMTTL,NMODES,NELM,FR
9000  FORMAT(//4X,A40,16X,'Page ',I1,' of ',I1,
1     /4X,'DAMAGE FILE USED : ',A20
1     /4X,'DAMAGE TITLE : ',A60
1     /4X,'NUMBER OF MODES : ',I2,
2     /4X,'NUMBER OF ELEMENTS : ',I2,
3     /4X,'DAMAGE FRACTION : ',F6.4)
      WRITE(6,9010)
9010  FORMAT(//4X,'MODE ',3X,'MAXIMUM ELEMENT ',3X,'ELEMENT ',
1     /4X,' NO. ',3X,' STRAIN ENERGY ',3X,' NO. ',/)
      DO 200 I=1,NMODES
        WRITE(6,9020) I,ESMX(I),LESMX(I)
200    CONTINUE
9020  FORMAT(5X,I2,6X,1PE10.3,8X,I2)
      WRITE(6,9021) FF
9021  FORMAT(A1)
      IPAGE = 2
      WRITE(6,9000) TITLE,IPAGE,NPG,DAMFIL,DAMTTL,NMODES,NELM,FR
      WRITE(6,9035)
9035  FORMAT(//20X,'ELEMENT DAMAGE SUMMARY')
      WRITE(6,9040)
9040  FORMAT(//4X,'ELEMENT ',27X,'MODE ',27X,'POSSIBLE ',
1     /4X,' NO. ',27X,' NO. ',28X,'DAMAGE')
      WRITE(6,9050) (I,I=1,NMODES)
9050  FORMAT(13X,15(I2,2X))
      DO 70 J=1,NELM
        WRITE(6,FMT) J,(AES(J,I),I=1,NMODES),PDAM(J)
        IF(MOD(J,40).NE.0) GO TO 70
        WRITE(6,9060)
        IPAGE = IPAGE + 1
        WRITE(6,9021) FF
        WRITE(6,9000) TITLE,IPAGE,NPG,DAMFIL,DAMTTL,NMODES,NELM,FR
        WRITE(6,9035)
        WRITE(6,9040)
        WRITE(6,9050) (I,I=1,NMODES)
70    CONTINUE
        WRITE(6,9060)
9060  FORMAT(//15X,'x indicates possible modal element damage')
C
C ALL DONE
C
      STOP
      END

```

```

$NOFLOATCALLS
      SUBROUTINE MODSSUM
      IMPLICIT INTEGER*2 (I-N)
      DIMENSION ES(100,20)
      CHARACTER*80 KEY
      CHARACTER*40 TITLE
C
C GET CURSOR
C
      CALL SCURXY(IC,IR)
      IR = IR + 1
C
C OPEN UP FILE
C
      READ(5) TITLE,NELM,NMODES
      DO 10 I=1,NMODES
        READ(5) (ES(J,I),J=1,NELM)
10    CONTINUE
      KEY = 'ENTER WHICH MODE TO SUMMARIZE : $'
      CALL KEYBD(KEY,R,IMODE,A,2,(3),0,IR)
      IR = IR + 1
C
C OPEN UP MODSUM.DD FILE
C
      OPEN(6,FILE='MODSUM.DD',STATUS='NEW')
      WRITE(6,8000) TITLE,NMODES,NELM
8000  FORMAT(A40,
1     /'NUMBER OF MODES : ',I2,
2     /'NUMBER OF ELEMENTS : ',I3)
      WRITE(6,8010) IMODE
8010  FORMAT(/20X,'SUMMARY FOR MODE NUMBER : ',I2)
      WRITE(6,8020)
8020  FORMAT(/'ELEMENT',5X,'MODAL STRAIN',
1     /' NO. ',5X,' ENERGY')
      DO 20 I=1,NELM
        WRITE(6,8030) I,ES(I,IMODE)
20    CONTINUE
8030  FORMAT(3X,I3,9X,1PE10.3)
      STOP
      END

```

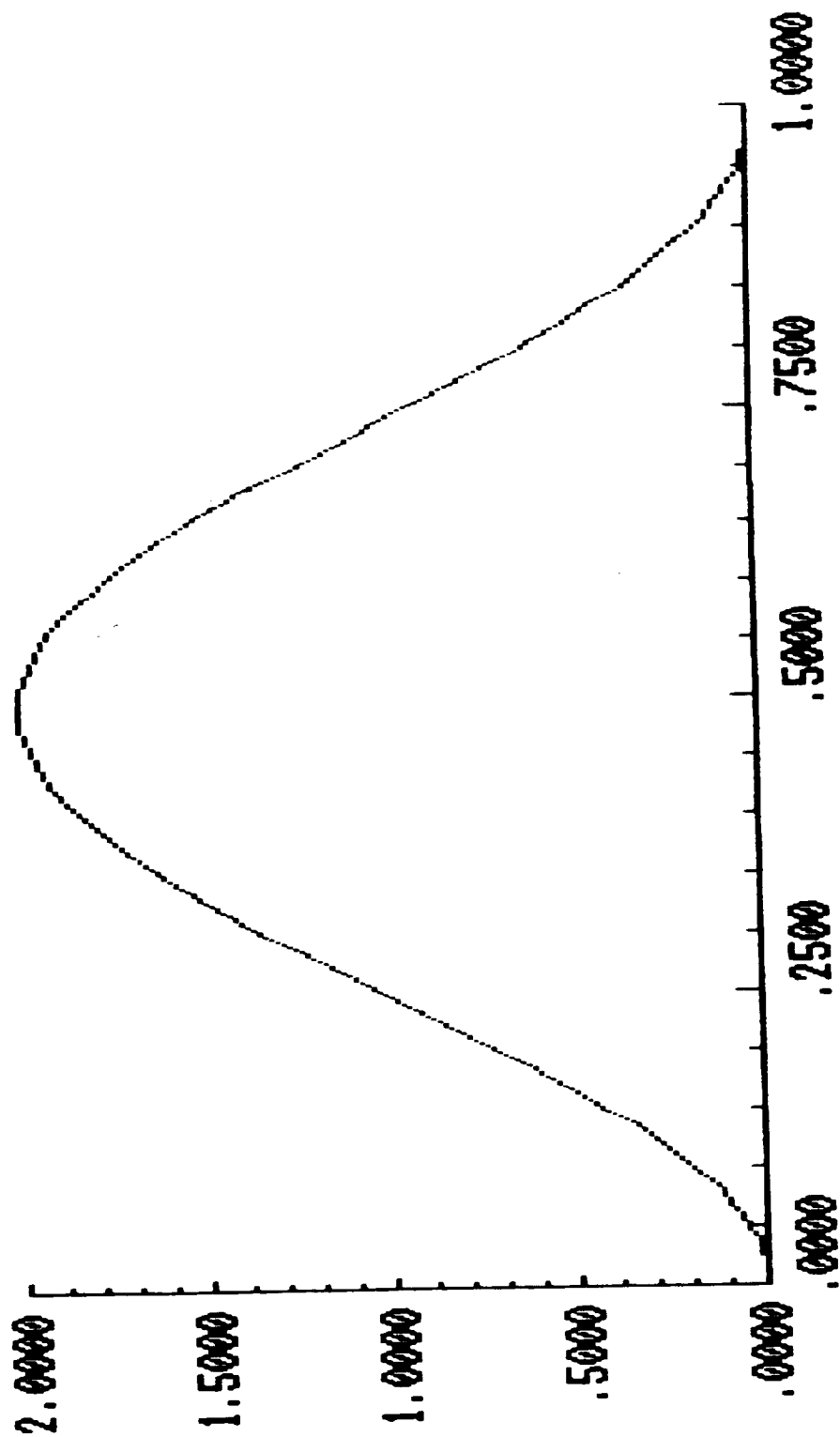
APPENDIX H

MODAL STRAIN ENERGY DISTRIBUTION  
PLOTS FOR SIMPLY SUPPORTED BEAM

This appendix contains the modal strain energy plots for the simply supported straight uniform beam referred to in Section 6.0. The modal strain energy distributions were obtained by using sixty beam segments. They were obtained for the first twelve modes.

MODAL STRAIN ENERGY 1ST MODE  
TEST : 1  
CHANNEL : 1

RANGE  
YMIN : .0000  
YMAX : 2.0000



Normalized Axial Position,  $x/\lambda$

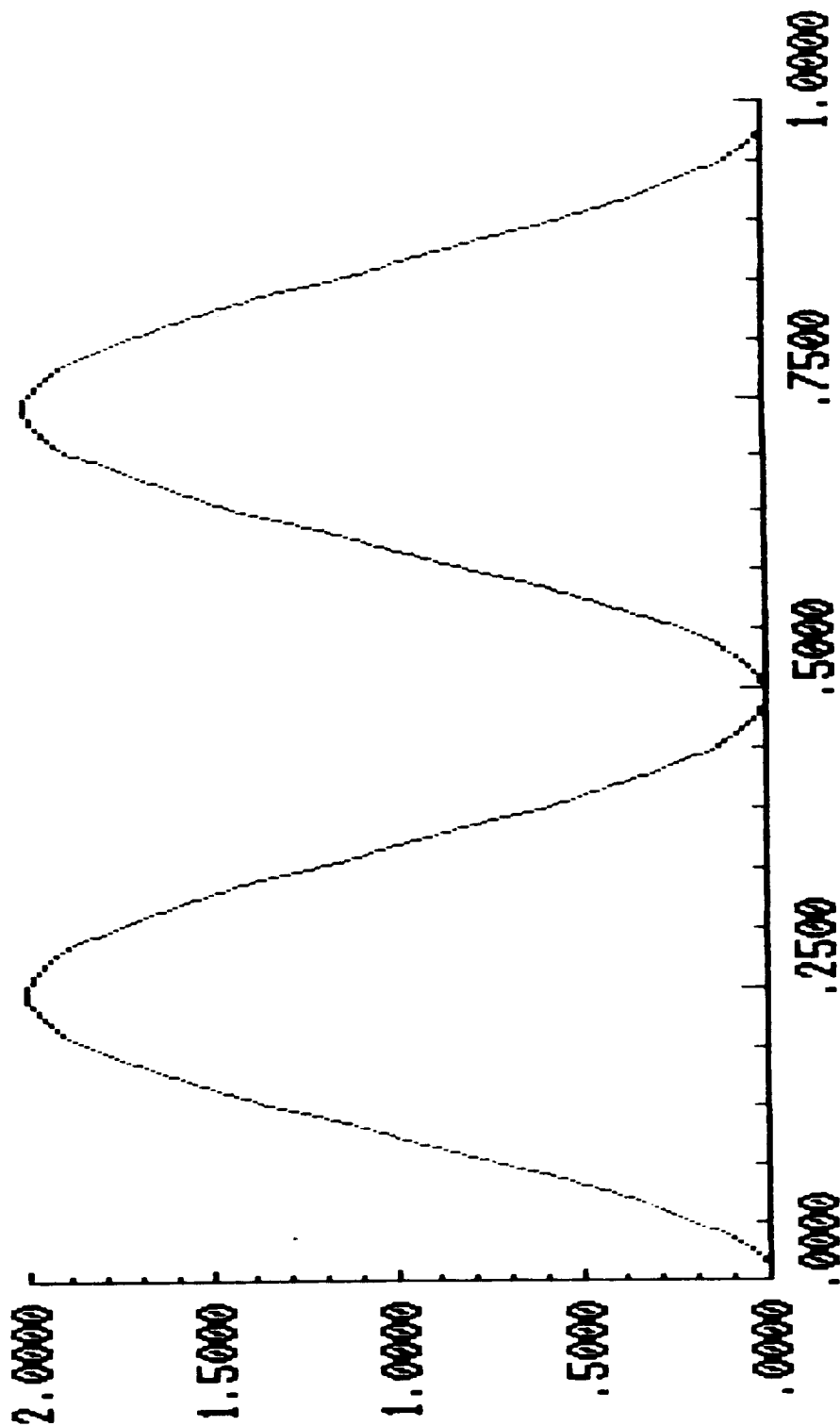
MODAL STRAIN ENERGY 2ND MODE

TEST : 1  
RUN : 1

CHANNEL : 1

RANGE

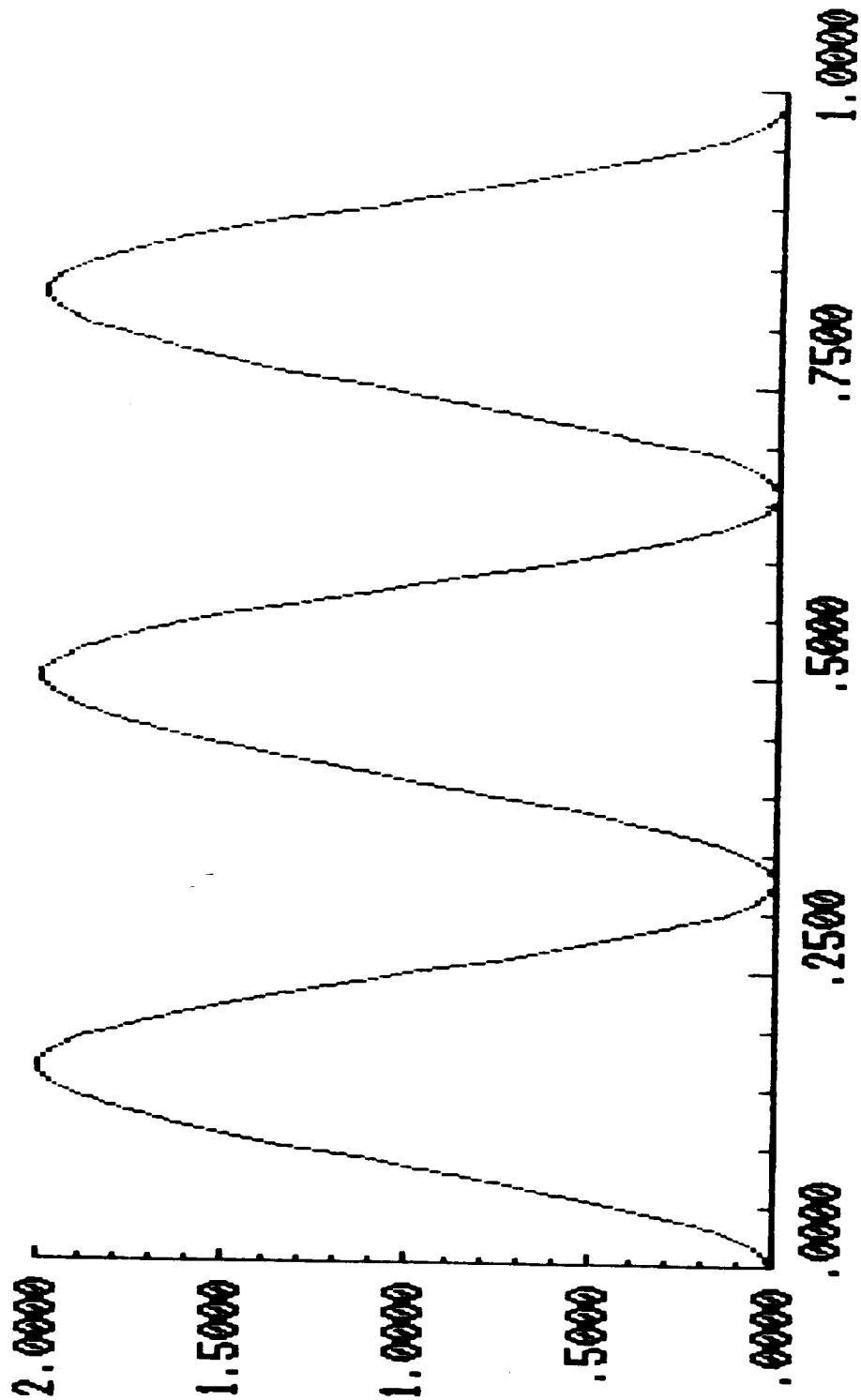
YMIN : .0000  
YMAX : 2.0000



Normalized Axial Position,  $x/l$

MODAL STRAIN ENERGY 3RD MODE  
TEST : 1  
CHANNEL : 1

RANGE  
YMIN : .0000  
YMAX : 2.0000

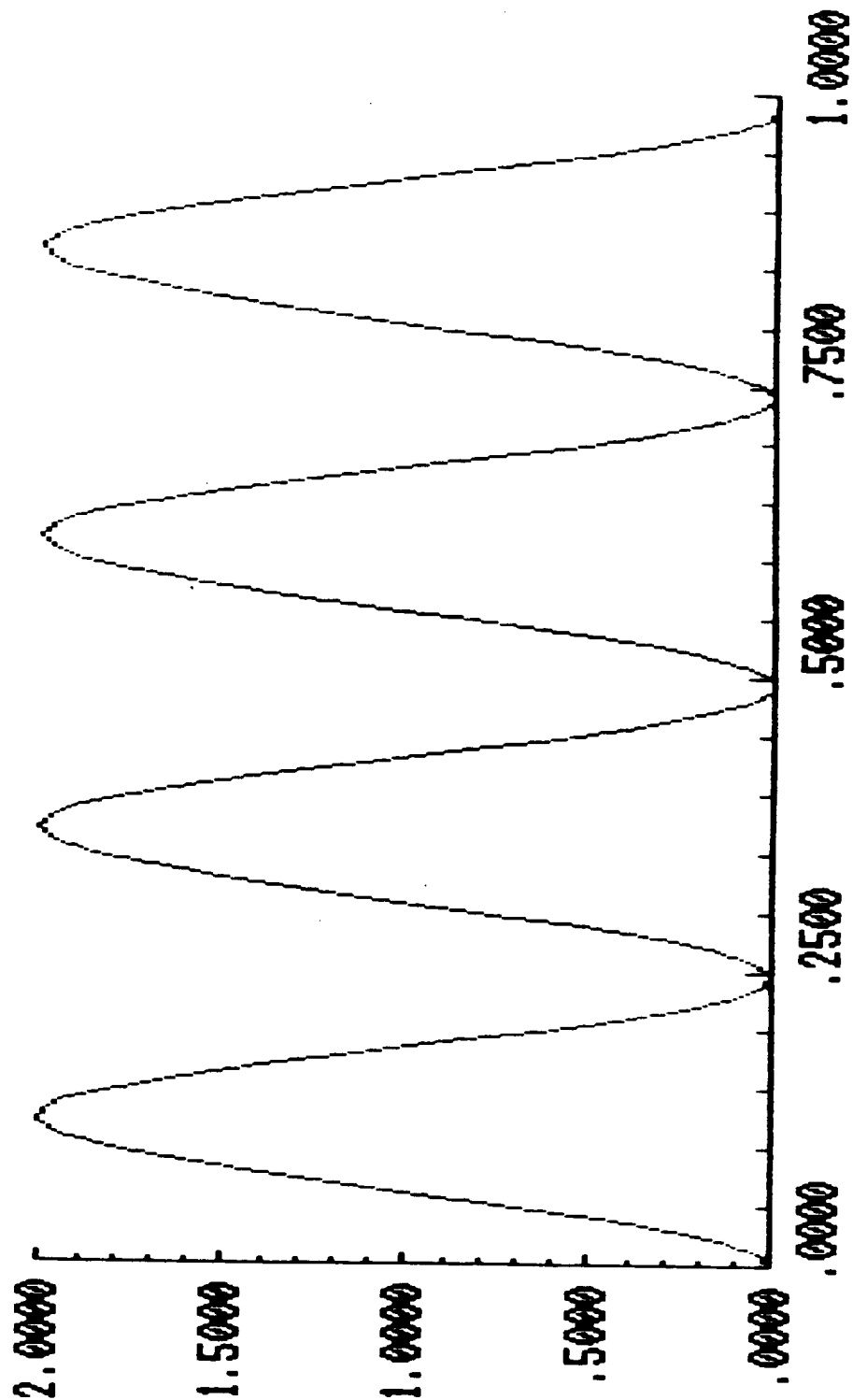


Normalized Axial Position,  $x/\ell$



MODAL STRAIN ENERGY 4TH MODE  
TEST : 1  
CHANNEL : 1

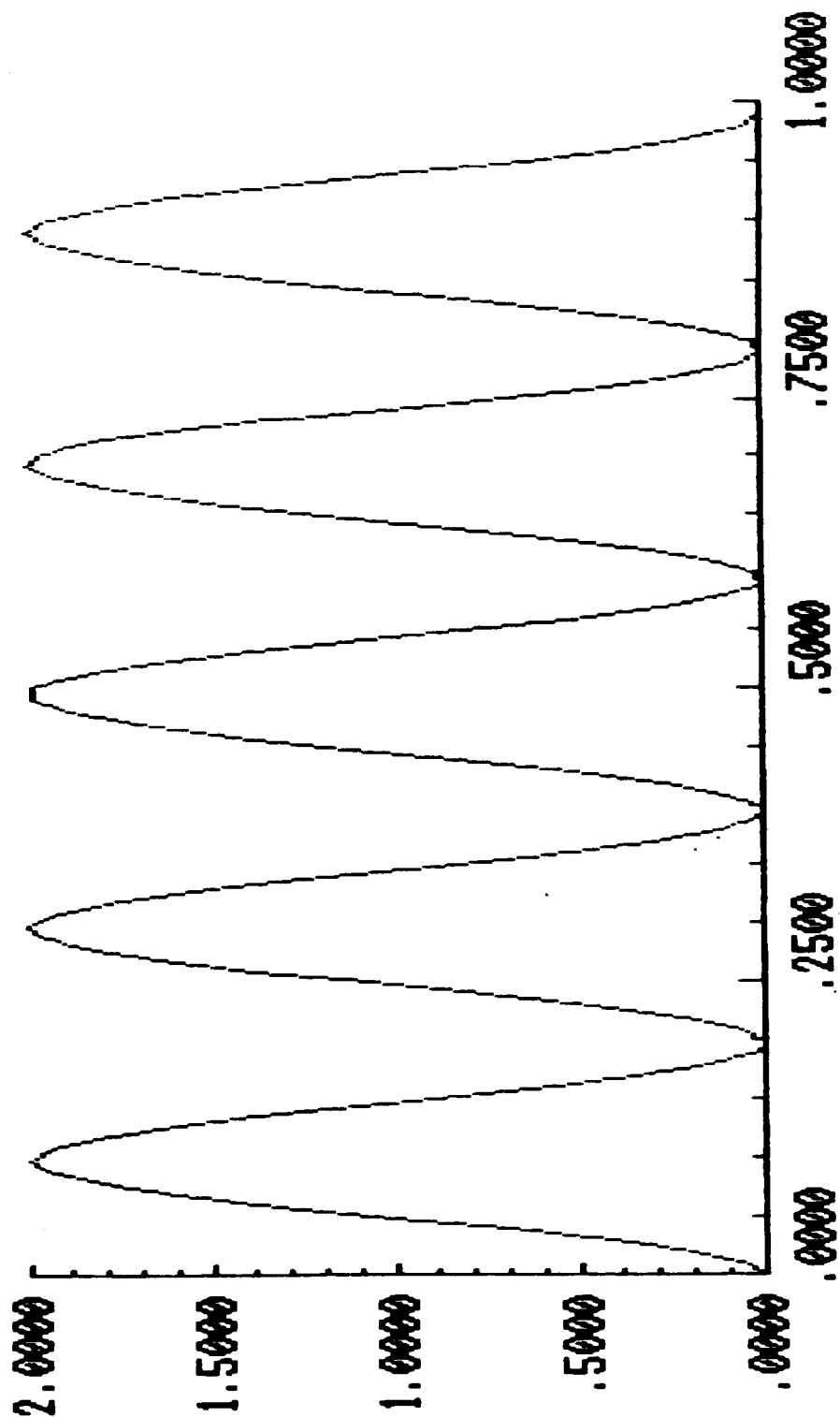
RANGE  
YMIN : .0000  
YMAX : 2.0000



Normalized Axial Position,  $x/l$

MODAL STRAIN ENERGY 5TH MODE  
TEST : 1  
CHANNEL : 1

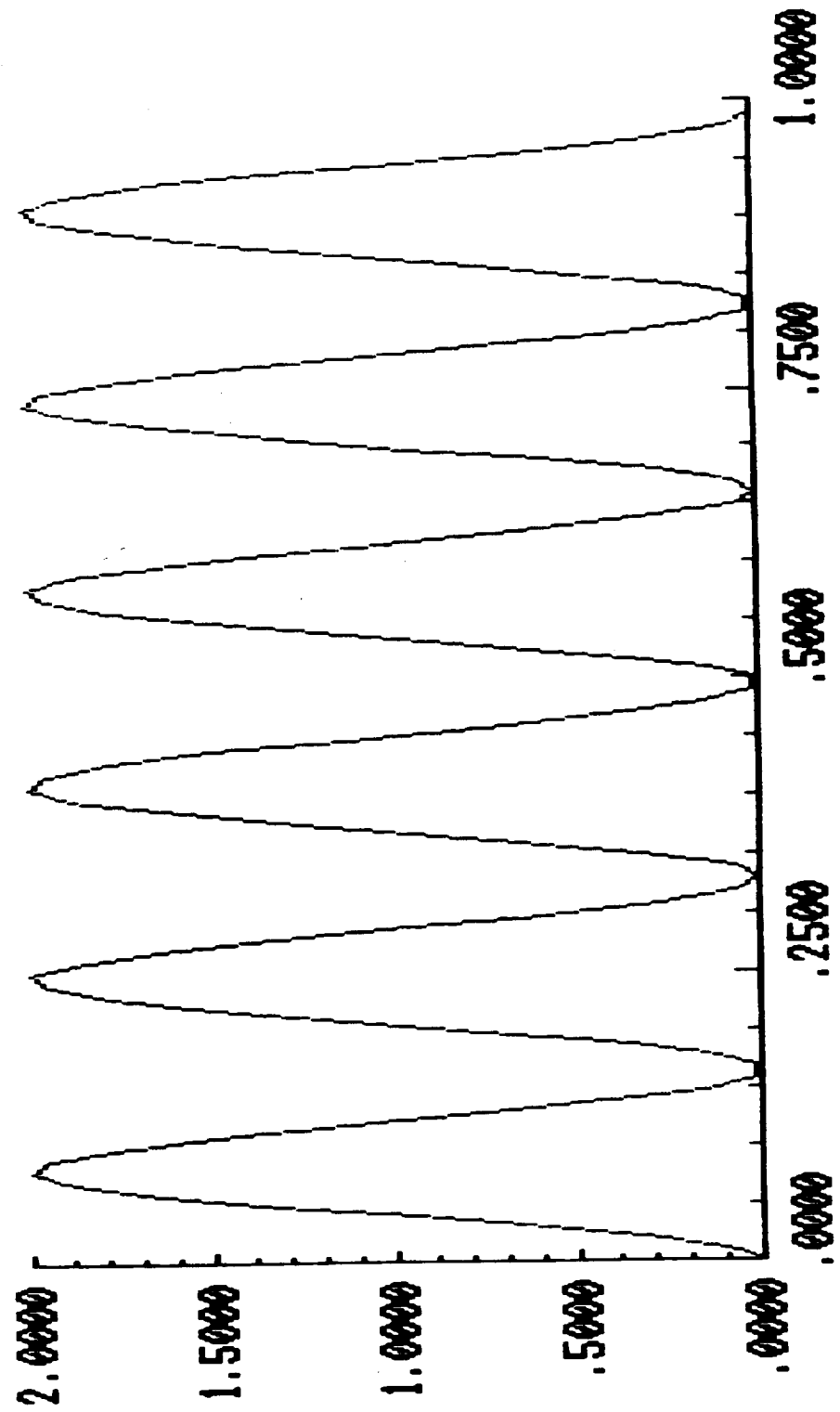
RANGE  
YMIN : .0000  
YMAX : 2.0000



Normalized Axial Position,  $x/l$

MODAL STRAIN ENERGY 6TH MODE  
TEST : 1  
CHANNEL : 1

RANGE  
YMIN : .0000  
YMAX : 2.0000



Normalized Axial Position,  $x/l$

MODAL STRAIN ENERGY 7TH MODE

TEST : 1

RUN : 1

CHANNEL : 1

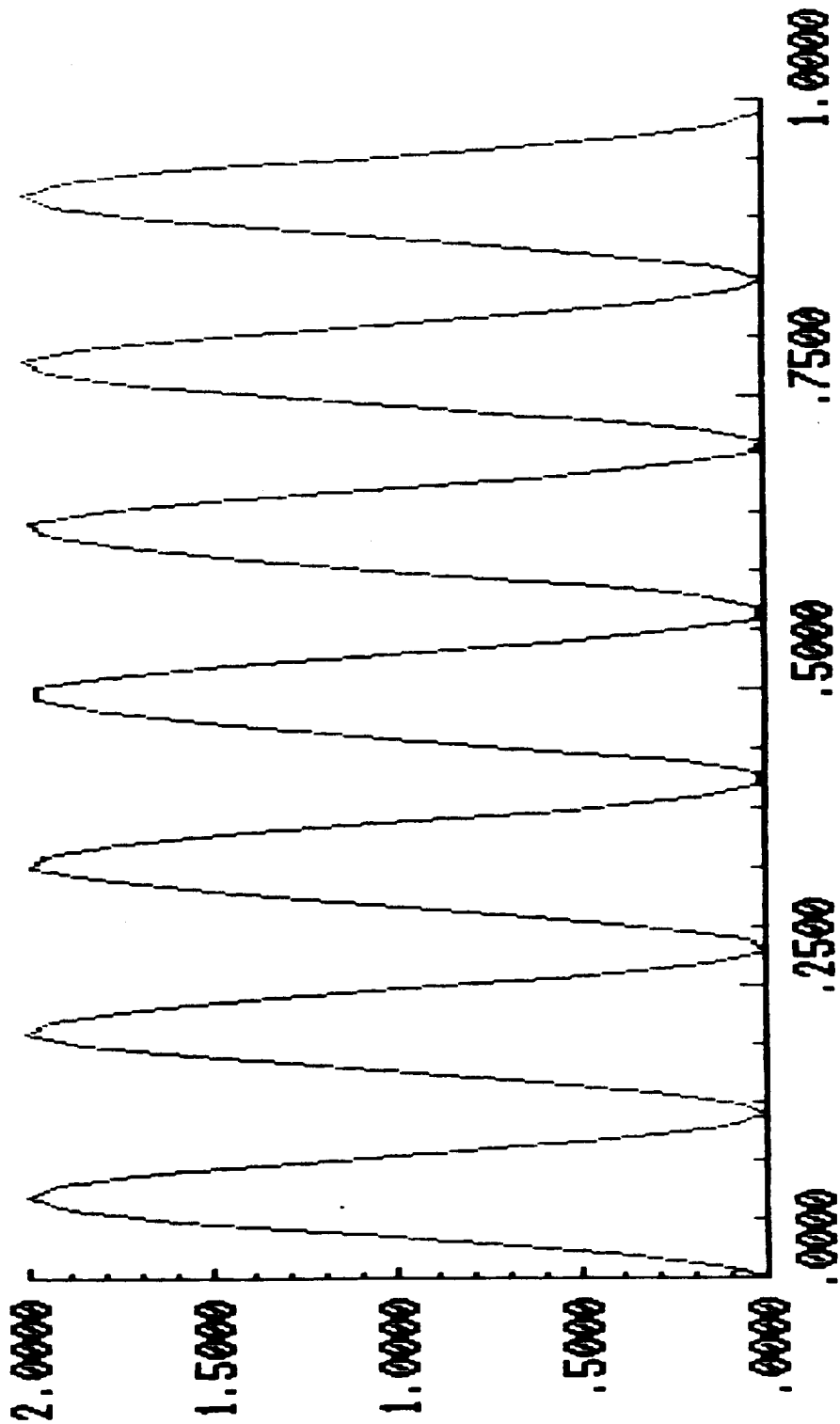
RANGE

YMIN :

.0000

YMAX :

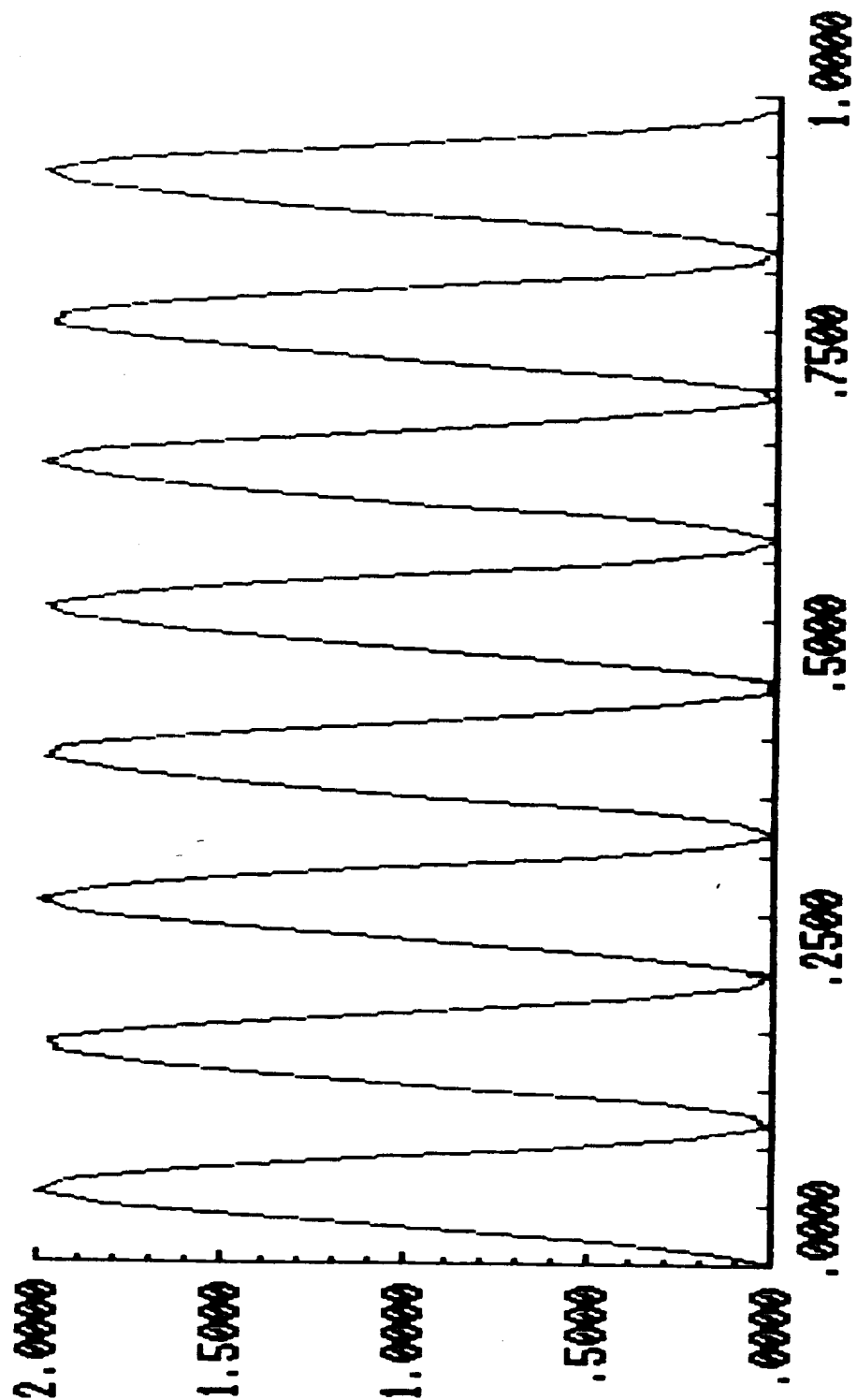
2.0000



Normalized Axial Position,  $x/l$

MODAL STRAIN ENERGY 8TH MODE  
TEST : 1  
CHANNEL : 1

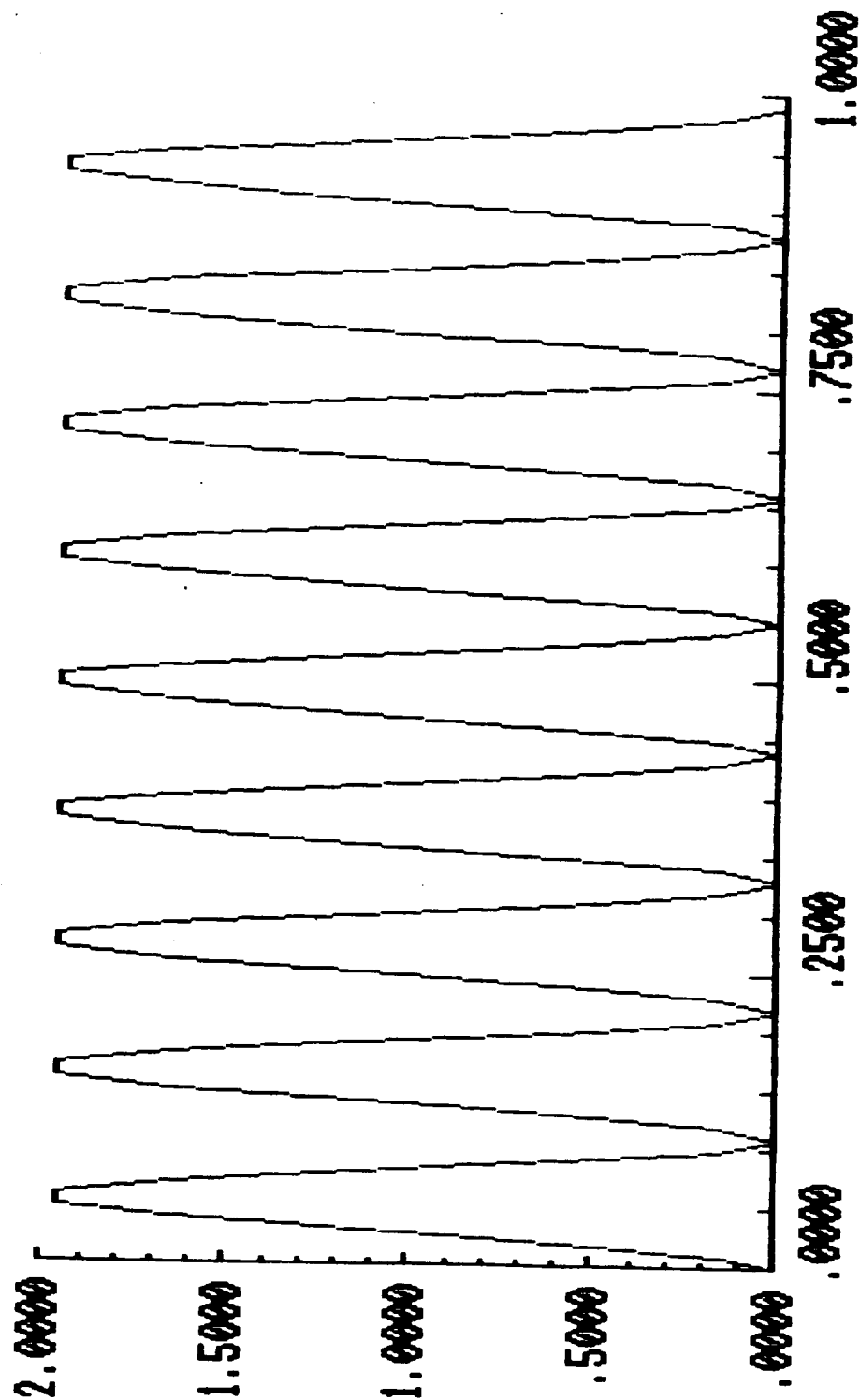
RANGE  
YMIN : .0000  
YMAX : 2.0000



Normalized Axial Position,  $x/l$

MODAL STRAIN ENERGY 9TH MODE  
TEST : 1  
CHANNEL : 1

RANGE  
YMIN : .0000  
YMAX : 1.9600



Normalized Axial Position,  $x/l$

MODAL STRAIN ENERGY 10TH MODE

TEST : 1

RUN : 1

CHANNEL : 1

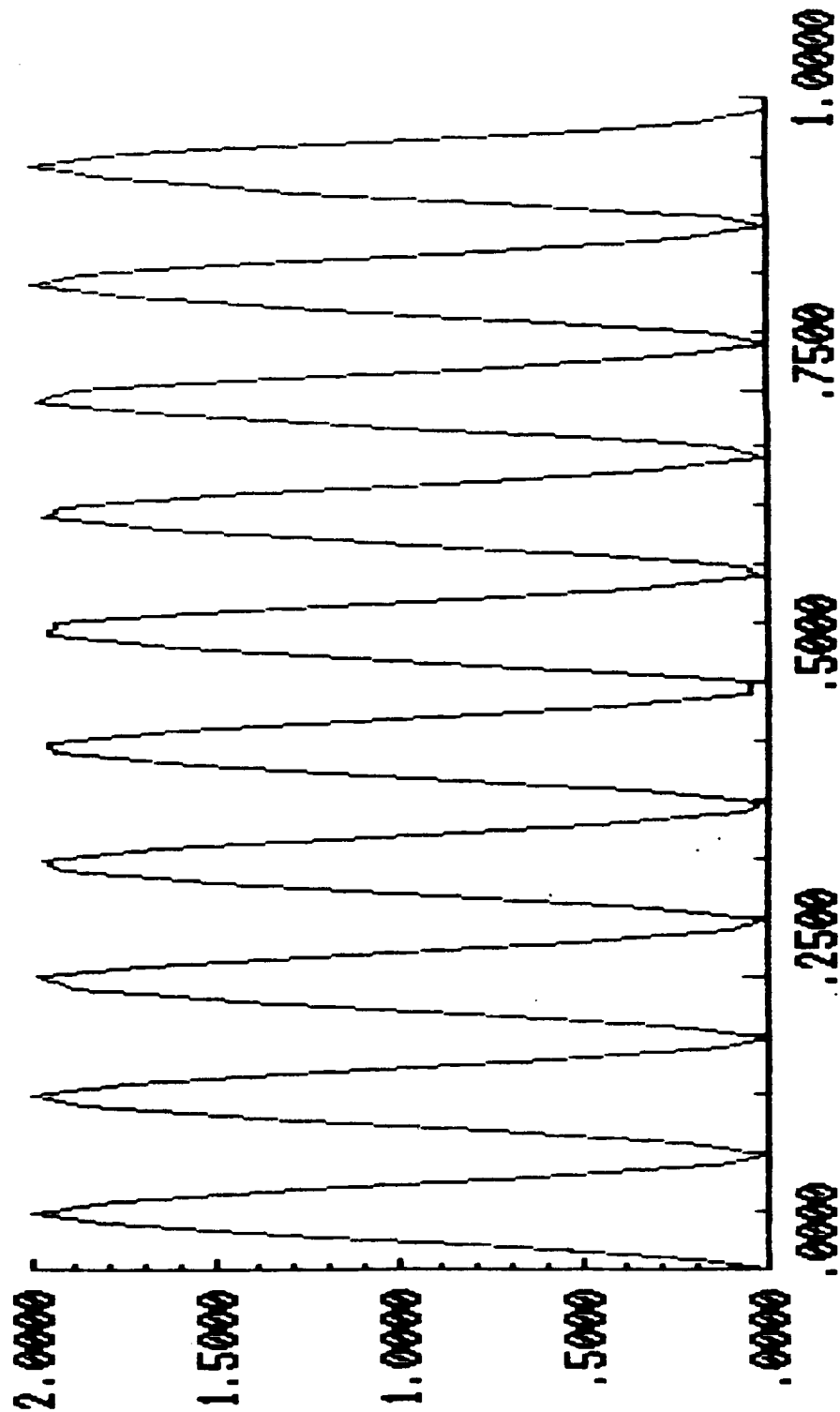
RANGE

YMIN :

.0000

YMAX :

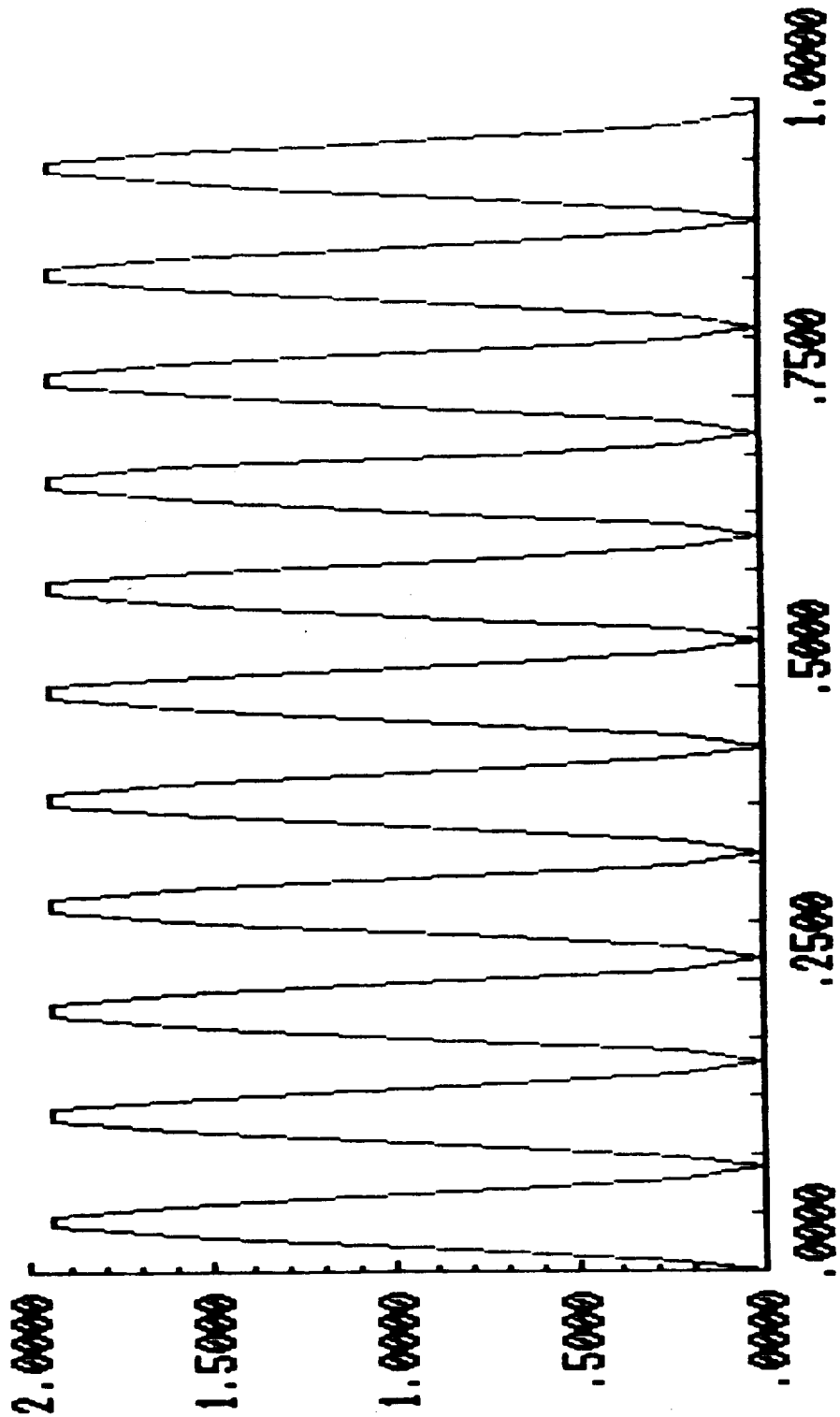
2.0000



Normalized Axial Position,  $x/l$

MODAL STRAIN ENERGY 11TH MODE  
TEST : 1  
CHANNEL : 1

RANGE  
YMIN : .0000  
YMAX : 1.9400



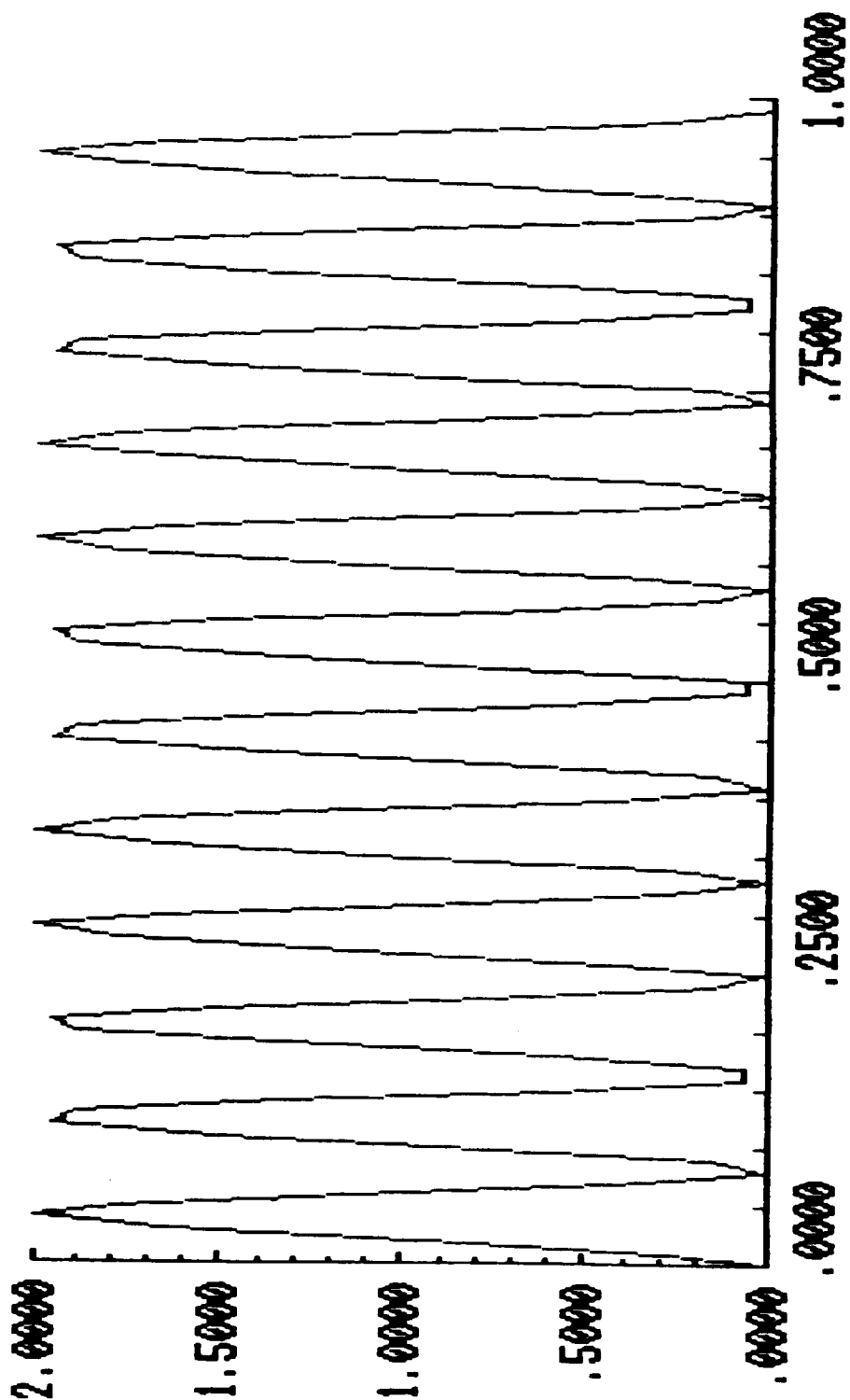
Normalized Axial Position,  $x/l$



MODAL STRAIN ENERGY 12TH MODE  
TEST : 1  
CHANNEL : 1

RANGE

YMIN : .0000  
YMAX : 2.0000



## NASA SCIENTIFIC AND TECHNICAL DOCUMENT AVAILABILITY AUTHORIZATION (DAA)

To be initiated by the responsible NASA Project Officer, Technical Monitor, or other appropriate NASA official for all presentations, reports, papers, and proceedings that contain scientific and technical information. Explanations are on the back of this form and are presented in greater detail in NHB 2200.2, "NASA Scientific and Technical Information Handbook."

☒ Original  
☐ Modified

(Facility Use Only)

Control No. \_\_\_\_\_

Date \_\_\_\_\_

I. DOCUMENT/PROJECT IDENTIFICATION (Information contained on report documentation page should not be repeated except title, date and contract number) SBIR Phase II Report  
Title: Providing Structural Modules with Self-Integrity Monitoring

Author(s): \_\_\_\_\_

Originating NASA Organization: NASA Resident Office-JPLPerforming Organization (if different) Anco Engineers, Inc.Contract/Grant/Interagency/Project Number(s) NAS7-961

Document Number(s) \_\_\_\_\_

Document Date: 1/6/86-7/6/88

(For presentations or externally published documents, enter appropriate information on the intended publication such as name, place, and date of conference, periodical or journal title, or book title and publisher: \_\_\_\_\_)

These documents must be routed to NASA Headquarters, International Affairs Division for approval. (See Section VII)

## II. AVAILABILITY CATEGORY

Check the appropriate category(ies):

Security Classification: ☐ Secret ☐ Secret RD ☐ Confidential ☐ Confidential RD ☐ Unclassified

Export Controlled Document - Documents marked in this block must be routed to NASA Headquarters International Affairs Division for approval.

☐ ITAR ☐ EAR

NASA Restricted Distribution Document

☐ FEDD ☐ Limited Distribution ☒ Special Conditions-See Section III

Document disclosing an invention

☐ Documents marked in this block must be withheld from release until six months have elapsed after submission of this form, unless a different release date is established by the appropriate counsel. (See Section IX)

Publicly Available Document

☐ Publicly available documents must be unclassified and may not be export-controlled or restricted distribution documents.  
☐ Copyrighted ☐ Not copyrighted

## III. SPECIAL CONDITIONS

Check one or more of the applicable boxes in each of (a) and (b) as the basis for special restricted distribution if the "Special Conditions" box under NASA Restricted Distribution Document in Section II is checked. Guidelines are provided on reverse side of form.

a. This document contains:

☐ Foreign government information☐ Commercial product test or evaluation results☐ Preliminary information☐ Other-Specify \_\_\_\_\_

b. Check one of the following limitations as appropriate:

☐ U.S. Government agencies and U.S. Government agency contractors only☐ NASA contractors and U.S. Government agencies only☐ NASA personnel and NASA contractors only☐ NASA personnel only☐ Available only with approval of issuing office

IN-31-012  
DAA 111111  
P.353  
SBIR-Proprietary for two years after acceptance

Final Report Accepted: 9/26/88

## IV. BLANKET RELEASE (OPTIONAL)

All documents issued under the following contract/grant/project number \_\_\_\_\_ may be processed as checked in Sections II and III.

The blanket release authorization granted \_\_\_\_\_ Date \_\_\_\_\_ is:

☐ Rescinded - Future documents must have individual availability authorizations.☐ Modified - Limitations for all documents processed in the STI system under the blanket release should be changed to conform to blocks as checked in Section II.

## V. PROJECT OFFICER/TECHNICAL MONITOR

Gordon S. ChapmanSJTG. S. Chapman7/17/91

Typed Name of Project Officer/Technical Monitor

Office Code

Signature

Date

## VI. PROGRAM OFFICE REVIEW

☐ Approved☐ Not Approved

Typed Name of Program Office Representative

Program Office and Code

Signature

Date

## VII. INTERNATIONAL AFFAIRS DIVISION REVIEW

☐ Open, domestic conference presentation approved.☐ Export controlled limitation is not applicable.☐ Foreign publication/presentation approved.☐ The following Export controlled limitation (ITAR/EAR) is assigned to this document: \_\_\_\_\_☐ Export controlled limitation is approved.

International Affairs Div. Representative

Title

Date

## VIII. EXPIRATION OF REVIEW TIME

The document is being released in accordance with the availability category and limitation checked in Section II since no objection was received from the Program Office within 20 days of submission, as specified by NHB 2200.2, and approval by the International Affairs Division is not required.

Name &amp; Title

Office Code

Date

Note: This release procedure cannot be used with documents designated as Export Controlled Documents, conference presentations or foreign publications.

## IX. DOCUMENTS DISCLOSING AN INVENTION

a. This document may be released on \_\_\_\_\_ Date \_\_\_\_\_

Installation Patent or Intellectual Property Counsel

Date

The document was processed on \_\_\_\_\_ Date \_\_\_\_\_

In accordance with Sections II and III as applicable.

NASA STI Facility

Date

## DISPOSITION

ed forms should be forwarded to the NASA Scientific and Technical Information Facility, P.O. Box 8757, B.W.I. Airport, Maryland 21240, with check box):

ted or reproducible copy of document enclosed

ect or Report Documentation Page enclosed. The issuing or sponsoring NASA installation should provide a copy of the document, when complete, NASA Scientific and Technical Information Facility at the above listed address.